Coseismic pore pressure changes linked to local, induced earthquakes

By
Alexis Ahlert
M.S., University of Kansas, 2021

Submitted to the graduate degree program in Geology and the Graduate Faculty of the University of Kansas in partial fulfillment of the requirements for the degree of Master of Science.

Chair: Dr. George Tsoflias

Dr. Megan Brown

Dr. Mary Hill

Dr. Eugene Holubnyak

Date Defended: December 8th, 2021

The thesis committee for Alexis Ahlert certifies that this is the approved version of the following thesis:

Coseismic pore pressure changes linked to local, induced earthquakes

Chair: Dr. George Tsoflias

Date Approved: December 8th, 2021

Abstract

An unprecedented increase in seismicity in south-central Kansas (KS), starting in 2013, has been linked to elevated pore fluid pressures in the subsurface resulting from high rate wastewater injections. Improving the understanding of pore pressure communication at local scales (~10s of km) through the shallow basement (upper 10 km in the subsurface) can help mitigate the risk of induced seismicity. Here, I examine whether induced earthquakes, typically small local events, can induce detectable pore fluid pressure changes in the subsurface. Previous research has demonstrated that fluid levels in wells are sensitive to large magnitude, regional, and teleseismic earthquakes. The effect of small, local earthquakes on pore pressures is unknown. I analyze pore pressure measurements obtained every second over a time period of 11 months in a deep borehole ~30 m above basement at Wellington Field in KS, USA. I identify pore pressure signals by adapting an STA/LTA trigger algorithm, analogous to earthquake detection methods. The pressure event triggers produced from this algorithm are compared to earthquake data recorded at Wellington field by a seismometer network surrounding the pressure monitoring borehole.

Results from this analysis show that small magnitude local earthquakes can induce detectable pore fluid pressure changes. Two hundred and seventy-nine earthquakes were detected using the pore pressure dataset; 183 of these events were above the background noise level of the data and can be confidently related to changes in downhole pore pressure. The detected pressure events correspond to seismometer identified earthquakes ranging in magnitude from 0.8 to 5.8 at distances of 2 to 180 km from the monitoring well. Out of the full catalog of interest only 20% of known earthquakes relate to changes in downhole pressure. Earthquakes related to pressure have detectable pressure changes at the time of the earthquake that differentiates them from

earthquakes that were not related to coseismic pressure changes. Earthquake characteristics like the phase, impulsiveness, magnitude, frequency, phase duration, and distance from the pressure well do not correlate to pressure events.

Not all seismometer recorded earthquakes cause detectable pore pressure changes. This can be due to the sparse sampling of the pressure data (1 Hz) compared to the earthquake data (200 Hz) resulting in potentially missing the earthquake pressure signal, pressure signals falling below noise level or below the instrument detection threshold, as well as geologic heterogeneity of the subsurface influencing pressure communication. By using downhole pressure measurements and earthquake data from the field, it was possible to detect coseismic pressure changes related to small magnitude, induced earthquakes. Water level monitors are commonly inexpensive compared to seismic monitoring systems. This investigation offers compelling evidence that pressure monitoring can be a viable, inexpensive method for detecting local earthquakes. However, additional studies are needed in a controlled setting to examine the factors that can influence pressure sensing of earthquakes.

Acknowledgments

This research was supported by the Kansas Geological Foundation, the University of Kansas Department of Geology, and the Kansas Geological Survey (KGS).

I would like to thank my advisor Dr. George Tsoflias for his mentorship and support throughout this project. Thank you to Dr. Alex Nolte for his guidance and input on this work. This project is an accumulation of three years of work, and it would have been impossible for it to be completed without their support and input. Thank you to my committee members Dr. Megan Brown, Dr. Mary Hill, and Dr. Eugene Holubnyak for their insights and feedback on the project.

Additionally, I would like to thank Wyatt Hansen for his continued support throughout my time in graduate school. I also would like to say thank you to my family for always supporting me throughout my academic career.

Table of Contents

List of Figures

Chapter 1: Introduction

Wastewater injection into subsurface reservoirs and saline aquifers has been common practice for disposing of fluid waste related to municipal and industrial activities. The Environmental Protection Agency (EPA) Underground Injection Control (UIC) program is responsible for placing injection wells into one of six different categories (Class I-VI). Each of these categories have their own set of regulations to protect underground sources for drinking water (Environmental Protection Agency, 2021). UIC Class II injection wells usually inject fluids related to the production of oil and gas. Most of these wells are used for enhanced oil recovery, but 20% of class II wells primarily function as saltwater disposal wells (SWD). SWD wells inject produced formation water (brine) and can also include flowback water from hydraulic fracturing operations.

The historical seismicity for the state of Kansas can be seen in Figure 2.1.1. From 1973 to 2012 there was on average one earthquake of magnitude 3 (M 3) or greater every two years within the state of Kansas (Dubois and Wilson, 1978; Steeples et al., 1990; Rubinstein et al., 2018). Seismicity has dramatically increased in the U.S. midcontinent in the past decade (Ellsworth, 2013; Rubinstein et al., 2015; Figure 2.1.2). This increase in earthquakes has been linked to wastewater injection from the increased activity of the oil and gas industry in the central United States (Frohlich, 2012; Horton, 2012; Ellsworth, 2013; Keranen et al., 2013; Frohlich et al., 2014; Keranen et al., 2014; Ellsworth et al., 2015; Alt and Zoback, 2016; Elsworth et al., 2016; Yeck et al., 2017). It has been shown that in some areas the increases in seismicity have closely followed a 5 to 10 fold increase in the rates at which the wastewater is being injected (Walsh and Zoback, 2015). This increase in seismicity has led to concerns relating to the safety and the effectiveness of underground wastewater injection. While these concerns

exist, there has been increased development of unconventional, low permeability, resource plays. These resource plays typically produce large amounts of wastewater, so the need for more SWD wells is growing.

Injection-induced seismicity, within the state of Oklahoma, has been extensively researched. Oklahoma has experienced an almost 900-fold increase in earthquakes since 2009 (Langenbruch and Zoback, 2016). Along with this increase in earthquakes, the state has also experienced some of the largest earthquakes in its history, including the 2011 M 5.6 Prague, the 2016 M 5.1 Fairview, and the 2016 M 5.8 Pawnee earthquakes (Keranen et al., 2013; Yeck et al., 2017). In late 2013, the seismicity occurring in Oklahoma was beginning to extend into Kansas. Since 2013, two counties in the south-central part of the state have experienced more than 2500 earthquakes, with more than 100 of these events recording as M 3 or greater (Walsh and Zoback, 2015). The largest earthquake to occur in Kansas was the Milan M 4.8 earthquake on November 12, 2014. This earthquake was located approximately 50 km SW of Wichita, KS.

The timing and location of these earthquakes has led researchers to believe that there is an association between the recent increase in earthquakes and major brine disposal operations across the midcontinent. Researchers from the USGS (Rubinstein et al., 2014; Benz et al., 2015; Ellsworth et al., 2015; Choy et al., 2016), Kansas Geological Survey (KGS; Bidgoli et al., 2015; Peterie et al., 2015; Buchanan, 2015; Bidgoli and Jackson, 2017), Oklahoma Geological Survey (Kroll et al., 2017; Walter, et al., 2017), and Oklahoma and Kansas Corporation Commissions, have all concluded that these seismic events are induced.

Past research relating to induced seismicity has focused on the temporal and spatial connection between injection activity and seismicity in the midcontinent (Frohlich, 2012; Horton, 2012; Ellsworth, 2013; Keranen et al., 2013; Frohlich et al., 2014; Keranen et al., 2014;

Ellsworth et al., 2015; Alt and Zoback, 2016; Elsworth et al., 2016; Yeck et al., 2017). In Oklahoma and Kansas, oil and gas operators inject wastewater at high rates into the Arbuckle group (Schoenball and Ellsworth, 2017). The Arbuckle group of the midcontinent is a highly heterogeneous, permeable and under-pressured carbonate reservoir (Franseen et al., 2004). Directly below the Arbuckle group is the fractured crystalline basement (Schoenball and Ellsworth, 2017). The fluid pressure from high rate injections migrates laterally within the Arbuckle group and into the crystalline basement where it reactivates preexisting faults, causing earthquakes (Schwab et al., 2017; Figure 2.2.1). It is important to note that the hydraulic properties of the Arbuckle group as well as basement rocks are poorly understood (Schnoeball and Ellsworth, 2017). Improving the understanding of pressure communication in the Arbuckle group and shallow basement at local scales (10s of km) can help mitigate the risk of induced seismicity.

The primary objective of this research is to determine whether small, induced earthquakes (M 5 and less) cause detectable pore pressure changes. It is known from previous research (Barbour et al., 2019; Manga et al., 2015; Ingebritsen and Manga, 2019) that fluid levels in wells are sensitive to large magnitude earthquakes. However, it is not known if small magnitude, local earthquakes induce pore fluid pressure changes. To address this question, I expand on the preliminary work presented by Watney et al. (2016) that observed distinct pressure and temperature signals recorded in a deep borehole at Wellington field in south KS, during the 2016 Pawnee earthquake. I use a year and half of continuous downhole pressure data and seismic data from Wellington Field, KS, to better understand how small seismic events relate to changes in subsurface fluid pressure changes. In the future, it is thought that pressure sensing

could potentially offer a low-cost, long-term earthquake monitoring method (Zhang et al., 2019; Zhang et al., 2018; Wang et al., 2017; Elkhoury et al. 2006).

Chapter 2: Background

Section 2.1: Historical and recent seismicity

The state of Kansas has experienced few earthquakes in the past. From 1867 to 1977, there were ~30 felt earthquakes within Kansas (DuBois and Wilson, 1978) (Figure 2.1.1). The largest event, which was a M 5.2, occurred in the northeast part of the state near Manhattan, KS. Between 1977 and 2012, there were over 200 earthquakes recorded by seismic instrumentation in the state (Figure 2.1.1). These earthquakes were recorded by a temporary network from the Kansas Geological Survey's Kansas-Nebraska Network (Hildebrand et al., 1988) and permanent stations operated by the U.S. Geological Survey. The over ~35 years of seismic data from these networks and stations help researchers conclude that historically Kansas has experienced one M 3 or greater earthquake every two years. From 1977 to 2012 there were approximately 30 earthquakes that were M 2 or greater (NEIC Catalog). However, since 2013, two counties in south-central Kansas (Harper and Sumner counties) have experienced a dramatic increase in the number of earthquakes, with 119 M 3 or greater events within these two counties (Choy et al., 2016; NEIC Catalog).

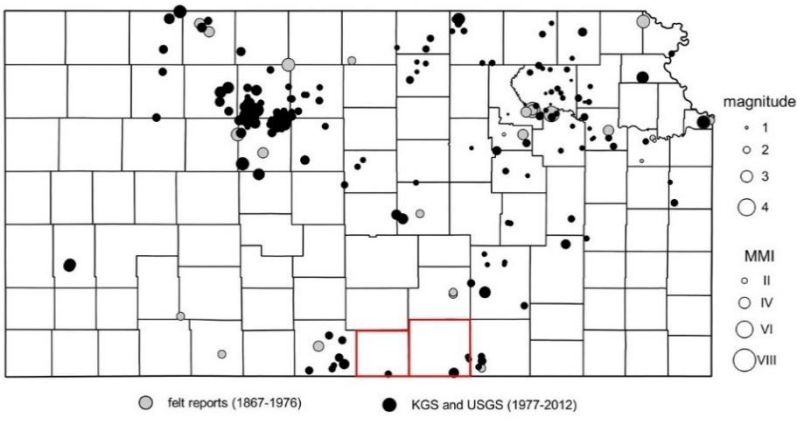

Figure 2.1.1: Historical Seismicity in the state of Kansas (Figure from Kansas Geological Survey (KGS) and uses data from the KGS; Dubois and Wilson, 1978; Steeples et al., 1990; and National Earthquake Information Center (NEIC)). Gray circles represent felt earthquakes from 1867 to 1976, while black circles are recorded events from

1977 to 2012. The red squares outline Harper and Sumner counties. Harper County is to the west, while Sumner County is to the east.

Past earthquake monitoring shows that the State of Oklahoma has experienced more historic seismicity than Kansas. Oklahoma experienced approximately 129 earthquakes from before 1962 to 1976. In 2009 there were 33 M 2.5 or greater events and more than 360 M 2.5 events just in the first half of 2017 (NEIC Catalog; Figure 2.1.2). The increase in seismicity in these two states, starting in the 2000's, is temporally and spatially correlated with the development of the Mississippian limestone play and other water-dominated resource plays. In 2009, these plays became more economical to produce from since the introduction of improved technologies relating to horizontal drilling and hydraulic fracturing of these reservoirs. These reservoirs produce large volumes of brine along with hydrocarbons. Within the Mississippian limestone play there can be water cuts as high as 90% (Mitchell and Simpson, 2015).

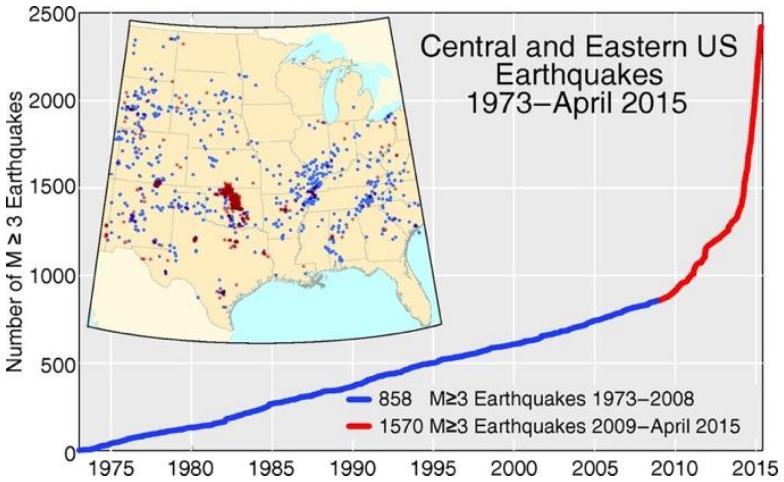

Figure 2.1.2: Seismicity in central and eastern U.S. from 1973 to 2015. Beginning in 2009, the rate of earthquakes increased and clustered in a few areas, like central and northern Oklahoma and southern Kansas (Rubinstein et al., 2015).

As oil and gas production in the midcontinent increased it led to an increase in wastewater injection due to the industry needing to dispose of large volumes of produced water. The number of SWD wells in Harper and Sumner counties, which is where induced seismicity is concentrated in Kansas, has tripled since 2005. During this same time, disposal volumes have increased and permitted daily injection rates in these counties have also heightened (Ellsworth, 2013). It has been shown that in some areas the increases in seismicity have closely followed a 5 to 10 fold increase in the rates at which the wastewater is being injected (Walsh and Zoback, 2015). These injection rates have increased from a maximum of 0.1-0.4 m^3/month to as high as 1.3 m^3/month (Langenbruch and Zoback, 2016). Recent state-ordered reductions have forced operators to lower injection rates to 0.7 m^3/month (Langenbruch and Zoback, 2016).

Both regional and local injections may influence the occurrence and location of the seismicity in South Central Kansas (Rubenstein et al., 2018). Seismicity in this area has been linked to high-rate disposal wells that are located 10 km's or more from the area of interest (Rubenstein et al., 2018). It is thought that fluid pressures near the well decrease quickly, but the fluid pressure remains high at greater distances from the well for months (Rubenstein et al., 2018). Near Wellington Field, there are low-rate injection wells that have been active for years and have not coincided with earthquakes. Recent seismicity in the area is thought to be caused by high-rate injection wells that are located 10 kms or more away from the field (Rubenstein et al., 2018). The closest high-rate injection well as noted by Rubinstein et al. (2018) is located 40 km's away from Wellington Field. Earthquakes in the area to date have been smaller magnitude events ($\leq$ M 5).

Section 2.2: Injection induced seismicity

Starting in the late 2000's injection induced earthquakes have become a recurring issue in Oklahoma and Kansas. Injection induced earthquakes have been observed in the past and studied extensively. For example, in the early 1960's seismicity related to the injection of waste fluid was noted at Rocky Mountain Arsenal near Denver, Colorado (Raleigh et al., 1976). In the late 1960's field experiments were conducted in Rangely, Colorado where they purposefully injected fluid into the subsurface with the goal of inducing earthquakes (Raleigh et al., 1976). Although injection induced seismicity is not a new phenomenon, it is within the states of Kansas and Oklahoma.

Changes in pore fluid pressure that are related to wastewater injection have been widely interpreted as the cause for triggering seismicity in Kansas (Keranen et al., 2013; Choy et al., 2016; McNamara et al., 2015), Arkansas (Horton, 2012), Oklahoma (Keranen et al., 2013), Ohio (Kim, 2013), and elsewhere (e.g., Segall et al., 1994). While it is accepted that fluid injection can trigger earthquakes, it should be noted that only a small number of injection wells have been conclusively linked to earthquakes. The principal wastewater injection zone in the U.S. midcontinent is the Cambro-Ordovician Arbuckle Group (Figure 2.2.1). The Arbuckle group of the midcontinent is a highly heterogeneous carbonate reservoir (Franseen et al., 2004). Continuous fluid pressure measurements in the Arbuckle have shown that the pressure of the reservoir is increasing by at least 5 kPa annually (Barbour et al., 2019). The Arbuckle overlies the crystalline basement, which is where the induced earthquakes are occurring. It is believed that the fluid pressure from high rate injections migrates laterally within the Arbuckle group and into the crystalline basement (Figure 2.2.1; Schoenball and Ellsworth, 2017).

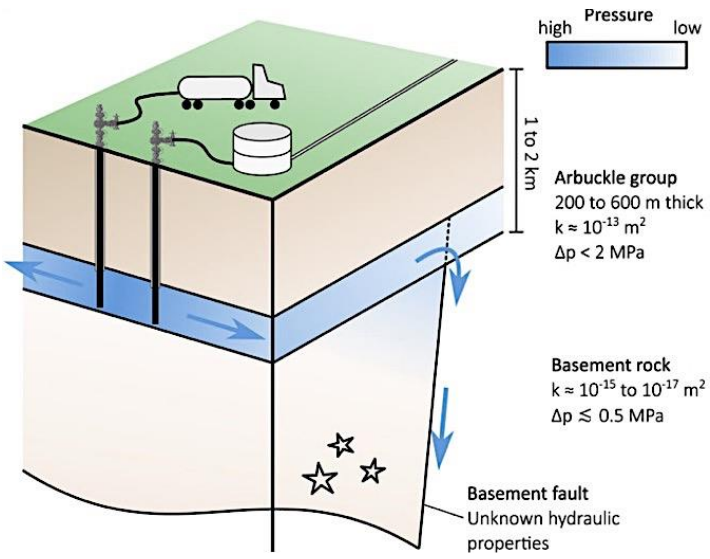

Figure 2.2.1: Schematic that describes how wastewater is being injected into the Arbuckle. Then the pressure migrates downward into the crystalline basement and triggers earthquakes (Schoenball and Ellsworth, 2017).

Improved understanding of how pore pressure changes relate to induced earthquakes may provide new knowledge relating to induced seismicity in Kansas. To date, small magnitude earthquakes (less than a magnitude 4) have not been related to downhole pore pressure changes. It is believed that if this relationship exists, pressure sensors could be used as an efficient measurement tool to monitor seismicity.

Section 2.3: Relating seismicity with well pressure data

Past research (Barbour et al., 2019, Manga et al., 2015, Ingebritsen and Manga, 2019) relates large felt earthquakes with well fluid level data. Large earthquakes, M7 and M8, can cause changes in water levels in wells across the globe (Manga et al., 2015). One example of this phenomenon is the 2017 earthquake that occurred in Tehunatepec, Mexico. At the time of this earthquake, there was a peak in the fluid level data in an Arbuckle well located in Oklahoma of 277 mm (Barbour et al., 2019). Along with relating earthquake and pressure, past studies (Zhang

et al., 2019, Zhang et al., 2018, Wang et al., 2017, Elkhoury et al. 2006) have used seismic events to calculate reservoir parameters, like permeability. The most common method used to estimate these parameters, is the tidal analysis method from downhole water-level measurement tools. This method compares synthetic tidal pressure to the tidal pressure collected from field data (Elkhoury et al., 2006). During an earthquake, the measured tide will either be ahead or lag behind the synthetic tide. These phase lags or leads can be interpreted as reservoir permeability changes (Elkhoury et al., 2006). Kroll et al. 2017 modeled the fluid level response in a well in Oklahoma by finding the static strains of earthquake events and poroelastic properties of the Arbuckle. They noted that changes in volumetric strain can cause increases or decreases in fluid level data in a reservoir (Kroll et al., 2017). Furthermore, they noted transient signals observed in their water level data that they believe are related to earthquake waves (Kroll et al., 2017), however the sampling rate was too sparse for transient signal monitoring. Many of these studies relating changes in pressure with seismicity have only involved large magnitude distant earthquakes and have not examined how pressure changes may relate to small magnitude, induced seismicity.

A preliminary study comparing observations of well pressure and earthquake recordings at the Wellington Field KS, the location of the proposed research, found that the Pawnee Earthquake (M 5.8) in Oklahoma coincided with pressure oscillations of 0.2 to 0.7 psi at Wellington (Watney et al., 2016; Figure 2.3.1). This preliminary study lends support to the hypothesis that seismic events can induce pore pressure changes that can be detected in well pressure data. However, a M 5.8 earthquake is a large magnitude event. It remains unknown if smaller magnitude earthquakes can induce detectable pore pressure changes and this study will attempt to answer this question.

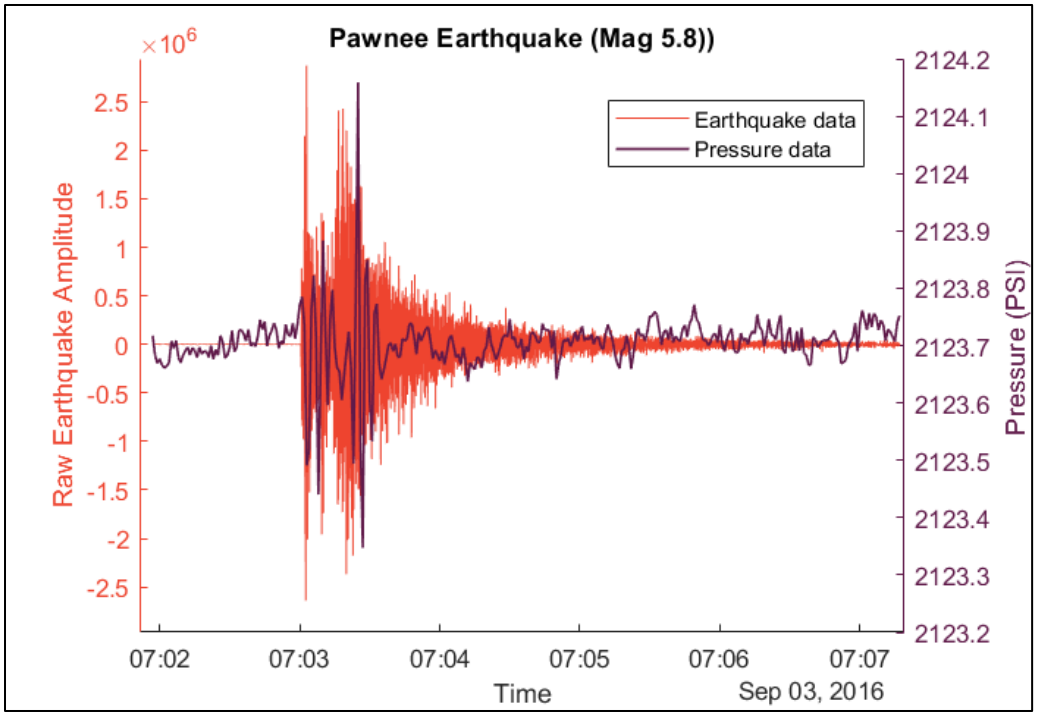

Figure 2.3.1: Overlay of 2016 Pawnee earthquake (M5.8) seismogram depicted in red and measured pore pressure of the Arbuckle depicted in purple (recreated from Watney et al., 2016). The pressure transducer located within the well at Wellington field was located in the Arbuckle at a depth of 1524 m (5030 ft), which is 30 m above the crystalline basement.

Chapter 3: Methods

Section 3.1: Data Acquisition

This work analyzes the pressure data collected at Wellington field that was used in the study of the Pawnee earthquake pressure response by Watney et al. (2016). Wellington Field lies between Wichita, KS and the Kansas-Oklahoma border in south central Kansas (Figure 3.1.1). Temperature and pressure were monitored downhole in the lower Arbuckle from April 2016 to August 2017. These datasets were collected at KGS well #1-28 at a depth of 1524 m (5030 ft), approximately 30 meters above the crystalline basement. A Badger LT downhole long term pressure recorder collected data at 1 sample per second continuously for a year and a half. The sensor had a resolution of ±0.018 psig and < 0.001 ℃ (Calscan Solutions). Seismicity data was collected by a local seismometer array, ran by the University of Kansas, and a regional array ran by the U.S. Geological Survey National Earthquake Information Center catalog (see Data and Resources; Figure 3.1.1). Seismic stations located at Wellington Field surround the well monitoring pressure and temperature continuously (Figure 3.1.1).

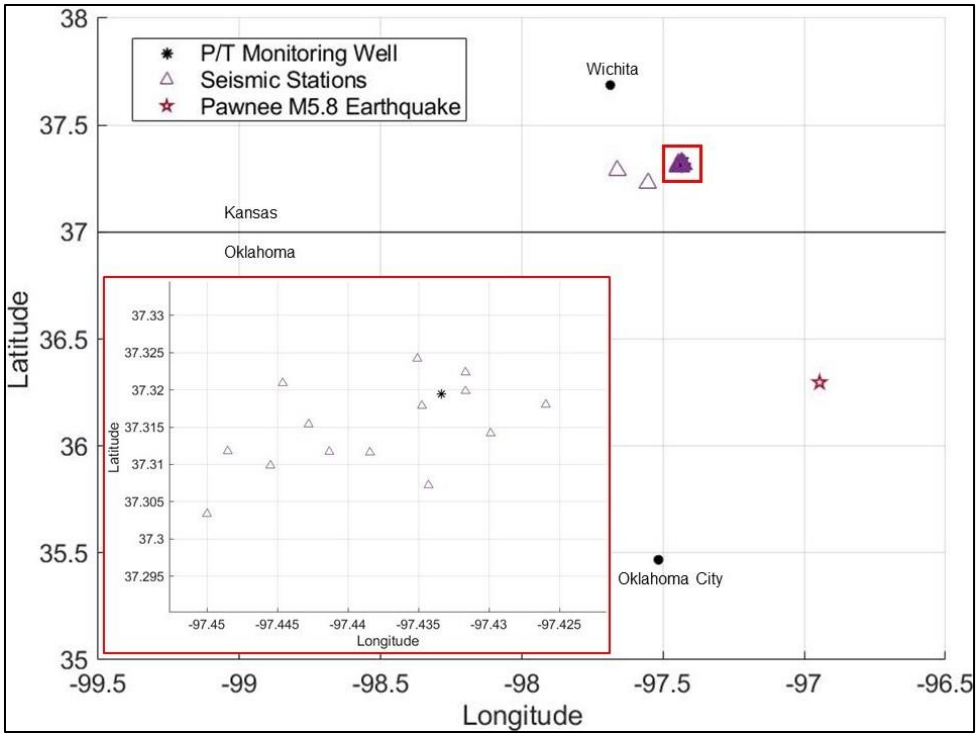

Figure 3.1.1: Map showing the geographic location of the seismic stations (purple triangles), the Pressure/Temperature monitoring well (black star), and the location of the Pawnee Earthquake (red star). The location of the Kansas-Oklahoma Border, Wichita, and Oklahoma City are also denoted for clarification of the field site location.

There were more than 16 seismic stations recording seismicity at Wellington Field during 2016 and 2017. The closest seismometer is 0.16 km away from the pressure monitoring well and the farthest seismometer is 19.6 km away from the well. The magnitude of completeness for the local seismometer array is a magnitude 1 earthquake. Earthquake data is recorded at a rate of 200 samples per second. Pressure and seismic data collected from Wellington Field were used in this research to determine whether small magnitude, anthropogenic earthquakes induce pore pressure changes in the subsurface.

Section 3.2: Data Processing

The pressure and temperature data are publicly available on the Kansas Geological Survey's website (see Data and Resources). The first step to processing this data was to combine the individual week-long files into one large dataset that consisted of a year and half of continuous pressure and temperature measurements. They were combined into one large dataset using MATLAB. After combining all the files, the pressure data was filtered to remove solar and tidal pressures and high frequency noise.

The pressure time series was initially filtered to remove solar and lunar tidal pressures which introduce water level variations in open wells (Victorine, 2016). Tidal pressures were calculated using equation 1 (Bredehoeft, 1967).

$$W_b = 0.75 * \left(\frac{GM_b}{D_b}\right)\left(\frac{a}{D_b}\right)^2 \left\{\left(\frac{(3\cos(2\lambda_b)-1)(3\cos(2\lambda_e)-1)}{12}\right) + \sin(2\lambda_b) + \sin(2\lambda_e)\right) * \cos(\omega t - \varphi_b - \varphi_w - \varphi_{corr}) + \cos^2(\lambda_b) * \cos^2(\lambda_e) * \cos[2(\omega t - \varphi_b - \varphi_w - \varphi_{corr})]\} \quad \text{(Eqn. 1)}$$

where W_b is the generating potential of the body, G is the gravitational constant (6.67408x10^{-11} m^3/kg*sec^2), M_b is the mass of the body, D_b is the distance between the earth and the body as it varies with time, a is the Earth's radius, λ_b is the latitude of the body, λ_e latitude of Wellington KGS 1-28, ω is the frequency of Earth's rotation, φ_b is the longitude of the body, φ_w is the longitude of Wellington KGS 1-28, and φ_{corr} is the correction angle due to the "starting time" of the pressure data file. Equation 1 contains the long-term cycle, the diurnal cycle, and the semi-diurnal cycle. The two bodies that affect the tidal pressure are the sun and the moon. This equation is calculated for both solar and then lunar tides. After finding each component, the two are summed to equal the total generating potential. The total generating potential can be related back to the pressure from tidal influence (Eqn. 2) (Bredehoeft, 1967).

$$P = \left(\frac{0.49}{a}\right)\left(\frac{W}{g}\right)(C_w\varphi) \qquad \text{(Eqn. 2)}$$

where P is the tidal pressure, a is the Earth's radius, W is the total generating potential, g is the acceleration due to gravity, C_w is the compressibility of water, and φ is the porosity of the aquifer. At Wellington KGS 1-28 in the Arbuckle, C_w was found to be about 0.4437 1/GPa and φ was around 0.13 [-] (Victorine, 2016). After calculating the tidal pressure, it was then subtracted from the raw pressure data. This removed the solar and lunar tidal pressures from the raw pressure data (Figure 3.2.1).

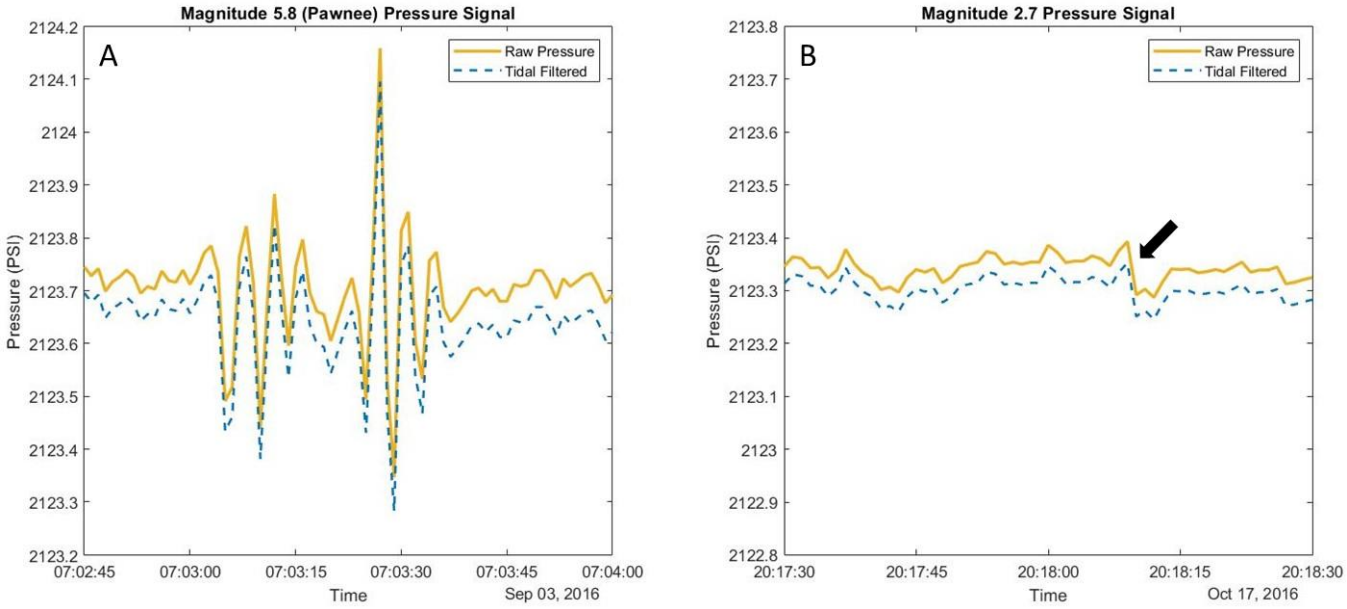

Figure 3.2.1: Overlay of raw and processed pressure data. A) The pressure signal from the 2016 M 5.8 Pawnee earthquake. B) The pressure signal corresponds to a magnitude 2.7 earthquake detected by the seismometers and identified in the pressure data. The location of the event is denoted by a black arrow. This signal denotes the noise level at the station and what a potential small magnitude earthquake signal may look like. Yellow denotes the raw pressure and the blue dashed line is the tidal filtered pressure.

A lowpass infinite impulse response (IIR) filter with an order of 1, a passband frequency of 0.4 Hz, a passband ripple of 0.2 dB, and a sample rate of 1 was originally applied to the data in an effort to remove high frequency noise possibly present in the data. It was not used due to there being little difference between the tidal filtered pressure and the lowpass filtered pressure. Furthermore, applying the filter would have further reduced the frequency of the pressure data, which was already lower in frequency than the earthquake data. Barometric Pressure was not removed from the pressure due to the exact height of the water column above the pressure sensor being unknown. Pressure changes due to barometric pressure are correlated over regional scales at periods of days or weeks (Barbour et al., 2019). The pressure changes of interest in this project will be at local scales over time periods of seconds to minutes. Therefore, the tidal filter described above is the only filter applied to the pressure data in the following analysis.

To compare the filtered pressure data to earthquake data, the derivative of the tidal filtered pressure was taken (Figure 3.2.2). This creates a pseudo sinusoidal pressure waveform that contains both positive and negative values and can be treated as an earthquake signal as described in the next section. The derivative of the pressure denotes the change in the pressure with time, which could accentuate subtle changes in pore fluid pressure resulting from the passage of earthquake waves. The sparsely sampled pressure data (1 Hz) is oversampled by two and then by four (Figure 3.2.2). This artificially increases the sampling rate of the data to facilitate comparison to the higher sampled earthquake data (200 Hz) and to allow use of an automated earthquake waveform picking utility (STA/LTA) described in the next section. By oversampling the pressure by four it increases the sampling rate of the data to four samples per second. Past studies have commonly collected pressure data at a maximum rate of one sample every 30 seconds (Kroll et al., 2017) to a minimum rate of one sample every 15 minutes (Quilty

and Roeloffs, 1997). Most commercially available pressure sensors do not collect data at rates higher than one sample per second.

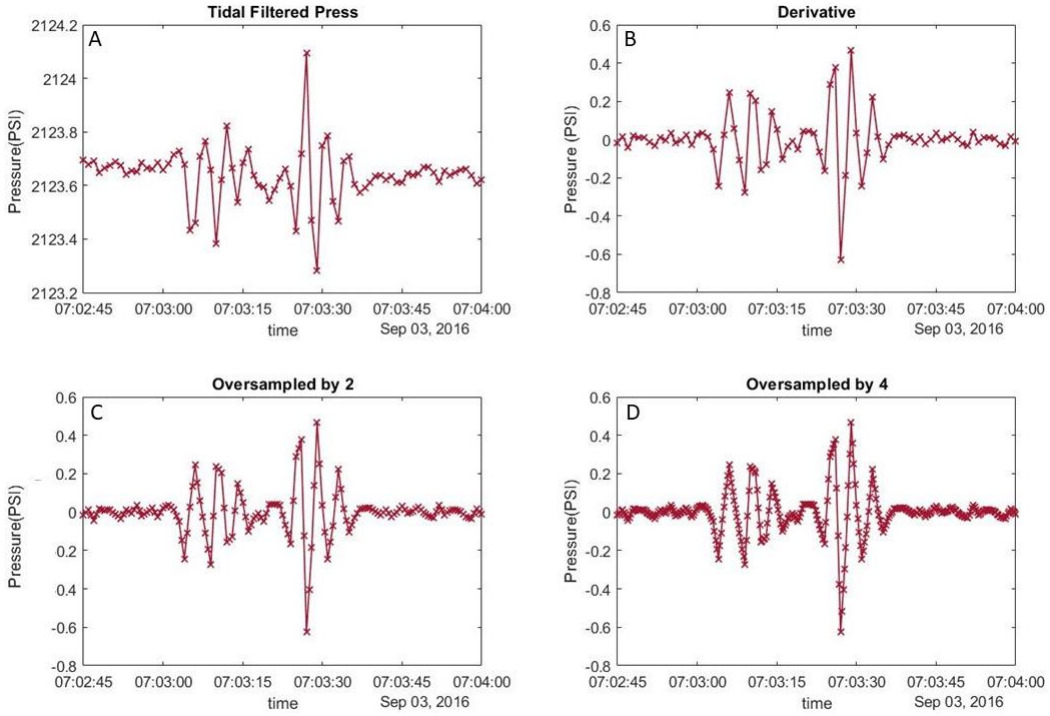

Figure 3.2.2: Pawnee earthquake (M 5.8) pressure data. A) Tidal filtered pressure data. Sample locations are denoted by the x's on each of the line plots. B) Derivative of filtered pressure data. C) Derivative data oversampled by 2. D) Derivative data oversampled by 4.

Section 3.3: Automated Detection of Pressure Signals (STA/LTA)

The pressure changes related to small magnitude (< 3), local, induced earthquakes are expected to be subtle and challenging to detect (e.g. Figure 3.2.1B). To overcome this challenge and to automate the detection of anomalous pressure signals potentially associated with earthquakes, the oversampled pressure data was ran through a short-time-average/long-time average trigger (STA/LTA) algorithm. STA/LTA trigger algorithms are commonly used in weak-motion seismology (Trnkoczy, 1999) for automated detection of earthquakes (Figure

3.3.1). The STA/LTA algorithm uses two sequential moving time windows to continuously calculate the average amplitude of a seismic signal (Trnkoczy, 1999). The LTA establishes the background amplitude level by capturing primarily ambient site noise and instrumentation noise at the site (Trnkoczy, 1999). The STA captures short duration amplitude windows which are influenced by the presence of short duration seismic events. When the ratio (STA/LTA) exceeds a pre-set threshold value, an event is identified (Trnkoczy, 1999).

Changing the STA window length can guide the algorithm to detect local vs. more distant events (Trnkoczy, 1999). Having a smaller STA value makes the trigger more sensitive to localized noise (e.g. thunder), but also increases the ability to detect the shorter lasting local earthquakes. A typical STA time window for regional events is one to two seconds, while a shorter STA value of 0.5 seconds is common for local events (Trnkoczy, 1999). Earthquake data at Wellington Field commonly uses STA values that range between one to three seconds and the LTA values range between 10 to 20 seconds due to the noise level at the field. When building a trigger algorithm, LTA windows should be long enough so that their duration is greater than the typical noise fluctuations (Trnkoczy, 1999). Long duration LTA windows increases the algorithms sensitivity to emergent earthquakes (e.g. earthquakes that have gradual changes in amplitude at the onset of the P wave as wave energy builds up over time), while reducing the window length decreases the trigger sensitivity to these events (Trnkoczy, 1999).

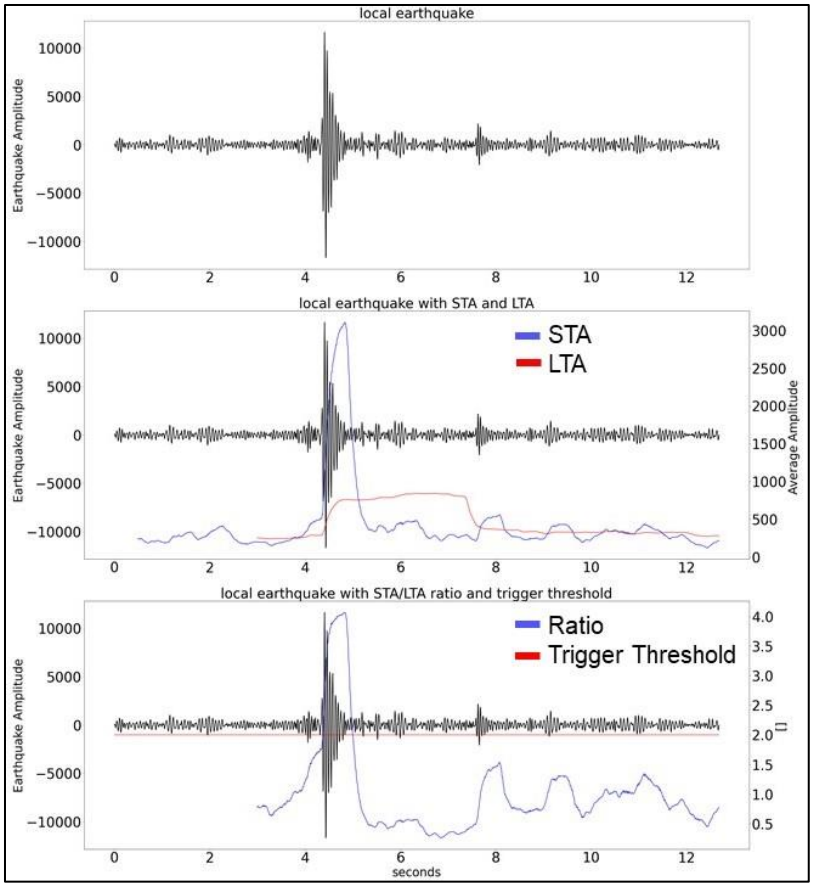

Figure 3.3.1: An example of how the STA/LTA algorithm is used on raw earthquake data to detect events. This figure shows STA/LTA results using earthquake data from a magnitude 1.0 earthquake. The top panel shows the raw earthquake data in black with the earthquake arriving at around 4 seconds. The middle panel shows the earthquake in black, the short term average (STA) in blue and the long term average (LTA) in red. The bottom panel has the ratio of the STA/LTA in blue, the trigger threshold in red, and the earthquake in black.

Here, I run an STA/LTA trigger algorithm on the derivative of the pressure data to test if pressure changes associated with earthquakes can be detected. This algorithm is a simplified version of the STA/LTA algorithm that is used on the earthquake data at Wellington field. It is a simplified version since the STA/LTA algorithm used for the pressure data has a set trigger threshold equal to 3. If the ratio of the STA divided by the LTA exceeds the trigger threshold of

3 then a trigger occurs. A trigger threshold of 3 was chosen due to it being low enough to detect earthquakes but high enough that there were less false triggers due to noise. STA values of 4, 6, 8, 12, 14, and 16 data samples (corresponding to 1, 1.5, 2, 3, 3.5 and 4 second time windows respectively) were tested to evaluate the effectiveness of the trigger algorithm. Lower STA values led to a large number of triggers, since the short window was only averaging over a few points of pressure data. This caused false triggers associated with noise compared to possible earthquake signals. Increasing the STA values to 14 and 16 decreased the number of triggers drastically. The longer STA window was successful in removing noise, but it also removed possible earthquake signals when compared to earthquakes identified in the seismograms. Using an STA value of 8 and 12 samples removed a significant portion of the noise triggers, while keeping potential earthquake signals. LTA values of 100 and 500 were also evaluated. The longer LTA window proved less sensitive to random noise in the data.

The entire filtered pressure derivative data was run through the STA/LTA, using STA values of 8 and 12 samples along with an LTA value of 500 samples. These values correspond to STA windows of 2 and 3 seconds in the pressure data. While oversampling the pressure data artificially increased the sampling rate, this rate is still much lower than the rate at which earthquake data is collected. The STA and LTA values and corresponding time windows used in the pressure data analysis are consistent with the times windows used to detect earthquakes automatically at Wellington Field. Using STA values of 8 and 12 samples ensures that a trigger only occurs when there is at least two points in the original pressure (not oversampled) data that relate to a pressure change. This reduces the number of false triggers related to noise. With these parameters, the full pressure dataset was analyzed by the STA/LTA trigger algorithm with the goal of noting coseismic pressure changes related to earthquake events. An example of the

automated detection trigger algorithm, with an STA of 8 and 12 samples and an LTA of 500 samples, used on the pressure data can be seen in Figure 3.3.2. This figure demonstrates how the STA/LTA algorithm detected pressure changes related to a magnitude 2.0 earthquake that occurred on December 23rd, 2016 (Figure 3.3.2).

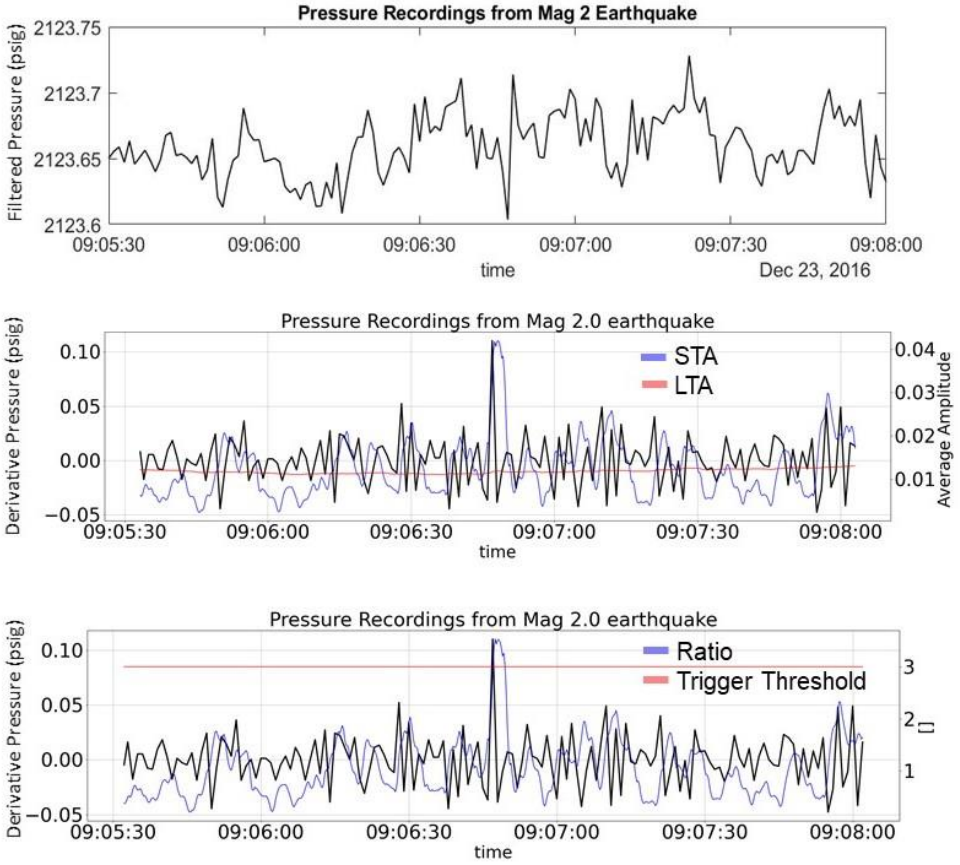

Figure 3.3.2: STA/LTA results using the pressure data from a magnitude 2.0 earthquake on December 23rd, 2016 at 09:05:06. This earthquake was located 11 km from the pressure monitoring station. The top panel shows the tidal filtered pressure data in black at the time of the event. The middle panel shows the derivative of the pressure in black, the short term average (STA) in blue and the long term average (LTA) in red. The bottom panel has the ratio of the STA/LTA in blue, the trigger threshold in red, and the derivative of the pressure in black.

Section 3.4: Time Drift Correction

Pressure sensors used in boreholes commonly exhibit time drift during periods of deployment. During the initial six months of deployment of the downhole pressure sensor at Wellington, there was no regular time drift calibration performed in the field because the intent was to monitor long-term (10s of minutes to hours resolution) of Arbuckle aquifer pore pressure changes. After noting what appeared as the Pawnee earthquake signal in the pressure data, it became apparent that time-stamps in pressure observations needed to be as accurate as possible. Therefore, after the September 2016 Pawnee earthquake, the time clock of the pressure sensor at Wellington Field was reset every two weeks to the correct time. The timing of the sensor clock reset can be seen in the raw pressure files at two-week increments as a jump forward or backward in time. When comparing pressure sensor recordings to seismometer recordings it is important to consider time drift between the instruments. Seismographs use GPS clocks to continuously time-stamp recordings to the actual time. Due to the pressure sensor experiencing time drift, the drift in time must be accounted for between the bi-weekly manual clock resets.

The pressure data collected before September 2016 cannot be used in this analysis due to the lack of time corrections resulting in large uncertainty in time (up to hours). This makes the data collected before September unsuitable for identifying specific earthquakes, since the difference in the time between the pressure and the earthquake data is unknown. To recalibrate the pressure sensor clock the instrument is pulled up from the well to the surface and time is reset manually. This leads to some inherent operator error being associated with the time recalibration. The first step to identifying the sensor time reset is to note the significant and abrupt time changes that occur during the recalibrations. These time changes are obvious within the data since they occur in two-week increments. It also is a significant adjustment in time of usually 6

to 10 minutes. The time difference is either ahead in time or behind in time depending on the specific recalibration. There were 21 obvious “jumps” in time from September 2016 to August 2017. The instrument on average exhibited a time drift of 6 minutes in time over each two-week period.

After noting the changes in time in the data files, it was assumed that the time drift would increase or decrease linearly over the two-week period. Figure 3.4.1 shows examples of the instrument time drift from March 2017 to May 2017. The time drift varies from being ten minutes ahead to 9 minutes behind during these months.

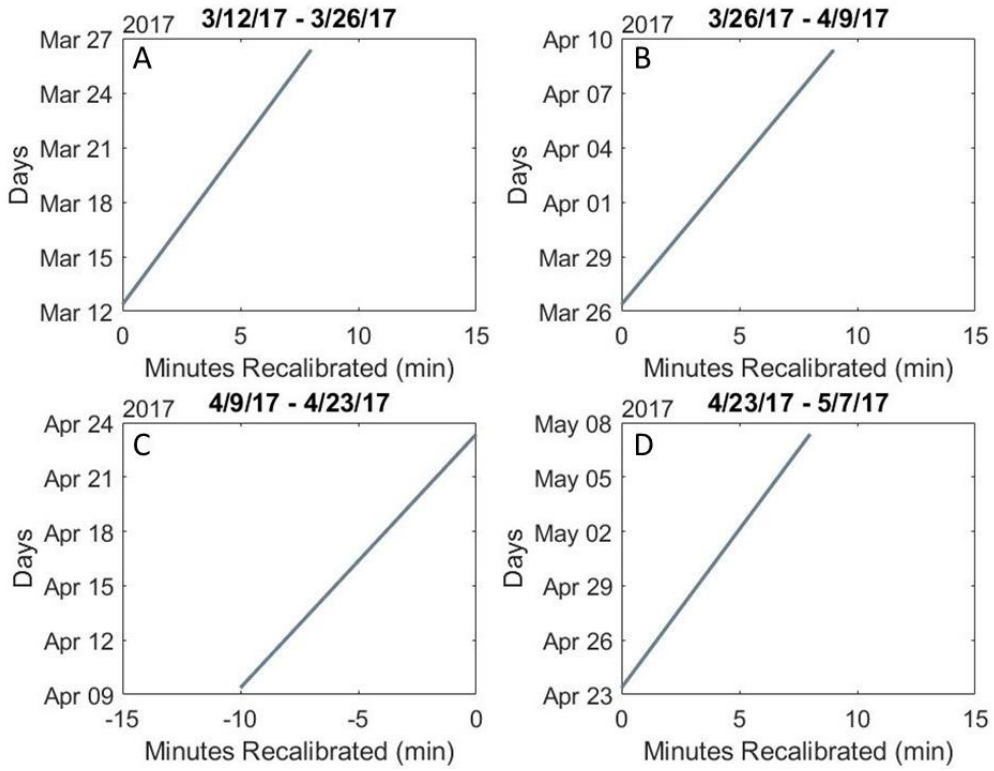

Figure 3.4.1: Time drift of pressure sensor at four recalibration points. A) Time drift from March 12th to March 26th where the pressure sensor was behind by 8 minutes. B) Instrument time drift from March 26th to April 9th. The pressure sensor was 9 minutes behind in time at the point of recalibration. C) Time drift from April 9th to April 23rd.

The pressure sensor time was 10 minutes ahead of real time when recalibrated. D) Time drift from April 23rd to May 7th where the time is 8 minutes behind real time.

Assuming linear time drift and correction of pressure data, the time difference between earthquakes and pressure triggers was within seconds of one another. It is important to note that it is unknown how the time resets were done in the field, and it was assumed that the pressure sensor clock would be set to the nearest minute in real time. Therefore, triggers in the pressure data that were a minute before and/or after an earthquake event were considered. Taking time drift into consideration made it possible to find potential earthquake signals within the pressure data.

Section 3.5: Interpretation of Earthquakes

The results of the pressure change analysis using the STA/LTA algorithm with the time drift correction were examined and related to all earthquakes detected by the seismic network from September 1st, 2016 to August 27th, 2017. Pressure recordings were collected during a time window of ±1.5 minutes around the time that the earthquake had occurred. A minimum and maximum pressure derivative value was recorded for each of the earthquakes in the catalog. This allowed for comparison later in the analysis between earthquakes that corresponded to an identifiable STA/LTA pressure trigger (referred as “detected earthquakes”) and those that were not detected by the STA/LTA pressure analysis.

In addition to earthquake magnitude and location and its relation to detected or not-detected pressure events, the earthquake waveform character was categorized as impulsive versus emergent (Figure 3.5.1). Impulsive vs. emergent is commonly used to classify the

characteristics of the wave onset for a given waveform (Bormann et al., 2002). An event is impulsive when the leading edge (or onset) of the wave arrival is steep and has large changes in amplitude (Bormann et al., 2002). Emergent waves are associated with more gradual changes in amplitude at the onset of the P wave as wave energy builds up over time. Figure 3.5.1 depicts the difference between an earthquake that is emergent versus impulsive. The Pawnee earthquake (M 5.8) is categorized as impulsive, while the Cushing earthquake (M 5.0) is categorized as emergent (Figure 3.5.1).

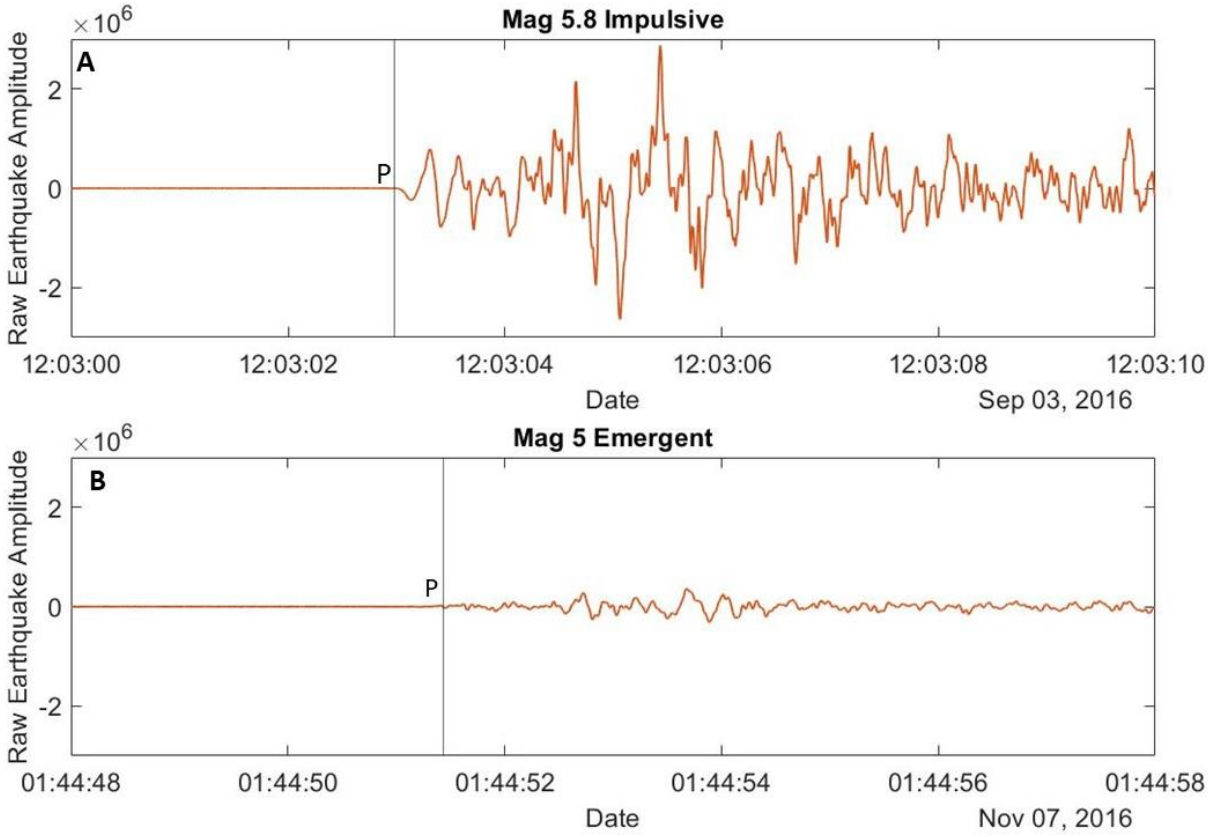

Figure 3.5.1: Impulsiveness comparison for two magnitude 5 earthquakes recorded at the Wellington network. A) Raw earthquake amplitude versus time of the Pawnee earthquake (M 5.8) on September 3, 2016. This event is classified as impulsive based on the large changes in amplitude at the P wave onset (Bormann et al., 2002). B) Raw earthquake amplitude versus time for the Cushing earthquake (M 5.0) on November 7th, 2016. This is classified as an emergent event due to the gradual increase in amplitude after the P wave onset (Bormann et al., 2002).

Past studies have commonly defined waveforms as impulsive versus emergent based on visual observation, without any quantitative measure. These studies have used the level of noise before the onset of the P wave arrival and the arrival of the P wave to qualitatively characterize impulsiveness. This determination is heavily dependent on the level of noise at the seismic station. Based on site conditions an event could look impulsive at some stations and emergent at others. This would be solely due to the background noise level at the station analyzed. A quantitative way to determine the impulsiveness of an earthquake was needed. It was noted that events that appeared impulsive had large changes in amplitude at the onset of the P wave that were followed by a sharp decrease in amplitude (Figure 3.5.2). Emergent events commonly had a smaller change in amplitude at the onset of the P wave followed by constant amplitude or gentler increase as the time progresses (Figure 3.5.2). Based on observations in the Wellington earthquake catalogue, it appears that by calculating the sum of the energy at the onset of the P wave and comparing it to the average sum of the energy in the cycles following the P wave it is possible to quantify impulsiveness. In this calculation, the sum of the first cycle is used right after the onset of the P wave and then it is directly compared to the average sum of the energy from the four cycles after the P wave. This process directly compares the first wave cycle directly after the onset of the P wave to a cycle that occurs later in time after the P wave arrival. Impulsive events should have higher calculated energy than emergent events when comparing the first cycle of the waveform to subsequent cycles (Figure 3.5.2).

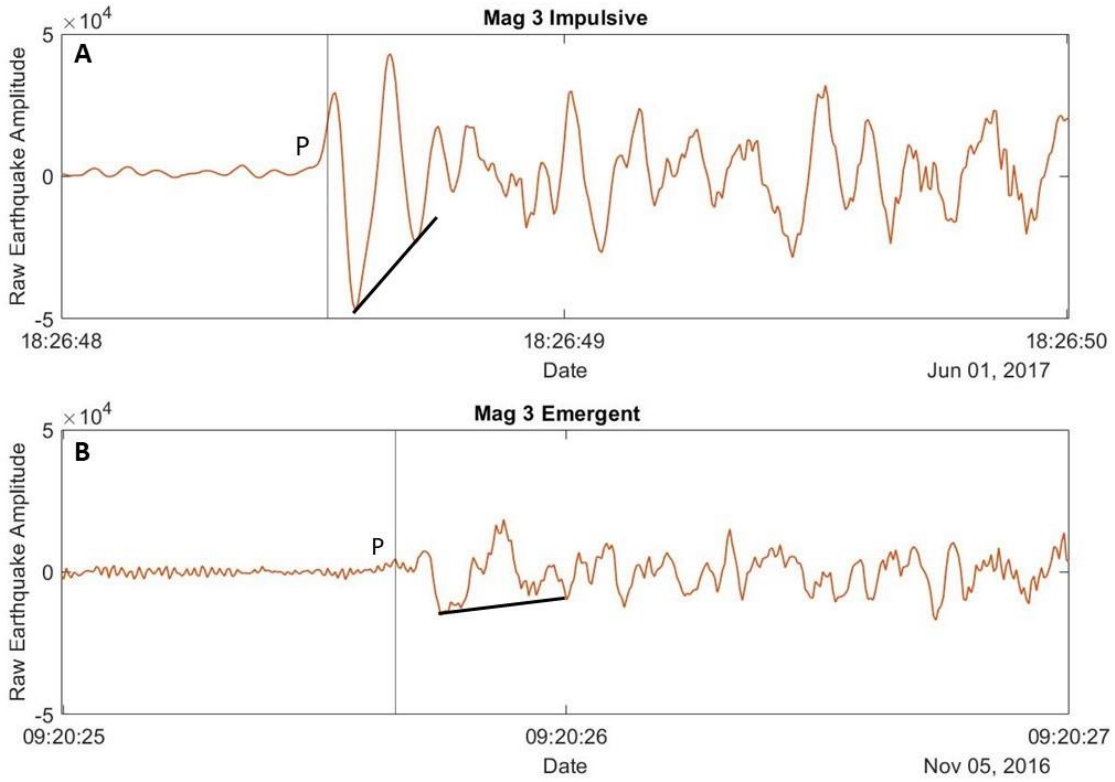

Figure 3.5.2: Impulsiveness characterization of waveforms. Plots show raw earthquake amplitude versus time for two magnitude 3 earthquakes. A) This magnitude 3 would be considered impulsive since there is a large change in amplitude at the onset of the P wave and then the amplitude decreases. The black line denotes the slope of amplitude change from the initial offset of the P wave to the cycles following. B) This event would be considered an emergent event, since at the onset of the P wave there is a small change in amplitude which stays relatively constant and does not decline rapidly in the cycles after the P wave. The black line denotes the slope of amplitude change from the initial P wave offset to the cycles following. The slope of the emergent event amplitude change is significantly less steep than the slope of the impulsive event.

Before conducting the waveform analysis to determine impulsiveness of the earthquakes, some processing steps were applied to the earthquake waveforms. Initially, the arrival of the P-wave and S-wave were determined for each event. The frequency of each earthquake was also determined. The earthquake data was then demeaned and a lowpass filter of 0.01 Hz to 10 Hz was applied. This filter is consistent with filters used in Seisan, which is a program that aids in

the analysis of earthquake data (Ottemöller et al., 2013). The envelope of the earthquakes was then calculated using the Hilbert transform (Figure 3.5.3; Eqn. 3).

$$F(t) = f(t) + jf^*(t) = A(t)e^{j\theta(t)} \quad \text{(Eqn. 3)}$$

$F(t)$ is the complex trace, $f(t)$ is the real seismic trace, $f^*(t)$ is the imaginary component of the seismic trace, $A(t)$ is the magnitude of the complex trace which is a measure of the energy in the waveform, and $\theta(t)$ is the instantaneous phase (Taner et al., 1979). The envelope provides information with regards to the signal strength, and it represents the time-dependent amplitude of the waveform (Figure 3.5.3; Taner et al., 1979). Figure 3.5.3 shows an example of the envelope calculation using the Hilbert transform and the complex trace equation.

Initially, the maximum value of the envelope was determined for each earthquake. Then it was decided that this was not an accurate representation of the impulsiveness. The sum of the energy was then calculated starting at the onset of the P wave and S wave. The energy was calculated by using the arrival times of the P and S waves and the frequency of the earthquake. A cycle after the wave arrivals was used to find the energy of the initial wave onset (Figure 3.5.3). Then the average energy from the next four cycles after the first cycle was calculated (Figure 3.5.3). The number of cycles used to calculate the energy was chosen to avoid the risk of calculating too far past the onset of P and S wave. Calculating the energy over too long of a time duration would lead to inaccuracies when determining the impulsiveness of an earthquake, due to impulsiveness being solely related to the wave onset. After calculating the energy at both locations along the waveform, the energy of the first cycle was divided by the average energy of the following four cycles (Figure 3.5.3).

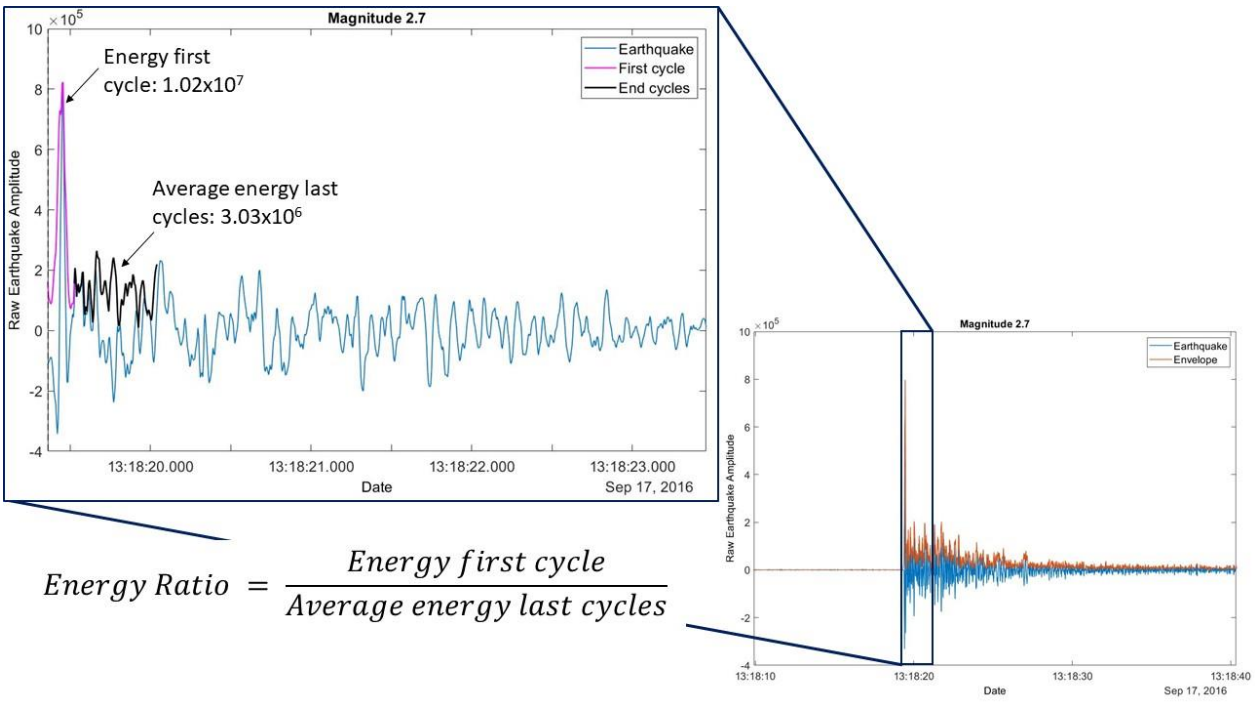

Figure 3.5.3: Energy calculation to determine impulsiveness. The plot to the right depicts the raw earthquake amplitude in blue and the calculated Hilbert envelope in orange. A small window of the waveform is taken right after the onset of the P wave arrival (dark blue box). The dark blue figure outlined to the left is a zoomed in image of the waveform. The dashed black line depicts the onset of the P wave arrival. The pink line depicts the first cycle of the Hilbert envelope after the P wave arrival. The earthquake amplitude is summed over the first cycle, which leads to the energy of the first cycle being 1.02x10^7 for this magnitude 2.7 event. The black line depicts the Hilbert envelope of the last four cycles after the first cycle. The raw earthquake amplitude is summed over the last four cycles and then divided by 4. This gives the average energy of the last cycles, which was 3.03x10^6 for this magnitude 2.7 event. Then the energy of the first cycle is divided by the energy of the last cycles, which yields an energy ratio of 3.36 for this event at this specific station. The energy ratios from all seismic network stations that recorded the event are then averaged to yield an average energy ratio for the earthquake.

A higher energy ratio was determined to be impulsive while a lower energy ratio was determined to be emergent. A threshold of 2 for the energy ratio was used to determine whether the P-wave arrival was impulsive versus emergent. Figure 3.5.4 shows an example of an

emergent event calculation. Ratios above 2 would be classified as impulsive, while ratios below 2 were emergent.

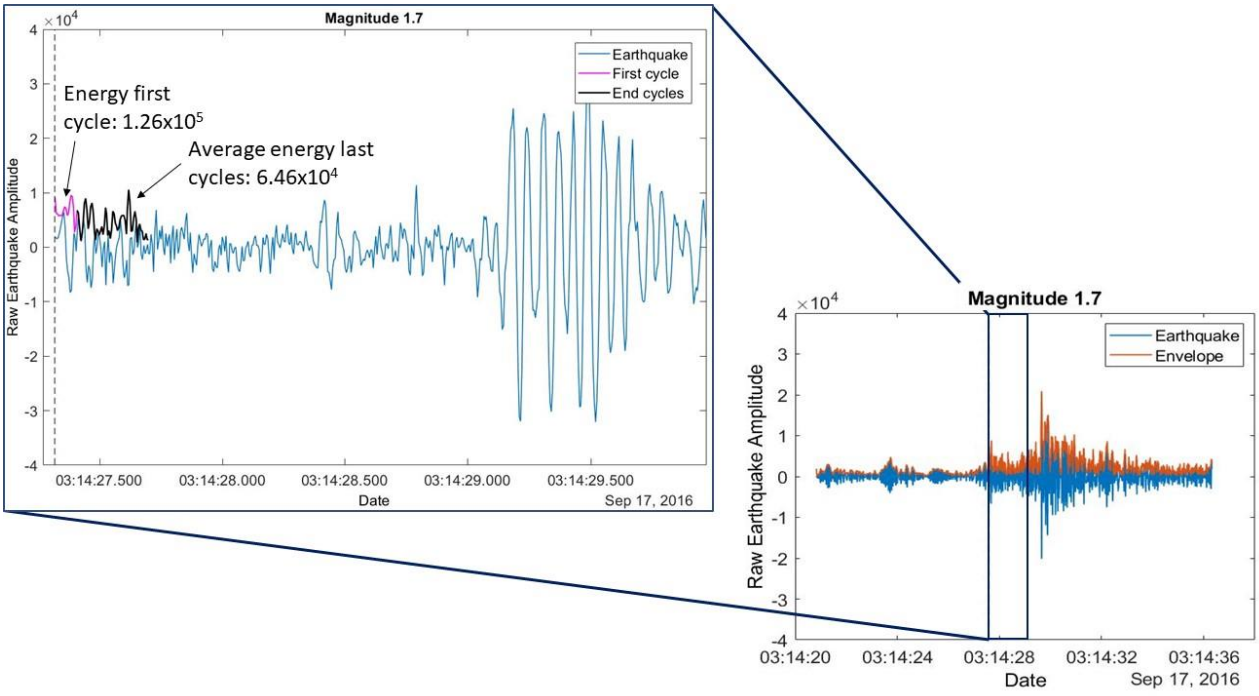

Figure 3.5.4: Energy calculation of emergent event. The plot to the right depicts the raw earthquake amplitude in blue and the calculated Hilbert envelope in orange. A small window of the waveform is taken right after the onset of the P wave arrival (dark blue box). The dark blue figure outlined to the left is a zoomed in image of the waveform. The dashed black line depicts the onset of the P wave arrival. The pink line depicts the first cycle of the Hilbert envelope after the P wave arrival. The earthquake amplitude is summed over the first cycle, which leads to the energy of the first cycle being $1.26x10^5$ for this magnitude 1.7 event. The black line depicts the Hilbert envelope of the last four cycles after the first cycle. The raw earthquake amplitude is summed over the last four cycles and then divided by 4. This gives the average energy of the last cycles to be $6.46x10^4$. Then the energy of the first cycle is divided by the energy of the last cycles, which yields an energy ratio of 1.82 for this event at this specific station. The energy ratios from all stations that recorded the event are then averaged to yield an average energy ratio for the earthquake.

This ratio was chosen based on visual inspection of each earthquake of interest and the definition

of what differentiated an impulsive event versus an emergent event. An energy ratio of 1.5 was used to determine the impulsiveness of the S-wave arrival. Energy ratios calculated from the S-wave arrivals commonly had higher energy ratios. Visual inspection of each earthquake event led to the energy ratio of 1.5 or greater to be chosen for impulsive S wave events (Figure 3.5.5).

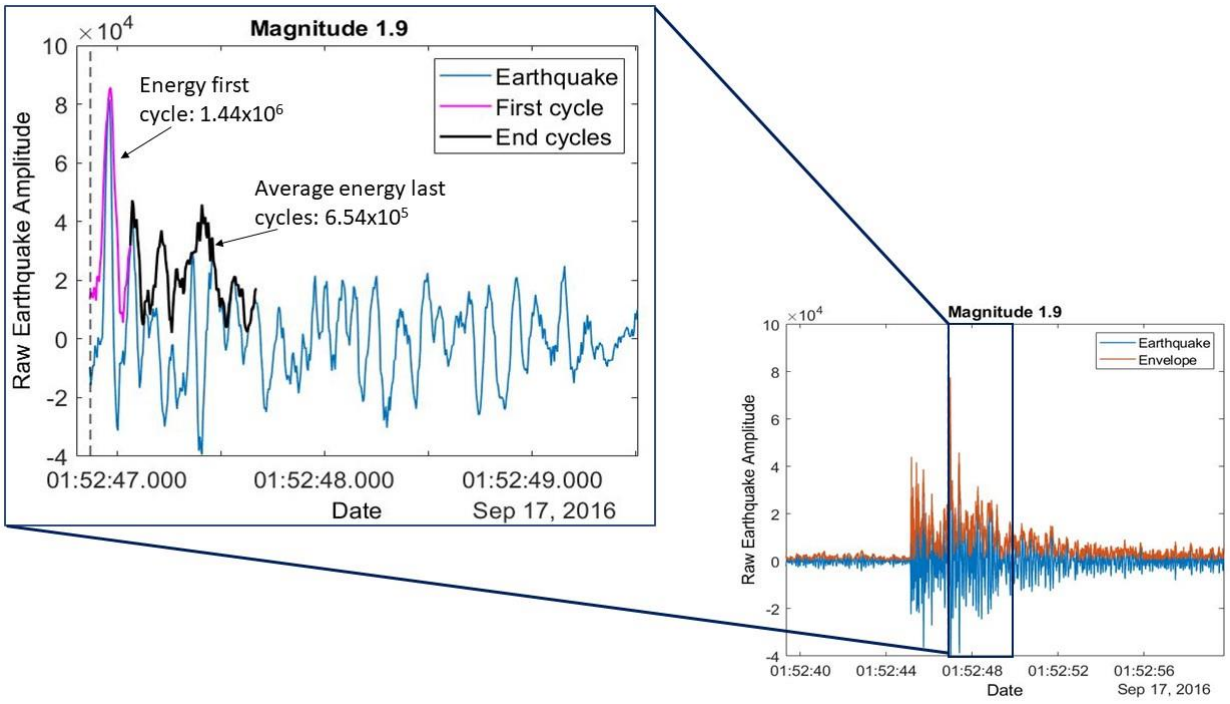

Figure 3.5.5: Energy calculation of an S wave impulsive event. The plot to the right depicts the raw earthquake amplitude in blue and the calculated Hilbert envelope in orange. A small window of the waveform is taken right after the onset of the S wave arrival (dark blue box). The dark blue figure outlined to the left is a zoomed in image of the waveform. The dashed black line depicts the onset of the S wave arrival. The pink line depicts the first cycle of the Hilbert envelope after the S wave arrival. The earthquake amplitude is summed over the first cycle, which leads to the energy of the first cycle being $1.44x10^6$ for this magnitude 1.9 event. The black line depicts the Hilbert envelope of the last four cycles after the first cycle. The raw earthquake amplitude is summed over the last four cycles and then divided by 4. This gives the average energy of the last cycles to be $6.54x10^5$. Then the energy of the first cycle is divided by the energy of the last cycles, which yields an energy ratio of 2.58 for this event at this specific station. The energy ratios from all stations that recorded the event are then averaged to yield an average energy ratio for the earthquake.

Stations that detected an earthquake could have variations in the impulsiveness for a single event. For example, one station could have the P wave arrival being emergent while another could classify the P wave arrival being impulsive. To account for this variation, the impulsiveness was analyzed from the station that was the closest to the pressure monitoring well. Analyzing the closest station to the well helps provide consistency for the impulsiveness results. The results from the impulsiveness analysis can be seen in section 4.3.2.

Chapter 4: Results

Section 4.1: STA/LTA Detection of Pressure Signals

From September 2016 to August 2017 there were a total of 1,373 earthquakes detected by the seismic stations at Wellington Field (Nolte, 2020). These earthquakes ranged in magnitude from 0.5 to 5.8 and their distances from the pressure station ranged from 0.55 km to 180 km. From the full catalog of interest 20 events were magnitude 0-1, 1035 were magnitude 1-2, 278 were magnitude 2-3, 35 were magnitude 3-4, and 5 were magnitude 4-6. Out of 1,373 earthquakes a total of 279 events were detected in the pressure data by the STA/LTA method described above. When using STA values of 8 and 12 samples, there were 69 common earthquake detections. In addition, 10 new events were detected with the STA of 12 samples and another 200 were detected with the STA of 8 samples. 87% of earthquakes detected using an STA of 12 samples were also detected when using an STA of 8 samples. Changes of the derivative of pressure that related to earthquakes ranged from +/- 0.01 psig for the smallest earthquakes up to +/- 0.6 psig for the largest earthquakes. Pressure measurements at the time of the earthquakes varied from 2123.13 psig to 2414.374 psig. The change in true pressure varied from +/- 0.038 psig to +/- 0.8 psig. Average rates of pressure, measured down well at Wellington Field from April 2016 to August 2017, showed an increasing rate of ~5 to 7 psig/year (Nolte et al., 2017). An example comparing the signal from the Pawnee earthquake and a potential magnitude 2 event can be seen in Figure 4.1.1. The Pawnee earthquake had a change in pressure that was 10 times greater than the smaller magnitude event (Figure 4.1.1). It is expected that small magnitude earthquakes would relate to small coseismic pressure changes, while larger magnitude earthquakes would be related to larger coseismic pressure changes.

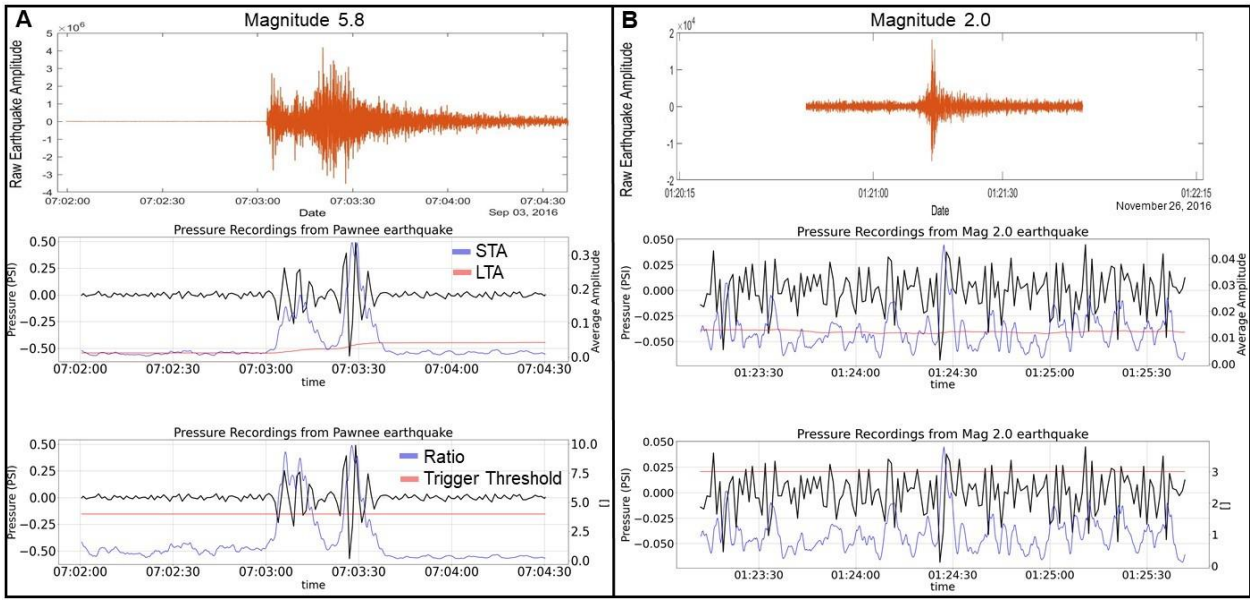

Figure 4.1.1: A) STA/LTA results from the Pawnee Earthquake (M 5.8) located 120 km from the pressure station. Note the change in pressure varied from -0.5 psig to 0.5 psig. B) STA/LTA results from a magnitude 2.0 earthquake, that was 27 km away from the pressure station. The change in pressure varied from -0.05 psig to 0.05 psig. The top panel shows the vertical channel of the earthquake seismogram. The middle panel shows the derivative of the pressure in black, the short term average (STA) in blue and the long term average (LTA) in red. The bottom panel has the ratio of the STA/LTA in blue, the trigger threshold in red, and the derivative of the pressure in black.

The earthquakes detected in the pressure data ranged in magnitude from 0.8 to 5.8. Their distance from the pressure station varied from 0.85 km to 150 km (Figure 4.1.2). The location of all the events in comparison to the pressure station can be seen in Figure 4.1.2.

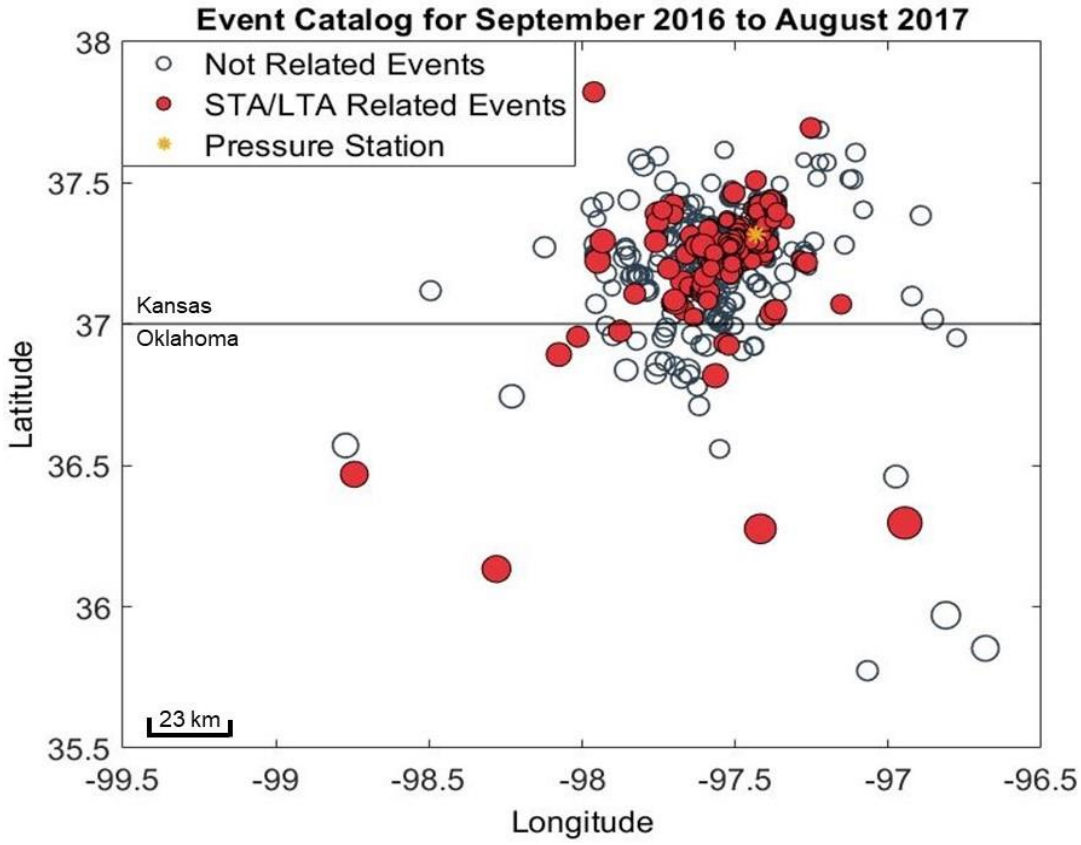

Figure 4.1.2: Location of 1,373 events obtained from the Wellington earthquake catalog (from Nolte, 2020). The size of the circles relates to the magnitude of the event. The larger the magnitude, the greater the size of the circle. The blue open circles are earthquakes that were not related to pressure changes. The orange filled circles are earthquakes that were related to pressure changes when using the STA/LTA method. The pressure station is denoted by the yellow star. Many of the earthquakes in the catalog are located to the south-west of the pressure station.

Section 4.2: Validation of STA/LTA Method

After interpreting the initial results, it was important to understand how noise within the pressure data effects the STA/LTA trigger algorithm. Noise in the pressure could potentially trigger the STA/LTA algorithm when there are no actual earthquake signals. These false triggers, which are related to the background noise of the pressure transducer, could also occur at the time of an earthquake. To determine whether the STA/LTA was differentiating noise versus signal, a

better understanding of the background noise level was required to build confidence in the results described above. False triggers were extremely common when using short STA/LTA windows. When using an STA of 8 samples (i.e. only 2 original measurements of pressure) there were commonly ~8,000 triggers per month. An STA of 12 samples commonly generated ~3,000 triggers per month. Many of these triggers were related to background noise in the pressure data. It is important to note that seismologists are aware that the STA/LTA method commonly generates many false triggers and visual inspection of each trigger is used to ensure that the false triggers are removed, and the earthquake data is kept. As a common practice, it is preferable to produce false triggers and reject them manually than to miss actual earthquakes by using conservative STA/LTA parameters.

To better understand the level of noise in the pressure recordings, false triggers from the STA/LTA method were examined. The false triggers used were chosen at time periods when no known earthquakes had occurred based on the Wellington catalogue. The false triggers were examined in time windows that were about three minutes in length, with the false STA/LTA trigger located at the middle of the window. The envelope of the tidal filtered pressure data and the derivative of the pressure was calculated for the first third of these time windows. By constraining the envelope to the first third of the time window, it allowed for the background noise level to be calculated before the false trigger occurred. Including the false trigger in the calculation would have led to the average of the background noise to be inaccurate. Figure 4.2.1 shows an example of how the difference from the background noise was calculated from the pressure using this method. The purple line represents the computed envelope for the first third of the time window (Figure 4.2.1). The average background pressure, shown by the black dashed line, was calculated from the computed envelope (Figure 4.2.1). The maximum or minimum

value in the pressure, which is always located in the center of the time window and was the cause of the STA/LTA to trigger, was then subtracted from the average pressure value (Figure 4.2.1). This yields the difference between the false trigger and the background noise level. Two hundred different time windows were considered for the assessment of background noise triggers. These 200 time windows examined false STA/LTA triggers when there were no known earthquakes recorded in the catalogue. Then the same analysis described above was conducted for the 279 pressure signals that were related to earthquakes.

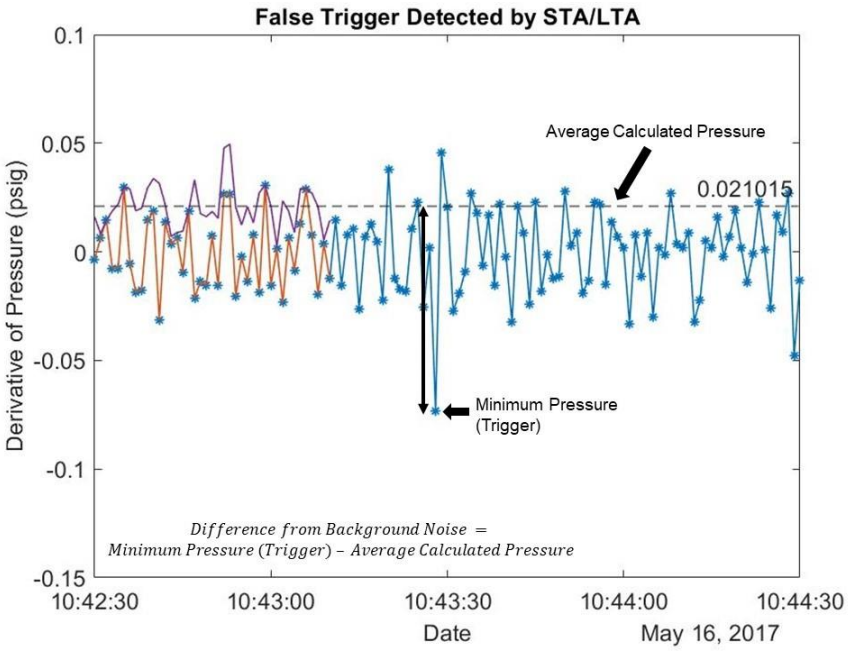

Figure 4.2.1: Example calculation used to determine the noise level in the pressure data. The blue line is the derivative of the pressure data, the purple line is the envelope calculated from the pressure data, the orange represents the data used to calculate the average envelope, and the dashed black line is the average pressure calculated from the envelope. The black arrow shows that the calculation was done from a minimum or maximum point to the average calculated pressure. This figure depicts the calculation from a false trigger that was purely noise and not related to an earthquake. The minimum/maximum value was subtracted from the average calculated pressure for 200 time windows related to noise. After averaging 200 of these calculations, it was found that the background noise level had an average difference in pressure from the calculated average noise of 0.047 psig.

This method of characterizing the noise level was used on both the tidal filtered pressure and the derivative of the tidal filtered pressure. Since the STA/LTA method uses the derivative of the pressure data, the difference from background noise for the tidal filtered pressure was not considered past this point. When looking at the derivative of the pressure, the false triggers had an average difference from the background noise of 0.047 psig. Figure 4.2.2 shows the distribution of these values for the 200 time windows analyzed. The median value for all 200 time windows was 0.047 psig, the maximum was 0.092 psig, and the minimum was 0.014 psig.

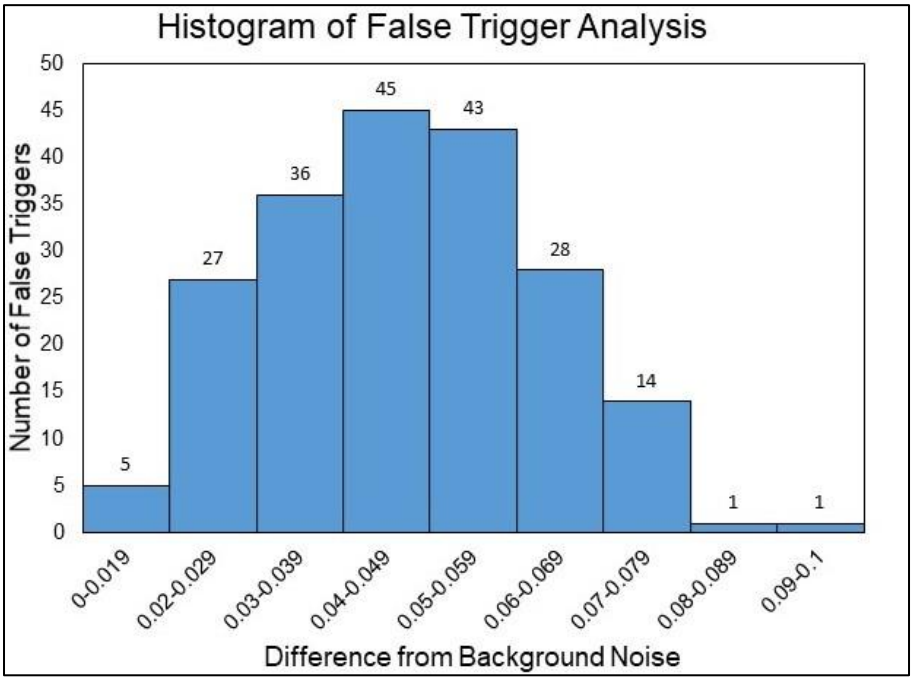

Figure 4.2.2: Distribution of difference values for the false trigger analysis. This plot is showing difference from the background noise versus the number of false triggers. The average difference from the background noise was 0.047 psig. The median was 0.047 psig, the maximum was 0.092 psig, and the minimum was 0.014 psig. 62% of false triggers had a difference from the background noise of 0.03 to 0.059 psig.

The average value of 0.047 psig was used to determine whether an earthquake event triggered by the STA/LTA was noise instead of signal. It would be expected that values above the threshold of 0.047 psig would be considered signal and not noise. When taking into account this threshold,

183 of the 279 potential earthquake events exceeded the noise threshold (Figure 4.2.3). These events ranged in magnitude from 0.8 to 5.4 and they ranged in distance from the pressure station from 2.09 km to 152 km (Figure 4.2.3).

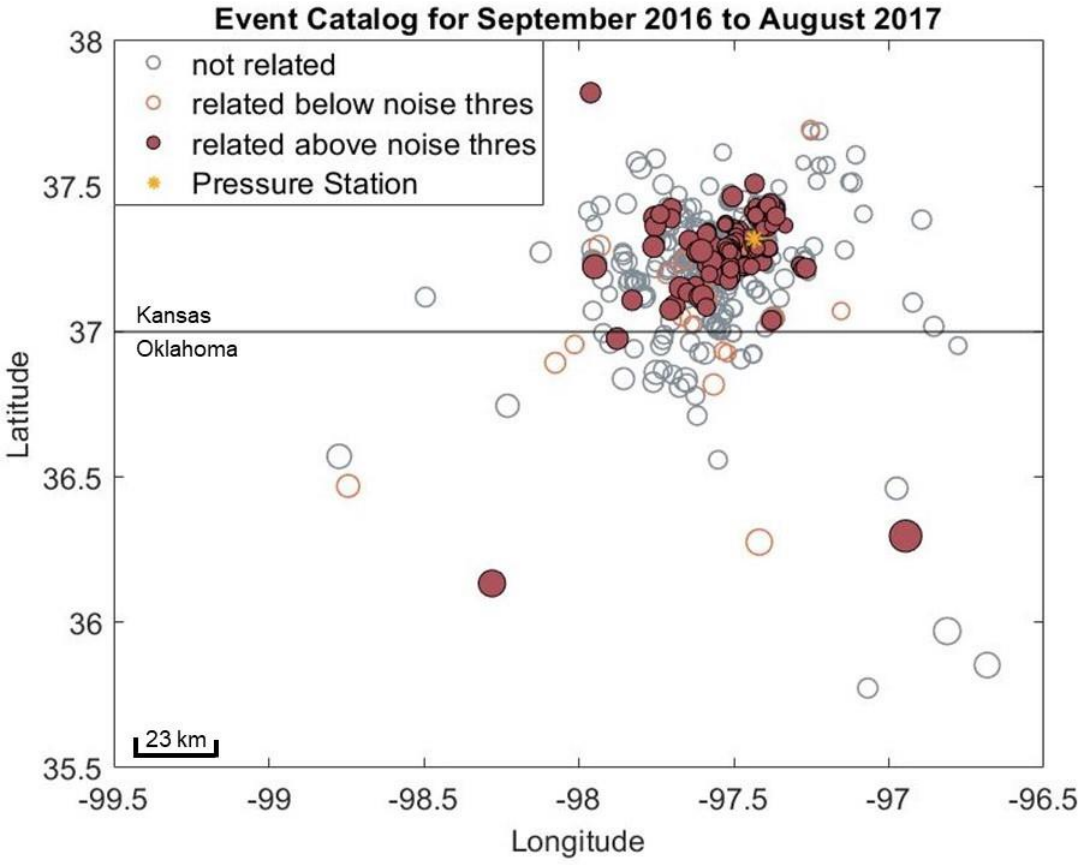

Figure 4.2.3: Location of all earthquake events in the catalog. The size of the circles relates to the magnitude of the event. The larger the magnitude, the greater the size of the circle. The blue open circles are earthquakes that were not related to pressure changes. Orange open circles were related to pressure changes, but they fell below the noise threshold. The green filled in circles are earthquakes that were related to pressure changes and their pressure change was above the calculated noise threshold. The pressure station is denoted by the yellow star.

When using STA values of 8 and 12 samples, there were 56 common earthquake detections. In addition, 8 new events were detected with the STA of 12 samples and another 119 were detected

with the STA of 8 samples. In total, these 183 events out of the original 279 were differentiable from the background noise level. The other 96 earthquakes that were detected by the STA/LTA could be related to earthquake signal, but since they are below the noise threshold they cannot be differentiated from noise with confidence, although their times coincide with known earthquakes.

Section 4.3: Earthquake Analysis

After determining the potential pressure signals that related to earthquakes with confidence, the individual events from the full catalog were then analyzed. The goal of this analysis was to determine why some earthquake events related to pore pressure changes, while others did not. For each of the earthquakes, I examined the phase, the impulsiveness, the magnitude, the frequency, the phase duration, the distance from the pressure station, and the changes in pressure.

Section 4.3.1: Earthquake Phase

Figure 4.3.1.1 depicts the earthquake phase of the full catalog of interest. The earthquake phase was determined by looking at the onset of the P wave. Downward motion directly after the onset was classified as dilatation, while upward motion was classified as compressional. The phase was determined from an earthquake station that was the closest to the pressure monitoring well and had a detected P wave arrival. Out of the 1,373 earthquakes analyzed, 726 of those events (or 53%) were dilatational in phase (i.e. the p-wave arrival onset was negative, indicating downward ground motion; a compressional phase onset is positive, indicating upward ground motion). Out of the 183 earthquakes related to pressure changes, 97 (or 53%) were dilatational in

phase (Figure 4.3.1.1). While most earthquakes with detectable pressure changes were dilatational (53%), overall earthquakes in the catalogue exhibit comparable dilatational behavior (53%) and therefore it cannot be concluded that earthquake phase affects pressure change detection.

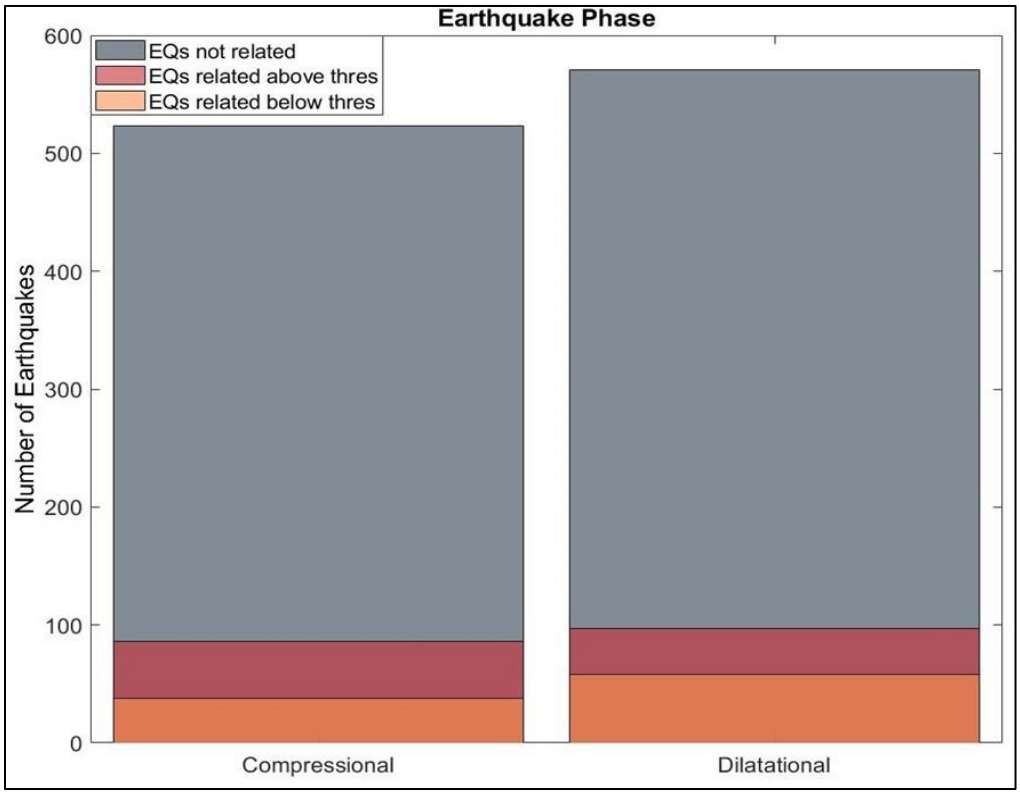

Figure 4.3.1.1: Earthquake phases for the full catalog of interest. The green bars represent the earthquakes that did not to detectable pressure changes. From the 1094 earthquakes not related to pressure, 52% were dilatational in phase and 48% were compressional in phase. The orange bars depict earthquakes related to pressure changes but below the noise threshold of 0.047. Out of the 96 earthquakes related to pressure but below the noise threshold, 60% were dilatational in phase. The purple bars are earthquakes related to pressure changes above the noise threshold. From the 183 earthquakes related to pressure, 53% were dilatational and 47% were compressional in phase.

Section 4.3.2: Earthquake Impulsiveness

From the full catalog of interest 728 events (53%) were found to have impulsive P waves, while 645 (47%) events were found to have emergent P waves (Figure 4.3.2.1). Earthquakes that related to pressure changes showed a similar distribution with 105 earthquakes (57%) being classified as impulsive and 78 (43%) being classified as emergent (Figure 4.3.2.1). When considering the S wave impulsiveness, 98 (54%) events that related to pressure changes were classified as being impulsive, while the other 85 (46%) were classified as being emergent (Figure 4.3.2.1). From the total catalog, 721 events (53%) were classified as having an impulsive S wave, while 652 events (47%) were classified as having an emergent S wave arrival (Figure 4.3.2.1). Earthquakes related to pressure changes but were below the noise threshold did follow the same P wave impulsiveness trends as those that were above the noise threshold. Out of the 96 earthquakes below the noise threshold, 55% had impulsive P waves. These earthquakes had different trends when comparing the S wave impulsiveness. For the earthquakes above the noise threshold, 54% had impulsive S waves, while only 48% of the earthquakes below the noise threshold had impulsive S waves.

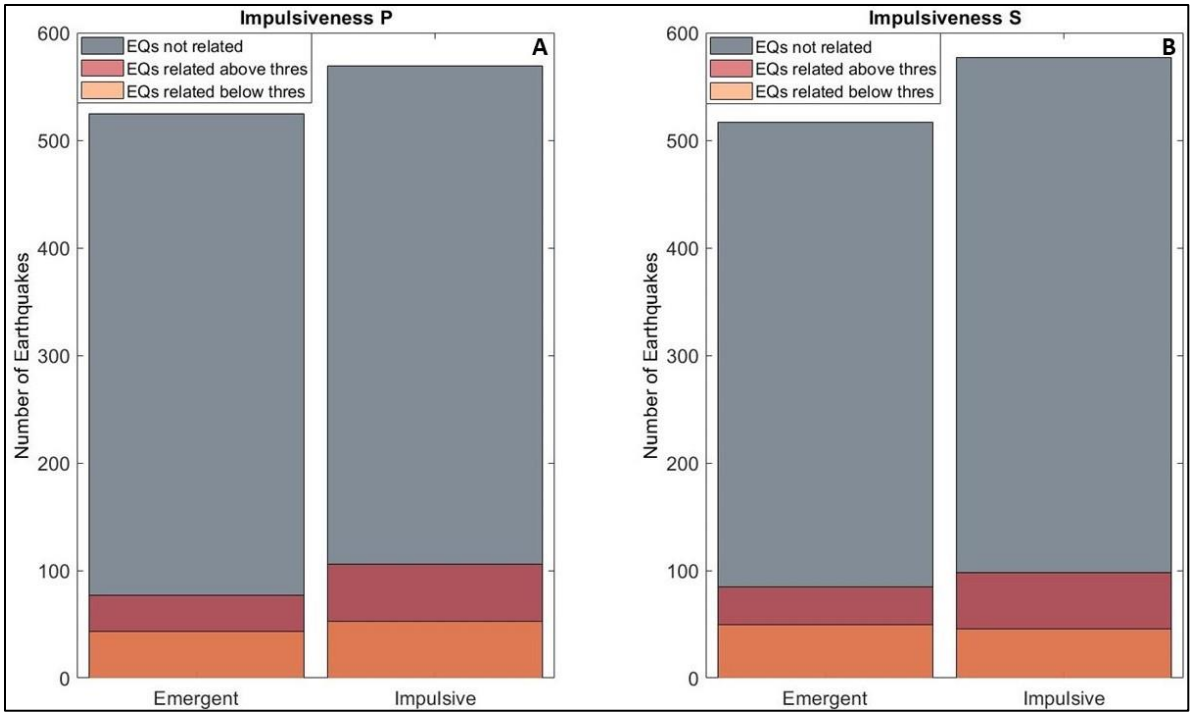

Figure 4.3.2.1: Earthquake impulsiveness analysis for the full catalog of interest. The green bars represent the earthquakes that did not relate to corresponding pressure changes, the orange bars depict earthquakes related to pressure changes but below the noise threshold of 0.047, and the purple bars denote earthquakes related to pressure changes above the noise threshold. A) Calculated P wave impulsiveness. From the 1094 earthquakes not related to pressure (green bars), 52% had an impulsive P wave and 48% had an emergent P wave. Out of the 96 earthquakes related to pressure but below the noise threshold (orange bars), 45% had emergent P waves and 55% had impulsive P waves. From the 183 earthquakes related to pressure (purple bars), 42% had emergent P waves and 58% had impulsive P waves. B) Calculated S wave impulsiveness for all earthquakes. From the 1094 earthquakes not related to pressure (green bars), 48% had an emergent S wave and 52% had an impulsive S wave. Out of the 96 earthquakes related to pressure but below the noise threshold (orange bars), 52% had emergent S waves and 48% had impulsive S waves. From the 183 earthquakes related to pressure (purple bars), 46% had emergent S waves and 54% had impulsive S waves.

The impulsiveness analysis suggests that earthquakes that are more impulsive are more likely to cause coseismic pressure changes. Based on the overall catalogue exhibiting comparable

impulsive behavior for both the P wave (53%) and the S wave (53%), it cannot be concluded that earthquake impulsiveness effects pressure change detection.

Section 4.3.3: Earthquake Magnitude, Frequency and Phase duration

When analyzing the magnitude of the earthquakes related to coseismic pressure changes, there were 3 (1.7%) events with a magnitude of 0-1, 143 (78%) with a magnitude of 1-2, 33 (18%) with a magnitude of 2-3, 3 (1.7%) with a magnitude 3-4, and 1 (0.55%) with a magnitude 4-6. Figure 4.3.3.1A compares magnitudes for earthquakes not related to coseismic pressure changes, those related but below the noise threshold, and those that are related and above the noise threshold. 78% of the earthquakes related to pressure changes had a magnitude that ranged from 1-2 (Figure 4.3.3.1A). This majority is consistent with trends seen in the overall catalog, since 75% of all the earthquakes had a magnitude range of 1-2 (Figure 4.3.3.1A).

After analyzing magnitude, the corner frequency for each individual earthquake the smaller magnitude events tend to have higher frequencies than the larger magnitude events (Figure 4.3.3.1B). Earthquakes related to pressure have a minimum frequency of 4 Hz and a maximum of 90 Hz, with 96% of all earthquakes having a frequency below 60 Hz (Figure 4.3.3.1B). Based on Figure 4.3.3.1B, earthquake corner frequency does not appear to correspond to pressure detection events.

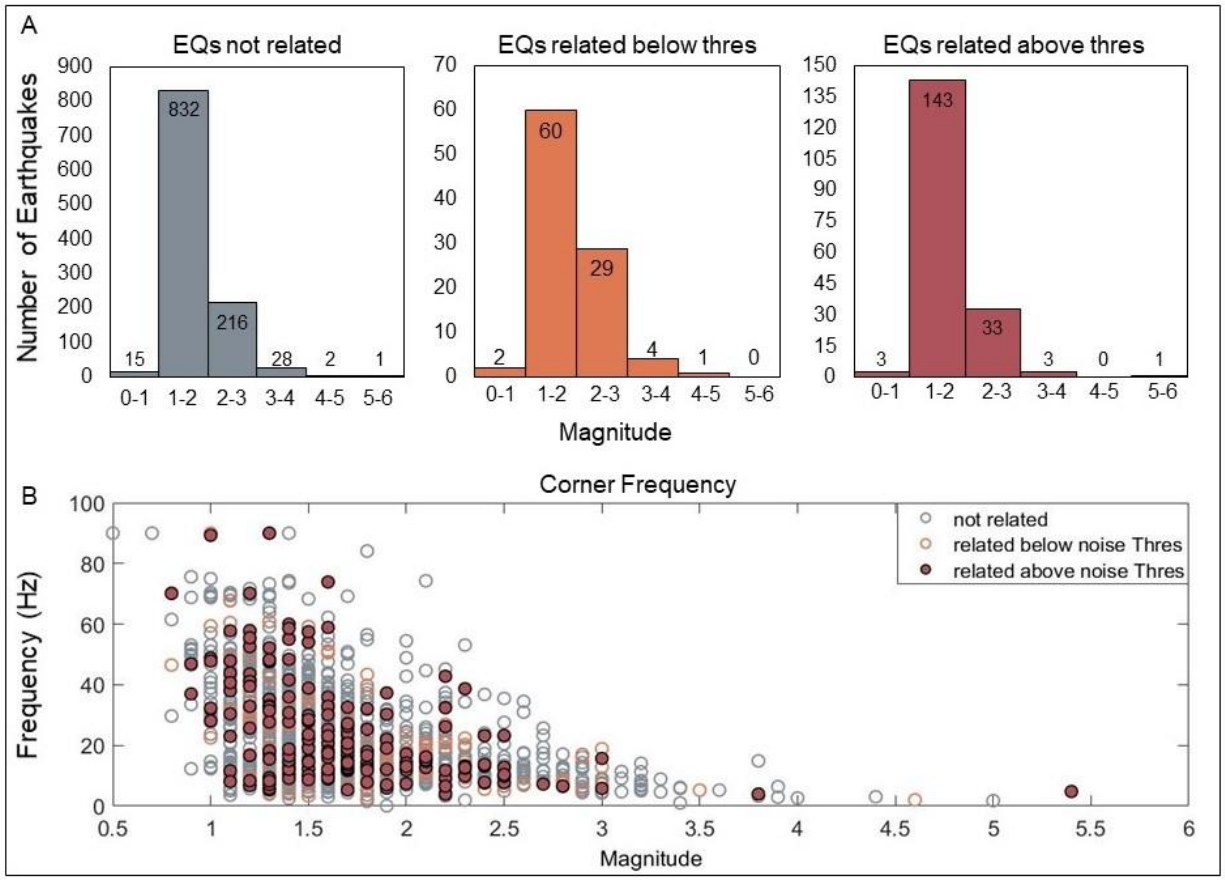

Figure 4.3.3.1: A) Comparison of earthquake magnitudes. The green bars represent the earthquakes that did not relate to corresponding pressure changes, the orange bars depict earthquakes related to pressure changes but below the noise threshold of 0.047, and the purple bars denote earthquakes related to pressure changes above the noise threshold. B) Comparison of magnitude versus corner frequency. The corner frequency is the frequency at which the energy moving through the system begins to decline. The corner frequency is highest in lower magnitude events and it decreases as the magnitude increases. The blue open circles are events that are not related to coseismic pressure changes, the orange open circles are events related to coseismic pressure chagnes but below the noise threshold of 0.047 psi, and the green circles are events related to coseismic pressure changes and above the noise threshold.

The length of the P wave was also considered to understand if there was any relationship between earthquake phase duration and detectable pressure changes. Earthquakes with longer P

waves (1 second or greater) may result in detectable pressure changes, due to the relatively sparse sampling rate of the pressure data. Earthquake recordings show that longer phase durations are associated with larger magnitude, more regional (distant) events. Pressure changes were not always captured in the during these specific events. Earthquakes that had phase durations of less than a second could have pressure changes that were detectable while other events, with that same phase length, did not have detectable pressure changes. Overall, there was no clear connection between the length of the P wave and the ability to detect pressures changes related to earthquakes.

Section 4.3.4: Distance

After analyzing phase duration, the earthquake distance from the pressure station was considered. Figure 4.3.4.1 displays observations of earthquake magnitude vs. distance from the pressure monitoring well and their relation to a detectable pressure change. As expected, larger earthquakes are detected by seismometers at greater distances whereas smaller earthquakes become undetectable as the distance from the seismometers increases. Earthquakes related to coseismic pressure changes are relatively lower in magnitude and closer to the pressure monitoring station (Figure 4.3.4.1). Increasing the distance from the pressure station decreases the likelihood that an earthquake will be detected within the pressure data. From the overall catalog, 91% of earthquakes occur at less than 30 km's away from the pressure monitoring well. When analyzing earthquakes that are related to pressure and above the noise threshold, 95% of these events are located less than 30 km's away (Figure 4.3.4.1). Based on these results there is a detection distance threshold at 30 km's away from the pressure monitoring well. When comparing distance versus magnitude, 93% of the earthquakes related to coseismic pressure

changes were ≤ M 2.5 and less than 30 km's away from the pressure station. This phenomenon is also seen in the overall catalog, since 88% of all the earthquakes analyzed were ≤ M 2.5 and less than 30 km's away from the pressure station.

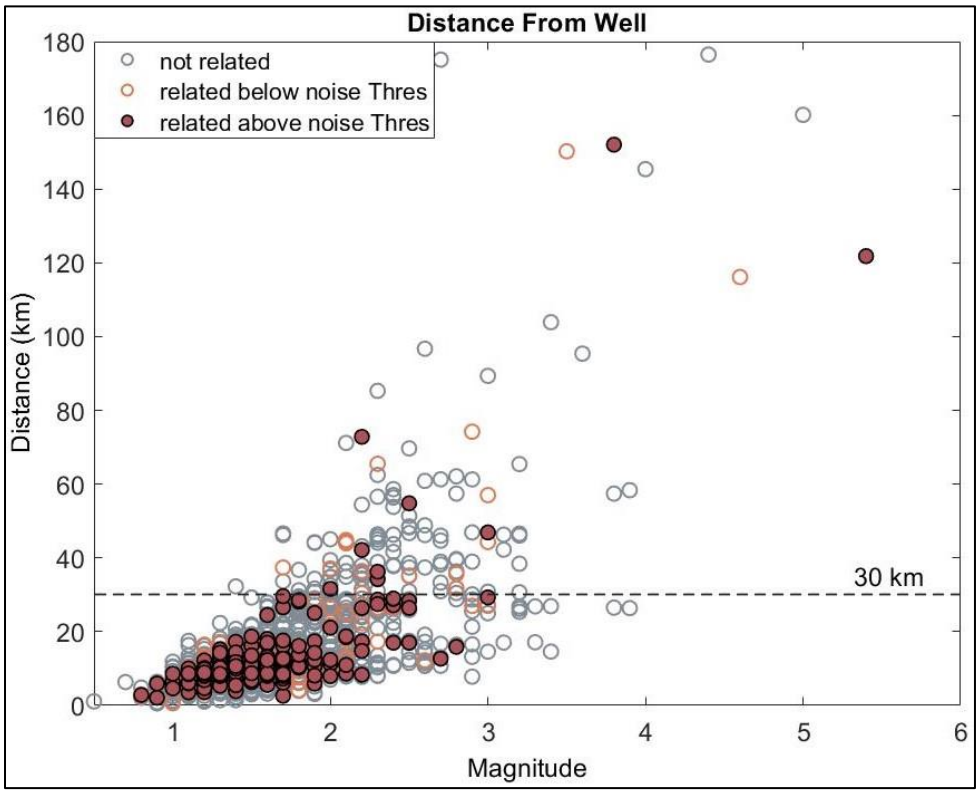

Figure 4.3.4.1: Comparison of magnitude versus versus distance from the pressure monitoring well. As distance increases the magnitude of the events also increases. The blue open circles are events that are not related to coseismic pressure changes, the orange open circles are events related to coseismic pressure chagnes but below the noise threshold of 0.047 psi, and the green circles are events related to coseismic pressure changes and above the noise threshold. The black dashed line represents 50 km's away from the pressure monitoring well. From the overall catalog, 1244 out of 1373 earthquakes are < 30 km's away from the well. From the earthquakes related to coseismic pressure changes, 174 out of 183 are < 30 km's away from the well.

Figure 4.3.4.2 is comparing the distance from the pressure monitoring station versus the percentage of earthquakes. This figure compares the full catalog of earthquakes versus the earthquakes related to pressure changes. From the overall catalog, 36% of earthquakes were 0-10 km's away, 42% were 10-20 km's away, and 13% were 20-30 km's away from the pressure station (Figure 4.3.4.2). From the earthquakes related to pressure changes and above the noise threshold, 37% were 0-10 km's away, 47% were 10-20 km's away, and 11% were 20-30 km's away from the pressure station (Figure 4.3.4.2).

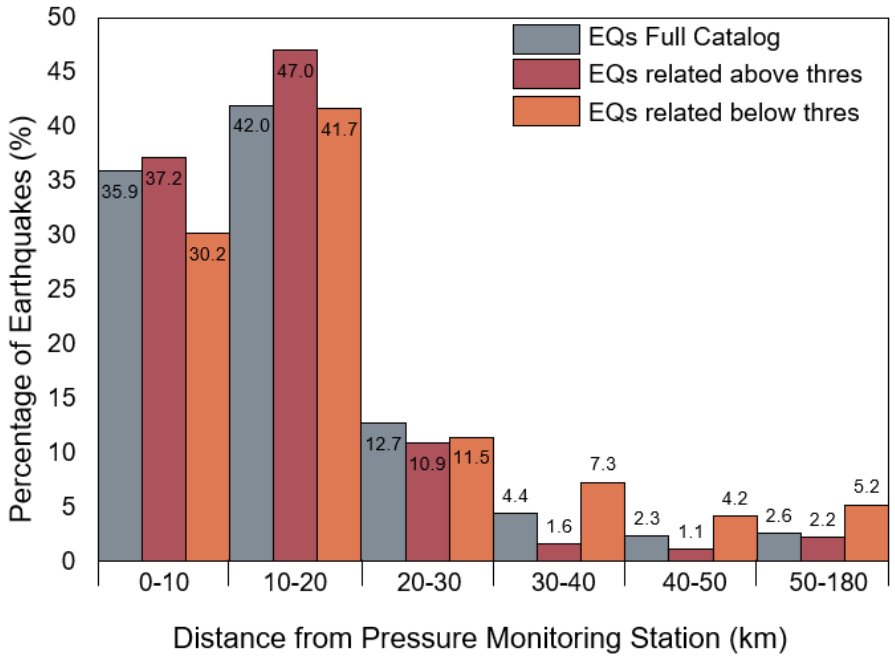

Figure 4.3.4.2: Comparison of distance from the pressure monitoring station versus the percentage of earthquakes. The green bars represent the full catalog of earthquakes, the orange bars depict earthquakes related to pressure changes but below the noise threshold of 0.047, and the purple bars denote earthquakes related to pressure changes above the noise threshold. The numbers at the end of the bars represent the percentage of earthquakes at that distance. For example, 36% of all the earthquakes in the catalog were 0-10 km's away from the pressure station.

Distance from the pressure monitoring well is related to earthquakes with detectable coseismic pressure changes but based on the overall catalogue exhibiting comparable trends in distance from the well, it cannot be concluded that earthquake distance effects pressure change detection.

Section 4.3.5: Maximum/Minimum Pressure Changes

Earthquakes related to pressure had maximum and minimum changes in pressure that were significant compared to the earthquakes that did not relate (Figure 4.3.5.1). To find the maximum and minimum pressure changes the derivative of the pressure data was used. A time window of three minutes was captured for each of the 1,373 known earthquakes. Using this time window, the difference in the maximum and minimum points of the derivative of the pressure data was calculated. After collecting values for each of the 1,373 earthquakes it was noted that the minimum pressure changes for earthquakes related to pressure ranged from -0.02 to -0.12 psig (Figure 4.3.5.1B). Many of these events clustered in a narrower range from -0.065 to -0.11 psig (Figure 4.3.5.1B). 87% of the earthquakes that related to pressure changes and were above the noise threshold fell within this range. When looking at earthquakes that related to coseismic pressure changes but were below the noise threshold only 35% fell within that pressure range and of the earthquakes that were not related only 0.5% fell within that data range. The minimum pressure changes for earthquakes that did not relate to pressure ranged from -0.065 to 0 psig (Figure 4.3.5.1B).

The maximum pressure changes for earthquakes detected by the STA/LTA method ranged from 0.02 to 0.1 psig (4.3.5.1A). The maximum pressure changes for earthquakes not related to pressure changes ranged from 0 to 0.06 psig, whereas events with related pressure changes had maximum values up to +0.1 psig (4.3.5.1A). From the earthquakes that

corresponded to pressure changes and were above the threshold, 12% had maximum pressure changes ≥ 0.065 psig. Of the earthquakes related to coseismic pressure changes but below the noise threshold only 4% had maximum pressure changes ≥ 0.065 psig and 0% of the non-pressure related earthquakes had maximum pressure changes ≥ 0.065 psig. It is noted that all events with minimum or maximum pressure changes that were greater or less than ±0.065 psig correspond to pressure related events (Figure 4.3.5.1).

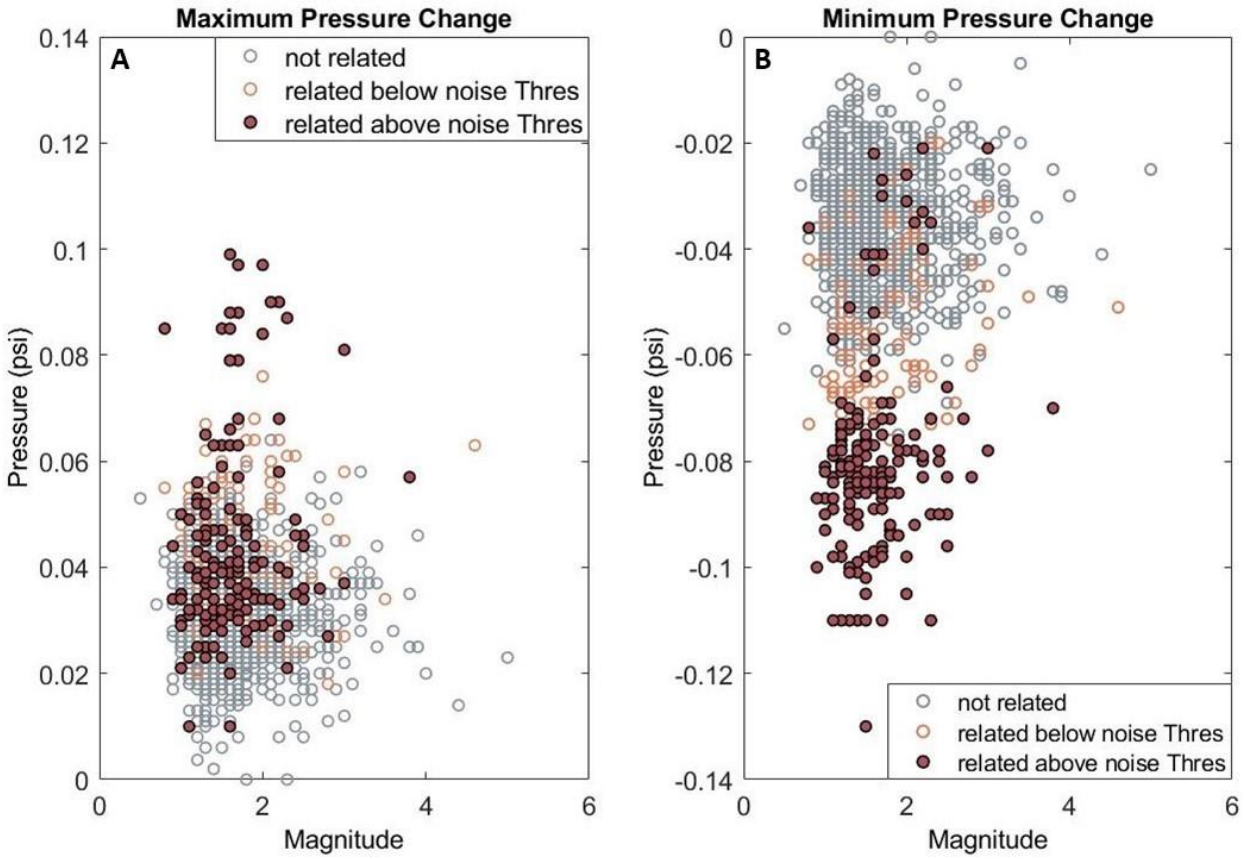

Figure 4.3.5.1: A) Comparison of earthquake magnitude versus maximum pressure changes for all earthquakes. Earthquakes related to pressure changes have a wide range of maximum pressure changes from 0.02 psig to 0.1 psig. B) Comparison of magnitude versus minimum pressure changes. Earthquakes related to pressure changes have a greater minimum pressure change of around –0.09 psig compared to other events in the catalogue. The blue open circles are events that are not related to coseismic pressure changes, the orange open circles are events

related to coseismic pressure changes but below the noise threshold of 0.047 psig, and the green circles are events related to coseismic pressure changes and above the noise threshold. It can be noted that events related to coseismic pressure changes that have low minimum pressure changes (B) commonly have large maximum pressure changes (A). From the 183 earthquakes related to pressure changes, 99% had pressure changes greater or less than ±0.065 psig. The Pawnee earthquake was not plotted due it having significantly larger pressure changes compared to the other earthquakes of interest. Based on this figure, pore pressure is a poor measure of the magnitude of an earthquake. Smaller magnitude earthquakes commonly have larger pore pressure changes than the larger magnitude earthquakes.

This was differentiable from the events that did not relate to pressure since they commonly had a maximum pressure change that was less than 0.065 psig (Figure 4.3.5.1A). The minimum pressure changes for non-pressure related earthquakes was commonly greater than -0.065 psig (Figure 4.3.5.1B). Earthquakes that were above the noise threshold that did not have significant minimum pressure changes commonly had significant maximum pressure changes above 0.065 psig (Figure 4.3.5.1). From these earthquakes, 181 out of 183 had pressure changes greater than or less than ±0.065 psig. When looking at the magnitude 2 events, this phenomenon is depicted (Figure 4.3.5.1). Events above the noise threshold that have a low minimum pressure change instead have a large maximum pressure change (Figure 4.3.5.1).

The vice versa relating to pressure changes is also depicted (Figure 4.3.5.1). Earthquakes that were above the noise threshold that did not have significant maximum pressure changes commonly related to significant minimum pressure changes below -0.065 psi (Figure 4.3.5.1). The magnitude 1 events depict how earthquakes above the noise threshold had significantly larger minimum pressure changes and if they did not then they had significant maximum pressure changes (Figure 4.3.5.1). Based on this figure pore pressure changes cannot be used to

determine the severity of an earthquake (Figure 4.3.5.1). Small magnitude earthquakes commonly have larger pore pressure changes than large magnitude earthquakes (Figure 4.3.5.1).

Earthquakes related to pressure commonly had significant changes in the minimum/maximum pressure. These events do not seem to be dependent on other earthquake characteristics presented earlier in this section. Based on this analysis, a significant change in the derivative of the pressure is needed for earthquakes to have coseismic pressure changes that are detectable by the STA/LTA method.

Section 4.4: Spatial and Temporal Distribution

When considering the full catalog (Nolte, 2020), earthquakes are more common to the southwest of the seismometer network and the pressure station (Figure 4.4.1). The earthquakes denoted by the STA/LTA method are also frequently located southwest of the pressure station (Figure 4.4.1). This is expected since the location of the large volume wastewater injection wells in this region is to the southwest of Wellington Field. One significant cluster of earthquakes was denoted within the pressure data, and it is to the northeast of the pressure station (Figure 4.4.1).

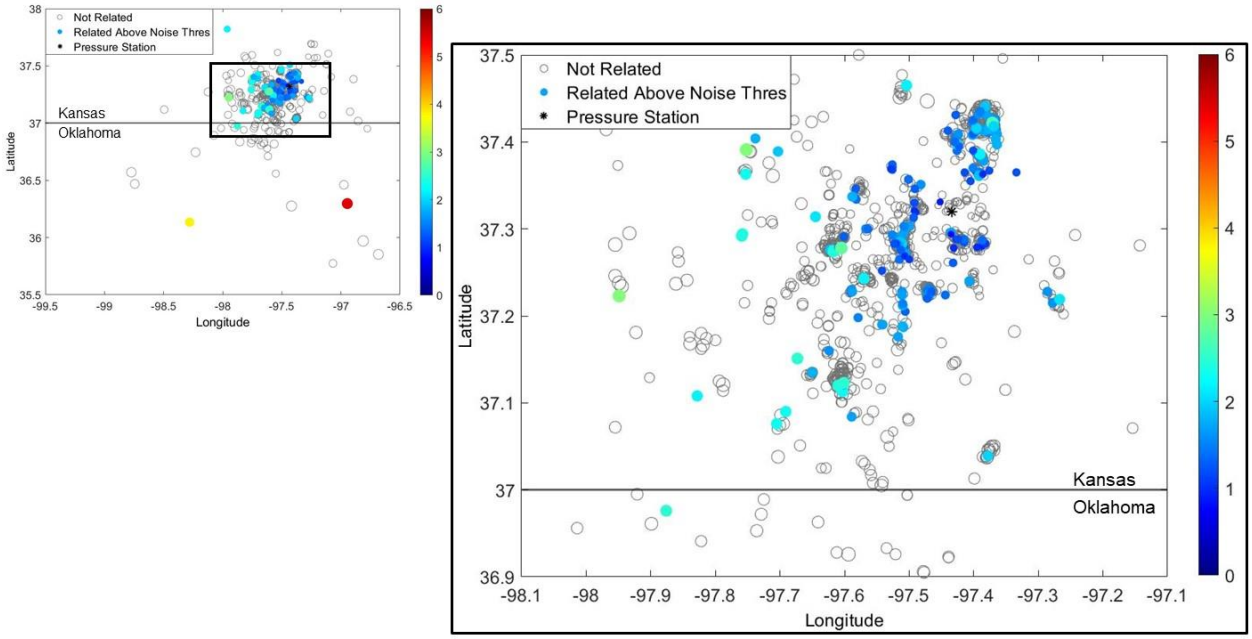

Figure 4.4.1: Map depicting the magnitude and location of the events that were related to coseismic pressure changes. The map to the left depicts the full area of interest, while the map to the right depicts a zoomed in area right around the pressure station. Events that were smaller in magnitude were commonly closer to the pressure station, while events that were larger in magnitude are farther away from the pressure station. The color bars to the right of both maps depict the magnitude. Blue relates to small magnitude events, while red relates to large magnitude events. The grey circles are locations of events that were not related to coseismic pressure changes and events that had pressure changes but were below the threshold. The size of these grey circles varies based on the magnitude of the event. The black star is the location of the pressure well.

The magnitude vs. distance relationship for earthquakes related to coseismic pressure changes is shown in Figure 4.4.2. This relationship was found by using a simplified ground motion equation (Tiira et al., 2016; Eqn.4).

$$M = b\log_{10}(D) + aD + c \qquad \text{(Eqn. 4)}$$

where M is magnitude, D is distance from the earthquake to the pressure monitoring station located in Wellington Field, a and b are coefficients of anelastic attenuation, and c is a baseline

correction (Tiira et al., 2016). By using random sampling and a least squares solution it was possible to solve the magnitude versus distance relationship for earthquakes related to pressure changes (Figure 4.4.2).

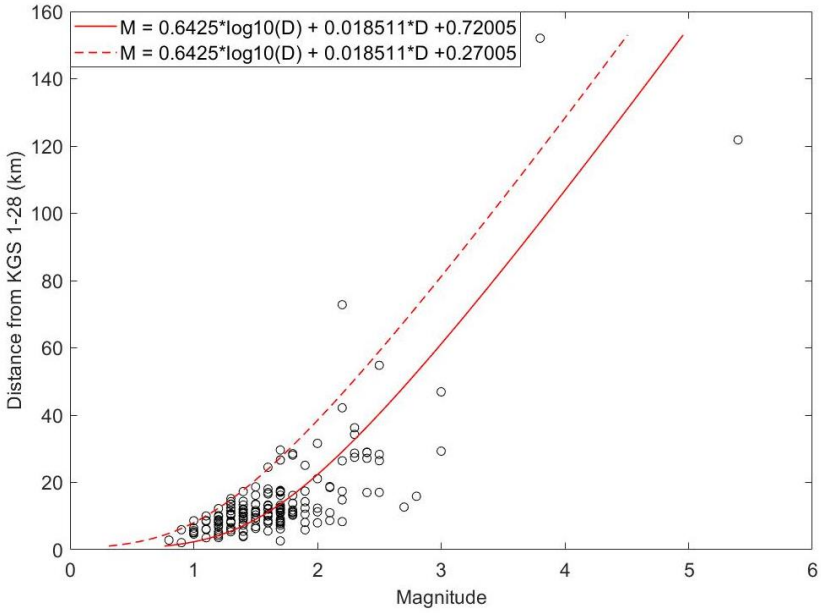

Figure 4.4.2: Magnitude versus distance relationship for the earthquakes related to pressure changes (Tiira et al., 2016). This relationship was found using bootstrapping, with 200 random samples, and least squares solution. The red line represents the best fit of the simplified ground motion equation with respect to the 183 earthquakes of interest. The best fit line has a correlation coefficient (R^2) of 0.98. The dashed red line is the ground motion equation, but it has been adjusted to represent detectability of minimum magnitude of events vs. distance. The dashed line represents the estimate for the minimum magnitude versus distance relationship for earthquakes related to coseismic pressure changes. The dashed line has a correlation coefficient (R^2) of 0.71.

Based on Figure 4.4.2, the detection of earthquakes in the pressure data is related to distance. Earthquakes with smaller magnitudes are commonly detected closer to the pressure station (Figure 4.4.2). Earthquakes related to pressure that were larger in magnitude (≥ M 3.5) were farther away from the pressure station (Figure 4.4.2). When looking at earthquakes related to pressure changes as the distance from the pressure station increases, the magnitude of the events

detected increases (Figure 4.4.2). This analysis is also in agreement with the visual observation of earthquake locations in Figure 4.4.1.

The next step was to look at interpreted faults in the area and compare earthquake locations to these faults. The fault locations found in the study by Nolte (2020) used earthquake data from Wellington field from 2014 to 2020. The faults were determined by using the orientation of the maximum horizontal stress to calculate slip potential at earthquake clusters (Nolte, 2020). Figure 4.4.3 shows the comparison between earthquakes that had detectable pressure changes and the fault locations. Clusters of earthquakes to the north, east, and south of Wellington field are associated with faults (Figure 4.4.3).

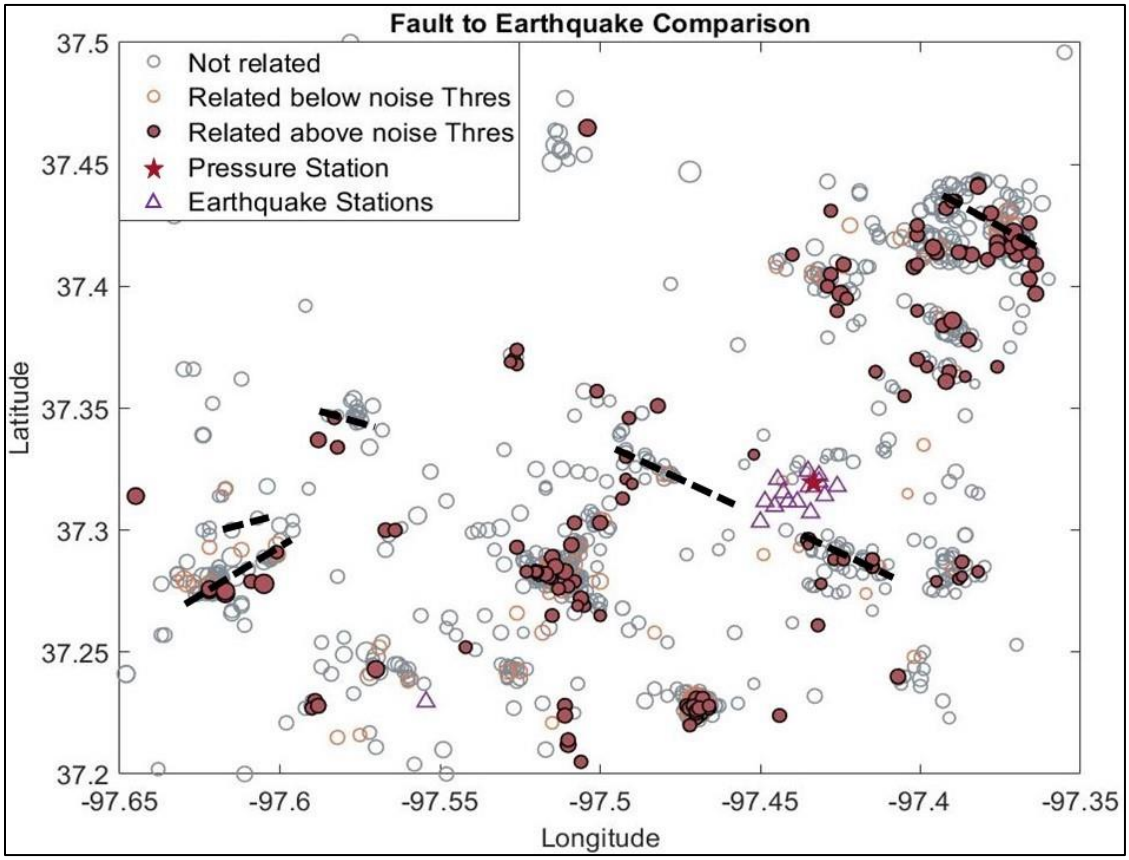

Figure 4.4.3: Comparison of earthquake locations to calculated fault locations in the area of interest. The size of the circles relates to the magnitude of the event. The blue open circles are events that are not related to coseismic

pressure changes, the orange open circles are events related to coseismic pressure changes but below the noise threshold of 0.047 psig. The green filled in circles are earthquakes that were related to pressure changes and their pressure change magnitude was above the calculated noise threshold. The pressure station is denoted by the dark red star and the earthquake stations are denoted by purple triangles. Calculated fault locations from Nolte (2020) are shown using black dashed black lines.

Some faults determined by Nolte (2020) are not associated with large clusters of earthquakes, which could be due to the fault analysis being conducted on six years of data compared to a year and a half. Earthquakes associated with coseismic pressure changes are clustered around the faults located in the northeast, southwest, and southeast on the map (Figure 4.4.3). The other fault locations do not correspond with the locations of earthquakes that are related to coseismic pressure changes (Figure 4.4.3).

Chapter 5: Discussion

The goal of this study was to determine whether small magnitude, local, induced earthquakes cause pore pressure changes that can be detected in well data and to examine which earthquake characteristics may relate to pressure changes. This work is significant since this is the first time that small magnitude, induced earthquakes were found to cause notable pore fluid pressure changes in the subsurface.

Section 5.1: Pressure Changes and Earthquakes

By using an STA/LTA trigger algorithm it was possible to detect small pressure changes within the data that potentially relate to earthquake signals. Use of the automated trigger algorithm removes human bias from the detection of subtle pressure anomalies. After testing different values and comparing the results, an STA window of 2 and 3 seconds (8 and 12 samples respectively) worked the best at removing noise and preserving signal. An STA value lower than 2 seconds was prone to triggering noise within the data and an STA value greater than 3 seconds was prone to removing possible earthquake signal. The one concern with using this method is the number of triggers produced. It is necessary to visually QC triggers from this method and to understand the background noise level of the data being used. Without knowing this information, it is impossible to differentiate between background noise and potential subtle signal.

The results from the STA/LTA method and the earthquake analysis indicate that small magnitude, induced earthquakes are detectable within pore pressure data. Small magnitude earthquakes are detectable in the pressure data by significant changes in pressure from the background level. Events that were above the noise threshold were shown to have significant

minimum and maximum pressure changes that were ±0.065 psig (Figure 4.3.5.1). After these pressure changes occur, the signal recovers back to background level or close to background level. It is believed that these changes in pressure are related to the passage of earthquake waves, which is commonly referred to as a transient signal (Kroll et al., 2017). The full earthquake signal is not detected due to the pressure sensor sampling at a low rate (Kroll et al., 2017). By having a sampling rate of one sample per second it was possible to clearly detect the full earthquake response for the Pawnee earthquake, but the sampling rate would need to be higher (~10 samples per second) to capture the full response for smaller magnitude events.

Past studies (Quitly and Roeloffs, 1997, Roeloffs ,1998, Rojstaczer and Wolf, 1992) have analyzed coseismic changes in water levels in shallow wells. In one study it was found that the recovery time for water levels after the coseismic changes depended on the confinement of the aquifer (Quitly and Roeloffs, 1997). Aquifers that are poorly confined and have low wellbore permeability commonly have rapid recovery rates (Quilty and Roeloffs, 1997). Their study looked at coseismic changes in shallow wells in a confined aquifer, while this research focuses on pressure changes in a deep well in the Arbuckle. The Arbuckle locally is a semiconfined aquifer with some leakage vertically (Barbour et al., 2019). Due to the Arbuckle being semiconfined it would be expected that the recovery rates would be rapid after coseismic pressure changes occur. The low permeability of the well studied could also lend to faster recovery rates. This provides a better understanding of the observations that depict a complete recovery in the pressure after an earthquake occurs.

The cause of these coseismic pressure changes is thought to be related to the passage of seismic waves (Roeloffs, 1996). The passage of seismic waves can cause pressure head fluctuations which produce water level fluctuations (Roeloffs, 1996). This oscillatory well

response depends on the wellbore storage response (i.e. water level behind the aquifer pressure) and the height of the water column above the aquifer (Roeloffs, 1996). These transient signals have been related to the passage of body waves and surface waves (Wang et al., 2009, Barbour et al., 2019). A past study has also shown that pressures in fluid filled fractures can be amplified by the passage of seismic waves (Jin et al., 2021). This amplification in pressure could be the cause of transient pressure changes associated with the passage of seismic waves.

Many earthquakes in the catalog had no significant changes in pressure during the time that they were expected to be observed. This could be related to the sampling rate of the pressure data being significantly lower than the sampling rate of the earthquake data. This would cause short duration earthquakes to be potentially missed in the pressure data. Also, since the pressure changes related to small magnitude earthquakes are subtle, these pressure changes could have been masked within the background noise. Another potential explanation of this phenomenon is described by Roeloffs (1998) in her studies on coseismic water level responses. In her study, Roeloffs notes that some earthquakes did not produce water level responses in the wells of interest (1998). Her conclusion to this phenomenon was that the coseismic responses are dependent on the dynamic strain orientation of the earthquake (Roeloffs, 1998). Earthquakes that are potentially off strike of the fault could be the cause of a lack of coseismic water level responses (Roeloffs, 1998). Earthquakes with a lack of coseismic pressure changes could potentially have a dynamic strain orientation that is not consistent with the earthquakes with coseismic pressure changes.

When comparing possible faults in the area calculated from the borehole breakouts at Wellington field (Nolte, 2020) to earthquakes related to coseismic pressure changes, no clear relationship can be seen. Some earthquakes that are on strike of the faults are more likely to be

related to coseismic pressure changes, but many of the earthquakes related to pressure were off strike of the faults (Figure 4.4.3). Overall, there is no clear relationship between fault orientation and earthquakes that are related to coseismic pressure changes. Further analysis should be done going forward to better understand the relationship between coseismic responses and fault orientation.

Section 5.2: Location of Events Detected

It is shown that the events detected by the STA/LTA method follow a magnitude versus distance relationship (Figures 4.4.1 & 4.4.2). Detected events that are closer to the pressure station are smaller in magnitude than events that are farther away from the pressure station. When looking at the spatial and temporal distribution of the earthquakes captured by the pressure data, many of the earthquakes occur to the southwest of the pressure station (Figure 4.2.2 & 4.4.1). This is expected since the injection wells that are the potential cause of these earthquakes are located to the southwest of Wellington field (Rubenstein et al., 2018). Since the full catalog of earthquakes commonly has similar locations to the southwest, new information relating to the hydraulic properties of the Arbuckle could not be determined. The distribution of these earthquakes around the pressure station is not consistent, which makes understanding the hydraulic properties of the subsurface unreliable. Having an increased number of wells monitoring pressure in the subsurface could help reduce this uncertainty. Past studies that have determined the hydraulic properties from the subsurface using coseismic water level changes have considered at least two wells to constrain their analysis (Roeloffs, 1998; Kroll et al., 2017; Elkhoury et al., 2006). Increasing the number of wells monitoring pressure could provide new

information relating to how the hydraulic properties of the Arbuckle vary spatially and temporally.

Section 5.3: Limitations and Future Work

The collection and the sampling of the pressure data is a limitation in this study. The pressure data was collected at a rate of one sample per second and then it was compared to earthquake data, which is collected at a rate of 200 samples per second. This difference in the sampling rate could have led to inaccuracies and the potential for small pressure changes that related to earthquakes not to be captured. To reduce this limitation, a pressure sensor that samples at a higher rate would be necessary. The time drift component of the pressure data is also of concern. It is crucial that the time of the pressure data is accurate when comparing it to earthquake data. Issues with time drift made it impossible to use the first three months of the pressure dataset. Having consistent time corrections or collecting the pressure data in real time could help resolve these time drift errors.

In the future it is recommended that similar pressure and earthquake data from this study be recollected. By collecting the pressure data at a higher sampling rate (~10 samples per second) and having multiple wells (~4 wells) monitoring pressure changes it will be possible to gain a better understanding of the hydraulic properties of the subsurface. In the case that data is recollected, pressure sensors should be as isolated as possible in wells to reduce the effect of site noise. It is recommended that these pressure sensors collect data in real time to avoid concerns with time drift. Also including seismometers that monitor downhole along with the pressure stations could be beneficial in providing new information relating to how pressure disturbances relate to earthquakes. For data management purposes, pressure and earthquake data should be

analyzed on a month-to-month basis. Improving the data collected in this project could provide a better understanding of coseismic pressure changes related to small magnitude, induced earthquakes. If the results are successful from this improved dataset, it is thought that pressure sensors could be used as a coarse substitute for earthquake monitoring.

Section 5.4: Significance

This research establishes a novel method for analyzing the relationship between induced seismicity and downhole pore pressure data. By using downhole pressure and earthquake data from the field, it was possible to detect coseismic pressure changes related to small magnitude, induced earthquakes. Going forward this relationship could provide information that is critical to the understanding of induced seismicity and for the mitigation of its impact to society. Earthquakes in Southern Kansas have to date been well below M 5, so it is important to understand the changes in pore fluid pressure that occur during smaller seismic events. By using the STA/LTA trigger method, small magnitude (M 5 and less), induced earthquakes were detectable within pore pressure data. Events that were detected were shown to have significant changes in pore pressure from background level. These pressure changes were consistent with past literature that studied coseismic well responses (Roeloffs, 1998; Kroll et al., 2017; Quilty and Roeloffs, 1997). From this study, changes in pore pressure have been related to earthquakes that range in magnitude from 0.8 to 5.8. These results are significant, since this is the first time that pore pressure changes measured down well have been found to relate to earthquakes that are magnitude 4 and smaller.

Chapter 6: Conclusion

I analyzed earthquake data and downhole pore pressure data collected at Wellington field, KS from September 2016 to August 2017. By using an STA/LTA trigger algorithm it was found that small magnitude, local, induced earthquakes cause pore pressure changes that are detectable in downhole well data. From the 1,373 events analyzed, 279 of these events were shown to have significant changes in pore pressure measured at the well site. Only 183 of the 279 events were considered since their pressure changes were above the approximated noise threshold. From these 183 events, 99% had minimum and/or maximum pressure changes that were greater than other earthquakes that were undetectable by the STA/LTA method. No other parameters like the phase, impulsiveness, corner frequency, magnitude, phase duration, and distance from the pressure monitoring well seemed to be correlated to earthquake events that related to pore pressure changes. This leads the authors to believe that these parameters do not impact whether earthquakes have detectable coseismic pressure variations.

A significant number of earthquakes were not related to pressure changes and this phenomenon could be due to the difference in the sampling rate of the datasets, the noise level at the well measuring pressure, or variations in the orientation of the dynamic strain of the earthquake. Future work could benefit from further analyzing the relationship between coseismic responses and fault orientation. The spatial and temporal distribution of the earthquakes with considerable pressure variations followed a magnitude versus distance relationship. Their locations were also consistent with the general trend of the full earthquake catalog.

With further data collection, new conclusions could be drawn relating to the hydraulic properties of the Arbuckle at Wellington Field. By increasing the number of wells monitoring pressure and having downhole seismic, a more thorough analysis of coseismic pressure changes could be

conducted. However, this study has demonstrated that using an STA/LTA algorithm is a potential method for detecting coseismic pressure changes and that induced seismic events that are magnitude 4 and smaller are detectable in continuous downhole pressure data. This investigation offers compelling evidence that pressure monitoring can be a viable, inexpensive method for detecting local earthquakes.

References

Alt, R.C., and Zoback, M.D. (2016). In situ stress and active faulting in Oklahoma. Bulletin of the Seismological Society of America.

Arditty, P. (1978). The Earth Tide Effects on Petroleum Reservoirs. *Department of Petroleum Engineering of Stanford University*.

Barbour AJ, Xue L, Roeloffs E, Rubinstein JL (2019). Leakage and Increasing Fluid Pressure Detected in Oklahoma's Wastewater Disposal Reservoir. *Journal of Geophysical Research: Solid Earth* 124:2896–2919. doi: 10.1029/2019JB017327

Benz, H.M., McMahon, N.D., Aster, R.C., McNamara, D.E., Harris D.B. (2015). Hundreds of Earthquakes per Day: The 2014 Guthrie, Oklahoma, Earthquake Sequence, Seismological Research Letters, 86.

Bidgoli, T.S., Holubnyak, Y., and FazelAlavi, M. (2015). Evaluating potential for induced seismicity through reservoir-geomechanical analysis of fluid injection in the Arbuckle saline aquifer, south-central Kansas: AAPG Datapages/Search and Discovery Article #90216.

Bidgoli, T.S., Jackson, C. (2017). Operational practices and their influence on injection-induced earthquakes: lessons learned from a statewide survey of brine disposal in Kansas. American Association of Petroleum Geology Annual Convention and Exhibition. April 5, 2017, Houston, Texas.

Bormann, P., Klinge, K., & Wendt, S. (2002). Data Analysis and Seismogram Interpretation. In *New manual of seismological observatory practice (NMSOP)* (pp. 1–102).

Bredehoeft, J. D. (1967). Response of well-aquifer systems to earth tides. *Journal of Geophysical Research*, *72*(12), 3075-3087.

Buchanan, R. C. (2015). Increased seismicity in Kansas. The Leading Edge, 34(6), 614-617.

Choy, G.L., Rubinstein, W.L., Yeck, W.L., Mcnamara, D.E, Mueller, C.S., Boyd, O.S. (2016). A rare moderate-sized (Mw 4.9) earthquake in Kansas: rupture process of the Milan, Kansas, earthquake of 12 November 2014 and its relationship to fluid injection. Seismological Research Letters, 87.

Dubois, S.M., Wilson, F.W. (1978). A revised and augmented list of earthquake intensities for Kansas, 1867-1977. Kansas Geological Survey Environmental Geology Series 2.

Elkhoury, JE, Brodsky, EE, Agnew, DC (2006). Seismic waves increase permeability. *Nature*, *441*(7097), 1135–1138. https://doi.org/10.1038/nature04798

Ellsworth, WL (2013). Injection-Induced Earthquakes. *Science*, *341*(6142), 1225942. https://doi.org/10.1126/science.1225942

Ellsworth, W.L., Llenos, A.L., McGarr, A.F., Michael, A.J., Rubinstein, J.L., Mueller, C.S., Peterson, M.D., Calais, E. (2015), Increasing seismicity in the U. S. midcontinent: Implications for earthquake hazard, The Leading Edge, 34, 618-626.

Elsworth, D., Spiers, D.J., Niemeijer, A.R. (2016). Understanding Induced Seismicity. Science, 354, 1380-1381.

Franseen, EK, Brynes AP, Cansler JR, Steinhauff MD, Carr TR. (2004). The geology of Kansas Arbuckle Group. *Midcontinent Geoscience*, 1-43.

Fritz, RD, Medlock P, Kuykendall MJ, and Wilson JL (2012). The geology of the Arbuckle Group in the midcontinent: Sequence stratigraphy, reservoir development, and the potential for hydrocarbon exploration. *AAPG Special Volumes*: 203-273. doi:10.1306/13331495M980077

Frohlich, C. (2012). Two-year survey comparing earthquake activity and injection-well locations

in the Barnett Shale, Texas. Proceedings of the National Academy of Sciences, 109(35), 13934-13938.

Frohlich, C., Ellsworth, W., Brown, W.A., Brunt, M., Luetgert, J., MacDonald, T., Walter, S. (2014). The 17 May 2012 M4.8 earthquake near Timpson, East Texas: an event possibly triggered by fluid injection. Journal of Geophysical Research: Solid Earth, 119.

Hildebrand, G.M., Steeples, D.W., Knapp, R.W., Miller, R.C., Bennett, B.C. (1988). Microearthquakes in Kansas and Nebraska 1977-87. Seismological Research Letters, 59.

Hill, AD (1990). Production logging: theoretical and interpretive elements. *Society of Petroleum Engineers* 14:1-154.

Horton, S. (2012). Disposal of hydrofracking waste fluid by injection into subsurface aquifers triggers earthquake swarm in central Arkansas with potential for damaging earthquake. Seismological Research Letters, 83(2), 250-260.

Ingebritsen SE, Manga M (2019). Earthquake Hydrogeology. *Water Resources Research* 55:5212–5216. doi: 10.1029/2019WR025341

Jin, Y., Dyaur, N., & Zheng, Y. (2021). Laboratory Evidence of Transient Pressure Surge in a Fluid-Filled Fracture as a Potential Driver of Remote Dynamic Earthquake Triggering. *The Seismic Record*, *1*(2), 66-74.

Keranen, K.M., Savage, H.M., Abers, G.A., Cochran, E.S. (2013). Potentially induced earthquakes in Oklahoma, USA: links between wastewater injection and the 2011 Mw 5.7 earthquake sequence. Geology, 41, 699-702.

Keranen, K.M., Weingarten, M., Abers, G.A., Bekins, B.A., Ge, S. (2014). Sharp increase in central Oklahoma seismicity since 2008 induced by massive wastewater injection. Science, 345, 448-451.

Kim, W.Y. (2013). Induced Seismicity associated with fluid injection into deep well in Youngstown, Ohio. Journal of Geophysical Research: Solid Earth, 118, 3506-3518.

Kroll KA, Cochran ES, Murray KE (2017). Poroelastic Properties of the Arbuckle Group in Oklahoma Derived from Well Fluid Level Response to the 3 September 2016 Mw 5.8 Pawnee and 7 November 2016 Mw 5.0 Cushing Earthquakes. *Seismological Research Letters* 88:963–970. doi: 10.1785/0220160228

Langenbruch, C., Zoback, M.D. (2016). How will induced seismicity in Oklahoma respond to decreased saltwater injection rates? Science Advances, 2.

Love, A. E. H. (1911). Some Problems of Geodynamics. *Cambridge University Press*; 180.

Manga, M, Rowland, JC (2009). Response of Alum Rock springs to the October 30, 2007 Alum Rock earthquake and implications for the origin of increased discharge after earthquakes. *Geofluids*, *9*(3), 237–250. https://doi.org/10.1111/j.1468-8123.2009.00250.x

Manga, M., Wang, CY (2015). 4.12. Earthquake hydrology. *Treatise on geophysics*: 305-328.

McClure M.W., Horne R.N. (2014). Correlations between formation properties and induced seismicity during
high pressure injection into granitic rock. *Engineering Geology* 175:74
80. doi: https://doi.org/10.1016/j.enggeo.2014.03.015

McNamara, D. E., Rubinstein, J. L., Myers, E., Smoczyk, G., Benz, H. M., Williams, R. A., Hayes, G., Wilson, D., Herrmann, R., McMahon, N. D., Aster, R. C., Bergman, E., Holland, A., & Earle, P. (2015). Efforts to monitor and characterize the recent increasing seismicity in central Oklahoma. *Leading Edge*, *34*(6), 628–639. https://doi.org/10.1190/tle34060628.1

Mitchell, B. T., & Simpson, K. (2015). A Regional Re-Evaluation of the Mississippi Lime Play, South-Central Kansas: The Risks and Rewards of Understanding Complex Geology in a

Resource Play. *Paper presented at the SPE/AAPG/SEG Unconventional Resources Technology Conference, San Antonio, Texas, USA*. https://doi.org/10.15530/URTEC-2015-2154477

Nolte, K. A., Tsoflias, G. P., Bidgoli, T. S., &Watney, W. L. (2017). Shear-wave anisotropy reveals pore fluid pressure–induced seismicity in the US midcontinent. *Science Advances*, 3(12), e1700443. https://doi.org/10.1126/sciadv.1700443

Nolte, K.A. (2020). *Investigation of Induced Seismicity in Southern Kansas* [Doctoral dissertation, University of Kansas]. University of Kansas Research Repository. https://kuscholarworks.ku.edu

Ottemöller, L., Voss, P., & Havskov, J. (2013). SEISAN EARTHQUAKE ANALYSIS SOFTWARE FOR WINDOWS, SOLARIS, LINUX and MACOSX..

Peterie, S.L., Miller, R.C., Intfen, J., Bidgoli, T.S., Buchanan, R. (2015). A geologically-based approach to mitigate potentially induced seismicity in Kansas. Society of Exploration Geophysicists Annual Meeting (Extended Abstract).

Prensky S (1992). Temperature Measurements in Boreholes - An Overview of Engineering and Scientific Applications. *The Log Analyst* 33:313–333

Quilty, E. G., & Roeloffs, E. A. (1997). Water-level changes in response to the 20 December 1994 earthquake near Parkfield, California. *Bulletin of the Seismological Society of America*, *87*(2), 310–317.

Raleigh, C. B., Healy, J. H., and Bredehoeft, J. D. (1976). An experiment in earthquake control at Rangely, Colorado, Science, 191, 1230-1237.

Roeloffs, E. (1996). Poroelastic techniques in the study of earthquake-related hydrologic phenomena. *Advances in geophysics*, *37*, 135-195.

Roeloffs, E. A. (1998). Persistent water level changes in a well near Parkfield, California, due to local and distant earthquakes. *Journal of Geophysical Research: Solid Earth*, *103*(1), 869–889. https://doi.org/10.1029/97jb02335

Rojstaczer, S., & Wolf, S. (1992). Permeability changes associated with large earthquakes: an example from Loma Prieta, California. *Geology*, *20*(3), 211–214. https://doi.org/10.1130/0091-7613

Rubinstein, J.L., Ellsworth, W.L., McGarr, A., Benz, H.M. (2014). The 2001-present induced earthquake sequence in the Raton basin of northern New Mexico and southern Colorado. Bulletin of the Seismological Society of America, 10.1785/0120140009.

Rubinstein, J.L., Mahani, A.B. (2015). Myths and Facts on Wastewater Injection, Hydraulic Fracturing, Enhanced Oil Recovery, and Induced Seismicity. Seismological Research Letters, 86, 1060-1067.

Rubinstein JL, Ellsworth WL, Dougherty SL (2018). The 2013–2016 Induced Earthquakes in Harper and Sumner Counties, Southern Kansas. *Bulletin of the Seismological Society of America* 108:674–689. doi: 10.1785/0120170209

Segall, P., Grasso, J.R., Mossop, A. (1994). Poroelastic stressing and induced seismicity near the Lacq gas field southwestern France. Journal of Geophysical Research Letters: Solid Earth, 99, 15423-15438.

Schoenball M, Ellsworth WL (2017). A Systematic Assessment of the Spatiotemporal Evolution of Fault Activation Through Induced Seismicity in Oklahoma and Southern Kansas. *Journal of Geophysical Research: Solid Earth* 122:10,110-189,206. doi: 10.1002/2017JB014850

Schwab DR, Bidgoli TS, Taylor MH (2017). Characterizing the Potential for Injection-Induced Fault Reactivation Through Subsurface Structural Mapping and Stress Field Analysis,

Wellington Field, Sumner County, Kansas. *Journal of Geophysical Research: Solid Earth* 122:10,110-132,154. doi: 10.1002/2017JB014071

Steeples, D.W., Bennett, B.C., Park, C.B., Miller, R.D., and Knapp, R.W., (1990), Microearthquakes in Kansas and Nebraska, 1977-1989: Kansas Geological Survey, Open-file Report 90-10.

Tiira, T., Uski, M., Kortström, J., Kaisko, O., & Korja, A. (2016). Local seismic network for monitoring of a potential nuclear power plant area. *Journal of Seismology*, *20*(2), 397–417. https://doi.org/10.1007/s10950-015-9534-8

Trnkoczy, A. (2009). Understanding and parameter setting of STA/LTA trigger algorithm. In *New Manual of Seismological Observatory Practice (NMSOP)* (pp. 1-20). Deutsches GeoForschungsZentrum GFZ.

United States. Environmental Protection Agency. Underground Injection Control Regulations and Safe Drinking Water Act Provisions. Washington, D.C.: GPO, 1974. Web. 15 Sept. 2021.

Walsh, FR, Zoback, MD (2015). Oklahoma's recent earthquakes and saltwater disposal. *Science Advances*, *1*(5), e1500195. https://doi.org/10.1126/sciadv.1500195

Walter, J.I., Chang, J.C., Dotray, P.J. (2017). Foreshock seismicity suggests gradual differential stress increase in the months prior to the 3 September 2016 Mw 5.8 Pawnee earthquake. Seismological Research Letters, doi:10.1785/0220170007.

Wang, C. Y., Chia, Y., Wang, P. L., & Dreger, D. (2009). Role of S waves and Love waves in coseismic permeability enhancement. *Geophysical Research Letters*, *36*(9), 1–5. https://doi.org/10.1029/2009GL037330

Wang, SJ, Hsu, KC, Wang, CL, Lai, WC, & Hsu, LT (2017). Evaluation of Hydraulic Properties of Aquitards Using Earthquake-Triggered Groundwater Variation. *Groundwater*, *55*(5), 747–756. https://doi.org/10.1111/gwat.12519

Watney, WL., Bidgoli TS, Victorine J, Simpson P, Holubnyak Y, Nolte K, Tsoflias GP, Wreath D, Birdie TR (2016). Continuous Pressure and Temperature Monitoring in Lower Arbuckle Saline Aquifer in Wellington Field, Sumner County, Kansas-Response to the M5. 8 Pawnee Earthquake. *AGU Fall Meeting Abstracts*.

Yeck, W.L., Hayes, G.P., Mcnamara, D.E., Rubinstein, J.L., Barnhart, W.D., Earle, P.S., Benz, H.M. (2017). Oklahoma experiences largest earthquake during ongoing regional wastewater injection hazard mitigation efforts. Geophysical Research Letters, 44.

Zhang, S, Shi, Z, & Wang, G (2019). Comparison of aquifer parameters inferred from water level changes induced by slug test, earth tide and earthquake – A case study in the three Gorges area. *Journal of Hydrology*, *579*, 124169. https://doi.org/https://doi.org/10.1016/j.jhydrol.2019.124169

Zhang, S, Shi, Z, Wang, G, & Zhang, Z (2018). Quantitative Assessment of the Mechanisms of Earthquake-Induced Groundwater-Level Change in the MP Well, Three Gorges Area. *Pure & Applied Geophysics*, *175*(7), 2475–2484. http://10.0.3.239/s00024-017-1643-6

Data and Resources

All data needed to evaluate the conclusions in this study are present in the paper and/or the Supplementary Materials. Project data is available through the IRIS Data Management Center. Additional data related to this paper may be requested from the authors. The regional earthquake catalog may be accessed at http://earthquake.usgs.gov/earthquakes/search/. The IRIS repository may be accessed at http://ds.iris.edu/ds/. The regional array ran by the USGS can be found at that link with a network ID of GS and the local array ran at Wellington Field has an ID of ZA. Pressure and temperature data are available through the Kansas Geological Survey oil and gas well database (http://www.kgs.ku.edu/PRS/Ozark/Summary/CO2_II.html). SEISAN is available through seisan.info. HYPOINVERSE was used directly in SEISAN. All websites were last accessed in September 2021

Appendix A: Extra Figures

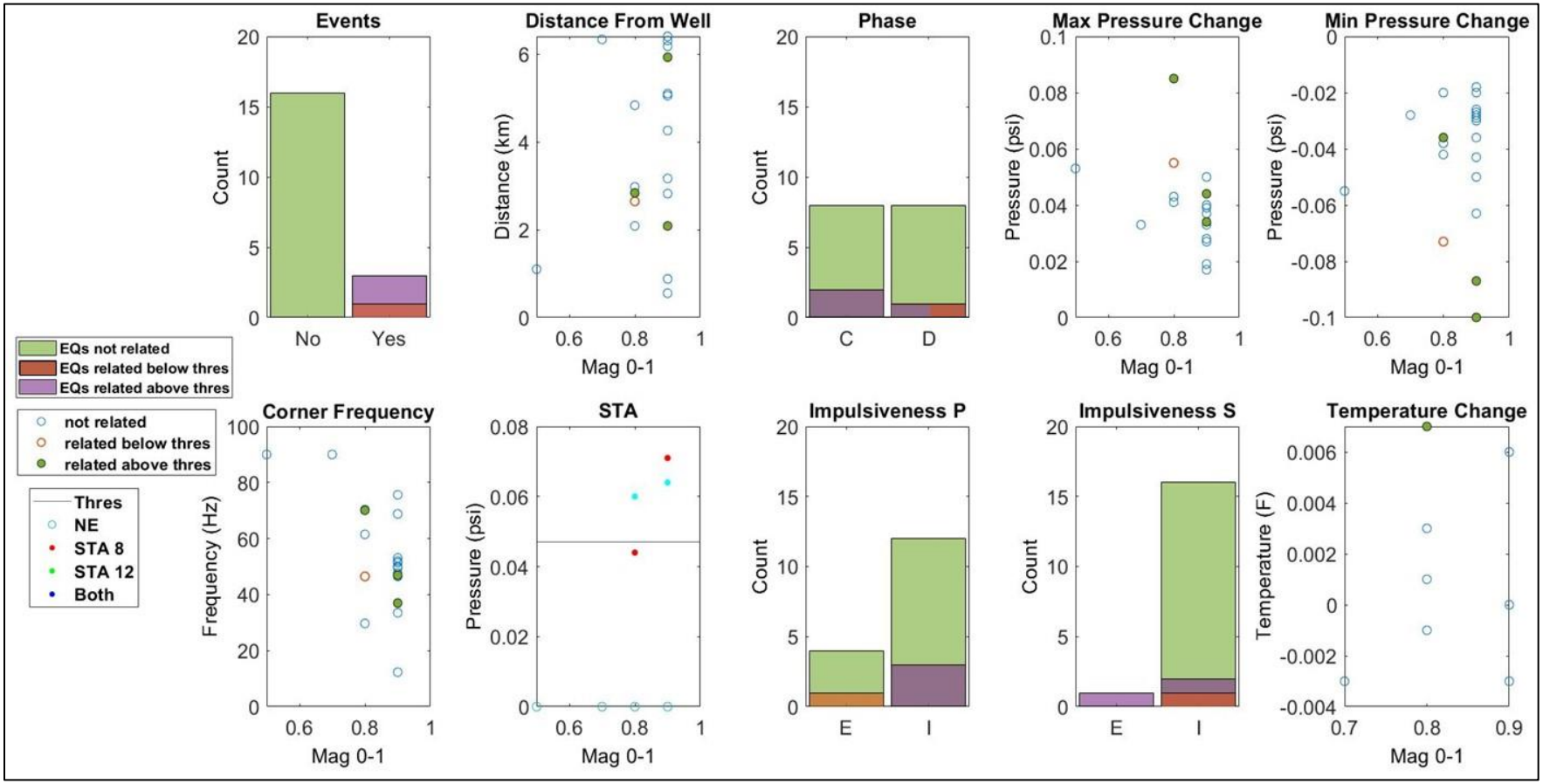

Earthquake, pressure, and temperature analysis for magnitude 0 to 1 events. There were 20 magnitude 0 to 1 events in the catalog. Sixteen of the events were not related to pressure changes, 4 events were related to pressure changes, and 3 were above the noise threshold. The bar graph and scatter plot colors differ based on whether the earthquakes related to pressure changes, whether they related to pressure changes but were below the noise threshold and whether they related to pressure changes and were above the noise threshold. The earthquakes with this range of magnitude were commonly dilatational in phase and had more impulsive S and P wave arrivals. Also, as the magnitude increased the distance from the pressure monitoring station increased. There is no strong correlation between events that related to pressure changes and the distance from the pressure station, the corner frequency, and the change in temperature. Events that related to pressure changes and were above the noise threshold had differentiable minimum/maximum pressure changes from events that were not noted by the STA/LTA. The STA plot depicts the STA value of the events that related to pressure changes and were above the noise threshold of 0.047. The black line depicts this noise threshold and everything above this line is events that had significant pressure changes above noise.

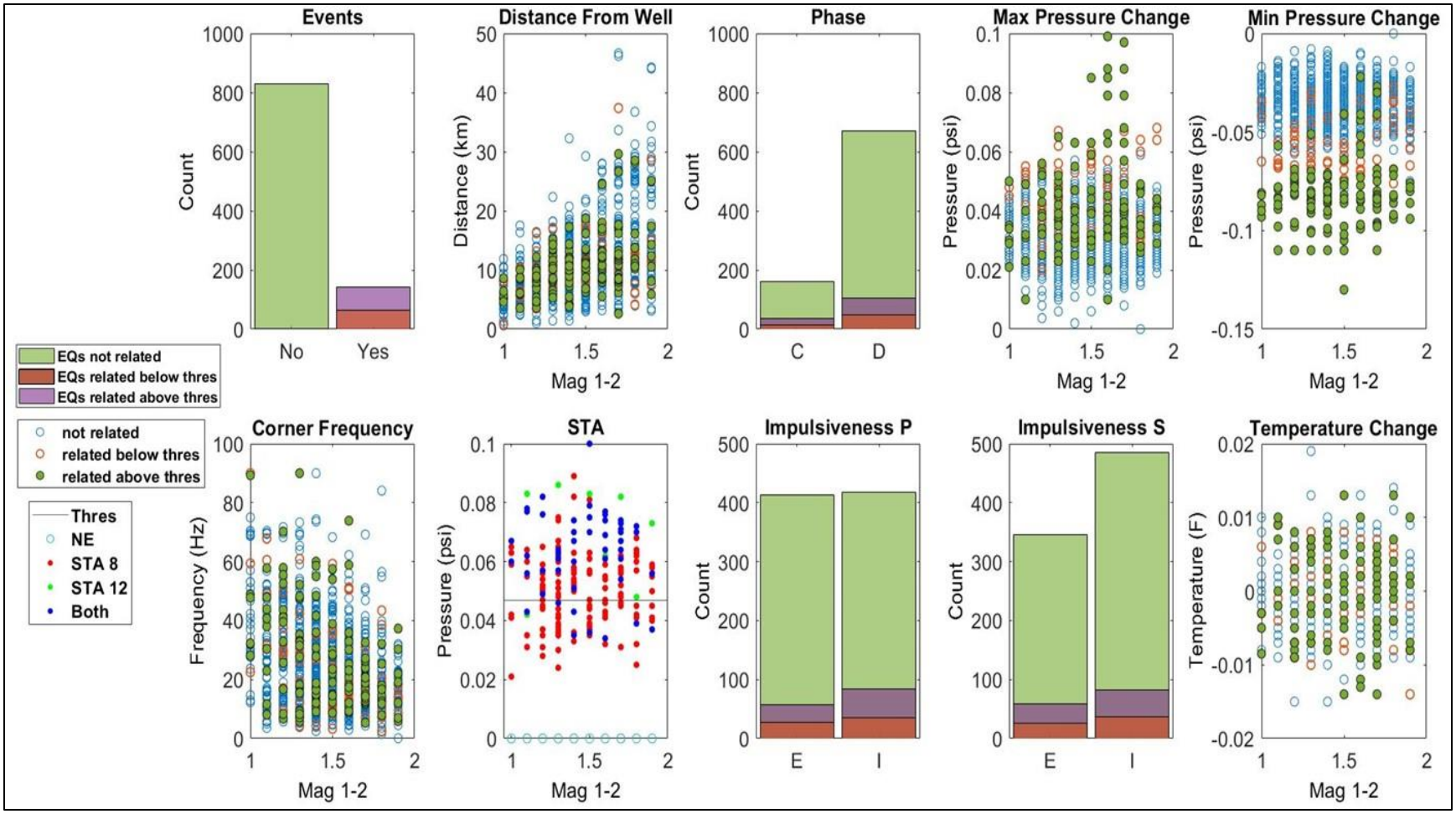

Earthquake, pressure, and temperature analysis for magnitude 1 to 2 events. There were 1035 magnitude 1 to 2 events in the catalog. Eight hundred and thirty-one events were not related to pressure changes, 204 events were related to pressure changes, and 141 were above the noise threshold. The bar graph and scatter plot colors differ based on whether the earthquakes related to pressure changes, whether they related to pressure changes but were below the noise threshold and whether they related to pressure changes and were above the noise threshold. The earthquakes with this range of magnitude were commonly dilatational in phase and had more impulsive S and P wave arrivals. Also, as the magnitude increased the distance from the pressure monitoring station increased. There is no strong correlation between events that related to pressure changes and the distance from the pressure station, the corner frequency, and the change in temperature. Events that related to pressure changes and were above the noise threshold had differentiable minimum/maximum pressure changes from events that were not noted by the STA/LTA. The STA plot depicts the STA value of the events that related to pressure changes and were above the noise threshold of 0.047. The black line depicts this noise threshold and everything above this line is events that had significant pressure changes above noise.

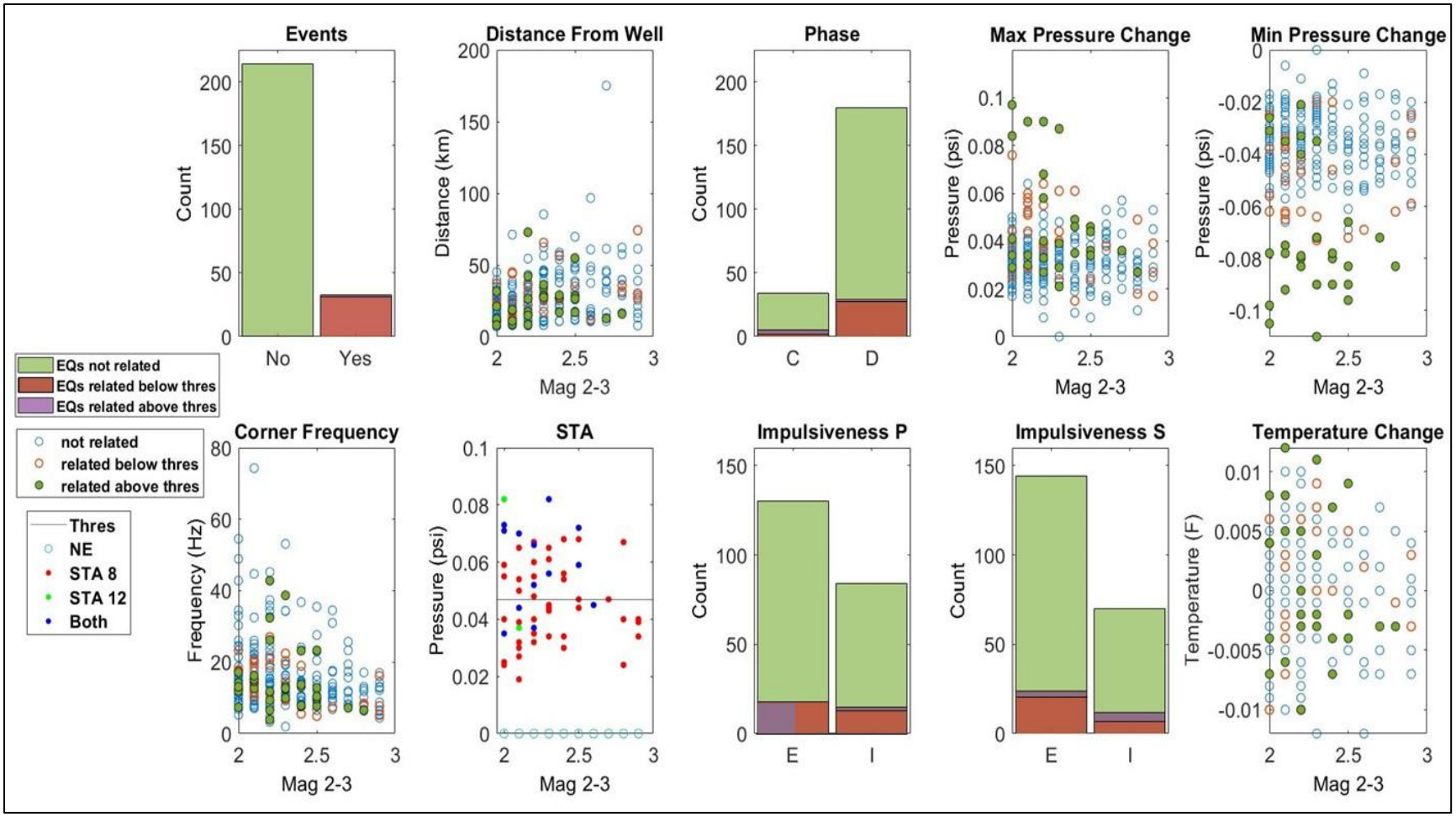

Earthquake, pressure, and temperature analysis for magnitude 2 to 3 events. There were 278 magnitude 2 to 3 events in the catalog. Two hundred and fourteen of the events were not related to pressure changes, 64 events were related to pressure changes, and 33 were above the noise threshold. The bar graph and scatter plot colors differ based on whether the earthquakes related to pressure changes, whether they related to pressure changes but were below the noise threshold and whether they related to pressure changes and were above the noise threshold. The earthquakes with this range of magnitude were commonly dilatational in phase and had more emergent S and P wave arrivals. Also, as the magnitude increased the distance from the pressure monitoring station only slightly increased. There is no strong correlation between events that related to pressure changes and the distance from the pressure station, the corner frequency, and the change in temperature. Events that related to pressure changes and were above the noise threshold had differentiable minimum/maximum pressure changes from events that were not noted by the STA/LTA. The STA plot depicts the STA value of the events that related to pressure changes and were above the noise threshold of 0.047. The black line depicts this noise threshold and everything above this line is events that had significant pressure changes above noise.

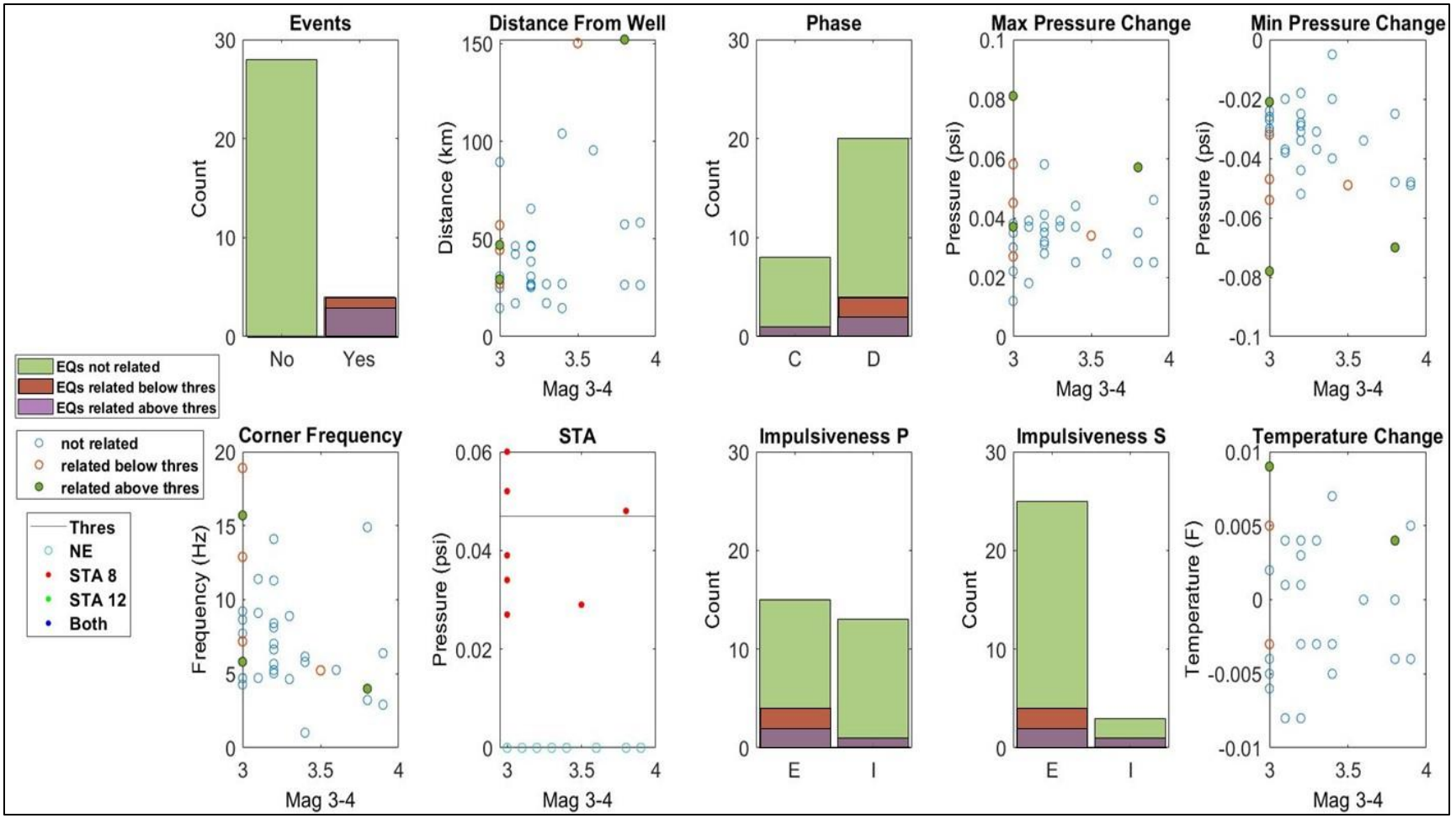

Earthquake, pressure, and temperature analysis for magnitude 3 to 4 events. There were 35 magnitude 3 to 4 events in the catalog. Twenty-eight of the events were not related to pressure changes, 7 events were related to pressure changes, and 3 events above the noise threshold. The bar graph and scatter plot colors differ based on whether the earthquakes related to pressure changes, whether they related to pressure changes but were below the noise threshold and whether they related to pressure changes and were above the noise threshold. The earthquakes with this range of magnitude were commonly dilatational in phase and had more emergent S and P wave arrivals. Also, as the magnitude increased the distance from the pressure monitoring station only slightly increased. There is no strong correlation between events that related to pressure changes and the distance from the pressure station, the corner frequency, and the change in temperature. Events that related to pressure changes and were above the noise threshold had differentiable minimum/maximum pressure changes from events that were not noted by the STA/LTA. The STA plot depicts the STA value of the events that related to pressure changes and were above the noise threshold of 0.047. The black line depicts this noise threshold and everything above this line is events that had significant pressure changes above noise.

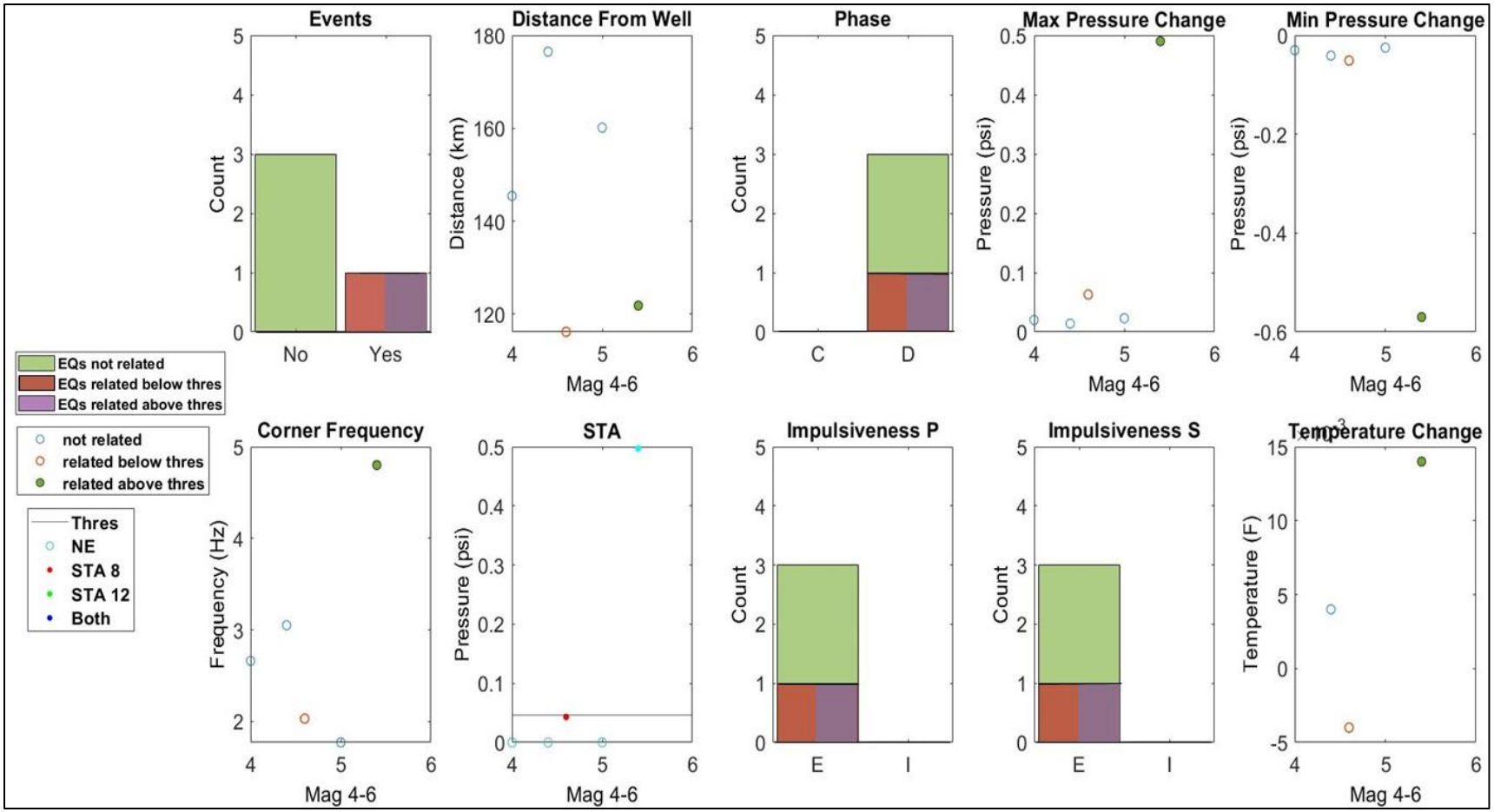

Earthquake, pressure, and temperature analysis for magnitude 4 to 6 events. There were 5 magnitude 4 to 6 events in the catalog. Three of the events were not related to pressure changes, 2 events were related to pressure changes, and only 1 was above the noise threshold. The bar graph and scatter plot colors differ based on whether the earthquakes related to pressure changes, whether they related to pressure changes but were below the noise threshold and whether they related to pressure changes and were above the noise threshold. The earthquakes with this range of magnitude were commonly dilatational in phase and had more emergent S and P wave arrivals. Also, as the magnitude increased the distance from the pressure monitoring station only slightly increased. There is no strong correlation between events that related to pressure changes and the distance from the pressure station, the corner frequency, and the change in temperature. Events that related to pressure changes and were above the noise threshold had differentiable minimum/maximum pressure changes from events that were not noted by the STA/LTA. STA plot depicts the STA value of the events that related to pressure changes and were above the noise threshold of 0.047. The black line depicts this noise threshold and everything above this line is events that had significant pressure changes above noise.of 0.047. The black line depicts this noise threshold and everything above this line is events that had significant pressure changes above noise.

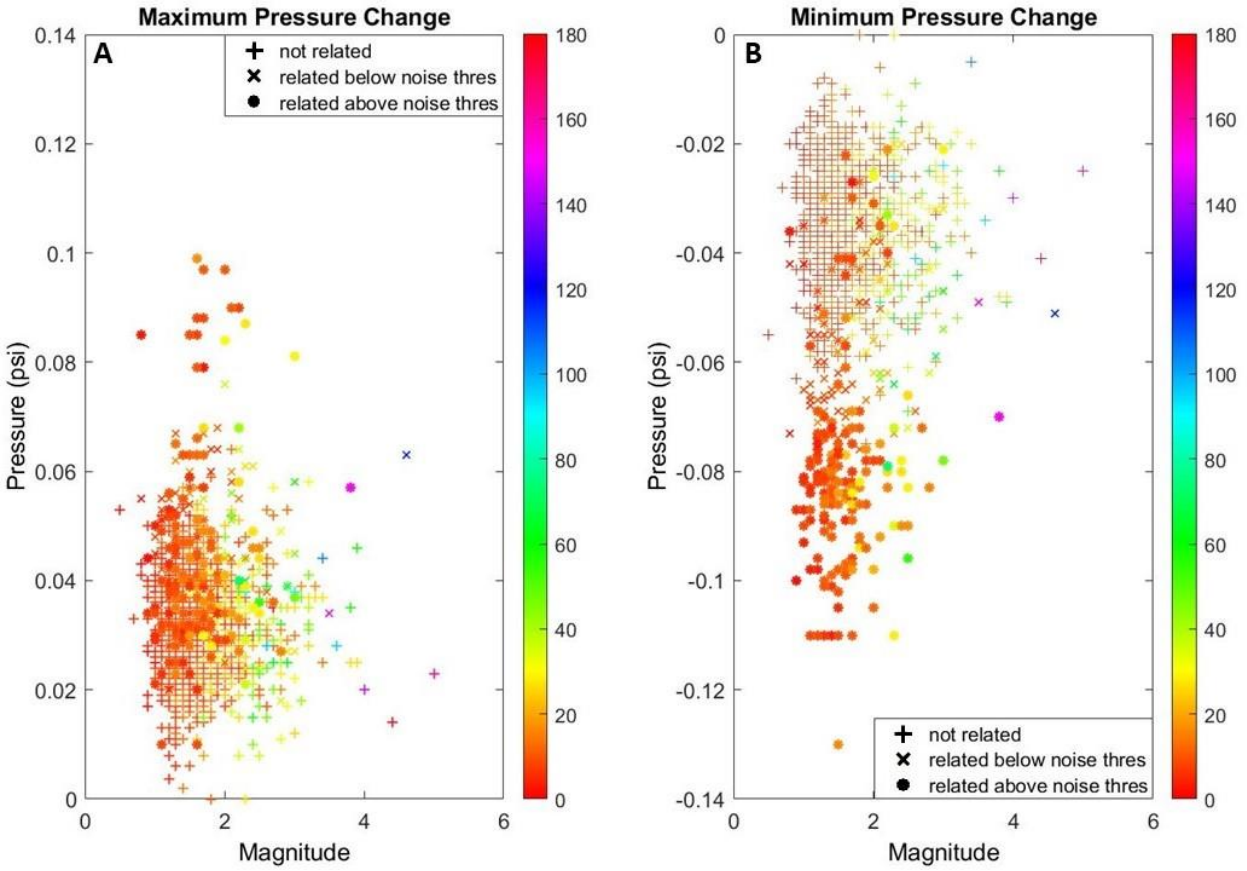

A) Comparison of earthquake magnitude versus maximum pressure changes for all earthquakes. Earthquakes related to pressure changes have a wide range of maximum pressure changes from 0.02 psig to 0.1 psig. B) Comparison of magnitude versus minimum pressure changes. Earthquakes related to pressure changes have a greater minimum pressure change of around –0.09 psig compared to other events in the catalogue. The plus signs are events that are not related to coseismic pressure changes, the x's are events related to coseismic pressure changes but below the noise threshold of 0.047 psig, and the stars are events related to coseismic pressure changes and above the noise threshold. The colors represent distance from the pressure monitoring station in km. Red is 0 km's away and pink is 180 km's away. Based on this figure earthquakes related to coseismic pressure changes are commonly closer to the pressure station. The Pawnee earthquake was not plotted due it having significantly larger pressure changes compared to the other earthquakes of interest.

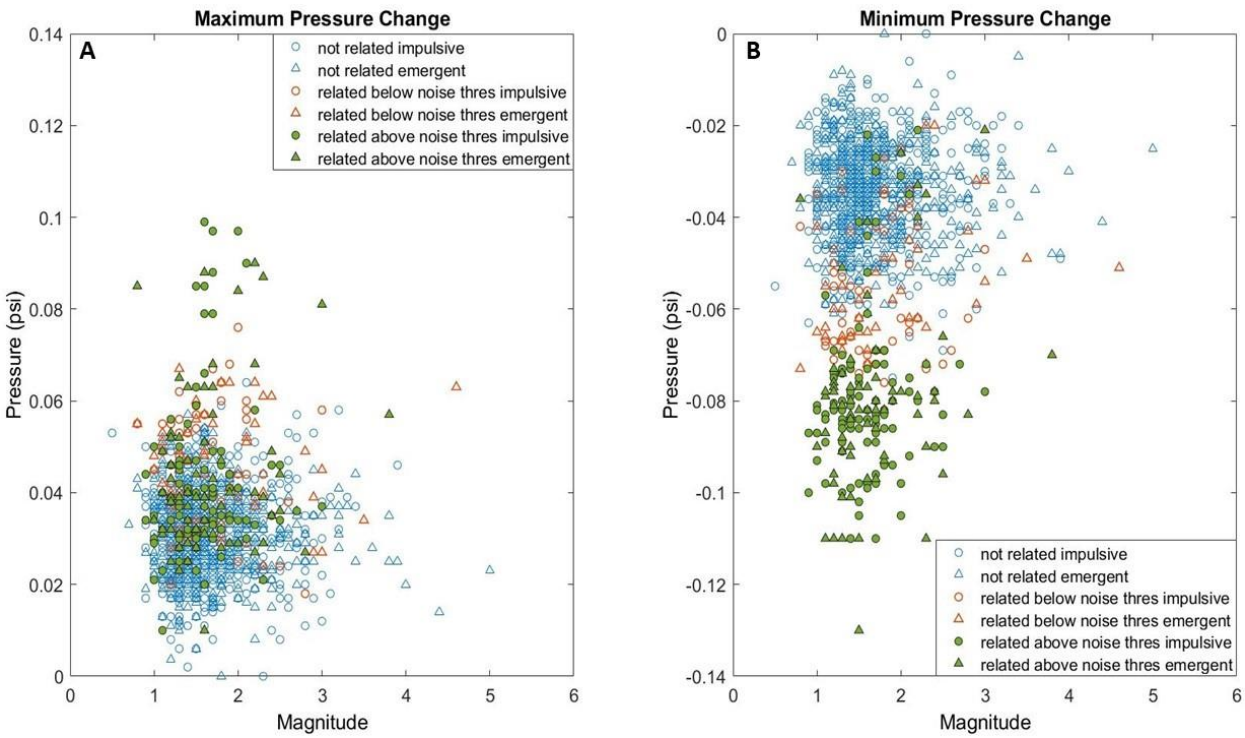

A) Comparison of earthquake magnitude versus maximum pressure changes for all earthquakes. Earthquakes related to pressure changes have a wide range of maximum pressure changes from 0.02 psig to 0.1 psig. B) Comparison of magnitude versus minimum pressure changes. Earthquakes related to pressure changes have a greater minimum pressure change of around –0.09 psig compared to other events in the catalogue. The blue open circles are events that are impulsive and not related to coseismic pressure changes. The blue open trianges are events that are emergent and not related to pressure. The orange open circles are events related to coseismic pressure changes but below the noise threshold of 0.047 psig and are impulsive. The orange open triangles are events below the noise threshold that are emergent. The green circles are events related to coseismic pressure changes and above the noise threshold and are impulsive. The green triangles are events that are above the noise threshold but are emergent. There is no clear relationship between impulsiveness and earthquakes related to pressure changes.The Pawnee earthquake was not plotted due it having significantly larger pressure changes compared to the other earthquakes of interest.

STA/LTA Results Continued

Earthquakes Related to Pressure but Below the Noise Threshold

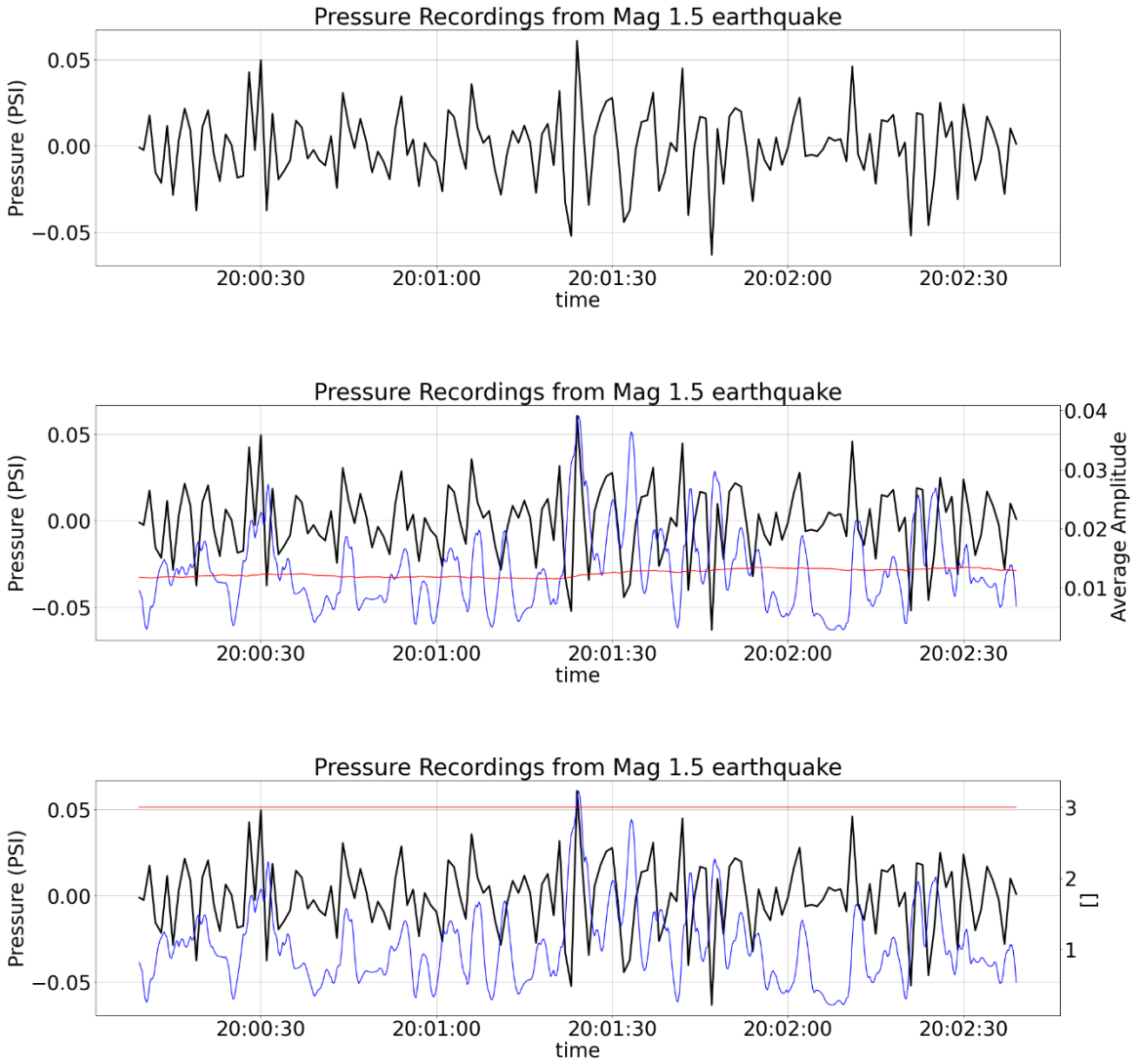

STA/LTA results using the pressure data from a magnitude 1.5 earthquake on October 1st, 2016 at 20:01:07. This earthquake was located 10 km from the pressure monitoring station. The top panel shows the tidal filtered pressure data in black at the time of the event. The middle panel shows the derivative of the pressure in black, the short term average (STA) in blue and the long term average (LTA) in red. The bottom panel has the ratio of the STA/LTA in blue, the trigger threshold in red, and the derivative of the pressure in black.

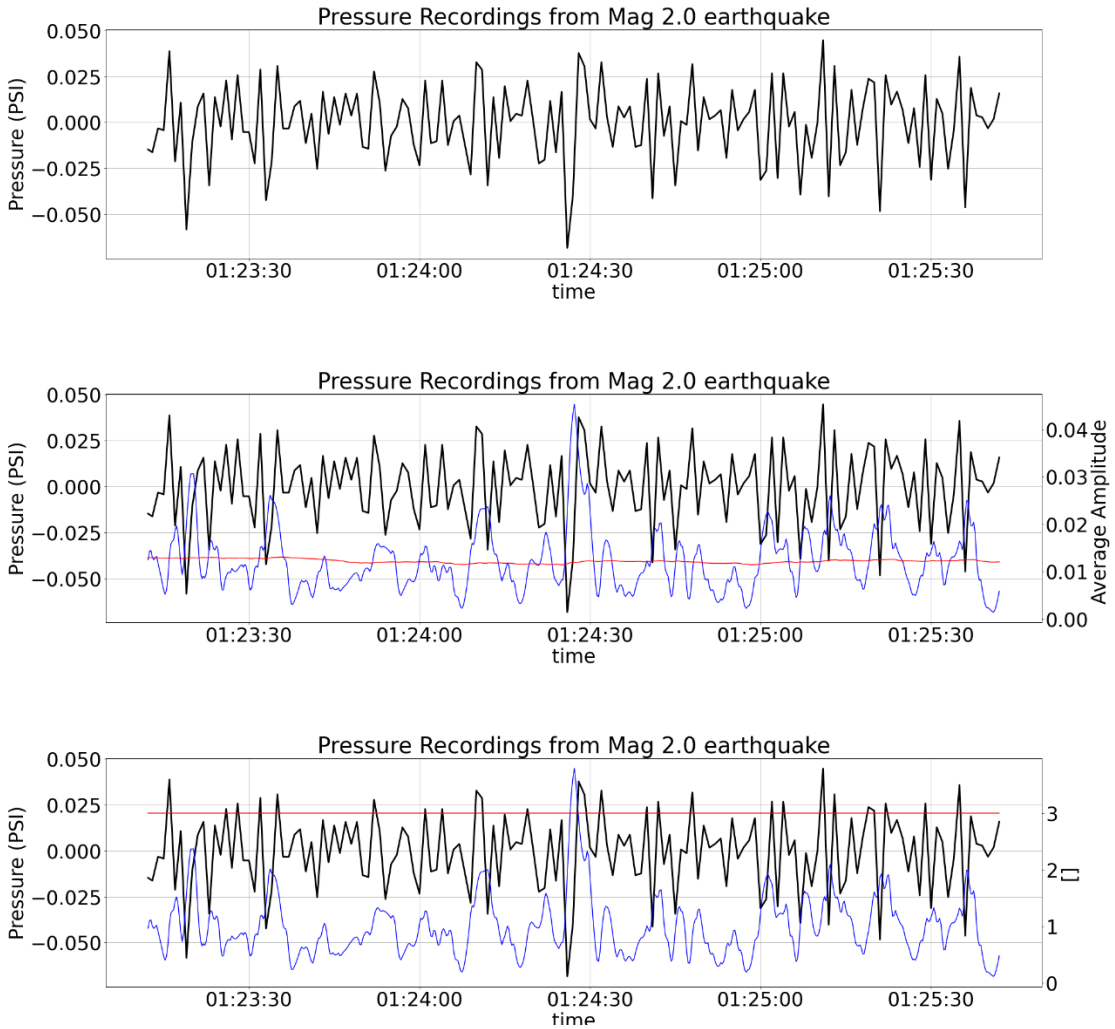

STA/LTA results using the pressure data from a magnitude 2.0 earthquake on November 26th, 2016 at 01:21:06. This earthquake was located 21 km from the pressure monitoring station. The top panel shows the tidal filtered pressure data in black at the time of the event. The middle panel shows the derivative of the pressure in black, the short term average (STA) in blue and the long term average (LTA) in red. The bottom panel has the ratio of the STA/LTA in blue, the trigger threshold in red, and the derivative of the pressure in black.

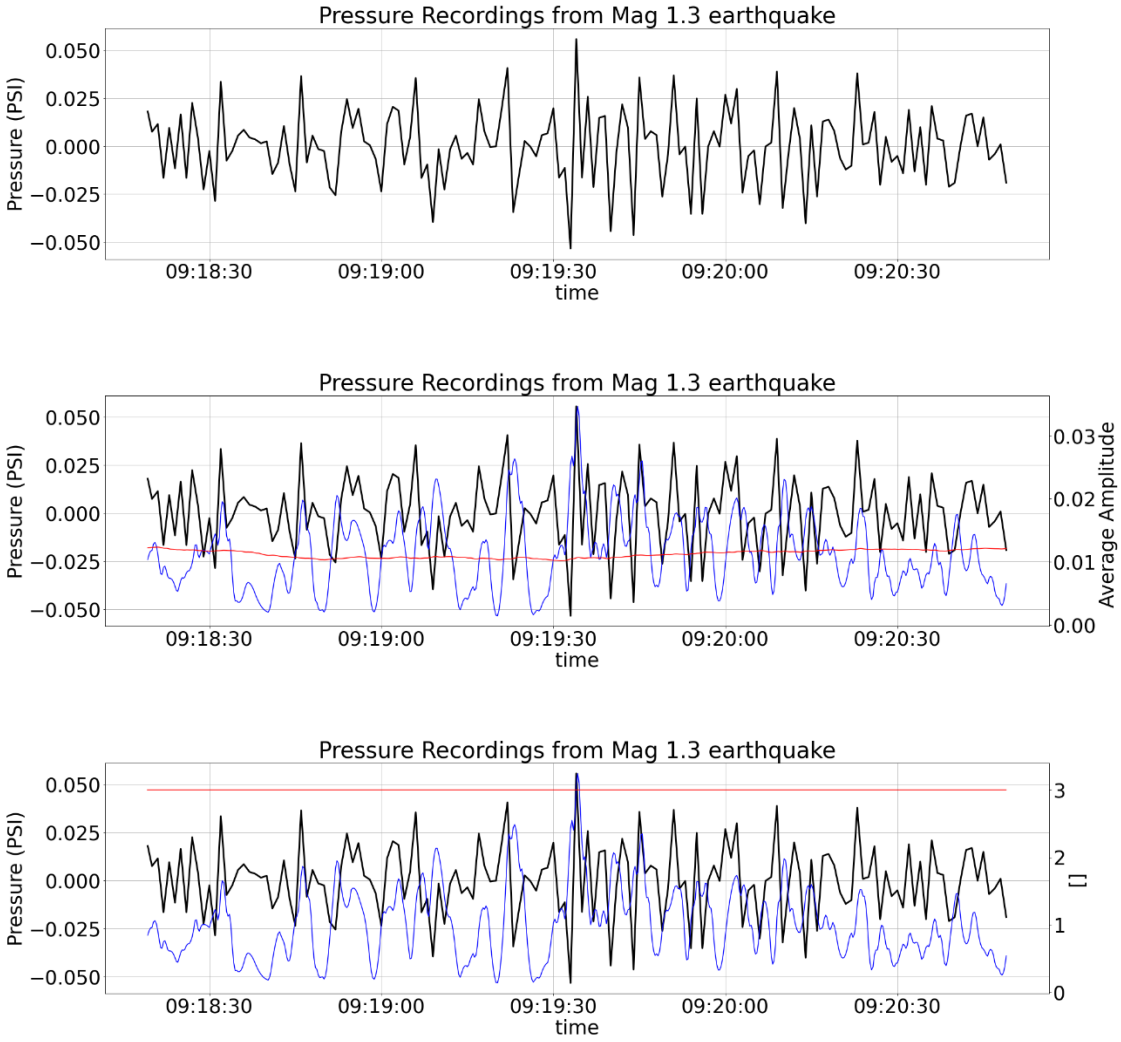

STA/LTA results using the pressure data from a magnitude 1.3 earthquake on December 12, 2016 at 09:10:57. This earthquake was located 10 km from the pressure monitoring station. The top panel shows the tidal filtered pressure data in black at the time of the event. The middle panel shows the derivative of the pressure in black, the short term average (STA) in blue and the long term average (LTA) in red. The bottom panel has the ratio of the STA/LTA in blue, the trigger threshold in red, and the derivative of the pressure in black.

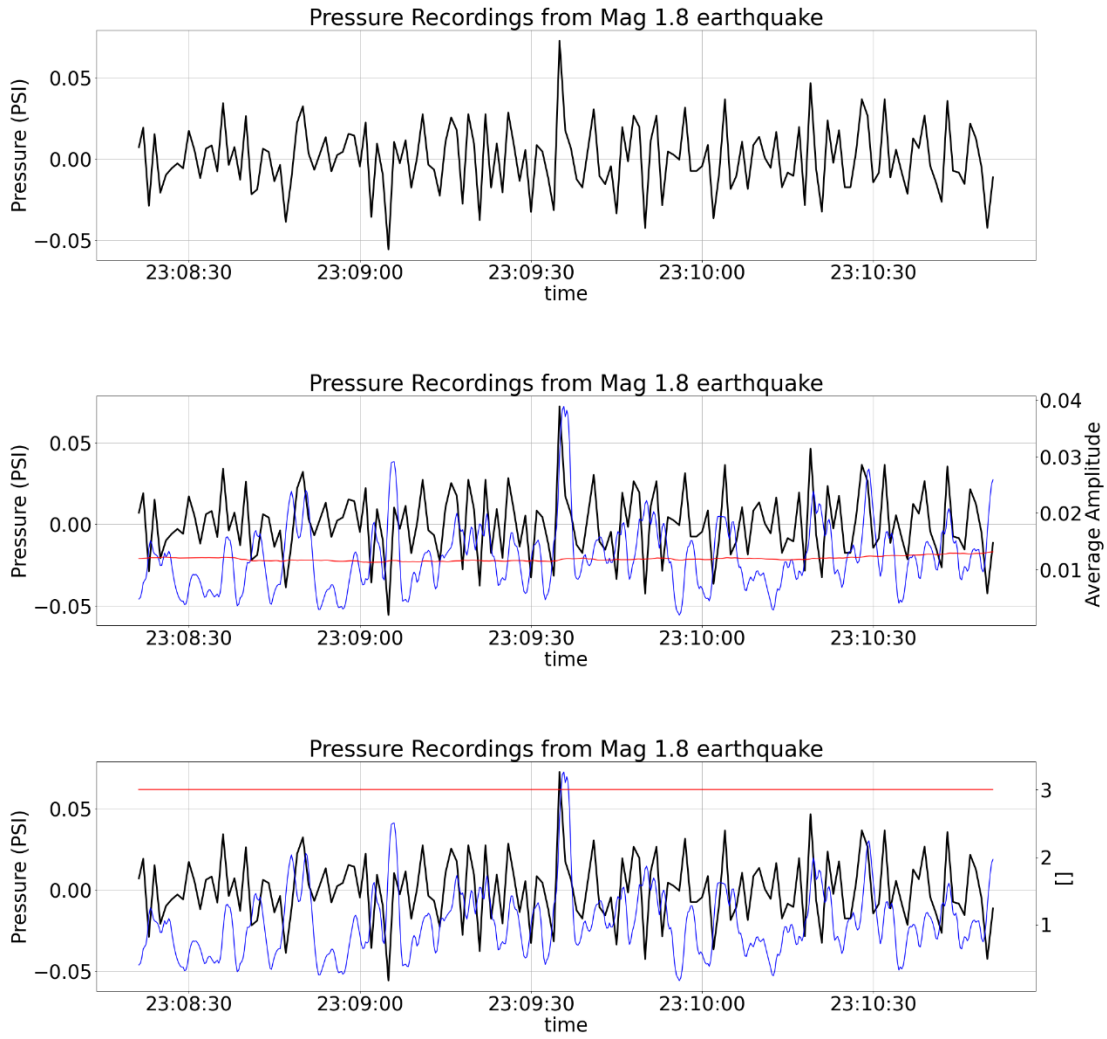

STA/LTA results using the pressure data from a magnitude 1.8 earthquake on January 1st, 2017 at 23:02:37. This earthquake was located 4 km from the pressure monitoring station. The top panel shows the tidal filtered pressure data in black at the time of the event. The middle panel shows the derivative of the pressure in black, the short term average (STA) in blue and the long term average (LTA) in red. The bottom panel has the ratio of the STA/LTA in blue, the trigger threshold in red, and the derivative of the pressure in black.

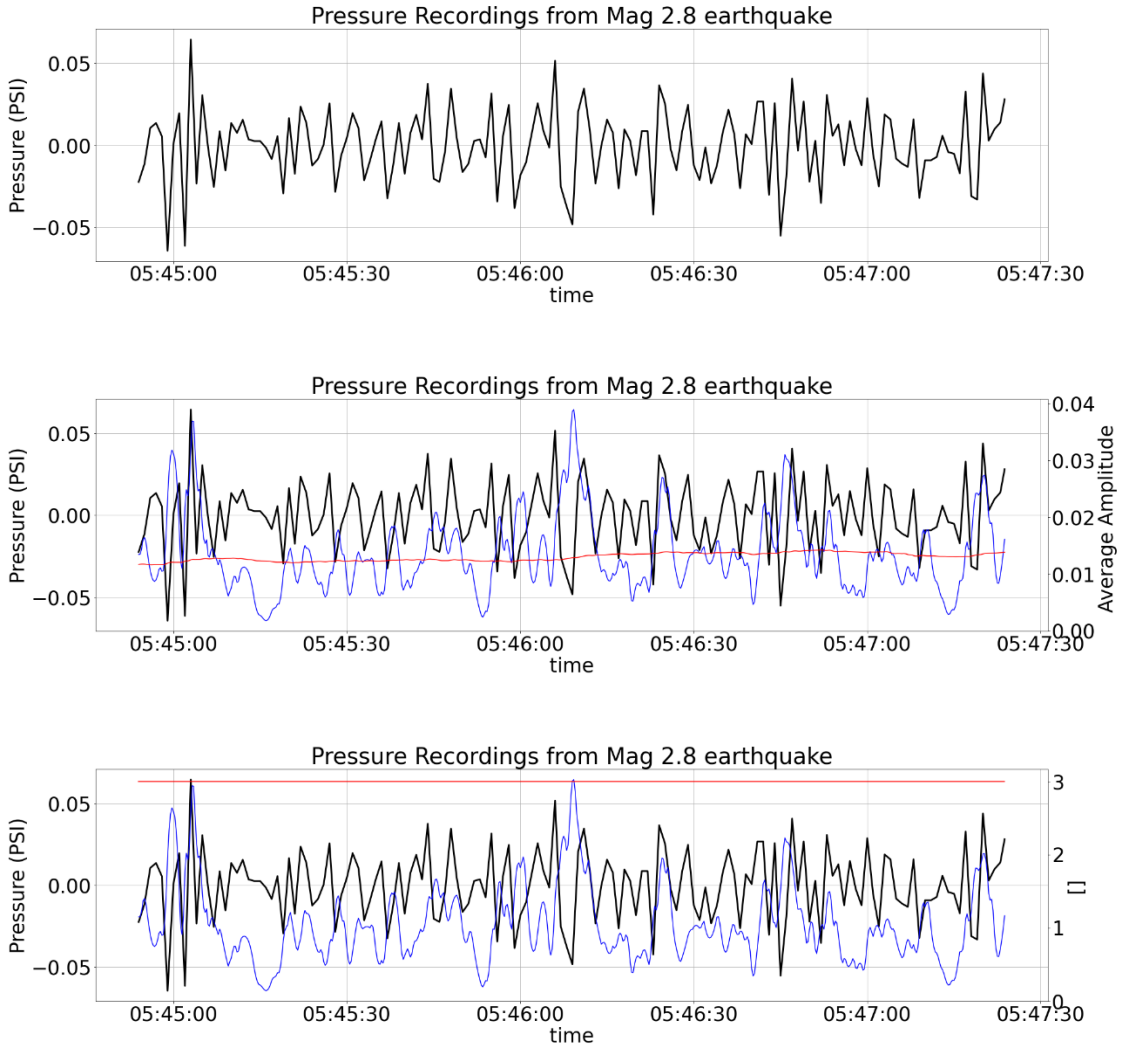

STA/LTA results using the pressure data from a magnitude 2.8 earthquake on February 25, 2017 at 05:36:43. This earthquake was located 32 km from the pressure monitoring station. The top panel shows the tidal filtered pressure data in black at the time of the event. The middle panel shows the derivative of the pressure in black, the short term average (STA) in blue and the long term average (LTA) in red. The bottom panel has the ratio of the STA/LTA in blue, the trigger threshold in red, and the derivative of the pressure in black.

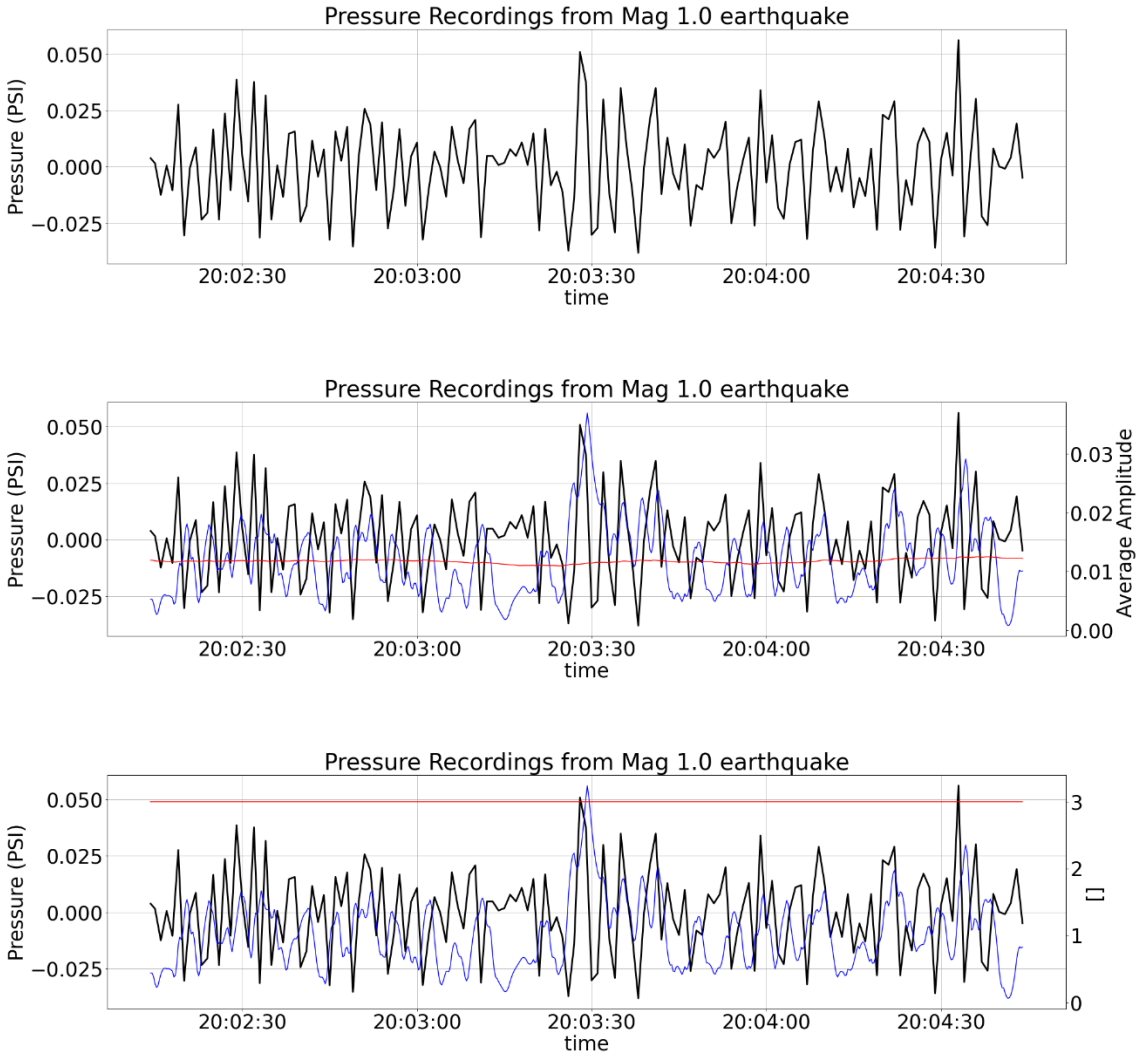

STA/LTA results using the pressure data from a magnitude 1.0 earthquake on March 12, 2017 at 19:58:09. This earthquake was located 0.85 km from the pressure monitoring station. The top panel shows the tidal filtered pressure data in black at the time of the event. The middle panel shows the derivative of the pressure in black, the short term average (STA) in blue and the long term average (LTA) in red. The bottom panel has the ratio of the STA/LTA in blue, the trigger threshold in red, and the derivative of the pressure in black.

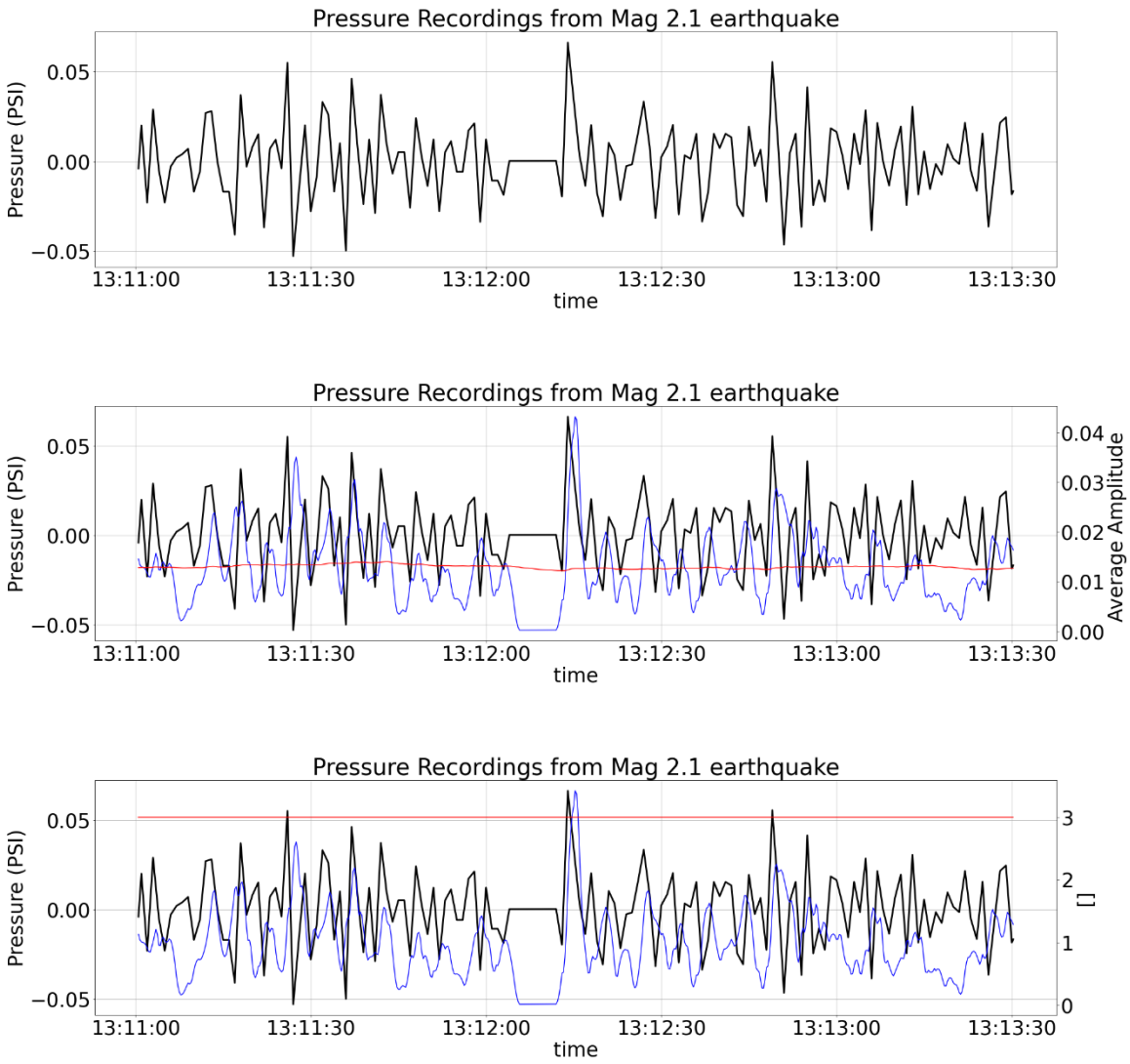

STA/LTA results using the pressure data from a magnitude 2.1 earthquake on April 21, 2017 at 13:21:41. This earthquake was located 10.4 km from the pressure monitoring station. The top panel shows the tidal filtered pressure data in black at the time of the event. The middle panel shows the derivative of the pressure in black, the short term average (STA) in blue and the long term average (LTA) in red. The bottom panel has the ratio of the STA/LTA in blue, the trigger threshold in red, and the derivative of the pressure in black.

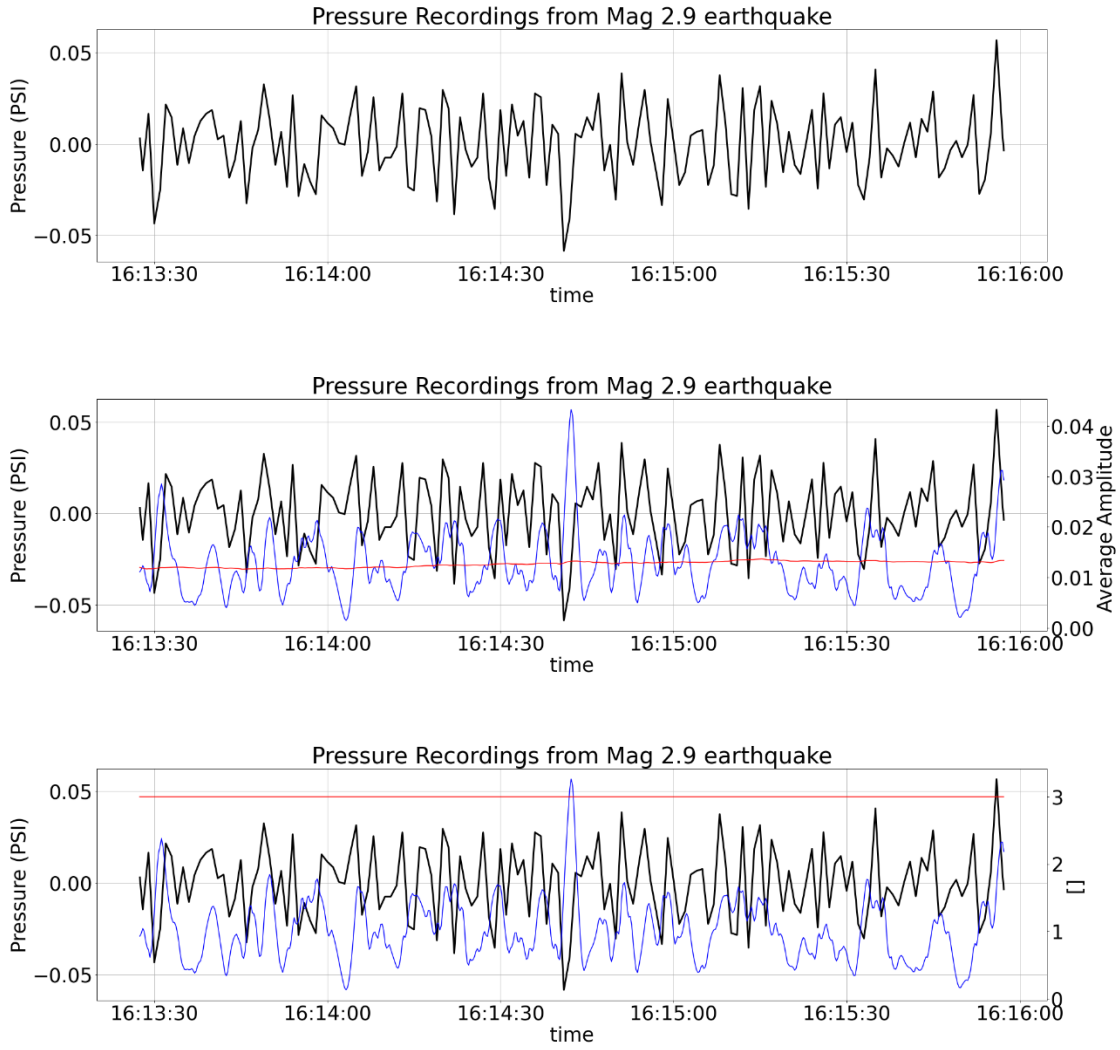

STA/LTA results using the pressure data from a magnitude 2.9 earthquake on May 7, 2017 at 16:08:21. This earthquake was located 74 km from the pressure monitoring station. The top panel shows the tidal filtered pressure data in black at the time of the event. The middle panel shows the derivative of the pressure in black, the short term average (STA) in blue and the long term average (LTA) in red. The bottom panel has the ratio of the STA/LTA in blue, the trigger threshold in red, and the derivative of the pressure in black.

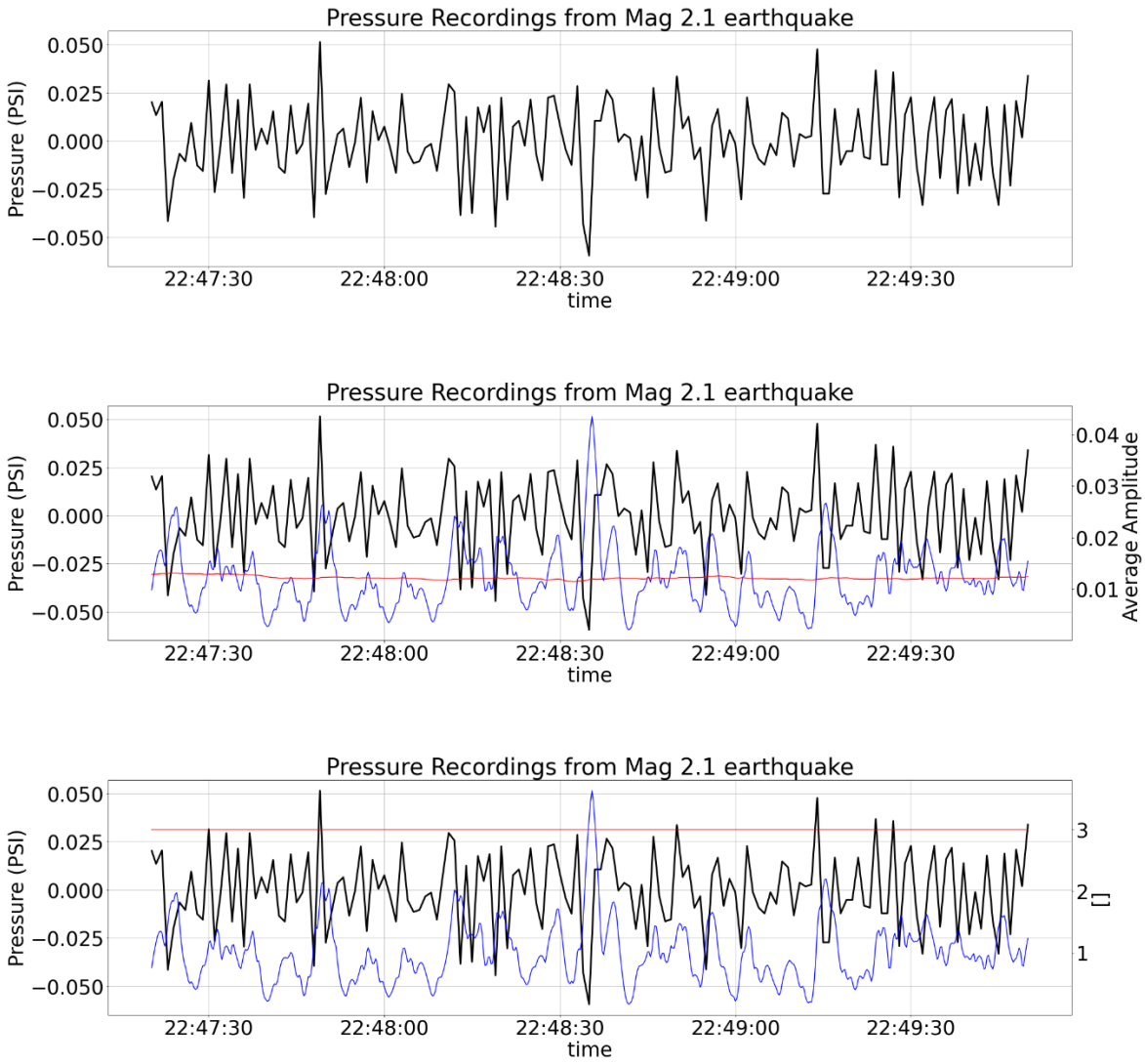

STA/LTA results using the pressure data from a magnitude 2.1 earthquake on June 1, 2017 at 22:48:38. This earthquake was located 12 km from the pressure monitoring station. The top panel shows the tidal filtered pressure data in black at the time of the event. The middle panel shows the derivative of the pressure in black, the short term average (STA) in blue and the long term average (LTA) in red. The bottom panel has the ratio of the STA/LTA in blue, the trigger threshold in red, and the derivative of the pressure in black.

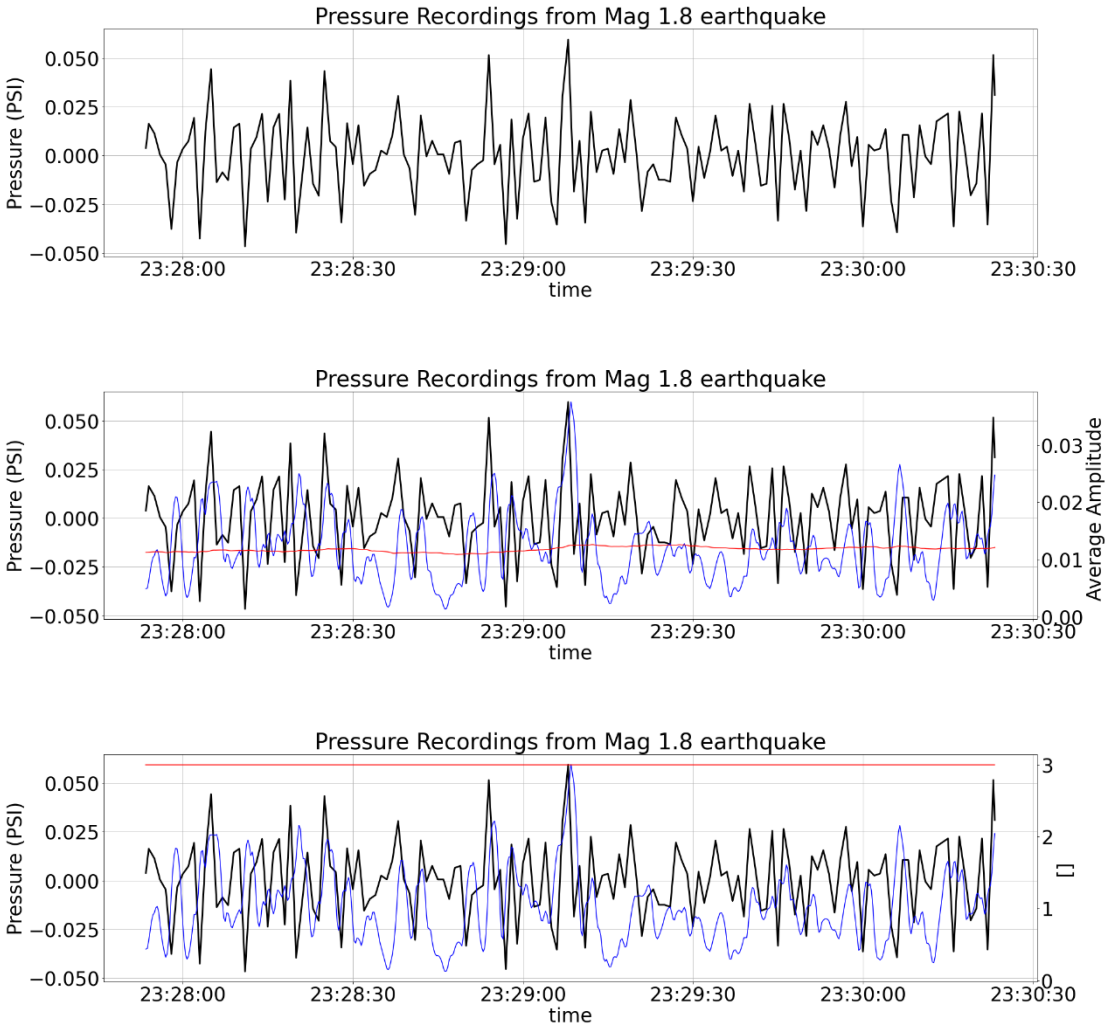

STA/LTA results using the pressure data from a magnitude 1.8 earthquake on July 29, 2017 at 23:28:05. This earthquake was located 6 km from the pressure monitoring station. The top panel shows the tidal filtered pressure data in black at the time of the event. The middle panel shows the derivative of the pressure in black, the short term average (STA) in blue and the long term average (LTA) in red. The bottom panel has the ratio of the STA/LTA in blue, the trigger threshold in red, and the derivative of the pressure in black.

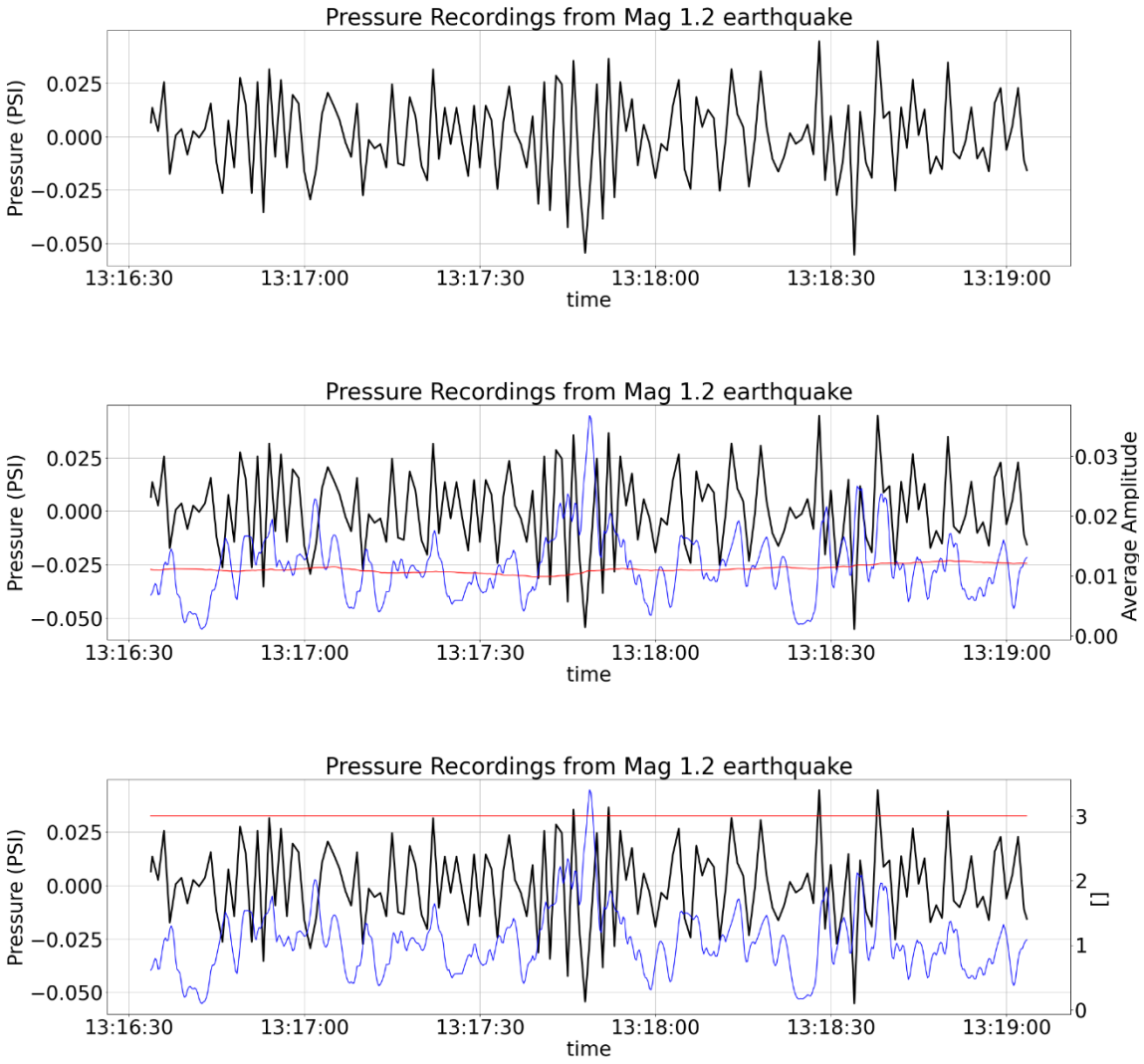

STA/LTA results using the pressure data from a magnitude 1.2 earthquake on August 22, 2017 at 13:17:40. This earthquake was located 32 km from the pressure monitoring station. The top panel shows the tidal filtered pressure data in black at the time of the event. The middle panel shows the derivative of the pressure in black, the short term average (STA) in blue and the long term average (LTA) in red. The bottom panel has the ratio of the STA/LTA in blue, the trigger threshold in red, and the derivative of the pressure in black.

Earthquakes Related to Pressure and Above the Noise Threshold

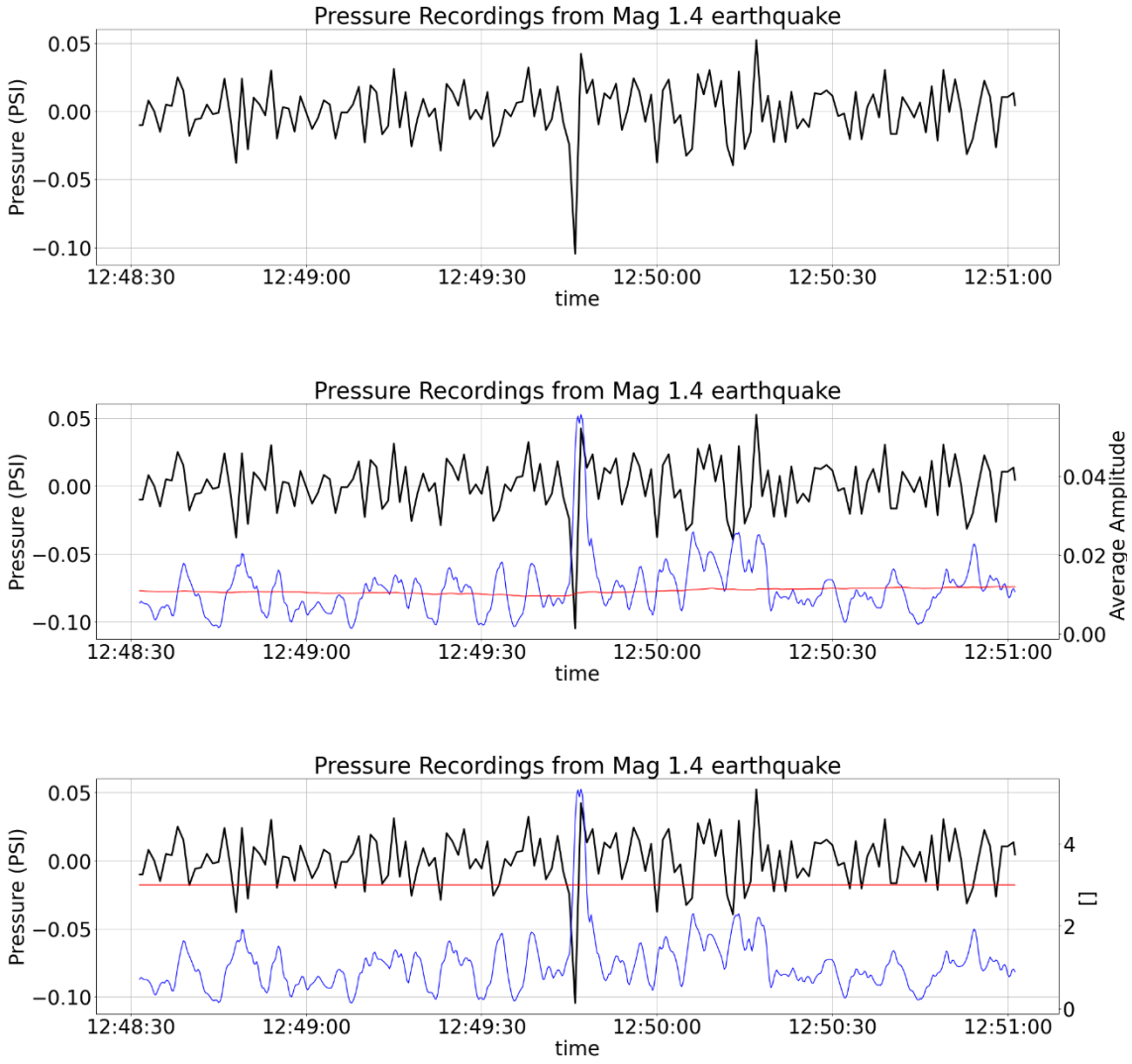

STA/LTA results using the pressure data from a magnitude 1.4 earthquake on October 4th, 2016 at 12:41:53. This earthquake was located 36 km from the pressure monitoring station. The top panel shows the tidal filtered pressure data in black at the time of the event. The middle panel shows the derivative of the pressure in black, the short term average (STA) in blue and the long term average (LTA) in red. The bottom panel has the ratio of the STA/LTA in blue, the trigger threshold in red, and the derivative of the pressure in black.

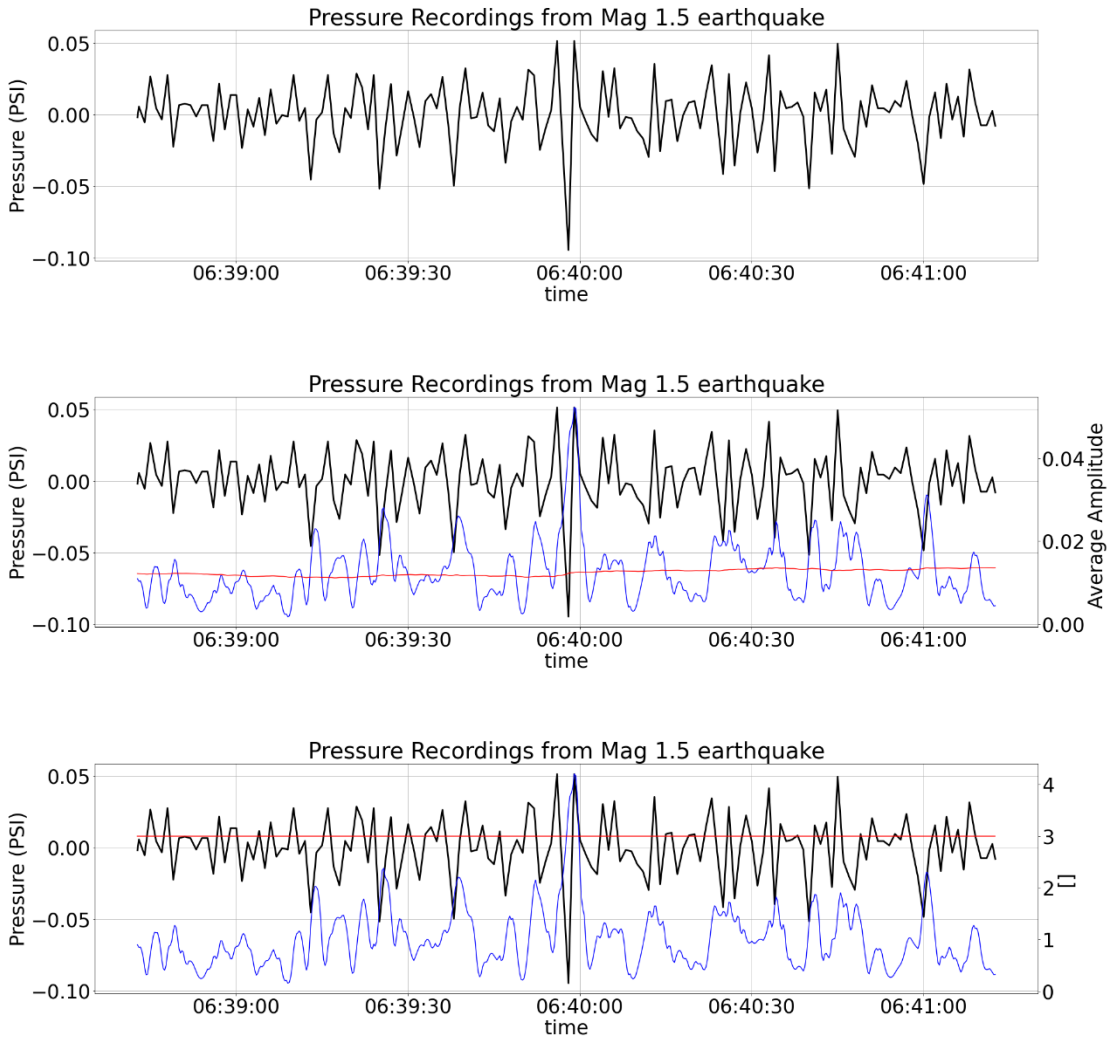

STA/LTA results using the pressure data from a magnitude 1.5 earthquake on November 28th, 2016 at 06:35:05. This earthquake was located 11 km from the pressure monitoring station. The top panel shows the tidal filtered pressure data in black at the time of the event. The middle panel shows the derivative of the pressure in black, the short term average (STA) in blue and the long term average (LTA) in red. The bottom panel has the ratio of the STA/LTA in blue, the trigger threshold in red, and the derivative of the pressure in black.

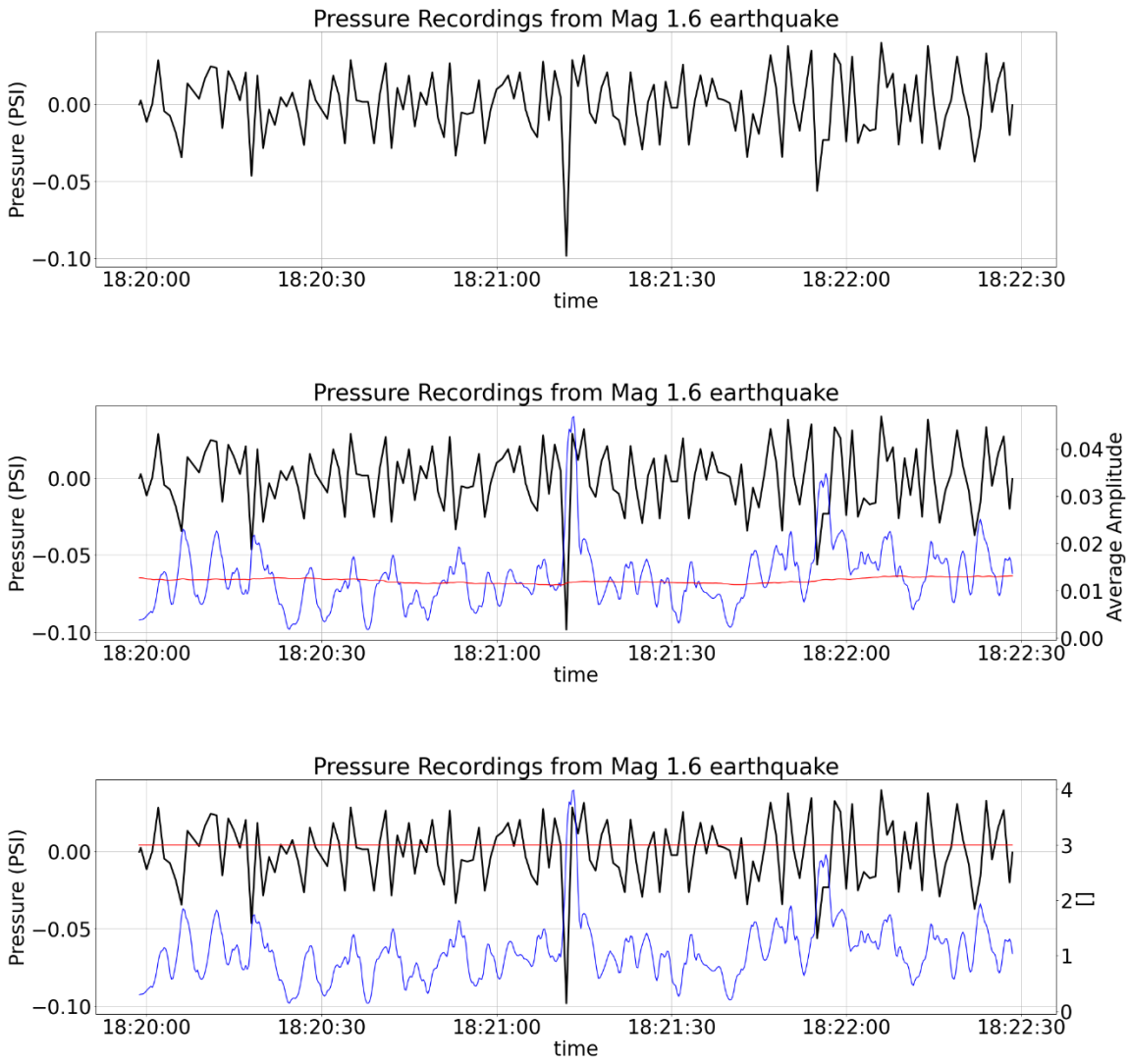

STA/LTA results using the pressure data from a magnitude 1.6 earthquake on December 29th, 2016 at 18:14:20. This earthquake was located 12 km from the pressure monitoring station. The top panel shows the tidal filtered pressure data in black at the time of the event. The middle panel shows the derivative of the pressure in black, the short term average (STA) in blue and the long term average (LTA) in red. The bottom panel has the ratio of the STA/LTA in blue, the trigger threshold in red, and the derivative of the pressure in black.

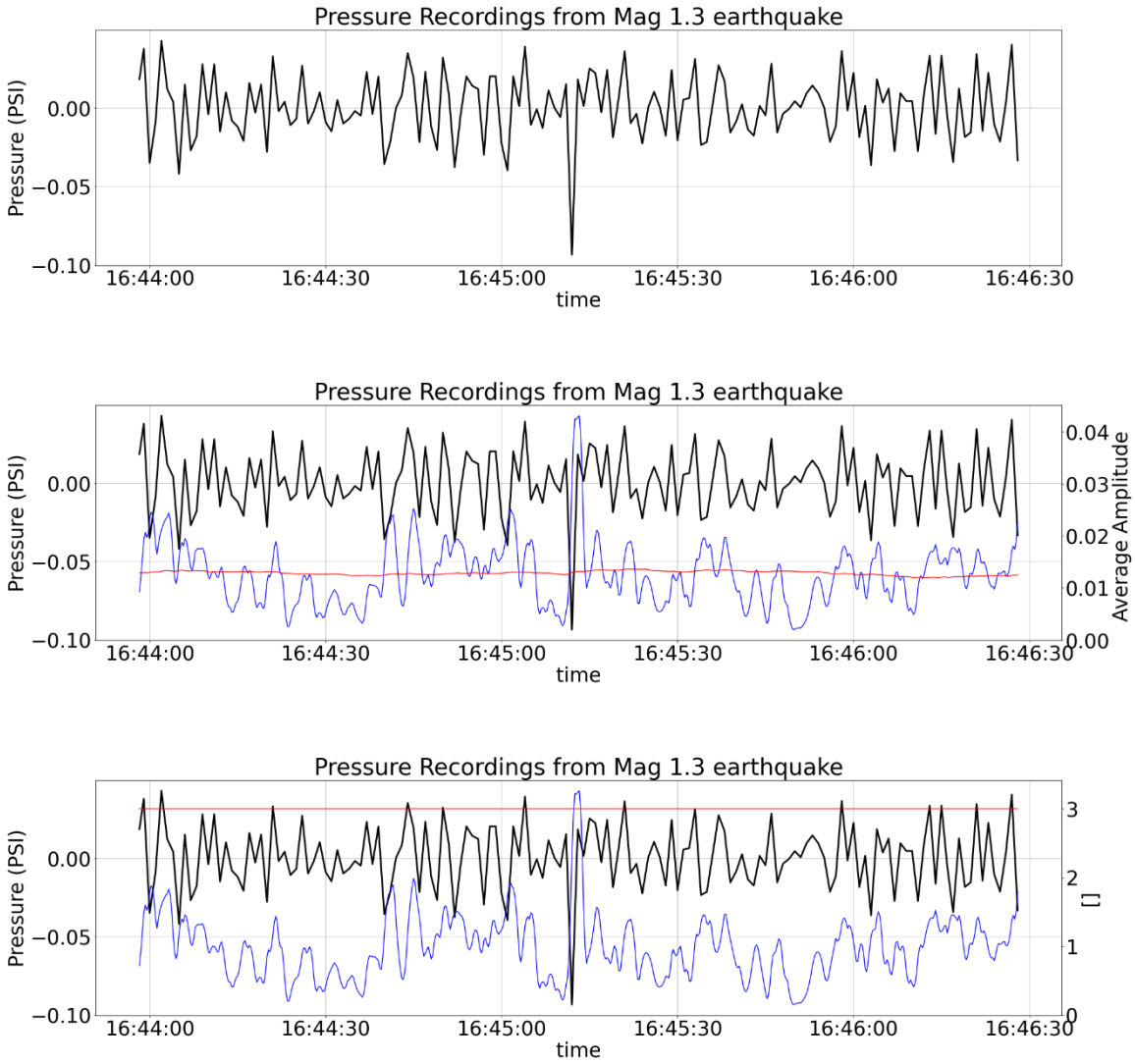

STA/LTA results using the pressure data from a magnitude 1.3 earthquake on January 15th, 2017 at 16:31:59. This earthquake was located 8.5 km from the pressure monitoring station. The top panel shows the tidal filtered pressure data in black at the time of the event. The middle panel shows the derivative of the pressure in black, the short term average (STA) in blue and the long term average (LTA) in red. The bottom panel has the ratio of the STA/LTA in blue, the trigger threshold in red, and the derivative of the pressure in black.

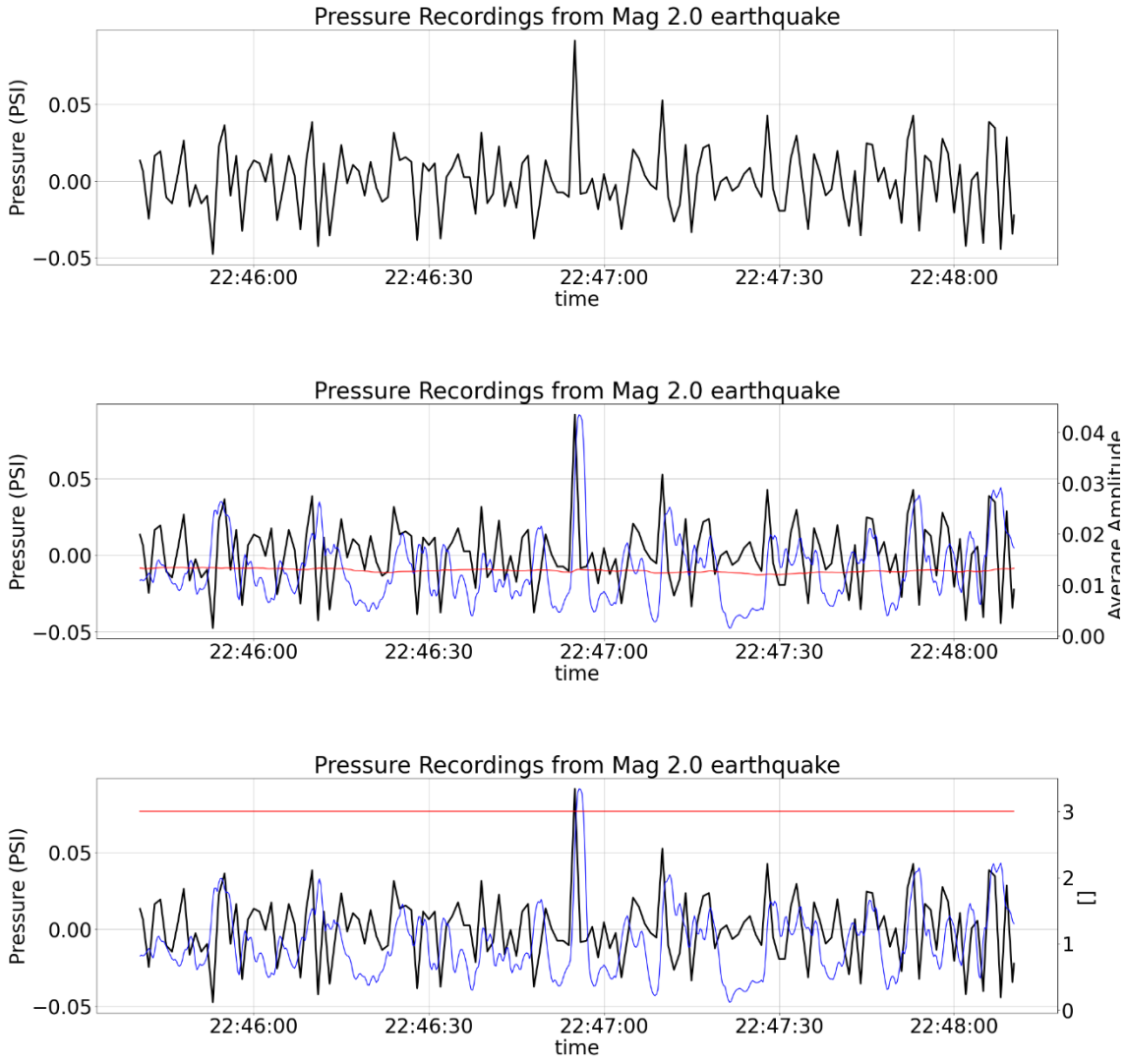

STA/LTA results using the pressure data from a magnitude 2.0 earthquake on February 1st, 2017 at 22:45:54. This earthquake was located 31 km from the pressure monitoring station. The top panel shows the tidal filtered pressure data in black at the time of the event. The middle panel shows the derivative of the pressure in black, the short term average (STA) in blue and the long term average (LTA) in red. The bottom panel has the ratio of the STA/LTA in blue, the trigger threshold in red, and the derivative of the pressure in black.

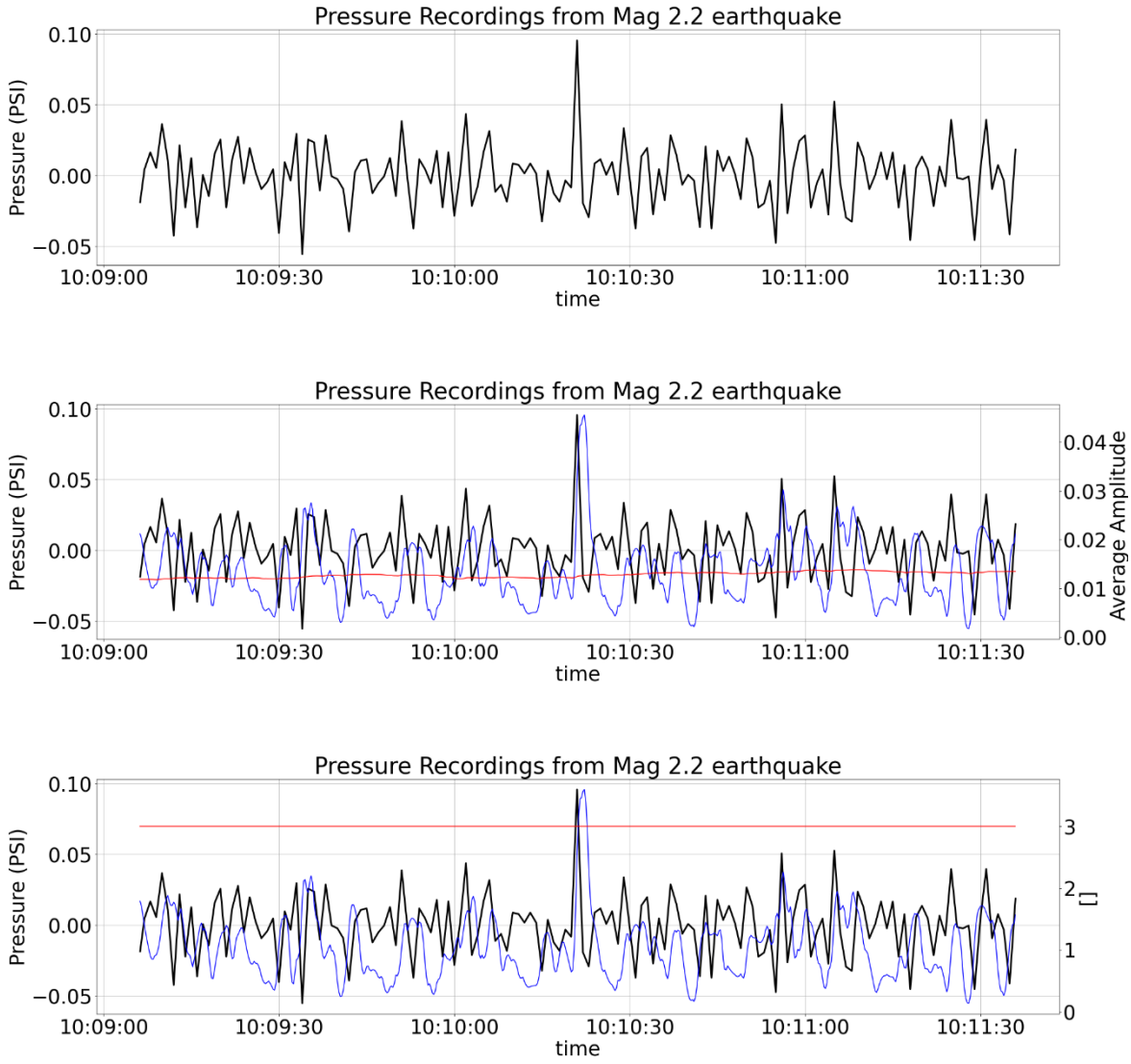

STA/LTA results using the pressure data from a magnitude 2.2 earthquake on March 30th, 2017 at 10:06:38. This earthquake was located 8.3 km from the pressure monitoring station. The top panel shows the tidal filtered pressure data in black at the time of the event. The middle panel shows the derivative of the pressure in black, the short term average (STA) in blue and the long term average (LTA) in red. The bottom panel has the ratio of the STA/LTA in blue, the trigger threshold in red, and the derivative of the pressure in black.

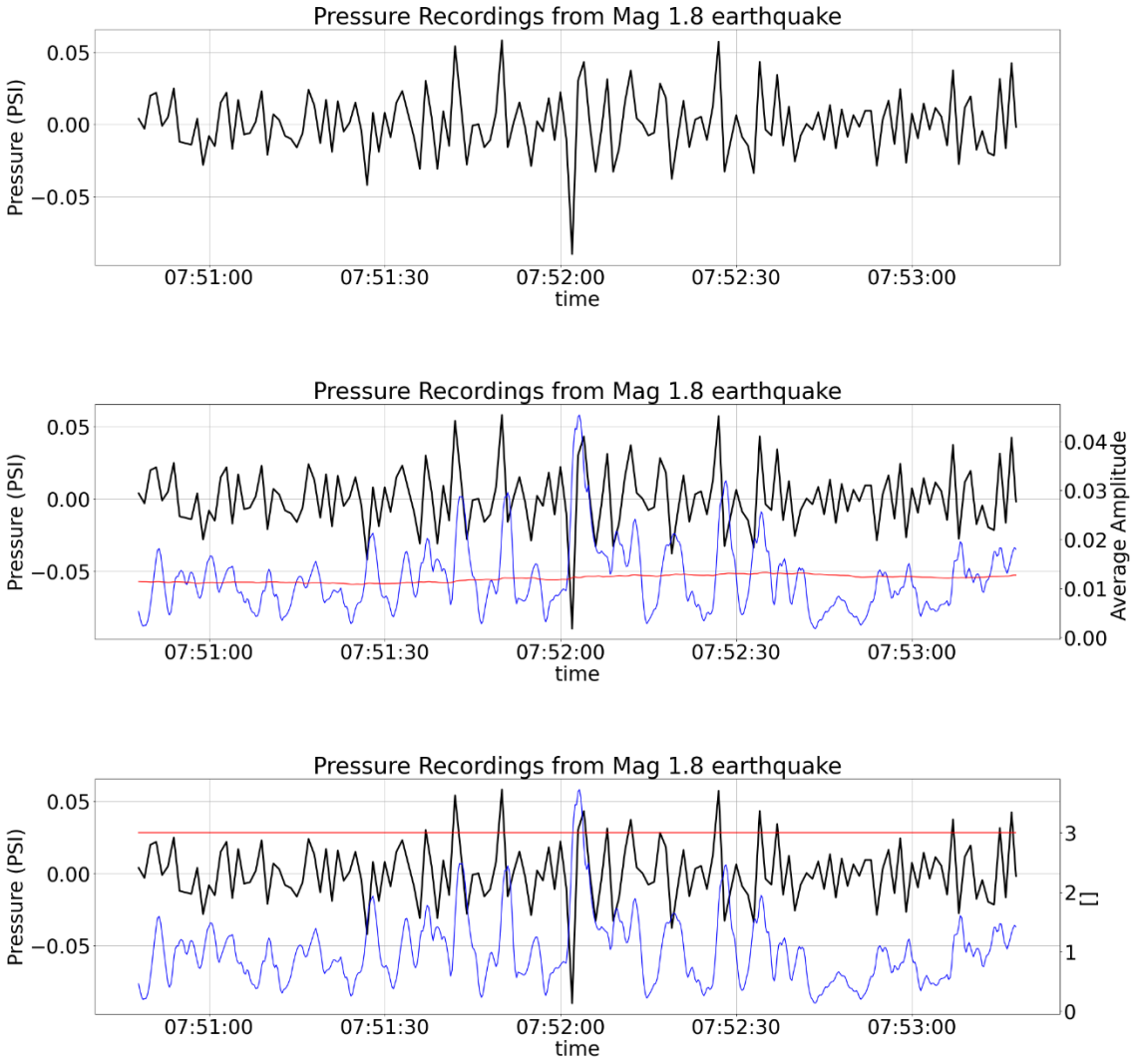

STA/LTA results using the pressure data from a magnitude 1.4 earthquake on April 10th, 2017 at 07:50:45. This earthquake was located 28 km from the pressure monitoring station. The top panel shows the tidal filtered pressure data in black at the time of the event. The middle panel shows the derivative of the pressure in black, the short term average (STA) in blue and the long term average (LTA) in red. The bottom panel has the ratio of the STA/LTA in blue, the trigger threshold in red, and the derivative of the pressure in black.

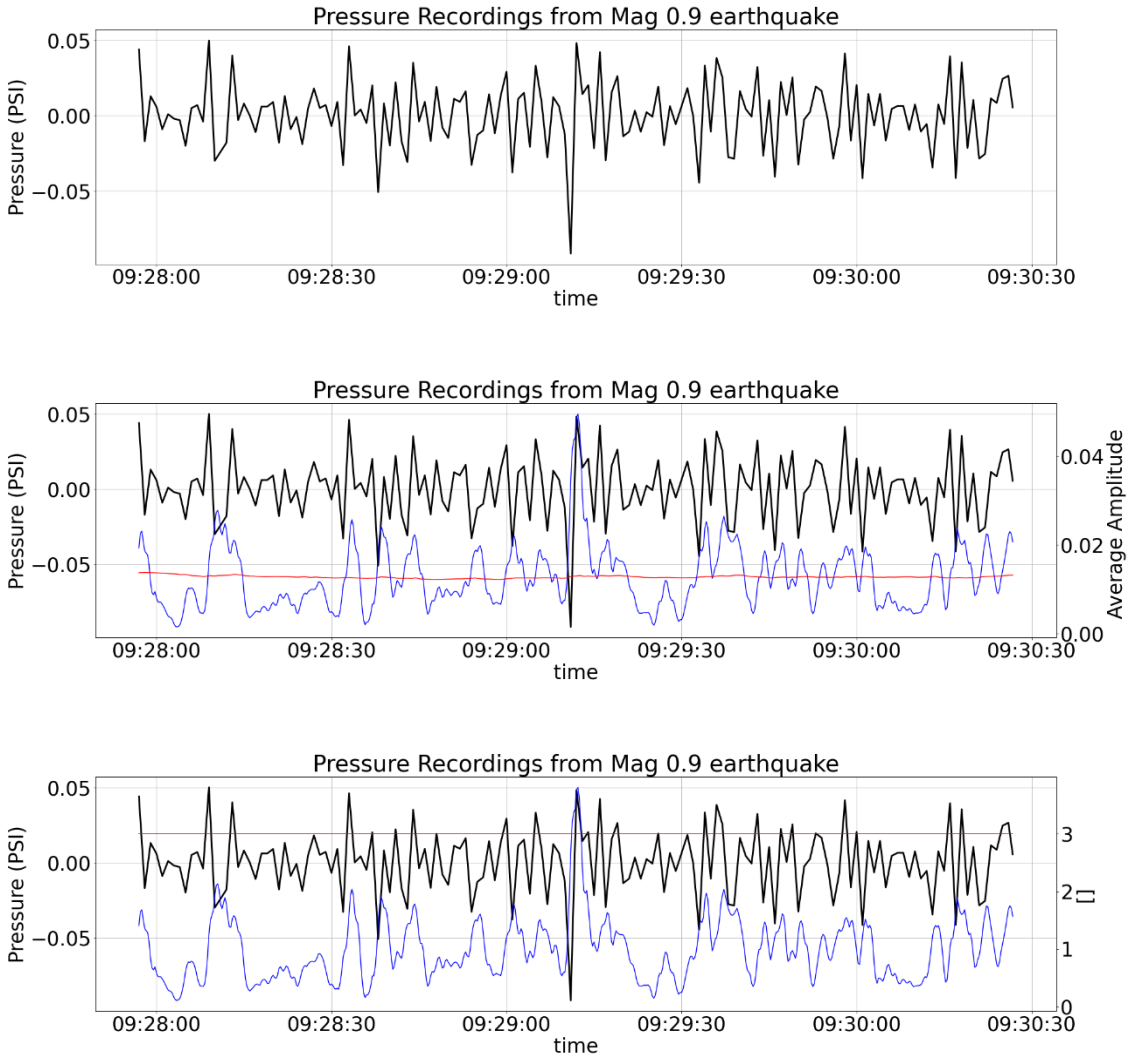

STA/LTA results using the pressure data from a magnitude 0.9 earthquake on May 2nd, 2017 at 09:25:25. This earthquake was located 5.9 km from the pressure monitoring station. The top panel shows the tidal filtered pressure data in black at the time of the event. The middle panel shows the derivative of the pressure in black, the short term average (STA) in blue and the long term average (LTA) in red. The bottom panel has the ratio of the STA/LTA in blue, the trigger threshold in red, and the derivative of the pressure in black.

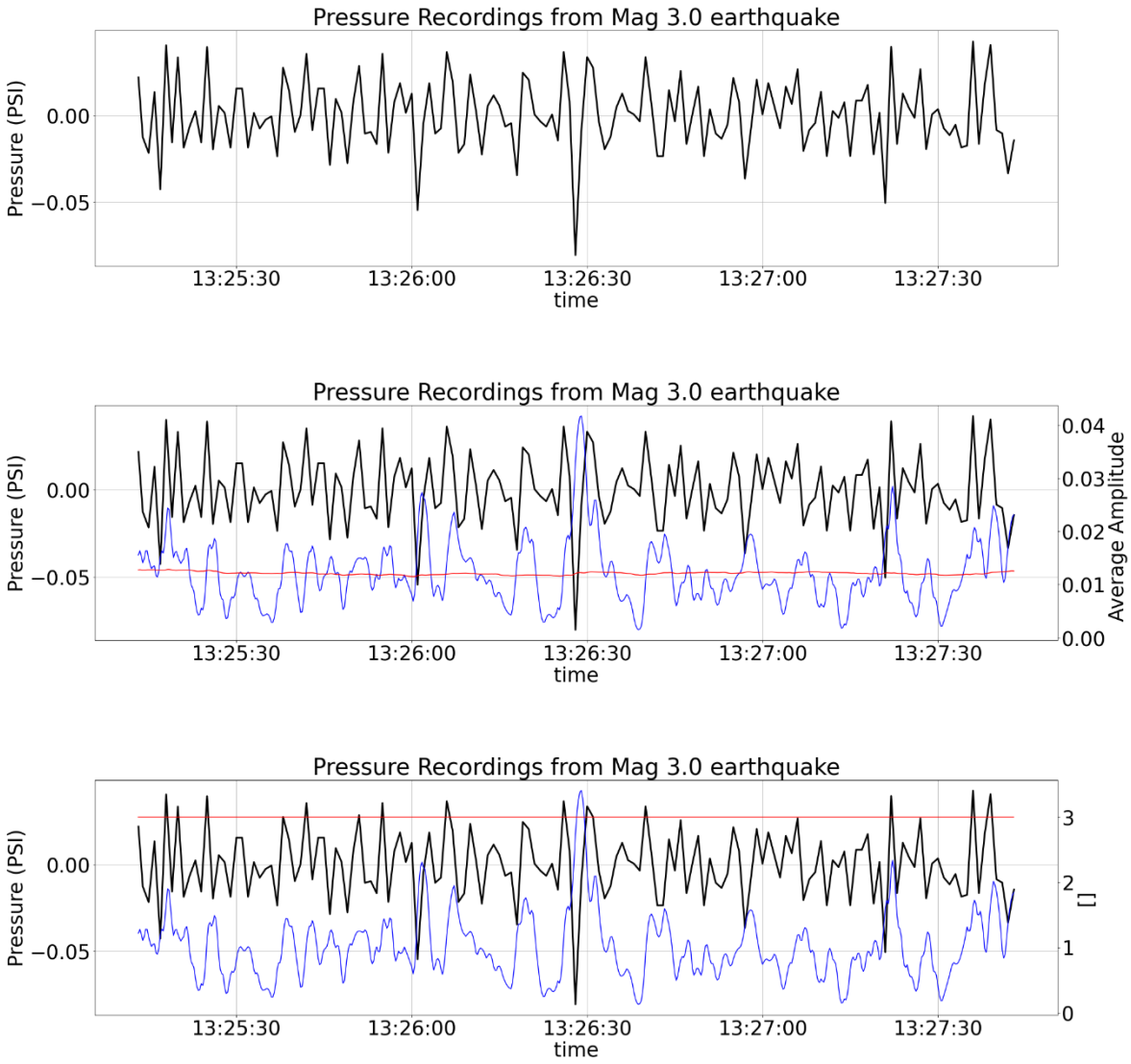

STA/LTA results using the pressure data from a magnitude 3.0 earthquake on June 1st, 2017 at 13:26:40. This earthquake was located 12 km from the pressure monitoring station. The top panel shows the tidal filtered pressure data in black at the time of the event. The middle panel shows the derivative of the pressure in black, the short term average (STA) in blue and the long term average (LTA) in red. The bottom panel has the ratio of the STA/LTA in blue, the trigger threshold in red, and the derivative of the pressure in black.

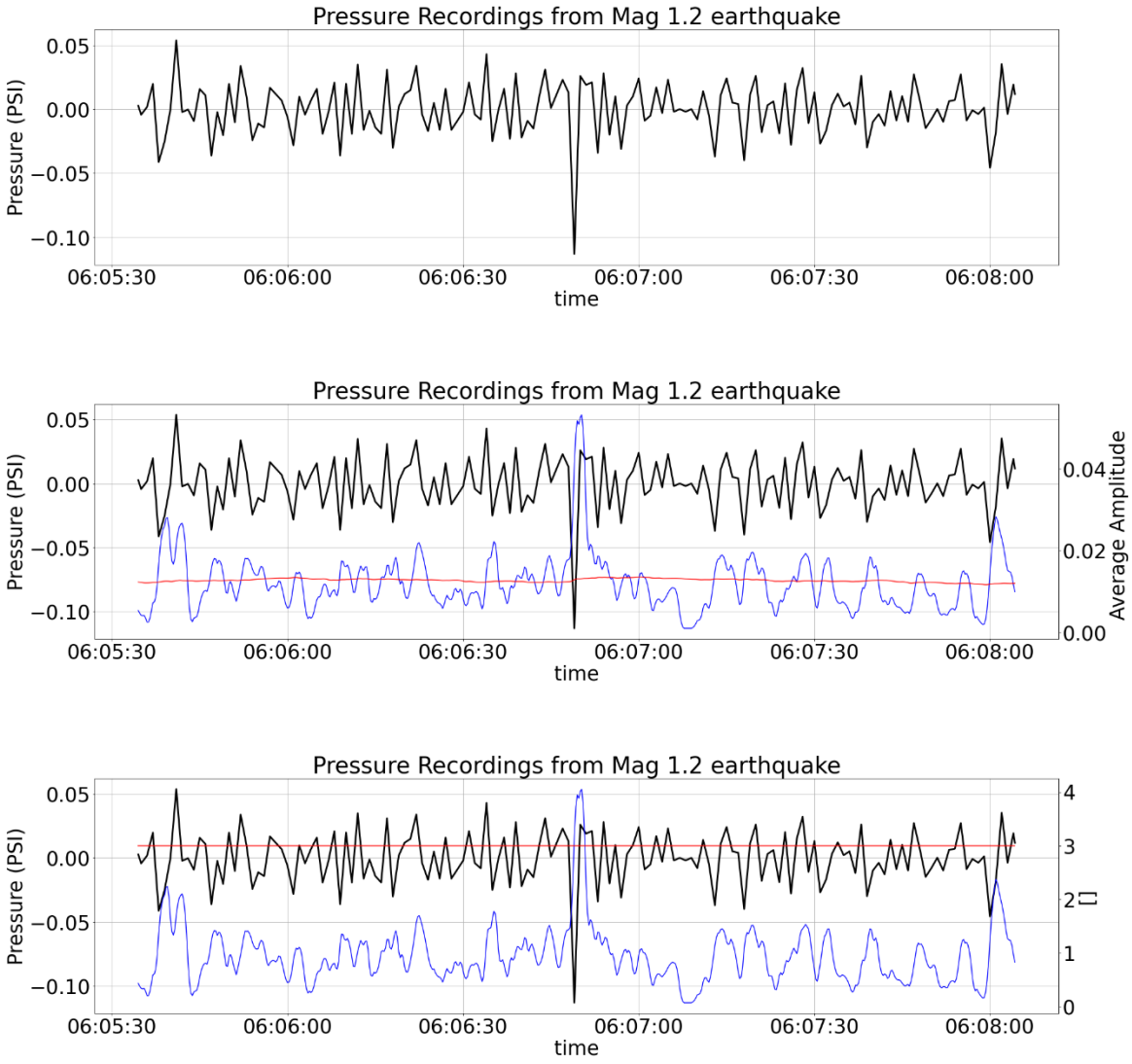

STA/LTA results using the pressure data from a magnitude 1.2 earthquake on July 1st, 2017 at 06:05:58. This earthquake was located 9.8 km from the pressure monitoring station. The top panel shows the tidal filtered pressure data in black at the time of the event. The middle panel shows the derivative of the pressure in black, the short term average (STA) in blue and the long term average (LTA) in red. The bottom panel has the ratio of the STA/LTA in blue, the trigger threshold in red, and the derivative of the pressure in black.

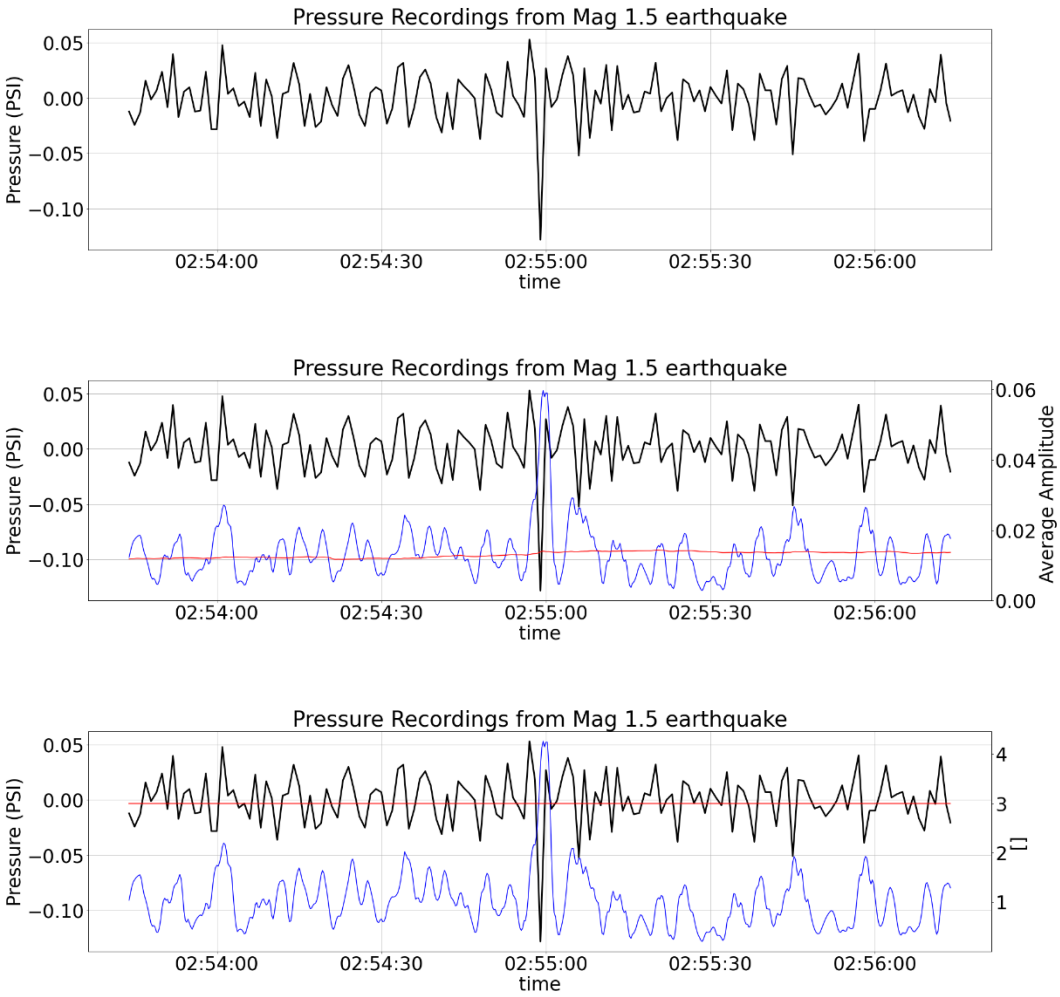

STA/LTA results using the pressure data from a magnitude 1.5 earthquake on August 6th, 2017 at 02:54:52. This earthquake was located 16 km from the pressure monitoring station. The top panel shows the tidal filtered pressure data in black at the time of the event. The middle panel shows the derivative of the pressure in black, the short term average (STA) in blue and the long term average (LTA) in red. The bottom panel has the ratio of the STA/LTA in blue, the trigger threshold in red, and the derivative of the pressure in black.

Appendix B: Temperature

Downhole temperature data was also analyzed along with the seismic events to better understand the connection between seismic events and temperature. Changes in the temperature data related to seismicity were used to determine how fluid is flowing in the subsurface around the borehole.

Continuous downhole temperature logging

Continuous downhole temperature measurements have been used to better understand fluid flow in reservoirs (Prensky, 1992). There is fluid in both the borehole and the formations surrounding the borehole. These fluids vary in temperature and as these fluids flow and interact it causes changes in downhole temperature readings. These temperature changes have been directly linked to fluid flowing into and out of the borehole (Hill, 1990). Liquids that enter the borehole from the formation usually will have warmer temperatures than the borehole fluids (Prensky, 1992).

This is just one scenario that can occur, since preliminary work at Wellington Field has shown that when brine enters the borehole, from a nearby brine injection well, it decreases the temperature of the fluid within the borehole (Watney et al., 2016). It was found in this research that when injection fluid enters the borehole there is a decrease in the temperature, but an increase in the pressure (Figure 4). This relationship can be used to better understand what pressure changes occur due to brine injection versus seismic events. Continuous downhole temperature data will also be used to gain knowledge regarding how fluid is flowing in the subsurface.

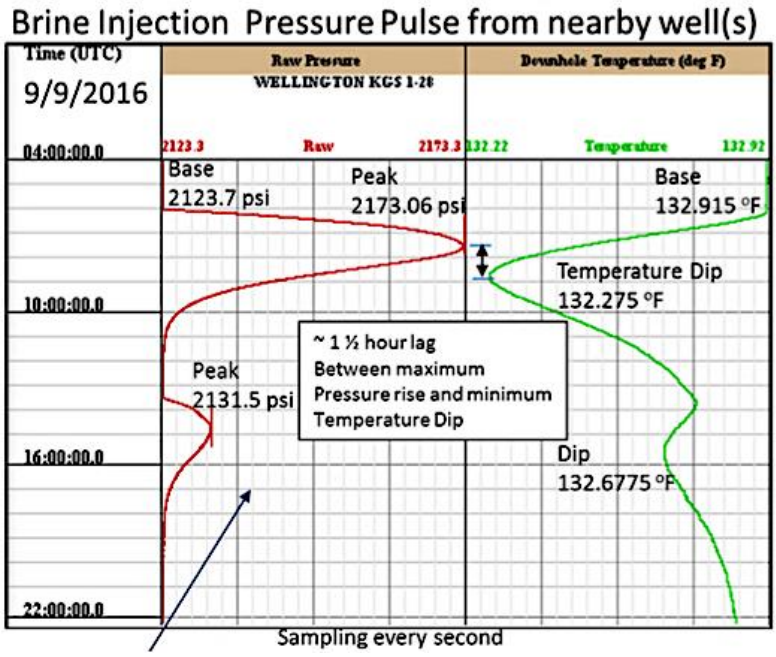

Raw Pressure (psi) and downhole temperature (°F) data from a brine injection that occurred in a nearby well. Pressure increases during the brine injection, while temperature decreases. There is a lag of an hour and half between the maximum pressure spike and the minimum temperature dip (Watney et al., 2016).

Appendix C: Earthquake Catalog

2016 9 1 0219 51.3 L 37.061 -97.534 6.6 TES 9 0.0 2.9WTES 1
2016 9 1 1457 27.1 L 37.249 -97.580 5.3 TES 9 0.0 2.0WTES 1
2016 9 3 0718 25.4 L 37.423 -97.704 5.1 TES 9 0.0 1.6WTES 1
2016 9 3 1202 42.5 L 36.297 -96.946 33.6 TES 10 0.1 5.4WTES 1
2016 9 4 1152 28.5 L 37.261 -97.432 6.7 TES 6 0.0 1.3WTES 1
2016 9 6 0637 20.8 L 37.311 -97.497 4.8 TES 9 0.0 1.7WTES 1
2016 9 6 1341 19.1 L 37.351 -97.482 0.5 TES 8 0.0 1.6WTES 1
2016 9 6 1531 2.1 L 37.348 -97.487 2.3 TES 6 0.0 1.4WTES 1
2016 9 6 1642 59.0 L 37.348 -97.487 2.4 TES 7 0.0 1.5WTES 1
2016 910 0802 14.7 L 37.279 -97.632 3.3 TES 7 0.0 1.3WTES 1
2016 911 0303 36.9 L 37.244 -97.587 9.8 TES 8 0.0 1.6WTES 1
2016 911 2229 51.3 L 37.261 -97.611 8.9 TES 5 0.0 1.5WTES 1
2016 912 0021 17.8 L 37.351 -97.571 3.0 TES 7 0.0 1.7WTES 1
2016 914 0218 4.2 L 37.496 -97.355 0.1 TES 8 0.0 1.6WTES 1
2016 915 0616 46.0 L 37.413 -97.398 4.5 TES 9 0.0 1.5WTES 1
2016 917 0152 42.7 L 37.420 -97.406 4.3 TES 8 0.0 1.9WTES 1
2016 917 0314 25.0 L 37.243 -97.560 4.0 TES 8 0.0 1.7WTES 1
2016 917 0525 40.6 L 37.331 -97.452 2.6 TES 6 0.0 0.9WTES 1
2016 917 1207 50.8 L 37.419 -97.403 2.5 TES 8 0.0 1.5WTES 1
2016 917 1318 17.0 L 37.411 -97.394 4.5 TES 8 0.0 2.7WTES 1
2016 917 1404 22.7 L 37.420 -97.390 3.7 TES 8 0.0 1.5WTES 1
2016 917 2309 16.5 L 37.421 -97.401 4.4 TES 8 0.0 1.5WTES 1
2016 918 1759 19.8 L 37.287 -97.629 4.3 TES 8 0.0 1.7WTES 1
2016 919 0816 10.9 L 37.209 -97.267 2.2 TES 7 0.0 1.4WTES 1
2016 920 0129 11.7 L 37.410 -97.391 5.3 TES 8 0.0 1.8WTES 1
2016 920 0131 16.4 L 37.423 -97.405 2.7 TES 8 0.0 1.7WTES 1
2016 920 1042 27.6 L 37.357 -97.505 2.4 TES 8 0.0 1.9WTES 1
2016 920 1111 36.6 L 37.353 -97.501 3.6 TES 8 0.0 1.2WTES 1
2016 920 1120 30.9 L 37.347 -97.508 0.3 TES 6 0.0 1.3WTES 1
2016 920 2041 57.1 L 37.210 -97.268 4.5 TES 8 0.0 1.7WTES 1

2016 920 2121 23.5 L 37.211 -97.275 0.1 TES 8 0.0 1.4WTES 1
2016 921 1934 40.8 L 37.235 -97.291 12.3 TES 9 0.0 1.6WTES 1
2016 921 2121 20.5 L 37.219 -97.276 7.5 TES 9 0.0 1.6WTES 1
2016 921 2243 6.8 L 37.225 -97.280 9.9 TES 8 0.0 1.3WTES 1
2016 922 0816 37.3 L 37.417 -97.400 4.6 TES 9 0.0 1.4WTES 1
2016 922 0823 25.1 L 37.200 -97.548 4.1 TES 7 0.0 1.5WTES 1
2016 922 1146 50.7 L 37.204 -97.558 5.0 TES 8 0.0 1.5WTES 1
2016 924 0458 19.9 L 37.219 -97.277 8.4 TES 9 0.0 1.7WTES 1
2016 924 2357 19.5 L 37.169 -97.450 11.8 TES 7 0.1 1.7WTES 1
2016 925 0411 7.8 L 37.211 -97.271 5.8 TES 6 0.0 1.5WTES 1
2016 925 1015 30.5 L 37.415 -97.399 4.7 TES 9 0.0 1.6WTES 1
2016 926 0339 40.2 L 37.265 -97.515 5.0 TES 7 0.0 1.4WTES 1
2016 926 0649 12.5 L 37.237 -97.555 3.8 TES 6 0.0 1.3WTES 1
2016 926 0934 54.5 L 37.328 -97.485 2.9 TES 9 0.0 1.6WTES 1
2016 926 1344 14.3 L 37.353 -97.497 4.5 TES 6 0.0 1.1WTES 1
2016 926 1447 31.4 L 37.326 -97.489 2.7 TES 7 0.0 1.1WTES 1
2016 927 2345 7.1 L 37.325 -97.482 3.4 TES 7 0.0 1.0WTES 1
2016 927 2359 39.5 L 37.333 -97.492 1.8 TES 8 0.0 1.5WTES 1
2016 10 1 2050 54.2 L 37.572 -97.224 16.2 TES 5 0.0 1.7WTES 1
2016 10 2 0101 7.3 L 37.266 -97.526 1.8 TES 8 0.0 1.5WTES 1
2016 10 3 1219 51.9 L 37.005 -97.543 14.5 TES 8 0.0 2.8WTES 1
2016 10 3 2341 15.1 L 37.417 -97.393 3.8 TES 8 0.0 1.6WTES 1
2016 10 4 1741 53.0 L 37.357 -97.501 2.6 TES 7 0.0 1.4WTES 1
2016 10 7 0643 21.8 L 37.305 -97.607 3.4 TES 5 0.0 1.4WTES 1
2016 10 7 0644 21.9 L 37.281 -97.582 9.7 TES 6 0.0 1.4WTES 1
2016 10 7 0725 33.8 L 37.300 -97.596 1.8 TES 7 0.1 1.6WTES 1
2016 10 7 0817 51.1 L 37.302 -97.600 3.9 TES 8 0.0 1.9WTES 1
2016 10 7 1609 44.9 L 36.972 -97.729 10.9 TES 9 0.0 2.5WTES 1
2016 10 7 1842 44.2 L 37.051 -97.669 5.8 TES 8 0.0 2.2WTES 1
2016 10 8 0423 36.8 L 37.228 -97.286 11.1 TES 7 0.0 1.6WTES 1
2016 10 8 0512 12.7 L 37.213 -97.273 6.3 TES 8 0.0 1.7WTES 1

2016 10 9 2304 30.4 L 37.608 -97.107 1.8 TES 8 0.1 2.2WTES 1
2016 1010 0428 21.1 L 37.379 -97.429 12.2 TES 8 0.0 1.3WTES 1
2016 1010 1104 26.7 L 37.408 -97.424 4.5 TES 8 0.0 1.3WTES 1
2016 1010 1954 27.1 L 37.403 -97.428 4.5 TES 8 0.0 1.7WTES 1
2016 1012 0829 27.3 L 37.422 -97.398 1.6 TES 8 0.0 1.9WTES 1
2016 1013 0227 46.2 L 37.333 -97.530 1.0 TES 6 0.0 1.4WTES 1
2016 1013 0248 42.5 L 36.745 -98.230 21.6 TES 9 0.1 3.6WTES 1
2016 1013 1430 18.4 L 37.365 -97.414 0.7 TES 6 0.0 1.2WTES 1
2016 1014 2252 48.8 L 36.961 -97.899 1.0 TES 8 0.1 2.8WTES 1
2016 1015 1441 17.3 L 37.403 -97.431 4.8 TES 8 0.0 1.9WTES 1
2016 1015 1545 14.6 L 37.407 -97.432 2.9 TES 8 0.0 1.5WTES 1
2016 1015 2340 10.3 L 37.390 -97.426 3.7 TES 8 0.0 1.4WTES 1
2016 1017 0909 54.6 L 37.090 -97.691 10.1 TES 8 0.0 2.3WTES 1
2016 1017 2048 52.5 L 37.440 -97.847 7.6 TES 9 0.0 2.7WTES 1
2016 1018 0115 39.9 L 36.976 -97.876 12.2 TES 8 0.1 2.5WTES 1
2016 1019 2107 16.9 L 36.822 -97.651 2.0 TES 8 0.1 2.4WTES 1
2016 1019 2233 35.9 L 36.838 -97.856 18.6 TES 8 0.1 3.2WTES 1
2016 1020 0106 25.4 L 37.119 -97.628 15.0 TES 8 0.3 2.0WTES 1
2016 1020 0124 46.7 L 37.296 -97.435 4.8 TES 8 0.0 1.7WTES 1
2016 1020 1214 8.6 L 36.926 -97.594 1.9 TES 8 0.1 3.2WTES 1
2016 1021 2026 1.3 L 36.134 -98.280 7.1 TES 9 0.8 3.8WTES 1
2016 1022 2244 34.1 L 37.423 -97.414 1.5 TES 8 0.0 1.2WTES 1
2016 1022 2309 17.8 L 37.412 -97.399 5.4 TES 8 0.0 1.4WTES 1
2016 1023 0146 31.6 L 37.386 -97.419 4.7 TES 6 0.0 1.1WTES 1
2016 1023 0225 8.9 L 37.327 -97.493 0.7 TES 6 0.0 1.1WTES 1
2016 1023 0618 5.1 L 37.226 -97.286 10.6 TES 8 0.0 1.6WTES 1
2016 1024 0033 34.6 L 36.818 -97.565 10.2 TES 8 0.0 3.0WTES 1
2016 1024 1325 55.2 L 37.121 -97.788 13.8 TES 8 0.1 3.2WTES 1
2016 1024 1342 1.1 L 36.989 -97.725 17.9 TES 8 0.0 2.3WTES 1
2016 1024 1350 13.8 L 37.038 -97.703 11.7 TES 7 0.0 2.8WTES 1
2016 1024 1404 42.9 L 37.416 -97.433 1.6 TES 8 0.0 2.1WTES 1

2016 1024 2310 5.9 L 37.403 -97.420 4.7 TES 7 0.0 1.4WTES 1
2016 1025 0248 19.4 L 37.410 -97.426 4.1 TES 8 0.0 1.7WTES 1
2016 1025 1559 8.1 L 37.125 -97.794 12.9 TES 8 0.0 2.5WTES 1
2016 1026 2339 25.2 L 37.688 -97.251 6.0 TES 8 0.0 1.9WTES 1
2016 1026 2340 9.1 L 37.689 -97.225 10.5 TES 8 0.0 2.0WTES 1
2016 1026 2352 58.0 L 37.696 -97.253 5.4 TES 8 0.0 2.1WTES 1
2016 1027 1033 9.8 L 37.089 -97.582 13.1 TES 6 0.0 2.0WTES 1
2016 1027 1124 56.3 L 36.928 -97.612 2.0 TES 7 0.0 2.3WTES 1
2016 1028 1757 5.8 L 37.406 -97.674 14.4 TES 7 0.0 2.1WTES 1
2016 1028 2104 39.9 L 37.424 -97.705 7.8 TES 8 0.0 1.8WTES 1
2016 1028 2211 11.3 L 37.408 -97.416 4.5 TES 7 0.0 1.3WTES 1
2016 1029 1443 17.5 L 37.009 -97.541 1.8 TES 8 0.1 2.2WTES 1
2016 1029 1533 11.7 L 37.265 -97.315 5.4 TES 8 0.0 1.5WTES 1
2016 1029 1652 18.4 L 37.431 -97.715 0.0 TES 8 0.0 2.0WTES 1
2016 1029 1835 3.8 L 37.423 -97.702 9.2 TES 8 0.0 2.2WTES 1
2016 1029 2256 36.8 L 37.291 -97.424 4.0 TES 8 0.0 1.5WTES 1
2016 1030 0402 23.8 L 37.284 -97.424 3.3 TES 8 0.0 1.0WTES 1
2016 1030 0503 55.0 L 37.294 -97.435 4.4 TES 6 0.0 0.8WTES 1
2016 1030 0509 56.5 L 37.291 -97.434 4.1 TES 8 0.0 0.9WTES 1
2016 1030 1631 53.2 L 37.289 -97.424 3.9 TES 8 0.0 1.4WTES 1
2016 1030 2058 36.5 L 37.292 -97.427 4.1 TES 8 0.0 1.9WTES 1
2016 1030 2106 16.1 L 37.030 -97.569 12.7 TES 8 0.0 2.2WTES 1
2016 1031 2152 1.1 L 37.227 -97.527 4.4 TES 8 0.0 1.6WTES 1
2016 11 1 2229 53.5 L 37.393 -97.373 1.8 TES 8 0.0 1.5WTES 1
2016 11 1 2235 9.6 L 37.383 -97.369 0.1 TES 8 0.0 1.3WTES 1
2016 11 2 0426 55.3 L 36.276 -96.792 20.2 TES 8 0.1 4.6WTES 1
2016 11 2 2238 36.4 L 37.288 -97.418 4.6 TES 8 0.0 1.4WTES 1
2016 11 2 2330 4.7 L 37.288 -97.417 4.2 TES 8 0.0 1.1WTES 1
2016 11 3 0151 40.2 L 37.285 -97.415 3.9 TES 8 0.0 1.4WTES 1
2016 11 3 0400 47.6 L 37.286 -97.417 4.1 TES 8 0.0 1.3WTES 1
2016 11 3 0514 45.6 L 37.285 -97.415 4.0 TES 8 0.0 1.2WTES 1

2016 11 3 0620 25.0 L 37.285 -97.413 3.7 TES 8 0.0 1.4WTES 1
2016 11 3 0706 53.9 L 37.288 -97.415 3.9 TES 8 0.0 1.4WTES 1
2016 11 3 0743 14.1 L 37.282 -97.413 3.4 TES 8 0.0 1.4WTES 1
2016 11 3 1036 50.2 L 37.282 -97.412 3.4 TES 7 0.0 1.2WTES 1
2016 11 3 2211 3.5 L 37.289 -97.418 4.6 TES 8 0.0 1.4WTES 1
2016 11 5 0202 7.3 L 37.329 -97.667 18.4 TES 8 0.0 2.4WTES 1
2016 11 5 0920 20.9 L 37.361 -97.711 14.2 TES 8 0.0 3.0WTES 1
2016 11 6 0311 7.4 L 37.408 -97.402 4.7 TES 9 0.0 1.8WTES 1
2016 11 6 0850 59.6 L 37.396 -97.657 8.2 TES 8 0.0 1.8WTES 1
2016 11 6 1133 37.9 L 37.246 -97.664 4.9 TES 7 0.0 1.7WTES 1
2016 11 7 0041 58.5 L 37.286 -97.427 3.6 TES 8 0.0 1.0WTES 1
2016 11 7 0144 25.0 L 35.970 -96.812 15.0 TES 9 0.1 5.0WTES 1
2016 11 7 0452 35.1 L 37.391 -97.752 8.1 TES 9 0.0 3.0WTES 1
2016 11 7 0701 43.3 L 37.166 -97.819 9.1 TES 8 0.0 2.7WTES 1
2016 11 7 0734 0.4 L 36.469 -98.744 6.5 TES 10 0.7 3.5WTES 1
2016 11 9 1040 50.9 L 37.331 -97.486 2.8 TES 8 0.0 1.3WTES 1
2016 11 9 1048 17.9 L 37.288 -97.427 3.7 TES 8 0.0 1.1WTES 1
2016 11 9 1728 0.9 L 37.221 -97.598 4.4 TES 6 0.0 1.5WTES 1
2016 11 9 2137 37.1 L 37.330 -97.486 2.6 TES 8 0.0 1.0WTES 1
2016 1110 0203 52.4 L 37.326 -97.439 2.5 TES 7 0.0 0.9WTES 1
2016 1112 0255 51.9 L 36.906 -97.478 7.4 TES 9 0.0 2.6WTES 1
2016 1112 0521 49.5 L 37.335 -97.399 2.8 TES 8 0.0 1.2WTES 1
2016 1112 1511 33.7 L 37.327 -97.480 3.5 TES 6 0.0 1.0WTES 1
2016 1113 1355 9.7 L 36.933 -97.535 20.2 TES 8 0.0 2.1WTES 1
2016 1114 0135 2.9 L 37.215 -97.278 7.7 TES 7 0.0 1.6WTES 1
2016 1114 1627 24.3 L 37.017 -97.559 8.4 TES 9 0.0 2.2WTES 1
2016 1114 1734 6.2 L 37.071 -97.154 2.0 TES 8 0.0 2.0WTES 1
2016 1114 2059 8.7 L 37.292 -97.423 4.1 TES 8 0.0 1.6WTES 1
2016 1116 0902 16.8 L 37.211 -97.570 3.2 TES 5 0.0 1.6WTES 1
2016 1117 0534 38.7 L 37.278 -97.637 4.6 TES 10 0.0 1.7WTES 1
2016 1117 0712 6.3 L 37.292 -97.423 3.6 TES 8 0.0 1.3WTES 1

2016 1117 0939 4.3 L 37.405 -97.428 3.5 TES 8 0.0 1.5WTES 1
2016 1118 2326 53.4 L 36.852 -97.697 12.5 TES 9 0.0 2.4WTES 1
2016 1124 1329 15.2 L 37.334 -97.582 0.1 TES 6 0.0 1.4WTES 1
2016 1125 0949 53.2 L 35.774 -97.068 48.5 TES 6 0.1 2.7WTES 1
2016 1125 1519 36.3 L 36.855 -97.742 15.3 TES 8 0.0 3.7WTES 1
2016 1125 2133 30.2 L 36.953 -97.736 21.0 TES 7 0.1 2.6WTES 1
2016 1126 0253 55.9 L 37.243 -97.652 2.2 TES 8 0.0 2.0WTES 1
2016 1126 0257 16.0 L 37.250 -97.658 3.8 TES 8 0.1 2.9WTES 1
2016 1126 0621 6.6 L 37.247 -97.661 4.1 TES 7 0.1 2.0WTES 1
2016 1126 1414 14.4 L 37.352 -97.621 2.1 TES 6 0.0 1.4WTES 1
2016 1126 1948 13.3 L 37.242 -97.661 4.3 TES 8 0.0 1.6WTES 1
2016 1127 0837 25.0 L 37.246 -97.667 5.6 TES 6 0.1 1.7WTES 1
2016 1127 1329 13.1 L 37.413 -97.392 5.1 TES 8 0.0 2.2WTES 1
2016 1127 1330 10.9 L 37.419 -97.408 1.1 TES 7 0.1 2.1WTES 1
2016 1127 2032 20.8 L 37.418 -97.401 5.0 TES 7 0.0 1.8WTES 1
2016 1127 2244 5.3 L 37.411 -97.387 5.5 TES 8 0.0 2.4WTES 1
2016 1128 0050 8.1 L 37.420 -97.398 0.2 TES 6 0.0 1.6WTES 1
2016 1128 1135 5.5 L 37.411 -97.379 4.9 TES 7 0.0 1.5WTES 1
2016 1129 0132 2.5 L 37.409 -97.385 5.1 TES 8 0.0 2.6WTES 1
2016 1129 0901 24.8 L 37.416 -97.391 4.5 TES 6 0.0 1.4WTES 1
2016 1130 0657 55.3 L 37.225 -97.508 2.1 TES 3 0.0 1.1WTES 1
2016 1130 0810 13.7 L 37.140 -97.575 10.8 TES 6 0.0 1.6WTES 1
2016 1130 1340 17.7 L 37.260 -97.548 3.3 TES 5 0.0 1.2WTES 1
2016 1130 1406 3.3 L 37.252 -97.542 4.0 TES 5 0.0 1.2WTES 1
2016 12 1 0408 59.4 L 37.421 -97.396 5.3 TES 8 0.0 1.6WTES 1
2016 12 1 0454 34.6 L 37.426 -97.415 1.1 TES 8 0.1 1.6WTES 1
2016 12 1 0723 57.5 L 37.296 -97.437 4.8 TES 7 0.0 1.2WTES 1
2016 12 1 1126 50.4 L 37.291 -97.431 4.6 TES 8 0.0 1.4WTES 1
2016 12 2 0852 49.0 L 37.423 -97.401 1.5 TES 8 0.0 2.1WTES 1
2016 12 2 0943 35.8 L 37.420 -97.394 3.2 TES 8 0.1 1.5WTES 1
2016 12 2 1348 31.8 L 37.264 -97.547 1.0 TES 8 0.0 1.8WTES 1

2016 12 2 1417 6.5 L 37.229 -97.518 4.3 TES 8 0.1 1.6WTES 1
2016 12 2 1441 19.7 L 37.265 -97.556 3.7 TES 7 0.0 1.5WTES 1
2016 12 2 1443 24.9 L 37.238 -97.526 4.7 TES 8 0.0 1.5WTES 1
2016 12 2 1445 56.9 L 37.251 -97.539 4.5 TES 7 0.0 1.4WTES 1
2016 12 2 1747 7.4 L 37.403 -97.370 4.6 TES 8 0.0 1.3WTES 1
2016 12 3 0419 27.3 L 36.995 -97.921 17.5 TES 8 0.0 2.4WTES 1
2016 12 3 2109 47.0 L 37.292 -97.415 3.4 TES 8 0.0 1.0WTES 1
2016 12 3 2147 31.3 L 37.214 -97.665 1.3 TES 8 0.0 2.1WTES 1
2016 12 3 2307 44.4 L 37.116 -97.544 8.6 TES 8 0.1 1.6WTES 1
2016 12 4 0331 7.1 L 37.212 -97.665 0.2 TES 8 0.0 1.9WTES 1
2016 12 4 0845 40.0 L 37.346 -97.491 1.5 TES 8 0.0 1.3WTES 1
2016 12 4 1726 49.4 L 37.365 -97.334 1.3 TES 8 0.2 1.2WTES 1
2016 12 5 0043 34.1 L 37.421 -97.398 2.8 TES 8 0.0 1.7WTES 1
2016 12 5 0216 20.4 L 37.421 -97.413 0.2 TES 7 0.0 1.3WTES 1
2016 12 6 0208 28.0 L 37.409 -97.401 7.0 TES 8 0.0 1.3WTES 1
2016 12 6 0214 42.4 L 37.390 -97.368 6.7 TES 8 0.0 1.3WTES 1
2016 12 6 0429 4.4 L 37.413 -97.399 5.3 TES 8 0.0 1.4WTES 1
2016 12 6 0429 29.7 L 37.412 -97.394 5.6 TES 8 0.0 1.6WTES 1
2016 12 7 0733 6.6 L 37.410 -97.380 4.5 TES 8 0.1 1.5WTES 1
2016 12 7 1951 55.9 L 37.292 -97.434 4.3 TES 8 0.0 1.1WTES 1
2016 12 7 2340 37.5 L 37.293 -97.426 4.3 TES 8 0.0 1.5WTES 1
2016 12 8 0503 9.2 L 37.295 -97.425 4.1 TES 8 0.0 0.9WTES 1
2016 12 8 2312 43.4 L 37.293 -97.438 4.5 TES 8 0.0 0.8WTES 1
2016 12 9 0117 27.5 L 37.304 -97.596 4.6 TES 9 0.1 1.3WTES 1
2016 12 9 0340 2.3 L 37.407 -97.442 0.9 TES 8 0.0 1.5WTES 1
2016 12 9 1049 53.5 L 37.410 -97.445 1.2 TES 8 0.0 1.7WTES 1
2016 12 9 1120 48.7 L 37.414 -97.387 6.0 TES 8 0.0 1.5WTES 1
2016 12 9 1531 21.9 L 37.405 -97.429 4.7 TES 9 0.0 1.3WTES 1
2016 12 9 1611 17.1 L 37.413 -97.440 0.1 TES 8 0.0 1.3WTES 1
2016 12 9 1904 40.8 L 37.405 -97.432 4.5 TES 8 0.0 1.6WTES 1
2016 1210 1023 23.4 L 37.362 -97.612 4.2 TES 7 0.0 1.5WTES 1

2016 1210 1800 52.0 L 37.173 -97.632 6.0 TES 8 0.0 2.0WTES 1
2016 1211 1128 36.7 L 37.413 -97.384 4.8 TES 9 0.0 1.8WTES 1
2016 1211 1440 45.7 L 37.242 -97.525 4.2 TES 9 0.0 1.5WTES 1
2016 1211 1449 16.2 L 37.257 -97.545 4.0 TES 5 0.0 1.3WTES 1
2016 1211 1531 9.7 L 37.239 -97.525 4.6 TES 9 0.0 1.5WTES 1
2016 1212 0108 51.0 L 37.411 -97.389 5.3 TES 8 0.0 1.8WTES 1
2016 1212 0715 34.2 L 37.405 -97.429 4.5 TES 9 0.0 1.5WTES 1
2016 1212 0734 55.9 L 37.411 -97.444 1.0 TES 8 0.0 1.3WTES 1
2016 1212 1410 57.2 L 37.408 -97.445 1.2 TES 8 0.0 1.3WTES 1
2016 1214 0620 24.8 L 37.243 -97.523 4.2 TES 6 0.0 1.3WTES 1
2016 1214 2342 43.7 L 37.202 -97.638 6.7 TES 5 0.1 1.3WTES 1
2016 1215 0139 12.7 L 37.376 -97.717 16.5 TES 8 0.0 2.5WTES 1
2016 1215 0209 58.7 L 37.414 -97.388 5.1 TES 9 0.0 1.7WTES 1
2016 1215 0302 45.5 L 37.301 -97.531 29.6 TES 9 0.2 2.2WTES 1
2016 1215 1621 30.5 L 37.389 -97.703 9.9 TES 8 0.0 1.9WTES 1
2016 1215 1937 28.9 L 37.329 -97.430 0.8 TES 7 0.0 0.5WTES 1
2016 1216 0438 59.8 L 37.243 -97.527 4.4 TES 8 0.0 1.3WTES 1
2016 1216 1316 37.3 L 37.111 -97.649 4.4 TES 9 0.0 2.0WTES 1
2016 1216 1729 54.3 L 37.273 -97.858 6.8 TES 8 0.0 2.2WTES 1
2016 1216 2345 39.0 L 37.199 -97.612 4.1 TES 7 0.0 1.4WTES 1
2016 1218 0030 2.2 L 37.341 -97.493 3.8 TES 8 0.0 1.4WTES 1
2016 1218 1515 12.7 L 36.905 -97.477 7.4 TES 9 0.0 2.4WTES 1
2016 1218 2031 27.9 L 37.244 -97.528 4.2 TES 5 0.0 1.0WTES 1
2016 1218 2355 37.3 L 37.219 -97.267 11.5 TES 8 0.0 2.1WTES 1
2016 1219 0749 12.1 L 37.200 -97.611 3.8 TES 9 0.1 1.8WTES 1
2016 1219 0928 33.8 L 37.242 -97.528 4.5 TES 8 0.0 1.3WTES 1
2016 1221 0653 39.8 L 37.240 -97.529 4.7 TES 7 0.0 1.3WTES 1
2016 1221 0751 45.6 L 37.239 -97.529 4.7 TES 5 0.0 1.1WTES 1
2016 1221 0757 45.9 L 37.244 -97.529 4.6 TES 9 0.0 1.8WTES 1
2016 1221 0820 54.4 L 37.242 -97.529 4.5 TES 9 0.0 1.8WTES 1
2016 1221 1138 7.1 L 37.245 -97.526 4.5 TES 8 0.0 1.4WTES 1

2016 1221 1512 49.3 L 37.563 -97.800 15.0 TES 8 0.1 3.1WTES 1
2016 1222 1446 57.3 L 37.241 -97.844 7.7 TES 9 0.1 2.6WTES 1
2016 1222 1525 31.8 L 37.317 -97.617 5.9 TES 8 0.0 1.6WTES 1
2016 1222 1547 10.8 L 37.413 -97.395 5.3 TES 8 0.0 1.4WTES 1
2016 1222 1606 46.3 L 37.414 -97.395 4.8 TES 8 0.0 1.7WTES 1
2016 1222 2343 34.8 L 37.146 -97.550 9.1 TES 8 0.2 1.5WTES 1
2016 1223 0254 28.2 L 37.314 -97.618 6.2 TES 4 0.0 1.1WTES 1
2016 1223 1405 6.9 L 37.416 -97.396 4.2 TES 9 0.0 2.0WTES 1
2016 1223 1719 59.5 L 37.244 -97.528 4.5 TES 8 0.0 1.5WTES 1
2016 1223 2012 21.0 L 37.243 -97.526 4.6 TES 9 0.0 1.5WTES 1
2016 1224 1211 54.2 L 37.419 -97.396 4.3 TES 9 0.0 2.5WTES 1
2016 1224 1318 34.3 L 36.926 -97.521 19.0 TES 8 0.0 2.1WTES 1
2016 1224 1521 15.4 L 37.409 -97.424 4.6 TES 9 0.0 1.6WTES 1
2016 1224 1755 40.4 L 37.408 -97.422 4.4 TES 9 0.0 2.0WTES 1
2016 1224 1757 31.0 L 37.408 -97.417 5.1 TES 9 0.0 1.6WTES 1
2016 1225 1741 58.7 L 37.217 -97.572 4.0 TES 6 0.0 1.4WTES 1
2016 1226 0351 19.7 L 37.258 -97.531 4.2 TES 9 0.0 1.7WTES 1
2016 1226 1404 12.2 L 37.431 -97.428 4.2 TES 8 0.0 1.3WTES 1
2016 1226 1642 31.8 L 37.191 -97.524 2.7 TES 7 0.0 1.5WTES 1
2016 1226 1819 0.9 L 37.265 -97.536 2.5 TES 9 0.1 1.5WTES 1
2016 1226 2124 45.3 L 37.425 -97.401 2.7 TES 8 0.0 1.4WTES 1
2016 1226 2129 53.7 L 37.420 -97.413 0.1 TES 7 0.0 1.4WTES 1
2016 1227 0922 50.2 L 36.869 -97.729 10.2 TES 7 0.1 2.3WTES 1
2016 1227 1729 29.9 L 36.963 -97.641 10.7 TES 9 0.0 2.4WTES 1
2016 1228 1112 56.9 L 37.182 -97.525 1.8 TES 8 0.0 1.4WTES 1
2016 1228 1936 52.7 L 37.404 -97.434 4.0 TES 8 0.0 1.5WTES 1
2016 1228 2229 55.6 L 37.416 -97.394 4.3 TES 9 0.0 1.7WTES 1
2016 1229 0550 23.8 L 37.298 -97.566 6.4 TES 6 0.0 1.5WTES 1
2016 1229 1056 41.3 L 37.314 -97.619 6.6 TES 5 0.0 1.2WTES 1
2016 1229 2314 20.9 L 37.300 -97.567 6.3 TES 7 0.0 1.6WTES 1
2016 1230 0212 40.1 L 37.301 -97.562 6.4 TES 5 0.0 1.1WTES 1

2016 1230 0457 24.7 L 37.216 -97.575 3.7 TES 4 0.0 1.3WTES 1
2016 1230 1809 25.9 L 37.434 -97.930 7.3 TES 9 0.1 2.3WTES 1
2016 1231 2115 8.7 L 37.506 -97.728 34.2 TES 9 0.2 2.7WTES 1
2017 1 1 1013 17.5 L 37.303 -97.501 4.5 TES 6 0.0 1.3WTES 1
2017 1 1 1058 52.9 L 37.108 -97.828 7.9 TES 8 0.0 2.2WTES 1
2017 1 2 1944 24.2 L 36.461 -96.975 0.2 TES 8 0.1 3.4WTES 1
2017 1 5 0726 2.4 L 37.411 -97.399 5.1 TES 5 0.0 1.2WTES 1
2017 1 5 0746 24.6 L 37.410 -97.400 5.5 TES 5 0.0 1.1WTES 1
2017 1 7 0440 41.0 L 37.114 -97.788 8.0 TES 6 0.1 2.3WTES 1
2017 1 8 1811 46.4 L 37.389 -97.747 1.2 TES 10 0.1 2.5WTES 1
2017 110 0107 2.7 L 37.402 -97.430 4.6 TES 9 0.0 1.2WTES 1
2017 110 0829 5.9 L 36.711 -97.618 3.7 TES 10 0.1 2.5WTES 1
2017 111 0115 12.8 L 37.401 -97.429 4.8 TES 11 0.0 1.9WTES 1
2017 111 0416 56.9 L 37.244 -97.528 3.6 TES 7 0.0 1.2WTES 1
2017 111 0621 38.6 L 37.172 -97.800 8.4 TES 10 0.1 2.1WTES 1
2017 111 0702 10.7 L 37.013 -97.399 2.2 TES 10 0.1 2.2WTES 1
2017 111 1515 23.6 L 37.115 -97.351 14.4 TES 11 0.0 2.2WTES 1
2017 111 1823 48.3 L 37.389 -97.746 1.1 TES 11 0.1 2.9WTES 1
2017 112 0312 56.6 L 37.023 -97.561 8.6 TES 10 0.0 2.1WTES 1
2017 112 1101 26.7 L 37.301 -97.622 4.3 TES 6 0.0 1.3WTES 1
2017 113 2122 47.8 L 37.398 -97.430 5.9 TES 7 0.0 1.3WTES 1
2017 113 2123 10.2 L 37.407 -97.432 4.0 TES 10 0.0 1.7WTES 1
2017 113 2353 39.9 L 37.406 -97.434 3.7 TES 7 0.0 1.4WTES 1
2017 115 0342 11.4 L 37.176 -97.840 10.0 TES 6 0.1 2.0WTES 1
2017 115 0613 47.1 L 37.317 -97.617 6.0 TES 5 0.0 1.2WTES 1
2017 115 1144 47.1 L 37.090 -97.556 4.4 TES 9 0.0 2.3WTES 1
2017 115 1415 40.4 L 37.270 -97.504 4.6 TES 6 0.0 1.3WTES 1
2017 115 2131 59.2 L 37.269 -97.505 4.5 TES 7 0.1 1.3WTES 1
2017 116 0924 11.9 L 37.332 -97.411 2.2 TES 6 0.0 1.1WTES 1
2017 116 0957 5.4 L 37.333 -97.412 2.2 TES 6 0.0 1.0WTES 1
2017 116 1129 9.0 L 37.332 -97.411 2.2 TES 6 0.0 1.1WTES 1

2017 116 1411 40.1 L 37.334 -97.411 2.0 TES 6 0.0 1.0WTES 1
2017 117 1607 45.3 L 37.230 -97.589 5.2 TES 7 0.0 1.6WTES 1
2017 117 1641 40.4 L 37.230 -97.589 5.0 TES 7 0.0 1.5WTES 1
2017 117 2149 23.3 L 37.230 -97.590 5.0 TES 6 0.0 1.3WTES 1
2017 118 0014 54.9 L 37.227 -97.590 5.1 TES 7 0.0 1.4WTES 1
2017 118 0041 1.5 L 37.230 -97.589 4.9 TES 7 0.0 1.3WTES 1
2017 118 0649 59.1 L 37.227 -97.592 4.9 TES 8 0.0 1.5WTES 1
2017 118 2259 28.4 L 37.228 -97.590 5.2 TES 8 0.0 1.8WTES 1
2017 121 2156 27.1 L 37.230 -97.589 4.4 TES 8 0.0 1.5WTES 1
2017 122 0114 31.6 L 37.317 -97.617 6.3 TES 5 0.0 1.2WTES 1
2017 122 0757 34.0 L 37.331 -97.429 2.4 TES 6 0.0 1.0WTES 1
2017 122 1252 32.5 L 37.228 -97.588 4.9 TES 9 0.0 1.7WTES 1
2017 123 1417 21.1 L 37.595 -97.752 1.9 TES 8 0.0 2.4WTES 1
2017 124 0811 24.3 L 37.581 -97.276 1.7 TES 5 0.1 1.4WTES 1
2017 124 1503 0.5 L 37.215 -97.582 3.0 TES 8 0.0 1.5WTES 1
2017 126 1738 50.4 L 37.321 -97.480 3.6 TES 7 0.0 1.5WTES 1
2017 128 0004 1.4 L 37.405 -97.433 3.7 TES 8 0.0 1.6WTES 1
2017 128 0031 3.5 L 37.399 -97.433 5.5 TES 7 0.0 1.4WTES 1
2017 128 0530 6.6 L 37.401 -97.430 4.8 TES 8 0.0 1.6WTES 1
2017 128 1707 33.6 L 37.397 -97.425 6.0 TES 5 0.0 1.3WTES 1
2017 129 0402 37.0 L 37.323 -97.480 3.7 TES 9 0.0 1.8WTES 1
2017 129 0404 1.6 L 37.322 -97.477 4.1 TES 9 0.0 1.4WTES 1
2017 129 0404 35.9 L 37.323 -97.479 3.9 TES 9 0.0 1.6WTES 1
2017 129 0411 50.7 L 37.323 -97.478 4.1 TES 9 0.0 1.8WTES 1
2017 129 0412 0.5 L 37.332 -97.492 1.9 TES 7 0.0 1.3WTES 1
2017 129 0434 25.3 L 37.321 -97.492 2.5 TES 6 0.0 1.0WTES 1
2017 129 0434 32.5 L 37.329 -97.485 3.2 TES 8 0.0 1.1WTES 1
2017 129 0516 36.4 L 37.321 -97.486 3.3 TES 4 0.0 1.0WTES 1
2017 129 0616 13.6 L 37.426 -97.366 5.9 TES 9 0.0 1.6WTES 1
2017 129 0657 51.8 L 37.082 -97.502 0.9 TES 7 0.0 1.9WTES 1
2017 129 0733 55.1 L 37.324 -97.478 3.8 TES 6 0.0 1.0WTES 1

2017 129 0753 42.7 L 37.319 -97.490 3.2 TES 5 0.0 1.0WTES 1
2017 131 0801 37.2 L 37.430 -97.372 3.4 TES 8 0.0 1.8WTES 1
2017 131 0810 42.5 L 37.430 -97.372 4.0 TES 9 0.0 1.8WTES 1
2017 131 1345 20.2 L 37.430 -97.372 3.3 TES 9 0.0 2.0WTES 1
2017 131 1437 33.2 L 37.435 -97.384 2.1 TES 7 0.0 1.3WTES 1
2017 131 2315 34.3 L 37.319 -97.476 4.2 TES 7 0.0 1.4WTES 1
2017 2 1 1412 29.4 L 37.425 -97.371 4.8 TES 8 0.0 1.7WTES 1
2017 2 2 0345 54.6 L 37.039 -97.378 6.8 TES 7 0.0 2.0WTES 1
2017 2 2 0541 14.9 L 37.441 -97.366 2.1 TES 9 0.1 1.6WTES 1
2017 2 3 1146 55.7 L 37.240 -97.407 0.3 TES 6 0.1 1.7WTES 1
2017 2 3 1149 23.0 L 37.236 -97.400 1.3 TES 6 0.0 1.4WTES 1
2017 2 3 1153 0.3 L 37.248 -97.402 4.8 TES 6 0.0 1.3WTES 1
2017 2 3 1349 6.6 L 37.250 -97.399 6.5 TES 6 0.0 1.3WTES 1
2017 2 3 1401 34.6 L 37.248 -97.400 5.8 TES 5 0.0 1.1WTES 1
2017 2 3 1412 43.7 L 37.223 -97.391 3.6 TES 5 0.0 1.1WTES 1
2017 2 3 1433 40.2 L 37.239 -97.407 0.1 TES 6 0.0 1.3WTES 1
2017 2 3 1446 9.7 L 37.239 -97.400 3.4 TES 6 0.0 1.8WTES 1
2017 2 3 1447 15.6 L 37.240 -97.405 3.8 TES 5 0.0 1.2WTES 1
2017 2 3 1549 12.7 L 37.243 -97.399 3.9 TES 4 0.0 1.2WTES 1
2017 2 3 1858 17.2 L 37.253 -97.370 0.1 TES 4 0.0 1.2WTES 1
2017 2 3 2004 45.8 L 37.237 -97.452 1.4 TES 3 0.0 1.0WTES 1
2017 2 3 2047 16.8 L 37.237 -97.406 3.3 TES 4 0.0 1.2WTES 1
2017 2 5 1239 29.8 L 37.244 -97.402 4.5 TES 7 0.0 1.2WTES 1
2017 2 5 1254 4.4 L 37.230 -97.393 6.3 TES 8 0.1 1.5WTES 1
2017 2 6 0937 38.7 L 37.050 -97.531 4.8 TES 7 0.0 1.8WTES 1
2017 2 6 1008 17.2 L 37.358 -97.408 3.3 TES 4 0.0 0.8WTES 1
2017 2 6 1252 34.1 L 37.293 -97.622 4.5 TES 6 0.0 1.5WTES 1
2017 2 7 0712 40.1 L 37.339 -97.449 3.1 TES 7 0.0 1.1WTES 1
2017 2 8 0314 48.6 L 37.050 -97.372 7.0 TES 10 0.0 2.8WTES 1
2017 2 8 2220 42.8 L 37.046 -97.377 6.7 TES 9 0.0 3.0WTES 1
2017 2 9 0002 55.2 L 37.047 -97.376 7.2 TES 10 0.0 2.0WTES 1

2017 2 9 150 5.8 L 37.321 -97.440 2.60 TES 6 .00 1.0WTES 1
2017 2 9 1128 42.6 L 37.202 -97.261 1.9 TES 6 0.0 1.6WTES 1
2017 2 9 1243 37.2 L 37.289 -97.514 4.7 TES 7 0.0 1.4WTES 1
2017 213 2139 59.1 L 37.048 -97.373 7.3 TES 10 0.1 3.2WTES 1
2017 214 0744 55.6 L 37.131 -97.653 7.8 TES 8 0.0 1.9WTES 1
2017 215 0232 10.4 L 37.044 -97.374 0.1 TES 7 0.0 2.3WTES 1
2017 216 1342 0.7 L 37.168 -97.839 8.1 TES 9 0.0 2.8WTES 1
2017 222 1018 53.3 L 37.298 -97.622 4.3 TES 5 0.0 1.4WTES 1
2017 222 1020 8.9 L 37.300 -97.624 5.1 TES 6 0.1 1.4WTES 1
2017 222 1132 29.1 L 37.417 -97.368 6.0 TES 8 0.0 1.6WTES 1
2017 222 1631 47.3 L 37.282 -97.955 1.4 TES 8 0.0 3.2WTES 1
2017 223 0218 3.6 L 37.328 -97.421 2.2 TES 6 0.0 1.4WTES 1
2017 223 0218 54.6 L 37.394 -97.405 3.8 TES 5 0.0 1.6WTES 1
2017 223 1442 44.6 L 37.300 -97.615 4.6 TES 9 0.0 1.8WTES 1
2017 223 1826 35.4 L 37.162 -97.822 8.8 TES 8 0.1 2.1WTES 1
2017 224 0124 48.0 L 37.160 -97.624 6.1 TES 8 0.1 1.6WTES 1
2017 224 0130 58.5 L 37.159 -97.627 5.0 TES 9 0.1 1.7WTES 1
2017 225 1036 43.0 L 37.038 -97.379 7.0 TES 10 0.0 2.8WTES 1
2017 225 1730 41.2 L 37.245 -97.531 2.3 TES 6 0.0 1.3WTES 1
2017 225 2143 40.3 L 37.244 -97.562 3.9 TES 8 0.1 1.4WTES 1
2017 226 0744 34.2 L 37.038 -97.386 7.4 TES 8 0.0 2.2WTES 1
2017 226 0753 21.2 L 37.038 -97.380 6.7 TES 8 0.0 1.9WTES 1
2017 228 2047 21.2 L 37.363 -97.389 4.3 TES 9 0.0 1.6WTES 1
2017 3 1 0125 36.8 L 37.367 -97.398 4.7 TES 6 0.0 1.1WTES 1
2017 3 1 0146 27.0 L 37.360 -97.383 4.3 TES 5 0.0 0.7WTES 1
2017 3 1 0212 46.3 L 37.371 -97.399 4.1 TES 6 0.0 1.2WTES 1
2017 3 2 1342 14.8 L 37.421 -97.376 5.1 TES 9 0.0 1.6WTES 1
2017 3 2 1828 51.8 L 37.309 -97.713 7.4 TES 9 0.0 2.1WTES 1
2017 3 3 0655 48.3 L 37.397 -97.425 5.7 TES 9 0.0 2.1WTES 1
2017 3 3 0710 36.9 L 37.396 -97.425 5.6 TES 8 0.0 1.4WTES 1
2017 3 4 0253 41.4 L 37.395 -97.423 5.8 TES 6 0.0 1.3WTES 1

2017 3 4 0358 15.8 L 37.306 -97.711 7.6 TES 9 0.0 1.6WTES 1
2017 3 4 0443 19.8 L 37.398 -97.424 5.0 TES 10 0.0 1.4WTES 1
2017 3 4 0742 15.3 L 37.399 -97.422 5.3 TES 9 0.0 1.3WTES 1
2017 3 4 1201 27.2 L 37.397 -97.421 5.2 TES 8 0.0 1.5WTES 1
2017 3 5 1206 36.7 L 37.080 -97.501 4.2 TES 9 0.1 2.2WTES 1
2017 3 6 2321 4.6 L 37.037 -97.380 2.0 TES 10 0.0 2.8WTES 1
2017 3 7 0459 11.8 L 37.341 -97.568 6.0 TES 6 0.0 1.4WTES 1
2017 3 8 1432 54.1 L 37.285 -97.509 4.8 TES 7 0.0 1.1WTES 1
2017 311 0612 36.8 L 37.418 -97.390 4.3 TES 8 0.0 2.3WTES 1
2017 311 0801 5.0 L 37.345 -97.575 4.7 TES 7 0.0 2.2WTES 1
2017 311 0808 43.6 L 37.346 -97.576 2.9 TES 7 0.0 1.5WTES 1
2017 311 2051 26.0 L 37.330 -97.492 2.7 TES 7 0.0 1.2WTES 1
2017 311 2328 46.2 L 37.324 -97.436 3.1 TES 7 0.0 0.9WTES 1
2017 312 0710 8.7 L 37.180 -97.822 9.3 TES 7 0.0 2.4WTES 1
2017 312 0954 43.5 L 37.418 -97.387 4.7 TES 6 0.0 1.4WTES 1
2017 312 1141 39.7 L 37.421 -97.392 4.0 TES 7 0.0 1.8WTES 1
2017 312 2019 54.3 L 37.046 -97.369 5.4 TES 7 0.0 2.7WTES 1
2017 312 2358 9.3 L 37.320 -97.443 3.2 TES 5 0.0 1.0WTES 1
2017 313 0220 13.2 L 37.051 -97.368 7.9 TES 7 0.0 2.2WTES 1
2017 313 2311 46.0 L 37.327 -97.455 1.2 TES 4 0.0 0.8WTES 1
2017 314 0905 22.8 L 37.228 -97.470 4.0 TES 10 0.0 1.5WTES 1
2017 315 0343 1.7 L 37.375 -97.372 4.6 TES 6 0.0 1.2WTES 1
2017 316 2351 24.0 L 37.229 -97.471 4.2 TES 10 0.0 1.4WTES 1
2017 317 0528 50.0 L 37.292 -97.567 2.8 TES 10 0.1 1.8WTES 1
2017 317 0905 58.2 L 37.230 -97.471 4.2 TES 8 0.0 1.3WTES 1
2017 317 1327 24.3 L 37.228 -97.470 4.1 TES 10 0.0 1.5WTES 1
2017 318 2011 16.1 L 37.228 -97.470 3.5 TES 10 0.0 1.6WTES 1
2017 318 2036 1.2 L 37.225 -97.471 4.5 TES 7 0.0 1.4WTES 1
2017 318 2129 43.8 L 37.228 -97.470 3.4 TES 10 0.0 1.5WTES 1
2017 319 0310 24.7 L 37.230 -97.470 4.2 TES 10 0.0 1.7WTES 1
2017 319 0311 17.3 L 37.235 -97.476 5.0 TES 6 0.0 1.3WTES 1

2017 319 1750 45.9 L 37.132 -97.658 6.6 TES 10 0.0 2.1WTES 1
2017 320 0352 4.5 L 37.230 -97.469 3.9 TES 7 0.0 1.2WTES 1
2017 320 0932 25.7 L 37.233 -97.470 3.9 TES 10 0.0 1.3WTES 1
2017 320 1020 29.9 L 37.229 -97.468 4.1 TES 7 0.0 1.2WTES 1
2017 320 1101 47.9 L 37.284 -97.390 1.4 TES 7 0.0 1.1WTES 1
2017 320 1221 4.0 L 37.229 -97.468 3.7 TES 8 0.0 1.2WTES 1
2017 320 2252 51.4 L 37.232 -97.472 4.6 TES 5 0.0 1.1WTES 1
2017 321 0105 51.5 L 37.229 -97.469 4.4 TES 10 0.0 1.4WTES 1
2017 321 0106 19.2 L 37.231 -97.469 4.0 TES 6 0.0 1.0WTES 1
2017 321 0903 4.1 L 37.230 -97.468 3.8 TES 10 0.0 1.7WTES 1
2017 322 0012 31.1 L 37.226 -97.469 3.7 TES 8 0.0 1.3WTES 1
2017 322 1445 54.0 L 37.045 -97.378 7.2 TES 10 0.0 2.5WTES 1
2017 323 1231 49.2 L 37.227 -97.469 3.4 TES 10 0.0 1.7WTES 1
2017 323 1234 21.5 L 37.229 -97.470 4.3 TES 8 0.0 1.4WTES 1
2017 324 1243 42.9 L 37.320 -97.443 3.1 TES 6 0.0 1.0WTES 1
2017 324 1949 47.2 L 37.234 -97.473 4.8 TES 7 0.0 1.3WTES 1
2017 324 2055 41.4 L 37.228 -97.472 3.8 TES 10 0.0 1.5WTES 1
2017 324 2342 32.3 L 37.226 -97.471 3.3 TES 7 0.0 1.2WTES 1
2017 324 2345 32.4 L 37.337 -97.410 15.0 TES 8 0.7 1.7WTES 1
2017 325 2115 47.9 L 37.383 -97.388 3.9 TES 10 0.0 2.3WTES 1
2017 325 2314 38.9 L 37.387 -97.397 3.2 TES 8 0.0 1.2WTES 1
2017 326 0010 18.5 L 37.389 -97.395 2.9 TES 9 0.0 1.4WTES 1
2017 326 0100 54.2 L 37.378 -97.385 4.0 TES 9 0.0 1.7WTES 1
2017 326 0131 8.1 L 37.380 -97.384 3.9 TES 8 0.0 1.3WTES 1
2017 326 0147 55.4 L 37.384 -97.393 3.9 TES 9 0.0 1.6WTES 1
2017 326 0201 50.5 L 37.384 -97.392 3.4 TES 9 0.0 1.5WTES 1
2017 326 0608 28.8 L 37.386 -97.391 3.7 TES 8 0.0 1.2WTES 1
2017 326 0652 41.2 L 37.387 -97.395 3.3 TES 9 0.0 1.6WTES 1
2017 326 1057 42.6 L 37.376 -97.383 4.2 TES 9 0.0 1.4WTES 1
2017 326 1614 5.8 L 37.222 -97.469 3.2 TES 6 0.0 1.2WTES 1
2017 326 1708 49.9 L 37.376 -97.383 4.0 TES 6 0.0 1.4WTES 1

2017 326 2022 2.5 L 37.227 -97.472 3.5 TES 7 0.0 1.3WTES 1
2017 326 2050 53.8 L 37.228 -97.473 4.4 TES 8 0.0 1.4WTES 1
2017 327 1302 29.5 L 37.227 -97.472 3.9 TES 10 0.0 2.0WTES 1
2017 327 1323 34.1 L 37.228 -97.472 3.3 TES 10 0.0 1.6WTES 1
2017 327 1727 31.9 L 37.435 -97.389 5.8 TES 9 0.0 1.3WTES 1
2017 327 1931 27.9 L 37.438 -97.391 4.7 TES 9 0.0 1.4WTES 1
2017 327 2345 59.1 L 37.439 -97.393 4.7 TES 8 0.0 1.4WTES 1
2017 327 2349 16.5 L 37.226 -97.472 3.9 TES 10 0.0 1.5WTES 1
2017 328 1707 32.3 L 37.437 -97.394 4.4 TES 5 0.0 2.3WTES 1
2017 329 0536 10.0 L 37.382 -97.389 3.9 TES 5 0.0 1.8WTES 1
2017 329 1411 18.2 L 37.230 -97.468 4.1 TES 5 0.0 1.6WTES 1
2017 329 1537 41.8 L 36.835 -97.656 6.1 TES 6 0.4 3.8WTES 1
2017 329 1749 16.7 L 37.384 -97.393 2.5 TES 4 0.0 1.4WTES 1
2017 330 0832 49.9 L 37.381 -97.391 3.4 TES 5 0.0 2.9WTES 1
2017 330 0901 40.9 L 37.346 -97.577 3.4 TES 5 0.0 1.5WTES 1
2017 330 0918 24.0 L 37.382 -97.388 3.4 TES 5 0.0 1.7WTES 1
2017 330 1006 26.0 L 37.313 -97.397 2.0 TES 3 0.1 1.0WTES 1
2017 330 1506 38.0 L 37.386 -97.390 2.2 TES 5 0.0 2.2WTES 1
2017 330 1854 56.0 L 37.381 -97.392 2.9 TES 5 0.0 2.2WTES 1
2017 330 1904 37.8 L 37.387 -97.393 3.3 TES 4 0.0 1.5WTES 1
2017 330 1920 48.4 L 37.225 -97.472 3.6 TES 5 0.0 1.3WTES 1
2017 330 1925 41.3 L 37.385 -97.390 3.1 TES 4 0.0 1.7WTES 1
2017 330 1926 9.8 L 37.385 -97.389 2.8 TES 4 0.0 1.8WTES 1
2017 330 1931 22.0 L 37.227 -97.472 3.7 TES 5 0.0 1.7WTES 1
2017 330 1957 33.4 L 37.385 -97.389 3.2 TES 4 0.0 1.5WTES 1
2017 4 1 0223 42.0 L 37.347 -97.577 3.6 TES 5 0.0 1.6WTES 1
2017 4 1 0912 42.7 L 37.286 -97.415 4.5 TES 4 0.0 1.5WTES 1
2017 4 1 1044 44.1 L 37.288 -97.418 4.4 TES 3 0.0 1.1WTES 1
2017 4 1 2338 24.6 L 37.227 -97.473 3.2 TES 5 0.0 1.6WTES 1
2017 4 2 0414 34.3 L 37.227 -97.472 3.8 TES 5 0.0 1.4WTES 1
2017 4 2 0718 20.3 L 37.378 -97.388 4.0 TES 4 0.0 1.4WTES 1

2017 4 2 1452 20.8 L 37.348 -97.575 3.2 TES 4 0.0 1.3WTES 1
2017 4 2 1617 19.8 L 37.228 -97.473 3.4 TES 5 0.0 1.4WTES 1
2017 4 2 2116 52.4 L 37.433 -97.393 4.9 TES 5 0.0 2.1WTES 1
2017 4 3 0258 59.1 L 37.231 -97.471 3.5 TES 5 0.0 1.8WTES 1
2017 4 3 0313 42.5 L 37.233 -97.470 2.7 TES 5 0.0 1.4WTES 1
2017 4 3 1339 51.2 L 37.232 -97.469 3.4 TES 5 0.0 2.1WTES 1
2017 4 3 1426 9.8 L 37.230 -97.468 3.6 TES 5 0.0 1.5WTES 1
2017 4 3 1433 46.8 L 37.229 -97.473 3.3 TES 5 0.0 1.5WTES 1
2017 4 3 1809 4.6 L 37.231 -97.467 3.2 TES 5 0.0 1.3WTES 1
2017 4 3 2145 14.1 L 37.231 -97.468 3.6 TES 5 0.0 1.4WTES 1
2017 4 3 2204 25.0 L 37.381 -97.393 3.5 TES 4 0.0 1.7WTES 1
2017 4 4 0031 30.0 L 37.381 -97.387 3.5 TES 10 0.0 2.1WTES 1
2017 4 4 0109 42.3 L 37.383 -97.390 3.5 TES 9 0.0 2.0WTES 1
2017 4 4 0112 29.2 L 37.379 -97.389 3.9 TES 9 0.0 1.4WTES 1
2017 4 4 0149 57.5 L 37.383 -97.391 3.6 TES 9 0.0 1.3WTES 1
2017 4 4 0159 16.7 L 37.386 -97.394 3.1 TES 9 0.0 1.8WTES 1
2017 4 4 0317 54.3 L 37.390 -97.401 3.1 TES 8 0.0 1.2WTES 1
2017 4 5 1601 55.3 L 37.225 -97.472 3.5 TES 10 0.0 2.0WTES 1
2017 4 6 0402 23.9 L 37.390 -97.397 2.6 TES 9 0.0 1.6WTES 1
2017 4 7 0516 4.8 L 37.229 -97.469 3.9 TES 10 0.0 1.9WTES 1
2017 4 7 0519 59.0 L 37.231 -97.471 4.0 TES 10 0.0 1.7WTES 1
2017 4 7 1747 46.3 L 37.300 -97.498 4.9 TES 10 0.1 1.8WTES 1
2017 4 8 1034 41.2 L 37.151 -97.673 6.8 TES 9 0.1 2.5WTES 1
2017 4 8 1944 21.3 L 37.133 -97.653 6.9 TES 9 0.0 2.1WTES 1
2017 4 9 0208 14.7 L 37.228 -97.469 4.0 TES 9 0.0 1.4WTES 1
2017 410 0017 44.7 L 37.434 -97.393 4.8 TES 10 0.0 2.1WTES 1
2017 410 0019 32.2 L 37.434 -97.391 4.7 TES 9 0.1 1.5WTES 1
2017 410 0105 14.7 L 37.431 -97.390 6.7 TES 10 0.0 1.5WTES 1
2017 410 1101 12.5 L 37.424 -97.385 7.2 TES 8 0.0 1.7WTES 1
2017 410 1102 49.5 L 37.428 -97.388 6.5 TES 9 0.0 1.5WTES 1
2017 410 1145 22.5 L 37.302 -97.502 4.6 TES 8 0.0 1.4WTES 1

2017 410 1250 45.7 L 37.135 -97.650 7.1 TES 9 0.0 1.8WTES 1
2017 410 1307 9.2 L 37.135 -97.650 7.3 TES 10 0.0 2.0WTES 1
2017 410 1420 46.5 L 37.224 -97.470 3.2 TES 9 0.0 1.5WTES 1
2017 410 1734 13.4 L 37.225 -97.469 3.6 TES 10 0.0 2.1WTES 1
2017 410 1819 37.3 L 37.364 -97.394 4.9 TES 10 0.0 1.5WTES 1
2017 410 1819 43.8 L 37.347 -97.386 5.6 TES 7 0.0 1.4WTES 1
2017 410 2015 15.2 L 37.365 -97.389 4.7 TES 9 0.0 1.1WTES 1
2017 410 2049 49.3 L 37.223 -97.470 3.2 TES 7 0.0 1.4WTES 1
2017 411 1039 34.6 L 37.226 -97.472 3.4 TES 5 0.0 1.8WTES 1
2017 412 0231 19.9 L 37.231 -97.469 3.7 TES 5 0.0 2.3WTES 1
2017 413 1741 22.0 L 37.306 -97.504 2.2 TES 5 0.0 1.2WTES 1
2017 413 1843 19.6 L 37.370 -97.401 4.1 TES 4 0.0 1.5WTES 1
2017 413 1844 9.6 L 37.365 -97.391 4.3 TES 4 0.0 1.5WTES 1
2017 413 1855 0.0 L 37.368 -97.391 4.6 TES 4 0.0 1.3WTES 1
2017 413 2343 10.1 L 37.232 -97.468 3.8 TES 5 0.0 1.4WTES 1
2017 414 0424 55.4 L 37.237 -97.861 7.8 TES 5 0.0 2.9WTES 1
2017 415 1927 13.2 L 37.361 -97.392 5.0 TES 5 0.0 1.9WTES 1
2017 416 0034 23.7 L 37.364 -97.391 4.5 TES 4 0.0 1.3WTES 1
2017 416 0034 43.9 L 37.435 -97.391 5.3 TES 4 0.0 1.5WTES 1
2017 416 0121 2.5 L 37.224 -97.473 4.0 TES 5 0.0 1.5WTES 1
2017 416 0201 36.9 L 37.228 -97.471 4.0 TES 5 0.0 1.6WTES 1
2017 416 0202 42.9 L 37.367 -97.392 4.5 TES 5 0.0 1.7WTES 1
2017 416 0448 39.8 L 37.317 -97.591 4.2 TES 4 0.0 1.2WTES 1
2017 416 1910 28.7 L 37.349 -97.576 3.1 TES 5 0.0 1.3WTES 1
2017 417 1010 18.0 L 37.303 -97.500 4.6 TES 5 0.0 1.7WTES 1
2017 418 1451 14.2 L 37.231 -97.467 4.4 TES 10 0.0 1.8WTES 1
2017 418 1856 36.8 L 37.431 -97.393 6.0 TES 10 0.0 2.0WTES 1
2017 419 0747 38.8 L 37.231 -97.470 3.8 TES 10 0.0 1.6WTES 1
2017 419 0807 5.2 L 37.433 -97.396 5.5 TES 10 0.0 2.7WTES 1
2017 419 1013 43.6 L 37.427 -97.389 6.8 TES 9 0.0 1.7WTES 1
2017 419 1013 46.2 L 37.429 -97.392 6.0 TES 9 0.0 1.6WTES 1

2017 419 1042 5.9 L 37.133 -97.651 7.4 TES 9 0.0 1.9WTES 1
2017 419 1109 54.1 L 37.230 -97.469 3.8 TES 10 0.0 1.6WTES 1
2017 419 1949 58.4 L 37.231 -97.473 4.0 TES 9 0.0 1.7WTES 1
2017 419 1950 23.3 L 37.232 -97.474 4.9 TES 10 0.0 1.7WTES 1
2017 420 0936 39.0 L 37.228 -97.471 3.5 TES 10 0.0 2.4WTES 1
2017 420 0958 34.9 L 37.228 -97.471 3.8 TES 10 0.0 2.6WTES 1
2017 420 1027 28.3 L 37.227 -97.472 3.5 TES 10 0.0 1.8WTES 1
2017 421 0037 47.9 L 37.231 -97.470 5.0 TES 7 0.0 1.3WTES 1
2017 421 0208 44.8 L 37.231 -97.468 4.2 TES 10 0.0 1.5WTES 1
2017 421 0229 25.8 L 37.231 -97.467 4.2 TES 8 0.0 1.4WTES 1
2017 421 0307 21.0 L 37.231 -97.467 4.2 TES 8 0.0 1.4WTES 1
2017 421 1821 41.6 L 37.230 -97.467 3.9 TES 10 0.0 2.1WTES 1
2017 422 0159 19.8 L 37.228 -97.471 3.7 TES 10 0.0 2.2WTES 1
2017 422 1102 35.4 L 37.144 -97.433 5.5 TES 9 0.0 2.0WTES 1
2017 422 1329 38.5 L 37.230 -97.467 4.0 TES 10 0.0 1.7WTES 1
2017 423 1812 2.5 L 37.415 -97.391 5.1 TES 10 0.0 1.5WTES 1
2017 424 0328 51.1 L 37.289 -97.603 3.0 TES 5 0.1 1.5WTES 1
2017 424 0329 7.1 L 37.290 -97.602 3.2 TES 6 0.1 1.2WTES 1
2017 424 0346 20.2 L 37.290 -97.602 3.3 TES 6 0.1 1.7WTES 1
2017 424 0412 36.2 L 37.289 -97.603 3.2 TES 8 0.1 1.3WTES 1
2017 424 0413 24.2 L 37.296 -97.600 3.8 TES 6 0.0 1.4WTES 1
2017 424 0414 8.4 L 37.291 -97.601 3.4 TES 6 0.1 1.4WTES 1
2017 424 0416 27.5 L 37.289 -97.602 3.0 TES 9 0.1 1.4WTES 1
2017 424 0417 8.8 L 37.294 -97.601 3.5 TES 8 0.1 1.9WTES 1
2017 424 0420 27.4 L 37.290 -97.601 1.9 TES 9 0.1 1.5WTES 1
2017 424 0421 21.0 L 37.288 -97.603 1.7 TES 10 0.1 1.4WTES 1
2017 424 0424 0.9 L 37.291 -97.601 2.2 TES 10 0.1 1.3WTES 1
2017 424 0440 6.7 L 37.290 -97.601 1.9 TES 9 0.1 2.2WTES 1
2017 424 0446 28.8 L 37.288 -97.603 2.4 TES 7 0.1 1.7WTES 1
2017 424 0610 19.4 L 37.289 -97.605 2.7 TES 10 0.1 1.4WTES 1
2017 424 0616 2.6 L 37.287 -97.605 2.6 TES 9 0.1 1.9WTES 1

2017 424 0736 10.9 L 37.130 -97.616 4.8 TES 8 0.0 2.0WTES 1
2017 424 1241 46.9 L 37.300 -97.442 5.3 TES 5 0.0 1.4WTES 1
2017 425 0126 59.1 L 37.074 -97.700 7.8 TES 10 0.0 2.3WTES 1
2017 425 1240 25.8 L 36.826 -97.760 8.6 TES 10 0.0 2.8WTES 1
2017 425 1547 39.6 L 37.432 -97.391 6.2 TES 10 0.0 2.0WTES 1
2017 425 1855 54.9 L 37.232 -97.469 4.5 TES 6 0.0 1.4WTES 1
2017 425 2243 27.1 L 37.432 -97.392 6.2 TES 9 0.0 1.6WTES 1
2017 426 0238 8.5 L 37.275 -97.396 2.6 TES 6 0.0 1.2WTES 1
2017 426 0820 20.7 L 37.287 -97.393 3.7 TES 7 0.0 1.4WTES 1
2017 426 1831 22.5 L 37.226 -97.469 3.5 TES 10 0.0 1.7WTES 1
2017 426 2011 16.9 L 37.228 -97.471 3.9 TES 9 0.0 1.3WTES 1
2017 427 0440 48.2 L 37.287 -97.392 3.6 TES 10 0.0 1.9WTES 1
2017 427 0443 48.1 L 37.282 -97.389 2.2 TES 7 0.0 1.4WTES 1
2017 427 0714 14.7 L 37.412 -97.391 5.6 TES 9 0.0 1.6WTES 1
2017 427 0841 28.3 L 37.288 -97.393 3.7 TES 7 0.0 1.0WTES 1
2017 427 1126 8.2 L 37.290 -97.393 3.9 TES 8 0.0 1.3WTES 1
2017 427 1134 9.2 L 37.281 -97.390 0.5 TES 5 0.0 1.4WTES 1
2017 427 1325 29.6 L 37.425 -97.422 5.9 TES 7 0.0 1.7WTES 1
2017 428 0706 46.2 L 37.280 -97.392 0.9 TES 5 0.0 1.3WTES 1
2017 428 0714 53.0 L 37.281 -97.391 2.2 TES 6 0.0 1.3WTES 1
2017 428 0720 32.7 L 37.279 -97.395 2.5 TES 6 0.0 1.0WTES 1
2017 428 0941 59.3 L 37.282 -97.396 3.4 TES 5 0.0 1.2WTES 1
2017 429 0026 9.2 L 37.289 -97.390 3.6 TES 9 0.0 1.2WTES 1
2017 429 1910 40.9 L 37.231 -97.467 3.9 TES 7 0.0 1.6WTES 1
2017 429 1942 32.2 L 37.276 -97.397 2.4 TES 6 0.0 1.5WTES 1
2017 429 1943 46.0 L 37.286 -97.386 2.7 TES 6 0.0 1.5WTES 1
2017 429 2010 21.8 L 37.279 -97.392 0.1 TES 5 0.0 1.2WTES 1
2017 429 2225 52.2 L 37.174 -97.814 9.9 TES 7 0.1 2.5WTES 1
2017 430 0512 57.1 L 37.318 -97.604 3.1 TES 7 0.0 1.8WTES 1
2017 430 1607 36.6 L 37.285 -97.380 0.3 TES 5 0.0 1.2WTES 1
2017 430 1815 2.8 L 37.278 -97.394 2.8 TES 6 0.0 1.1WTES 1

2017 430 1824 29.7 L 37.298 -97.429 6.2 TES 5 0.0 1.1WTES 1
2017 5 1 0137 23.9 L 37.280 -97.388 0.6 TES 7 0.0 1.1WTES 1
2017 5 1 0429 38.4 L 37.286 -97.388 3.0 TES 7 0.0 1.1WTES 1
2017 5 1 0430 15.4 L 37.286 -97.388 3.3 TES 9 0.0 1.4WTES 1
2017 5 1 0525 30.8 L 37.290 -97.390 4.1 TES 8 0.0 1.5WTES 1
2017 5 1 1122 27.7 L 37.275 -97.393 1.2 TES 5 0.0 1.1WTES 1
2017 5 2 0021 55.8 L 37.400 -97.429 5.7 TES 7 0.0 1.4WTES 1
2017 5 2 1146 14.8 L 37.274 -97.389 2.0 TES 5 0.0 0.9WTES 1
2017 5 2 1148 6.9 L 37.281 -97.387 0.3 TES 6 0.0 0.9WTES 1
2017 5 2 1246 8.4 L 37.281 -97.383 2.1 TES 7 0.0 0.9WTES 1
2017 5 2 1246 15.4 L 37.281 -97.381 1.2 TES 7 0.0 0.9WTES 1
2017 5 2 1425 25.2 L 37.281 -97.387 2.3 TES 6 0.0 0.9WTES 1
2017 5 2 1619 45.2 L 37.279 -97.386 0.1 TES 6 0.0 1.1WTES 1
2017 5 2 1620 15.1 L 37.283 -97.382 2.1 TES 7 0.0 1.2WTES 1
2017 5 2 1655 54.7 L 37.283 -97.382 2.3 TES 7 0.0 1.1WTES 1
2017 5 2 1658 26.4 L 37.287 -97.387 3.4 TES 9 0.0 1.4WTES 1
2017 5 2 1733 19.9 L 37.295 -97.397 5.1 TES 8 0.0 1.1WTES 1
2017 5 2 2355 30.0 L 37.239 -97.560 5.8 TES 9 0.0 1.6WTES 1
2017 5 3 0124 46.1 L 37.238 -97.560 5.9 TES 9 0.0 1.3WTES 1
2017 5 4 0258 52.8 L 37.267 -97.415 3.1 TES 6 0.0 1.0WTES 1
2017 5 4 0934 16.2 L 37.363 -97.386 4.7 TES 8 0.0 1.0WTES 1
2017 5 4 1038 1.3 L 37.239 -97.559 5.7 TES 9 0.0 1.4WTES 1
2017 5 5 0351 11.1 L 37.302 -97.502 4.9 TES 9 0.0 1.2WTES 1
2017 5 5 0618 14.0 L 37.166 -97.632 7.8 TES 9 0.0 2.1WTES 1
2017 5 5 1653 22.3 L 37.296 -97.402 5.2 TES 8 0.0 1.3WTES 1
2017 5 5 2147 38.2 L 37.289 -97.391 3.6 TES 6 0.0 0.9WTES 1
2017 5 7 0709 1.0 L 37.315 -97.404 2.3 TES 5 0.0 0.8WTES 1
2017 5 7 1104 47.2 L 37.229 -97.469 4.2 TES 9 0.0 1.4WTES 1
2017 5 7 2108 21.7 L 36.893 -98.076 5.4 TES 8 0.0 2.9WTES 1
2017 5 8 0454 13.4 L 37.279 -97.393 0.6 TES 7 0.0 1.3WTES 1
2017 5 8 0732 33.3 L 37.347 -97.582 2.9 TES 7 0.0 1.1WTES 1

2017 5 8 0735 47.1 L 37.346 -97.583 2.9 TES 8 0.0 1.3WTES 1
2017 5 8 1056 14.1 L 37.347 -97.585 2.9 TES 7 0.1 1.2WTES 1
2017 5 9 2140 31.2 L 37.225 -97.470 3.7 TES 9 0.0 1.5WTES 1
2017 510 1024 18.7 L 37.429 -97.393 6.3 TES 9 0.0 1.5WTES 1
2017 510 1052 28.8 L 37.367 -97.753 5.7 TES 9 0.0 2.8WTES 1
2017 510 2055 55.5 L 37.228 -97.468 3.9 TES 9 0.0 1.9WTES 1
2017 511 0639 13.4 L 37.227 -97.466 3.6 TES 9 0.0 1.4WTES 1
2017 511 0907 18.6 L 37.320 -97.391 3.1 TES 8 0.0 1.5WTES 1
2017 511 0936 36.6 L 37.316 -97.384 2.0 TES 7 0.0 1.2WTES 1
2017 511 0947 16.0 L 37.324 -97.389 3.0 TES 9 0.0 1.7WTES 1
2017 511 1207 48.1 L 37.228 -97.469 4.2 TES 9 0.0 1.2WTES 1
2017 511 1525 39.0 L 37.224 -97.472 3.5 TES 9 0.0 1.5WTES 1
2017 511 1753 2.9 L 37.226 -97.470 4.1 TES 9 0.0 1.4WTES 1
2017 511 1850 21.6 L 37.226 -97.467 4.2 TES 8 0.0 1.5WTES 1
2017 511 2023 59.0 L 37.231 -97.466 4.3 TES 9 0.0 1.5WTES 1
2017 511 2027 32.0 L 37.231 -97.466 4.1 TES 9 0.0 1.5WTES 1
2017 512 0437 8.7 L 37.365 -97.753 5.3 TES 9 0.0 2.0WTES 1
2017 512 0437 59.7 L 37.367 -97.757 5.4 TES 9 0.0 1.8WTES 1
2017 512 0440 3.1 L 37.283 -97.422 4.2 TES 8 0.0 1.4WTES 1
2017 512 0534 16.2 L 37.226 -97.468 3.6 TES 9 0.0 1.3WTES 1
2017 512 1416 29.6 L 37.227 -97.470 4.6 TES 9 0.0 1.5WTES 1
2017 512 2042 23.0 L 37.228 -97.471 4.9 TES 9 0.0 1.5WTES 1
2017 512 2157 40.8 L 37.274 -97.417 0.6 TES 5 0.0 1.0WTES 1
2017 513 0832 38.2 L 36.571 -98.773 1.2 TES 10 0.4 4.0WTES 1
2017 513 1339 56.6 L 37.225 -97.470 4.3 TES 9 0.0 1.5WTES 1
2017 513 1402 41.0 L 37.438 -97.419 5.7 TES 9 0.0 1.6WTES 1
2017 513 1455 28.5 L 37.282 -97.418 3.0 TES 7 0.0 1.1WTES 1
2017 513 2023 37.1 L 37.278 -97.431 3.2 TES 6 0.0 1.0WTES 1
2017 513 2318 35.8 L 37.288 -97.424 4.1 TES 8 0.0 1.2WTES 1
2017 514 0045 18.5 L 37.224 -97.465 3.1 TES 9 0.0 1.4WTES 1
2017 514 1010 23.6 L 37.288 -97.426 4.5 TES 9 0.0 1.7WTES 1

2017 514 1102 43.2 L 37.276 -97.411 1.5 TES 5 0.0 1.0WTES 1
2017 514 1759 25.3 L 37.439 -97.419 4.8 TES 9 0.0 1.7WTES 1
2017 515 0543 30.7 L 37.122 -97.566 3.8 TES 9 0.0 1.8WTES 1
2017 515 0825 5.0 L 37.225 -97.471 4.3 TES 9 0.0 1.6WTES 1
2017 515 1241 6.8 L 37.274 -97.426 4.1 TES 7 0.0 0.9WTES 1
2017 517 0348 42.4 L 37.443 -97.429 0.2 TES 9 0.0 1.7WTES 1
2017 517 2139 16.8 L 37.275 -97.424 4.3 TES 8 0.0 1.3WTES 1
2017 518 0310 49.4 L 37.230 -97.467 3.9 TES 9 0.0 1.6WTES 1
2017 518 0337 18.8 L 37.231 -97.467 4.2 TES 9 0.0 1.4WTES 1
2017 518 0940 0.3 L 37.288 -97.426 4.7 TES 9 0.0 1.5WTES 1
2017 518 1055 51.5 L 37.286 -97.426 4.4 TES 9 0.0 1.5WTES 1
2017 519 0732 50.2 L 37.246 -97.955 10.4 TES 9 0.0 2.9WTES 1
2017 519 1245 6.9 L 37.226 -97.469 4.1 TES 9 0.0 1.7WTES 1
2017 519 1402 21.3 L 37.464 -97.514 4.0 TES 9 0.0 1.6WTES 1
2017 519 1602 2.8 L 37.463 -97.513 5.0 TES 9 0.0 2.2WTES 1
2017 520 0016 0.9 L 37.452 -97.510 8.0 TES 8 0.0 1.4WTES 1
2017 520 0524 41.2 L 37.226 -97.474 0.2 TES 8 0.0 1.3WTES 1
2017 520 2040 20.0 L 37.366 -97.630 2.1 TES 8 0.0 1.7WTES 1
2017 521 1451 16.6 L 37.227 -97.469 3.8 TES 9 0.0 1.6WTES 1
2017 521 1814 53.5 L 37.221 -97.472 2.3 TES 8 0.0 1.5WTES 1
2017 522 0213 37.5 L 37.227 -97.468 4.3 TES 9 0.0 1.7WTES 1
2017 522 0224 57.9 L 37.224 -97.468 2.9 TES 9 0.0 1.3WTES 1
2017 523 0601 37.5 L 37.415 -97.368 6.4 TES 8 0.0 1.4WTES 1
2017 523 1328 30.8 L 37.366 -97.627 0.1 TES 8 0.0 1.5WTES 1
2017 523 1420 46.4 L 37.225 -97.469 3.6 TES 8 0.0 2.2WTES 1
2017 524 1258 28.4 L 37.419 -97.371 6.2 TES 9 0.0 1.4WTES 1
2017 524 2115 59.9 L 37.227 -97.469 4.7 TES 9 0.0 1.4WTES 1
2017 524 2120 29.5 L 37.220 -97.472 1.1 TES 8 0.0 1.3WTES 1
2017 524 2140 57.6 L 37.415 -97.368 6.1 TES 10 0.0 1.5WTES 1
2017 525 0206 60.0 L 37.225 -97.469 3.1 TES 10 0.0 1.6WTES 1
2017 525 0719 31.8 L 37.226 -97.469 3.4 TES 10 0.0 1.8WTES 1

2017 525 0916 8.7 L 37.226 -97.472 3.7 TES 10 0.0 2.1WTES 1
2017 525 2003 49.9 L 37.413 -97.370 7.2 TES 10 0.0 1.7WTES 1
2017 526 0303 27.8 L 37.262 -97.440 2.2 TES 6 0.0 1.1WTES 1
2017 526 0417 14.1 L 37.423 -97.376 5.5 TES 9 0.0 2.0WTES 1
2017 526 0429 35.0 L 37.428 -97.375 4.1 TES 8 0.0 1.4WTES 1
2017 526 0458 29.3 L 37.411 -97.371 7.4 TES 9 0.0 2.6WTES 1
2017 526 0533 50.7 L 37.419 -97.371 6.2 TES 10 0.0 1.9WTES 1
2017 526 0741 23.0 L 37.421 -97.371 5.8 TES 10 0.0 1.8WTES 1
2017 526 1605 21.4 L 37.424 -97.375 5.1 TES 10 0.0 1.6WTES 1
2017 526 1606 53.1 L 37.424 -97.378 5.2 TES 10 0.0 1.6WTES 1
2017 526 1722 47.5 L 37.423 -97.374 5.5 TES 10 0.0 2.1WTES 1
2017 526 1840 2.7 L 37.277 -97.433 4.8 TES 9 0.0 1.2WTES 1
2017 526 1917 28.3 L 37.420 -97.375 5.8 TES 10 0.0 1.7WTES 1
2017 526 1948 26.5 L 37.277 -97.434 4.6 TES 10 0.0 1.1WTES 1
2017 526 2011 0.9 L 37.416 -97.372 6.3 TES 10 0.0 1.4WTES 1
2017 526 2135 7.4 L 37.414 -97.370 6.9 TES 10 0.0 2.1WTES 1
2017 527 0012 48.8 L 37.278 -97.435 3.7 TES 7 0.0 1.1WTES 1
2017 527 0033 21.4 L 37.416 -97.372 5.3 TES 10 0.0 1.4WTES 1
2017 527 0728 12.1 L 37.275 -97.429 4.3 TES 9 0.0 1.0WTES 1
2017 527 1040 50.1 L 37.423 -97.374 5.9 TES 10 0.0 1.5WTES 1
2017 527 2141 21.1 L 37.419 -97.374 5.9 TES 10 0.0 1.6WTES 1
2017 528 0257 39.4 L 37.420 -97.374 6.1 TES 9 0.0 1.7WTES 1
2017 528 0723 13.1 L 37.418 -97.370 6.9 TES 8 0.0 1.3WTES 1
2017 528 1332 25.6 L 37.414 -97.366 7.0 TES 9 0.0 1.6WTES 1
2017 528 1336 14.5 L 37.290 -97.449 5.7 TES 9 0.0 1.1WTES 1
2017 528 1558 12.0 L 37.414 -97.370 6.7 TES 10 0.0 1.7WTES 1
2017 528 1724 26.5 L 37.417 -97.372 6.4 TES 10 0.0 2.0WTES 1
2017 528 2017 26.6 L 37.416 -97.370 6.4 TES 10 0.0 2.6WTES 1
2017 528 2238 24.9 L 37.411 -97.367 7.4 TES 9 0.0 1.4WTES 1
2017 528 2326 17.3 L 37.418 -97.373 6.0 TES 10 0.0 1.5WTES 1
2017 529 0610 46.7 L 37.420 -97.367 6.1 TES 10 0.0 1.5WTES 1

2017 529 0613 33.9 L 37.409 -97.364 7.7 TES 10 0.0 1.7WTES 1
2017 529 1047 18.3 L 37.419 -97.367 6.6 TES 10 0.0 1.8WTES 1
2017 529 2048 49.9 L 37.274 -97.621 3.7 TES 10 0.0 1.8WTES 1
2017 529 2147 15.6 L 37.414 -97.365 7.1 TES 9 0.0 1.3WTES 1
2017 529 2231 39.7 L 37.427 -97.374 4.1 TES 9 0.0 1.4WTES 1
2017 529 2231 55.0 L 37.277 -97.623 4.2 TES 10 0.0 1.6WTES 1
2017 529 2240 48.8 L 37.278 -97.622 4.0 TES 10 0.0 2.3WTES 1
2017 530 0029 48.9 L 37.403 -97.360 8.5 TES 7 0.0 1.2WTES 1
2017 530 0048 35.6 L 37.274 -97.622 4.2 TES 9 0.0 1.6WTES 1
2017 530 0244 6.0 L 37.426 -97.374 4.6 TES 6 0.0 1.4WTES 1
2017 530 0445 3.9 L 37.418 -97.373 5.9 TES 10 0.0 2.6WTES 1
2017 530 0510 3.5 L 37.418 -97.376 6.2 TES 10 0.0 1.7WTES 1
2017 530 0513 46.2 L 37.419 -97.371 7.1 TES 10 0.0 1.9WTES 1
2017 530 0721 17.8 L 37.275 -97.622 3.9 TES 10 0.0 1.7WTES 1
2017 530 0808 52.8 L 37.277 -97.623 4.1 TES 10 0.0 1.6WTES 1
2017 530 0809 39.6 L 37.276 -97.622 4.2 TES 10 0.0 1.6WTES 1
2017 530 1105 40.1 L 37.456 -97.512 7.3 TES 10 0.0 2.7WTES 1
2017 530 1433 47.3 L 37.422 -97.378 5.1 TES 9 0.0 1.7WTES 1
2017 530 1807 25.8 L 37.420 -97.369 5.9 TES 9 0.0 1.5WTES 1
2017 530 1811 34.0 L 37.418 -97.368 6.2 TES 10 0.0 1.8WTES 1
2017 530 1954 55.1 L 37.423 -97.372 5.4 TES 10 0.0 2.1WTES 1
2017 530 2022 27.6 L 37.431 -97.373 2.1 TES 10 0.0 1.8WTES 1
2017 530 2050 2.2 L 37.420 -97.368 6.1 TES 9 0.0 1.6WTES 1
2017 530 2055 56.3 L 37.458 -97.514 6.9 TES 10 0.0 2.5WTES 1
2017 531 0406 57.9 L 37.419 -97.372 5.9 TES 8 0.0 1.3WTES 1
2017 531 1137 8.4 L 37.430 -97.381 0.6 TES 8 0.0 1.4WTES 1
2017 531 1210 5.7 L 37.415 -97.376 6.5 TES 10 0.0 1.8WTES 1
2017 531 1227 24.2 L 37.425 -97.370 5.1 TES 10 0.0 2.1WTES 1
2017 531 1233 10.8 L 37.403 -97.366 8.3 TES 10 0.0 1.8WTES 1
2017 531 1618 11.7 L 37.276 -97.622 4.3 TES 10 0.0 1.9WTES 1
2017 6 1 0138 26.7 L 37.289 -97.508 4.8 TES 9 0.0 1.3WTES 1

2017 6 1 0232 21.0 L 37.427 -97.377 4.9 TES 10 0.0 2.1WTES 1
2017 6 1 0923 22.6 L 37.430 -97.378 0.8 TES 10 0.0 1.7WTES 1
2017 6 1 1826 40.4 L 37.223 -97.949 7.6 TES 9 0.0 3.0WTES 1
2017 6 1 2048 7.5 L 37.451 -97.515 8.2 TES 10 0.0 2.8WTES 1
2017 6 2 0012 22.8 L 37.418 -97.372 6.8 TES 7 0.0 2.6WTES 1
2017 6 2 0015 15.8 L 37.420 -97.376 6.6 TES 7 0.0 1.9WTES 1
2017 6 2 0019 1.9 L 37.417 -97.376 7.1 TES 7 0.0 2.1WTES 1
2017 6 2 0348 38.4 L 37.419 -97.371 6.1 TES 10 0.0 2.1WTES 1
2017 6 2 0533 4.8 L 37.364 -97.413 3.0 TES 6 0.0 1.1WTES 1
2017 6 2 0700 8.0 L 37.419 -97.371 6.2 TES 10 0.0 2.5WTES 1
2017 6 2 1053 32.3 L 37.419 -97.371 6.6 TES 10 0.0 1.9WTES 1
2017 6 2 1058 42.7 L 37.359 -97.409 3.0 TES 8 0.0 1.2WTES 1
2017 6 2 1144 0.5 L 37.355 -97.405 3.3 TES 8 0.0 1.2WTES 1
2017 6 2 1341 46.8 L 37.417 -97.369 6.6 TES 8 0.0 1.7WTES 1
2017 6 2 1432 30.1 L 37.415 -97.373 6.9 TES 8 0.0 1.9WTES 1
2017 6 2 1501 33.4 L 37.288 -97.510 4.6 TES 9 0.0 1.4WTES 1
2017 6 2 1512 35.7 L 37.289 -97.511 4.8 TES 7 0.0 1.3WTES 1
2017 6 2 1552 3.3 L 37.418 -97.368 5.8 TES 8 0.0 1.7WTES 1
2017 6 2 2314 12.2 L 37.422 -97.371 5.9 TES 9 0.0 2.7WTES 1
2017 6 3 0024 44.5 L 37.418 -97.369 6.6 TES 8 0.0 2.0WTES 1
2017 6 3 0215 3.4 L 37.414 -97.375 6.3 TES 9 0.0 1.8WTES 1
2017 6 3 0326 8.8 L 37.418 -97.374 6.2 TES 9 0.0 1.9WTES 1
2017 6 3 1235 8.4 L 37.230 -97.467 4.4 TES 7 0.0 1.6WTES 1
2017 6 4 0109 23.0 L 37.230 -97.469 3.2 TES 9 0.0 1.6WTES 1
2017 6 4 0332 59.2 L 37.334 -97.572 6.6 TES 9 0.1 2.0WTES 1
2017 6 4 0424 45.8 L 37.228 -97.466 3.6 TES 8 0.0 1.3WTES 1
2017 6 4 0451 48.3 L 37.228 -97.465 3.2 TES 8 0.0 1.1WTES 1
2017 6 4 0531 50.1 L 37.411 -97.372 6.7 TES 9 0.0 2.0WTES 1
2017 6 4 0558 23.8 L 37.233 -97.474 5.3 TES 7 0.0 2.1WTES 1
2017 6 6 2044 37.3 L 37.401 -97.478 5.5 TES 8 0.0 1.3WTES 1
2017 6 8 1121 27.6 L 37.369 -97.397 4.7 TES 6 0.0 1.2WTES 1

2017 6 8 1206 27.1 L 37.285 -97.501 4.8 TES 6 0.0 1.1WTES 1
2017 6 9 0659 3.4 L 37.070 -97.704 6.7 TES 8 0.0 2.0WTES 1
2017 6 9 2047 35.7 L 37.076 -97.705 8.8 TES 7 0.0 2.3WTES 1
2017 6 9 2219 19.1 L 37.316 -97.750 10.2 TES 7 0.0 2.0WTES 1
2017 610 0248 10.4 L 37.363 -97.753 6.1 TES 8 0.0 2.3WTES 1
2017 610 0443 29.2 L 37.367 -97.376 4.3 TES 5 0.0 1.2WTES 1
2017 610 0558 19.8 L 37.434 -97.370 3.2 TES 9 0.0 1.7WTES 1
2017 610 0626 11.8 L 37.234 -97.945 8.6 TES 9 0.0 3.1WTES 1
2017 610 0727 0.7 L 37.433 -97.368 2.0 TES 7 0.0 2.1WTES 1
2017 613 1426 8.2 L 37.306 -97.557 3.4 TES 8 0.1 2.3WTES 1
2017 614 2152 50.7 L 37.456 -97.512 7.2 TES 5 0.0 1.6WTES 1
2017 615 0529 43.3 L 37.230 -97.472 5.4 TES 6 0.0 1.2WTES 1
2017 616 0711 15.0 L 37.454 -97.505 9.0 TES 8 0.1 1.8WTES 1
2017 617 0846 31.8 L 37.237 -97.507 4.7 TES 7 0.0 1.3WTES 1
2017 617 0915 32.1 L 37.033 -97.573 12.0 TES 9 0.1 2.3WTES 1
2017 618 0142 5.5 L 37.283 -97.430 4.7 TES 7 0.0 1.7WTES 1
2017 618 1026 37.4 L 37.515 -97.127 12.5 TES 8 0.0 2.0WTES 1
2017 618 2059 29.3 L 37.228 -97.463 3.6 TES 8 0.0 1.5WTES 1
2017 619 0421 0.1 L 37.573 -97.201 2.1 TES 9 0.1 2.0WTES 1
2017 619 0542 40.7 L 37.427 -97.370 5.2 TES 8 0.0 1.9WTES 1
2017 619 0925 6.2 L 37.259 -97.491 0.9 TES 9 0.3 1.6WTES 1
2017 619 1000 7.4 L 37.228 -97.464 3.5 TES 8 0.0 1.6WTES 1
2017 619 1000 59.0 L 37.228 -97.464 3.2 TES 8 0.0 1.3WTES 1
2017 619 1630 19.7 L 37.224 -97.472 3.0 TES 8 0.0 1.7WTES 1
2017 620 0313 31.0 L 37.513 -97.118 7.6 TES 8 0.0 2.5WTES 1
2017 620 1128 48.6 L 37.228 -97.467 3.7 TES 7 0.0 1.3WTES 1
2017 620 2214 57.4 L 37.273 -98.123 11.8 TES 7 0.1 2.9WTES 1
2017 621 0955 36.8 L 37.234 -97.469 4.7 TES 6 0.0 1.4WTES 1
2017 622 0336 32.0 L 37.292 -97.500 4.3 TES 5 0.0 1.1WTES 1
2017 622 1244 51.8 L 37.238 -97.949 9.7 TES 8 0.0 3.2WTES 1
2017 622 2102 30.0 L 37.224 -97.471 0.6 TES 7 0.0 1.4WTES 1

2017 622 2119 43.7 L 37.232 -97.471 5.7 TES 6 0.0 1.5WTES 1
2017 623 0527 41.9 L 37.315 -97.382 2.3 TES 6 0.0 1.2WTES 1
2017 623 0920 58.7 L 37.237 -97.683 4.9 TES 8 0.0 1.9WTES 1
2017 623 0929 21.0 L 37.234 -97.679 3.8 TES 8 0.0 1.9WTES 1
2017 623 2118 3.1 L 37.008 -97.556 4.3 TES 8 0.0 2.2WTES 1
2017 624 0527 4.9 L 36.763 -98.013 3.3 TES 7 0.0 2.0WTES 1
2017 625 0258 49.0 L 37.234 -97.684 4.3 TES 8 0.0 1.6WTES 1
2017 625 0412 51.1 L 37.228 -97.467 5.4 TES 8 0.0 1.4WTES 1
2017 625 1512 48.8 L 37.241 -97.584 3.7 TES 8 0.1 1.6WTES 1
2017 625 1542 6.8 L 37.584 -97.814 8.2 TES 8 0.0 2.7WTES 1
2017 629 0841 49.8 L 37.320 -97.498 4.7 TES 8 0.1 1.4WTES 1
2017 630 0257 9.2 L 37.292 -97.463 3.4 TES 5 0.0 1.1WTES 1
2017 7 1 0613 13.7 L 37.369 -97.527 3.7 TES 7 0.0 1.3WTES 1
2017 7 1 0757 55.6 L 37.371 -97.526 2.9 TES 7 0.0 1.2WTES 1
2017 7 1 1021 0.0 L 37.370 -97.527 1.7 TES 6 0.0 1.4WTES 1
2017 7 1 1034 54.0 L 37.374 -97.526 5.0 TES 5 0.0 1.3WTES 1
2017 7 1 1106 7.2 L 37.368 -97.526 3.1 TES 6 0.0 1.2WTES 1
2017 7 1 1712 39.6 L 37.369 -97.528 1.5 TES 6 0.0 1.1WTES 1
2017 7 1 1824 46.1 L 37.372 -97.528 1.7 TES 6 0.0 1.4WTES 1
2017 7 1 2020 44.3 L 37.232 -97.479 5.8 TES 4 0.0 1.2WTES 1
2017 7 6 2158 4.1 L 37.278 -97.435 3.5 TES 8 0.0 1.0WTES 1
2017 7 9 1802 5.8 L 37.323 -97.503 4.8 TES 9 0.0 1.5WTES 1
2017 713 1353 2.6 L 37.235 -97.483 6.5 TES 9 0.0 1.4WTES 1
2017 714 1347 35.2 L 35.853 -96.683 17.8 TES 9 0.1 4.4WTES 1
2017 716 0505 49.4 L 37.294 -97.506 5.0 TES 9 0.0 1.4WTES 1
2017 716 0511 2.7 L 37.295 -97.507 4.7 TES 9 0.0 1.5WTES 1
2017 716 0618 33.4 L 37.294 -97.507 4.8 TES 9 0.0 1.2WTES 1
2017 716 0728 20.7 L 37.296 -97.508 4.8 TES 9 0.0 1.3WTES 1
2017 716 0830 29.2 L 37.295 -97.506 4.6 TES 9 0.0 1.2WTES 1
2017 716 1915 17.8 L 37.294 -97.509 5.0 TES 9 0.0 1.7WTES 1
2017 716 2044 34.1 L 37.240 -97.560 3.5 TES 7 0.0 1.4WTES 1

2017 717 0724 42.4 L 37.263 -97.857 11.7 TES 10 0.0 2.4WTES 1
2017 717 1755 36.1 L 37.313 -97.493 11.6 TES 8 0.1 1.3WTES 1
2017 717 2115 56.4 L 37.295 -97.507 5.0 TES 9 0.0 1.5WTES 1
2017 718 0108 0.3 L 37.294 -97.508 5.1 TES 8 0.0 1.2WTES 1
2017 718 0349 45.6 L 37.291 -97.508 3.8 TES 9 0.0 1.1WTES 1
2017 718 0450 26.2 L 37.294 -97.507 4.8 TES 9 0.0 1.3WTES 1
2017 718 0712 44.4 L 37.293 -97.507 4.8 TES 9 0.0 1.5WTES 1
2017 718 0747 3.8 L 37.294 -97.508 5.1 TES 9 0.0 1.2WTES 1
2017 718 0848 59.8 L 37.293 -97.508 4.9 TES 9 0.0 1.3WTES 1
2017 718 1329 38.0 L 37.294 -97.507 4.6 TES 8 0.0 1.6WTES 1
2017 718 1350 37.8 L 37.376 -97.457 4.1 TES 9 0.0 1.5WTES 1
2017 718 1355 42.2 L 37.072 -97.955 6.4 TES 10 0.1 2.4WTES 1
2017 718 1527 47.8 L 37.293 -97.508 4.7 TES 9 0.0 1.4WTES 1
2017 719 0949 3.6 L 37.290 -97.506 4.0 TES 9 0.0 1.1WTES 1
2017 720 1026 0.2 L 37.291 -97.509 4.7 TES 9 0.0 1.6WTES 1
2017 720 1146 52.0 L 37.288 -97.508 3.6 TES 9 0.0 1.1WTES 1
2017 720 2332 56.5 L 37.350 -97.413 12.6 TES 9 0.1 1.5WTES 1
2017 723 0154 48.0 L 37.296 -97.504 4.5 TES 9 0.0 1.4WTES 1
2017 723 0225 3.2 L 37.298 -97.460 4.1 TES 8 0.0 1.0WTES 1
2017 723 1857 56.0 L 37.293 -97.506 4.8 TES 9 0.0 1.3WTES 1
2017 724 0128 11.1 L 37.425 -97.376 4.0 TES 9 0.0 1.8WTES 1
2017 724 0228 1.1 L 37.417 -97.373 5.4 TES 10 0.1 1.6WTES 1
2017 725 0043 14.2 L 37.295 -97.933 12.7 TES 10 0.1 3.0WTES 1
2017 727 1854 39.5 L 37.125 -97.605 4.0 TES 9 0.0 2.1WTES 1
2017 728 2122 59.3 L 37.126 -97.610 4.3 TES 9 0.0 2.0WTES 1
2017 729 0604 49.7 L 37.289 -97.514 4.7 TES 9 0.0 1.4WTES 1
2017 729 1949 55.7 L 37.308 -97.503 4.9 TES 8 0.0 1.2WTES 1
2017 729 2220 26.4 L 37.331 -97.425 2.7 TES 8 0.0 1.2WTES 1
2017 729 2340 32.9 L 37.314 -97.645 4.4 TES 10 0.1 2.1WTES 1
2017 730 0228 7.7 L 37.307 -97.502 4.5 TES 9 0.0 1.0WTES 1
2017 730 0428 15.2 L 37.304 -97.499 5.2 TES 9 0.0 1.8WTES 1

2017 730 2019 15.9 L 37.076 -97.695 8.6 TES 9 0.0 2.8WTES 1
2017 731 0315 14.6 L 37.331 -97.426 2.6 TES 8 0.0 1.3WTES 1
2017 731 1942 47.1 L 37.258 -97.458 4.0 TES 10 0.0 1.5WTES 1
2017 8 1 0625 12.9 L 37.132 -97.612 6.7 TES 13 0.0 3.2WTES 1
2017 8 1 0625 13.0 L 37.137 -97.605 7.9 TES 13 0.2 3.2WTES 1
2017 8 1 0709 22.7 L 37.134 -97.607 1.9 TES 12 0.0 1.8WTES 1
2017 8 1 0709 22.8 L 37.138 -97.607 1.2 TES 12 0.0 1.9WTES 1
2017 8 1 0822 31.4 L 37.125 -97.605 6.0 TES 13 0.0 1.8WTES 1
2017 8 1 0822 31.4 L 37.129 -97.597 7.9 TES 13 0.2 1.8WTES 1
2017 8 1 0934 45.1 L 37.131 -97.611 6.7 TES 13 0.0 2.4WTES 1
2017 8 1 0934 45.2 L 37.139 -97.603 8.0 TES 13 0.2 2.4WTES 1
2017 8 1 0936 1.8 L 37.113 -97.603 1.5 TES 12 0.0 2.3WTES 1
2017 8 1 0936 1.8 L 37.113 -97.603 1.5 TES 12 0.0 2.3WTES 1
2017 8 1 1106 54.6 L 37.121 -97.602 2.0 TES 12 0.0 1.7WTES 1
2017 8 1 1106 54.6 L 37.121 -97.601 2.6 TES 12 0.0 1.7WTES 1
2017 8 1 1215 42.5 L 37.324 -97.553 9.3 TES 8 0.1 1.7WTES 1
2017 8 1 1215 37.5 L 37.157 -97.593 18.4 TES 12 0.0 1.9WTES 1
2017 8 1 1632 11.8 L 37.242 -97.561 3.2 TES 11 0.1 1.7WTES 1
2017 8 1 1632 9.5 L 37.183 -97.562 12.3 TES 12 0.0 1.8WTES 1
2017 8 1 1850 3.0 L 37.109 -97.603 4.3 TES 12 0.0 2.1WTES 1
2017 8 1 1850 3.0 L 37.109 -97.603 4.3 TES 12 0.0 2.1WTES 1
2017 8 1 2150 15.3 L 37.118 -97.601 1.2 TES 12 0.0 2.0WTES 1
2017 8 1 2150 15.3 L 37.118 -97.601 1.2 TES 12 0.0 2.0WTES 1
2017 8 2 0441 50.2 L 37.119 -97.610 6.3 TES 13 0.0 3.0WTES 1
2017 8 2 0441 50.4 L 37.132 -97.600 8.0 TES 13 0.3 2.9WTES 1
2017 8 2 0625 24.2 L 37.245 -97.563 2.1 TES 12 0.0 1.7WTES 1
2017 8 2 0625 24.2 L 37.245 -97.564 2.1 TES 12 0.0 1.8WTES 1
2017 8 2 1153 55.6 L 37.110 -97.596 2.2 TES 12 0.0 2.0WTES 1
2017 8 2 1153 55.6 L 37.110 -97.596 2.2 TES 12 0.1 2.0WTES 1
2017 8 2 1154 20.9 L 37.128 -97.619 1.1 TES 12 0.0 1.7WTES 1
2017 8 2 1154 20.9 L 37.128 -97.618 1.2 TES 12 0.0 1.6WTES 1

2017 8 2 1509 21.3 L 37.145 -97.617 8.2 TES 12 0.0 1.8WTES 1
2017 8 2 1509 21.3 L 37.145 -97.617 8.2 TES 12 0.0 1.8WTES 1
2017 8 3 1317 21.4 L 37.120 -97.610 7.4 TES 12 0.0 2.4WTES 1
2017 8 3 1317 21.4 L 37.120 -97.610 7.4 TES 12 0.0 2.4WTES 1
2017 8 3 1518 3.7 L 37.126 -97.615 5.3 TES 12 0.0 2.4WTES 1
2017 8 3 1518 3.7 L 37.125 -97.615 4.9 TES 12 0.0 2.4WTES 1
2017 8 4 0438 2.7 L 37.157 -97.626 7.4 TES 12 0.0 1.9WTES 1
2017 8 4 0438 2.7 L 37.157 -97.627 7.3 TES 12 0.0 1.9WTES 1
2017 8 5 0314 10.4 L 37.124 -97.611 6.1 TES 12 0.0 3.3WTES 1
2017 8 5 0314 10.4 L 37.124 -97.611 6.1 TES 12 0.0 3.2WTES 1
2017 8 5 0332 52.2 L 37.124 -97.612 6.7 TES 12 0.0 3.4WTES 1
2017 8 5 0332 52.2 L 37.124 -97.612 6.7 TES 12 0.0 3.4WTES 1
2017 8 5 0515 50.8 L 37.442 -97.383 4.0 TES 13 0.1 2.6WTES 1
2017 8 5 0515 50.9 L 37.434 -97.396 5.5 TES 12 0.0 2.9WTES 1
2017 8 5 0539 59.2 L 37.118 -97.603 2.9 TES 12 0.0 2.9WTES 1
2017 8 5 0539 59.2 L 37.118 -97.603 2.8 TES 12 0.0 3.0WTES 1
2017 8 5 0611 2.6 L 37.133 -97.603 7.4 TES 12 0.0 2.1WTES 1
2017 8 5 0611 2.6 L 37.134 -97.603 7.4 TES 12 0.0 2.1WTES 1
2017 8 5 0619 27.2 L 37.136 -97.601 7.7 TES 13 0.0 1.8WTES 1
2017 8 5 0619 27.1 L 37.134 -97.600 7.7 TES 12 0.1 1.9WTES 1
2017 8 5 0622 29.0 L 37.431 -97.400 5.2 TES 12 0.0 1.7WTES 1
2017 8 5 0622 29.0 L 37.431 -97.400 5.2 TES 12 0.0 1.9WTES 1
2017 8 5 0720 27.9 L 37.444 -97.382 3.4 TES 13 0.0 1.4WTES 1
2017 8 5 0720 27.7 L 37.437 -97.372 8.2 TES 13 0.1 1.4WTES 1
2017 8 5 0723 19.4 L 37.443 -97.380 3.8 TES 13 0.0 1.4WTES 1
2017 8 5 0723 19.4 L 37.443 -97.380 3.8 TES 13 0.0 1.6WTES 1
2017 8 5 0726 5.5 L 37.443 -97.375 7.8 TES 10 0.0 1.3WTES 1
2017 8 5 0726 5.3 L 37.434 -97.362 10.3 TES 9 0.2 1.9WTES 1
2017 8 5 0747 9.4 L 37.443 -97.382 3.4 TES 11 0.1 1.6WTES 1
2017 8 5 0747 9.4 L 37.442 -97.385 2.1 TES 11 0.1 1.8WTES 1
2017 8 5 1016 19.1 L 37.119 -97.612 5.1 TES 12 0.0 1.7WTES 1

2017 8 5 1016 19.1 L 37.119 -97.612 5.1 TES 12 0.0 1.7WTES 1
2017 8 5 1552 21.0 L 37.274 -97.617 3.4 TES 12 0.0 2.5WTES 1
2017 8 5 1552 21.0 L 37.275 -97.617 3.4 TES 12 0.0 2.4WTES 1
2017 8 5 1902 23.3 L 37.267 -97.615 1.4 TES 12 0.0 1.6WTES 1
2017 8 5 1902 23.4 L 37.266 -97.615 0.0 TES 12 0.1 1.9WTES 1
2017 8 5 2013 0.8 L 37.276 -97.618 4.0 TES 13 0.0 3.1WTES 1
2017 8 5 2013 0.8 L 37.276 -97.619 4.1 TES 13 0.1 3.3WTES 1
2017 8 5 2209 14.7 L 37.241 -97.648 3.8 TES 12 0.0 2.1WTES 1
2017 8 5 2209 14.7 L 37.241 -97.648 3.8 TES 12 0.1 2.3WTES 1
2017 8 5 2210 5.2 L 37.252 -97.655 2.9 TES 12 0.0 1.7WTES 1
2017 8 5 2210 5.2 L 37.252 -97.655 2.9 TES 12 0.0 2.0WTES 1
2017 8 5 2357 2.4 L 37.133 -97.606 6.5 TES 13 0.0 2.3WTES 1
2017 8 5 2357 2.4 L 37.132 -97.606 6.4 TES 13 0.1 2.3WTES 1
2017 8 6 0238 2.6 L 37.281 -97.614 4.2 TES 13 0.0 2.9WTES 1
2017 8 6 0238 2.6 L 37.281 -97.614 4.2 TES 13 0.0 2.9WTES 1
2017 8 6 0648 56.2 L 37.433 -97.375 2.0 TES 13 0.0 1.9WTES 1
2017 8 6 0648 56.1 L 37.431 -97.372 4.0 TES 13 0.1 2.0WTES 1
2017 8 6 0754 52.8 L 37.279 -97.609 3.3 TES 13 0.0 1.5WTES 1
2017 8 6 0754 52.8 L 37.279 -97.609 3.3 TES 13 0.0 1.5WTES 1
2017 8 6 0941 39.4 L 37.275 -97.623 3.2 TES 11 0.0 1.1WTES 1
2017 8 6 0941 39.4 L 37.282 -97.620 3.4 TES 11 0.2 1.8WTES 1
2017 8 6 1024 3.1 L 37.284 -97.610 2.1 TES 13 0.0 1.6WTES 1
2017 8 6 1024 3.1 L 37.284 -97.610 2.2 TES 13 0.0 1.5WTES 1
2017 8 6 1154 44.1 L 37.279 -97.618 3.1 TES 12 0.0 1.4WTES 1
2017 8 6 1154 44.1 L 37.280 -97.618 3.1 TES 12 0.1 1.6WTES 1
2017 8 6 1505 34.5 L 37.292 -97.612 3.7 TES 12 0.0 1.6WTES 1
2017 8 6 1505 34.5 L 37.292 -97.612 3.7 TES 12 0.0 1.6WTES 1
2017 8 6 1856 28.4 L 37.277 -97.619 1.3 TES 11 0.0 1.3WTES 1
2017 8 6 1856 28.4 L 37.279 -97.620 1.0 TES 11 0.1 1.3WTES 1
2017 8 6 2150 22.3 L 37.269 -97.612 8.3 TES 13 0.0 1.7WTES 1
2017 8 6 2150 22.3 L 37.270 -97.612 8.2 TES 13 0.1 1.7WTES 1

2017 8 6 2311 42.3 L 37.282 -97.620 3.9 TES 13 0.0 1.3WTES 1
2017 8 6 2311 42.4 L 37.281 -97.618 3.7 TES 13 0.1 1.4WTES 1
2017 8 6 2342 42.4 L 37.263 -97.662 4.5 TES 12 0.0 1.6WTES 1
2017 8 6 2342 42.4 L 37.263 -97.662 4.5 TES 12 0.0 1.6WTES 1
2017 8 7 0448 45.9 L 37.274 -97.625 4.0 TES 12 0.0 1.5WTES 1
2017 8 7 0448 45.9 L 37.274 -97.626 4.1 TES 12 0.1 1.9WTES 1
2017 8 7 0951 42.0 L 37.132 -97.609 7.0 TES 12 0.0 2.2WTES 1
2017 8 7 0951 42.1 L 37.138 -97.603 8.0 TES 12 0.2 2.3WTES 1
2017 8 7 1104 24.4 L 37.123 -97.601 7.3 TES 12 0.0 2.5WTES 1
2017 8 7 1104 24.4 L 37.123 -97.601 7.3 TES 12 0.0 2.5WTES 1
2017 8 7 1150 50.3 L 37.301 -97.497 6.9 TES 9 0.0 1.2WTES 1
2017 8 7 1150 50.3 L 37.301 -97.497 6.9 TES 9 0.0 1.3WTES 1
2017 8 7 1354 19.1 L 37.276 -97.620 2.7 TES 10 0.0 1.4WTES 1
2017 8 7 1354 19.1 L 37.276 -97.620 2.7 TES 10 0.0 1.7WTES 1
2017 8 7 1545 58.4 L 37.340 -97.494 2.2 TES 9 0.0 1.1WTES 1
2017 8 7 1545 58.4 L 37.339 -97.494 2.4 TES 9 0.0 1.3WTES 1
2017 8 7 2037 36.0 L 36.922 -97.439 7.1 TES 13 0.0 1.9WTES 1
2017 8 7 2037 36.0 L 36.923 -97.439 7.1 TES 13 0.0 2.3WTES 1
2017 8 7 2117 33.8 L 37.215 -97.713 9.4 TES 9 0.0 1.8WTES 1
2017 8 7 2117 32.9 L 37.235 -97.750 13.2 TES 12 0.1 1.8WTES 1
2017 8 8 0413 35.7 L 37.339 -97.624 2.1 TES 10 0.1 1.4WTES 1
2017 8 8 0413 35.7 L 37.339 -97.624 2.1 TES 10 0.1 1.9WTES 1
2017 8 8 0727 27.0 L 37.257 -97.637 7.4 TES 12 0.0 1.5WTES 1
2017 8 8 0727 27.0 L 37.257 -97.636 7.5 TES 12 0.0 1.6WTES 1
2017 8 9 0707 14.8 L 37.442 -97.382 3.4 TES 12 0.0 1.4WTES 1
2017 8 9 0707 14.8 L 37.441 -97.382 3.6 TES 12 0.1 1.9WTES 1
2017 8 9 1523 4.6 L 37.190 -97.542 1.1 TES 12 0.0 1.7WTES 1
2017 8 9 1523 4.6 L 37.190 -97.541 0.7 TES 12 0.1 1.7WTES 1
2017 8 9 2115 31.0 L 37.126 -97.608 7.6 TES 12 0.0 3.8WTES 1
2017 8 9 2115 31.0 L 37.127 -97.607 7.8 TES 12 0.1 3.9WTES 1
2017 8 9 2221 55.7 L 37.117 -97.591 8.0 TES 12 0.0 2.4WTES 1

2017 8 9 2221 55.7 L 37.117 -97.591 8.0 TES 12 0.0 2.3WTES 1
2017 810 0154 49.6 L 37.328 -97.438 1.6 TES 7 0.0 1.2WTES 1
2017 810 0154 41.7 L 37.477 -97.511 23.1 TES 10 0.0 2.0WTES 1
2017 810 0248 56.6 L 37.303 -97.508 6.3 TES 10 0.0 1.2WTES 1
2017 810 0248 56.6 L 37.303 -97.508 6.3 TES 10 0.0 1.5WTES 1
2017 810 0445 49.0 L 37.142 -97.606 9.9 TES 12 0.0 2.1WTES 1
2017 810 0445 48.9 L 37.141 -97.606 10.0 TES 12 0.1 2.1WTES 1
2017 810 0545 47.4 L 37.153 -97.582 7.0 TES 12 0.0 1.8WTES 1
2017 810 0545 47.4 L 37.153 -97.582 7.0 TES 12 0.0 1.8WTES 1
2017 810 0547 52.5 L 37.210 -97.549 2.5 TES 9 0.0 2.0WTES 1
2017 810 0547 49.5 L 37.135 -97.579 12.4 TES 10 0.0 2.2WTES 1
2017 810 0602 18.1 L 37.101 -97.605 6.0 TES 12 0.0 1.9WTES 1
2017 810 0602 18.1 L 37.101 -97.604 6.1 TES 12 0.0 1.9WTES 1
2017 810 0609 28.8 L 37.141 -97.594 8.2 TES 12 0.0 1.6WTES 1
2017 810 0609 28.8 L 37.140 -97.595 8.2 TES 12 0.0 1.8WTES 1
2017 810 1238 15.6 L 37.227 -97.691 6.4 TES 11 0.0 1.7WTES 1
2017 810 1238 15.7 L 37.225 -97.689 6.1 TES 10 0.0 1.8WTES 1
2017 810 1247 31.8 L 37.206 -97.716 9.9 TES 12 0.0 1.7WTES 1
2017 810 1247 31.8 L 37.205 -97.716 10.2 TES 12 0.0 1.7WTES 1
2017 810 1708 26.5 L 37.300 -97.564 7.5 TES 11 0.0 1.4WTES 1
2017 810 1708 25.8 L 37.337 -97.588 9.3 TES 12 0.4 1.8WTES 1
2017 811 1237 52.3 L 37.170 -97.606 6.5 TES 12 0.0 2.0WTES 1
2017 811 1237 52.3 L 37.170 -97.606 6.5 TES 12 0.0 2.1WTES 1
2017 811 1330 45.8 L 37.156 -97.618 2.1 TES 12 0.0 1.7WTES 1
2017 811 1330 45.8 L 37.156 -97.618 1.7 TES 12 0.0 1.7WTES 1
2017 811 1850 42.7 L 37.147 -97.428 11.0 TES 13 0.0 2.1WTES 1
2017 811 1850 42.6 L 37.146 -97.430 11.3 TES 12 0.0 2.2WTES 1
2017 811 2022 12.3 L 37.190 -97.548 1.5 TES 9 0.0 1.7WTES 1
2017 811 2022 12.3 L 37.190 -97.548 1.5 TES 9 0.0 1.8WTES 1
2017 812 1005 7.2 L 37.258 -97.518 4.6 TES 7 0.0 1.7WTES 1
2017 812 1004 49.9 L 36.956 -98.014 32.2 TES 11 0.1 2.3WTES 1

2017 812 1530 27.2 L 37.472 -97.678 6.5 TES 10 0.0 1.8WTES 1
2017 812 1530 27.2 L 37.472 -97.678 6.7 TES 10 0.1 1.8WTES 1
2017 812 1542 33.6 L 37.127 -97.413 5.3 TES 11 0.0 2.2WTES 1
2017 812 1542 31.5 L 37.182 -97.337 25.1 TES 12 0.0 2.5WTES 1
2017 812 2142 14.8 L 37.274 -97.623 6.0 TES 10 0.0 1.4WTES 1
2017 812 2142 14.8 L 37.274 -97.623 6.0 TES 10 0.0 1.6WTES 1
2017 812 2232 39.6 L 36.994 -97.503 9.3 TES 11 0.0 1.8WTES 1
2017 812 2232 39.6 L 36.994 -97.503 9.3 TES 11 0.0 2.0WTES 1
2017 812 2246 32.3 L 37.465 -97.504 6.8 TES 12 0.1 2.2WTES 1
2017 812 2246 32.3 L 37.465 -97.504 6.8 TES 12 0.1 2.2WTES 1
2017 812 2356 23.6 L 37.145 -97.603 6.9 TES 12 0.0 2.0WTES 1
2017 812 2356 23.7 L 37.146 -97.603 6.9 TES 12 0.1 2.0WTES 1
2017 813 0444 16.9 L 37.282 -97.619 5.6 TES 10 0.0 1.4WTES 1
2017 813 0444 16.9 L 37.283 -97.619 5.6 TES 10 0.0 1.4WTES 1
2017 813 0543 10.4 L 37.088 -97.585 7.2 TES 12 0.1 1.8WTES 1
2017 813 0543 10.4 L 37.088 -97.585 7.2 TES 12 0.1 1.9WTES 1
2017 813 1354 23.1 L 36.779 -97.624 1.7 TES 11 0.0 2.3WTES 1
2017 813 1354 23.3 L 36.808 -97.676 16.5 TES 11 0.3 2.6WTES 1
2017 813 1705 42.7 L 37.134 -97.596 8.0 TES 12 0.0 1.8WTES 1
2017 813 1705 42.7 L 37.134 -97.596 8.0 TES 12 0.0 1.8WTES 1
2017 813 2227 9.5 L 35.789 -96.476 0.3 TES 10 0.3 2.5WTES 1
2017 813 2228 1.0 L 37.230 -97.486 4.5 TES 8 0.0 1.9WTES 1
2017 814 0021 11.7 L 37.298 -97.386 4.1 TES 11 0.0 1.4WTES 1
2017 814 0021 11.7 L 37.298 -97.386 4.1 TES 11 0.0 1.7WTES 1
2017 814 0224 24.4 L 37.110 -97.608 7.9 TES 12 0.0 1.6WTES 1
2017 814 0224 24.4 L 37.111 -97.608 7.9 TES 12 0.0 1.6WTES 1
2017 814 1221 14.5 L 37.268 -97.493 9.7 TES 10 0.0 1.5WTES 1
2017 814 1221 14.5 L 37.268 -97.493 9.7 TES 10 0.0 1.6WTES 1
2017 814 1422 7.9 L 37.281 -97.513 4.9 TES 9 0.0 1.2WTES 1
2017 814 1422 7.9 L 37.281 -97.513 4.9 TES 9 0.0 1.5WTES 1
2017 814 1834 3.8 L 37.254 -97.479 5.1 TES 8 0.0 1.2WTES 1

2017 814 1834 3.8 L 37.262 -97.488 5.8 TES 7 0.1 1.4WTES 1
2017 814 1952 16.9 L 37.279 -97.502 9.0 TES 9 0.0 1.1WTES 1
2017 814 1952 16.9 L 37.279 -97.502 9.0 TES 9 0.0 1.1WTES 1
2017 814 2053 33.6 L 37.250 -97.268 8.0 TES 10 0.0 1.5WTES 1
2017 814 2053 33.6 L 37.249 -97.268 8.0 TES 10 0.0 2.2WTES 1
2017 814 2252 7.1 L 37.287 -97.516 4.4 TES 10 0.0 1.0WTES 1
2017 814 2252 7.1 L 37.287 -97.516 4.3 TES 9 0.0 1.6WTES 1
2017 815 0456 38.9 L 37.438 -97.373 10.4 TES 12 0.0 1.3WTES 1
2017 815 0456 38.9 L 37.437 -97.370 10.7 TES 11 0.0 1.5WTES 1
2017 815 0525 59.8 L 37.279 -97.508 5.5 TES 10 0.0 1.2WTES 1
2017 815 0525 59.8 L 37.279 -97.508 5.5 TES 10 0.0 1.3WTES 1
2017 815 0557 50.5 L 37.289 -97.515 5.8 TES 10 0.0 1.6WTES 1
2017 815 0557 50.4 L 37.289 -97.515 6.0 TES 10 0.0 1.7WTES 1
2017 815 0600 56.2 L 37.290 -97.517 2.7 TES 11 0.1 1.3WTES 1
2017 815 0600 56.3 L 37.284 -97.515 0.0 TES 10 0.1 1.7WTES 1
2017 815 0715 20.4 L 37.282 -97.510 3.0 TES 10 0.0 1.2WTES 1
2017 815 0715 20.4 L 37.281 -97.509 2.8 TES 10 0.1 1.4WTES 1
2017 815 0923 44.5 L 37.286 -97.509 4.4 TES 10 0.0 1.1WTES 1
2017 815 0923 44.5 L 37.286 -97.509 4.4 TES 10 0.0 1.5WTES 1
2017 815 1012 52.4 L 37.284 -97.514 1.1 TES 10 0.0 1.2WTES 1
2017 815 1012 52.4 L 37.284 -97.514 1.1 TES 10 0.0 1.6WTES 1
2017 815 1020 49.2 L 37.285 -97.619 4.6 TES 10 0.0 1.3WTES 1
2017 815 1020 49.2 L 37.285 -97.619 4.6 TES 10 0.0 1.5WTES 1
2017 815 1203 6.7 L 37.283 -97.513 3.1 TES 10 0.0 1.6WTES 1
2017 815 1203 6.7 L 37.283 -97.513 3.1 TES 10 0.0 1.9WTES 1
2017 815 1227 14.6 L 37.294 -97.758 11.2 TES 12 0.0 2.4WTES 1
2017 815 1227 14.6 L 37.292 -97.759 11.6 TES 12 0.1 2.4WTES 1
2017 815 1514 53.4 L 37.283 -97.514 1.6 TES 9 0.0 1.1WTES 1
2017 815 1514 53.4 L 37.283 -97.514 1.6 TES 9 0.0 1.1WTES 1
2017 815 1516 4.3 L 37.429 -97.633 5.5 TES 8 0.1 2.0WTES 1
2017 815 1515 44.4 L 38.019 -97.931 1.5 TES 9 0.3 3.0WTES 1

2017 815 1634 54.4 L 37.283 -97.512 1.6 TES 9 0.1 1.2WTES 1
2017 815 1634 54.4 L 37.283 -97.512 1.5 TES 9 0.0 1.3WTES 1
2017 815 1648 45.0 L 37.281 -97.508 6.5 TES 9 0.0 1.1WTES 1
2017 815 1648 45.0 L 37.281 -97.508 6.5 TES 9 0.0 1.6WTES 1
2017 815 1709 25.9 L 37.280 -97.630 4.3 TES 10 0.0 2.1WTES 1
2017 815 1709 26.0 L 37.278 -97.629 4.1 TES 9 0.0 2.1WTES 1
2017 815 1829 9.5 L 37.282 -97.632 5.1 TES 9 0.0 1.4WTES 1
2017 815 1829 9.5 L 37.282 -97.632 5.1 TES 9 0.0 1.7WTES 1
2017 815 2258 38.5 L 37.281 -97.507 1.5 TES 9 0.0 1.0WTES 1
2017 815 2258 38.5 L 37.281 -97.507 1.5 TES 9 0.0 1.8WTES 1
2017 816 0041 23.8 L 37.283 -97.514 1.1 TES 9 0.0 1.0WTES 1
2017 816 0041 23.7 L 37.283 -97.513 0.8 TES 9 0.0 1.3WTES 1
2017 816 0117 20.2 L 37.189 -97.625 2.2 TES 12 0.0 1.9WTES 1
2017 816 0117 20.2 L 37.188 -97.625 2.2 TES 12 0.1 1.9WTES 1
2017 816 0322 55.7 L 37.284 -97.511 3.5 TES 9 0.0 1.4WTES 1
2017 816 0322 55.7 L 37.284 -97.511 3.5 TES 9 0.0 1.8WTES 1
2017 816 1029 15.1 L 37.281 -97.511 1.2 TES 9 0.0 1.1WTES 1
2017 816 1029 15.1 L 37.281 -97.511 1.2 TES 9 0.0 1.2WTES 1
2017 816 1058 44.9 L 37.284 -97.512 2.3 TES 9 0.0 1.3WTES 1
2017 816 1058 44.8 L 37.283 -97.510 0.3 TES 9 0.0 1.5WTES 1
2017 816 2052 27.7 L 37.287 -97.514 4.9 TES 10 0.0 2.1WTES 1
2017 816 2052 27.7 L 37.287 -97.514 4.9 TES 10 0.0 2.3WTES 1
2017 816 2109 0.5 L 37.285 -97.511 5.4 TES 10 0.0 1.4WTES 1
2017 816 2109 0.5 L 37.285 -97.511 5.4 TES 10 0.0 1.5WTES 1
2017 816 2157 22.5 L 37.124 -97.600 8.5 TES 10 0.0 1.8WTES 1
2017 816 2157 22.5 L 37.124 -97.600 8.4 TES 10 0.0 1.7WTES 1
2017 816 2335 33.1 L 37.284 -97.516 3.9 TES 10 0.0 1.3WTES 1
2017 816 2335 33.1 L 37.285 -97.516 3.8 TES 10 0.1 1.3WTES 1
2017 817 0343 5.9 L 37.284 -97.509 5.6 TES 10 0.0 1.3WTES 1
2017 817 0343 5.9 L 37.284 -97.509 5.6 TES 10 0.0 1.6WTES 1
2017 817 0520 0.2 L 37.283 -97.514 3.2 TES 10 0.0 1.4WTES 1

2017 817 0520 0.2 L 37.282 -97.513 3.2 TES 10 0.0 1.6WTES 1
2017 817 0718 5.6 L 37.318 -97.517 2.4 TES 7 0.0 1.0WTES 1
2017 817 0718 5.6 L 37.317 -97.517 2.1 TES 7 0.0 1.2WTES 1
2017 818 0223 33.9 L 37.260 -97.516 2.8 TES 9 0.1 1.9WTES 1
2017 818 0223 30.5 L 37.423 -97.651 0.0 TES 10 0.6 2.4WTES 1
2017 818 0315 58.8 L 37.280 -97.621 4.2 TES 9 0.0 1.3WTES 1
2017 818 0315 58.8 L 37.279 -97.621 4.1 TES 9 0.3 1.6WTES 1
2017 818 0615 58.5 L 37.384 -97.421 5.5 TES 7 0.1 1.2WTES 1
2017 818 0615 52.0 L 37.232 -97.433 30.4 TES 9 0.2 1.6WTES 1
2017 818 1749 49.8 L 37.277 -97.627 6.1 TES 10 0.0 1.6WTES 1
2017 818 1749 40.9 L 37.414 -97.969 14.3 TES 8 0.8 2.5WTES 1
2017 818 2255 47.4 L 37.437 -97.386 2.1 TES 10 0.1 1.7WTES 1
2017 818 2255 34.7 L 37.100 -96.923 0.2 TES 9 0.5 2.5WTES 1
2017 819 0036 40.3 L 37.123 -97.610 5.4 TES 10 0.0 1.7WTES 1
2017 819 0036 49.8 L 37.405 -97.082 2.1 TES 9 1.3 2.0WTES 1
2017 819 0546 44.3 L 37.442 -97.391 2.2 TES 11 0.0 1.7WTES 1
2017 819 0546 32.5 L 37.385 -96.894 3.0 TES 8 1.5 2.5WTES 1
2017 819 0825 41.3 L 37.279 -97.620 4.0 TES 9 0.0 1.4WTES 1
2017 819 0825 29.4 L 37.181 -97.923 37.5 TES 8 0.5 2.7WTES 1
2017 819 0833 44.1 L 37.440 -97.388 2.1 TES 11 0.0 1.6WTES 1
2017 819 0833 39.0 L 37.281 -97.143 0.0 TES 10 0.7 2.2WTES 1
2017 819 0922 43.4 L 37.442 -97.390 3.2 TES 9 0.1 1.4WTES 1
2017 819 0922 20.3 L 37.447 -97.472105.1 TES 7 0.6 3.4WTES 1
2017 819 0954 36.9 L 37.067 -97.525 5.3 TES 9 0.0 1.5WTES 1
2017 819 0954 20.6 L 36.559 -97.551 0.4 TES 8 0.5 2.3WTES 1
2017 819 1131 19.2 L 37.308 -97.729 1.1 TES 9 0.0 1.8WTES 1
2017 819 1130 59.3 L 37.119 -98.495 0.2 TES 9 1.0 2.6WTES 1
2017 819 1401 54.2 L 37.275 -97.504 1.1 TES 7 0.1 1.0WTES 1
2017 819 1401 53.9 L 37.281 -97.506 4.6 TES 8 0.1 1.5WTES 1
2017 819 1430 24.7 L 37.284 -97.513 3.0 TES 9 0.0 1.0WTES 1
2017 819 1430 15.8 L 37.081 -97.564 29.2 TES 7 0.4 2.2WTES 1

2017 819 1913 5.8 L 37.285 -97.516 1.6 TES 8 0.0 1.2WTES 1
2017 819 1912 44.2 L 37.517 -97.233 93.2 TES 8 0.6 1.8WTES 1
2017 819 1919 25.9 L 37.440 -97.385 7.4 TES 9 0.0 1.5WTES 1
2017 819 1919 10.7 L 37.018 -96.855 0.1 TES 7 0.4 2.7WTES 1
2017 820 0054 11.7 L 37.086 -97.699 9.9 TES 12 0.0 2.5WTES 1
2017 820 0054 14.0 L 37.197 -97.717 8.1 TES 11 0.7 2.3WTES 1
2017 820 0308 34.4 L 37.268 -97.500 6.8 TES 9 0.1 1.1WTES 1
2017 820 0308 27.4 L 37.617 -97.536 2.2 TES 10 0.3 1.9WTES 1
2017 820 0818 34.3 L 37.229 -97.457 3.4 TES 8 0.0 1.2WTES 1
2017 820 0818 22.4 L 37.263 -97.275 53.6 TES 10 0.4 1.9WTES 1
2017 820 0911 52.7 L 37.441 -97.394 2.1 TES 10 0.0 1.4WTES 1
2017 820 0911 49.2 L 37.293 -97.243 9.4 TES 10 0.4 2.2WTES 1
2017 820 0915 30.3 L 37.215 -97.755 9.5 TES 10 0.0 1.9WTES 1
2017 820 0915 23.5 L 36.941 -97.822 0.0 TES 10 1.8 2.2WTES 1
2017 820 1818 47.1 L 37.281 -97.516 2.0 TES 10 0.0 1.2WTES 1
2017 820 1818 47.0 L 37.277 -97.516 2.8 TES 9 0.2 1.2WTES 1
2017 820 1829 35.2 L 37.431 -97.371 3.2 TES 8 0.0 1.3WTES 1
2017 820 1829 16.5 L 36.952 -96.777 0.1 TES 9 0.6 2.1WTES 1
2017 820 2307 23.7 L 37.281 -97.622 4.2 TES 10 0.0 2.6WTES 1
2017 820 2307 23.7 L 37.289 -97.615 4.3 TES 12 0.2 2.8WTES 1
2017 821 0019 48.2 L 37.276 -97.506 6.1 TES 10 0.0 1.3WTES 1
2017 821 0019 37.6 L 37.425 -97.678 41.0 TES 8 0.3 1.6WTES 1
2017 821 0257 49.4 L 37.270 -97.505 6.6 TES 10 0.1 1.3WTES 1
2017 821 0257 45.0 L 37.500 -97.578 0.0 TES 10 1.3 2.0WTES 1
2017 821 0348 23.7 L 37.822 -97.962 50.3 TES 8 0.2 2.2WTES 1
2017 821 0348 44.8 L 37.282 -97.518 3.6 TES 9 0.0 1.1WTES 1
2017 821 0616 48.1 L 37.280 -97.515 4.0 TES 10 0.1 1.1WTES 1
2017 821 0616 48.2 L 37.281 -97.516 3.4 TES 10 0.1 1.6WTES 1
2017 821 0757 55.2 L 37.243 -97.570 3.2 TES 12 0.0 2.2WTES 1
2017 821 0757 54.6 L 37.278 -97.605 5.3 TES 12 0.4 2.8WTES 1
2017 821 0920 5.5 L 37.300 -97.511 1.9 TES 9 0.1 1.4WTES 1

2017 821 0920 5.3 L 37.281 -97.515 0.1 TES 10 0.2 1.6WTES 1
2017 821 0931 3.0 L 37.258 -97.524 2.3 TES 8 0.0 1.0WTES 1
2017 821 0931 3.6 L 37.282 -97.515 1.0 TES 9 0.2 1.2WTES 1
2017 821 1034 27.4 L 37.277 -97.510 5.0 TES 10 0.0 1.3WTES 1
2017 821 1034 27.7 L 37.283 -97.519 1.1 TES 6 0.3 1.2WTES 1
2017 821 1041 16.0 L 37.282 -97.516 1.6 TES 10 0.0 1.2WTES 1
2017 821 1041 15.9 L 37.281 -97.516 1.6 TES 10 0.3 1.5WTES 1
2017 821 1155 16.1 L 37.242 -97.569 3.5 TES 12 0.0 2.1WTES 1
2017 821 1155 16.0 L 37.248 -97.570 4.3 TES 12 0.2 2.5WTES 1
2017 821 1211 49.4 L 37.278 -97.508 6.6 TES 11 0.0 1.8WTES 1
2017 821 1211 49.4 L 37.286 -97.530 4.3 TES 11 0.3 1.7WTES 1
2017 821 1213 1.0 L 37.271 -97.503 7.0 TES 10 0.0 1.6WTES 1
2017 821 1213 1.4 L 37.280 -97.515 3.7 TES 11 0.1 1.5WTES 1
2017 821 1221 55.6 L 37.279 -97.514 4.5 TES 10 0.0 1.3WTES 1
2017 821 1221 55.5 L 37.299 -97.540 1.2 TES 9 0.3 1.3WTES 1
2017 821 1729 51.6 L 37.435 -97.390 4.0 TES 12 0.0 1.5WTES 1
2017 821 1729 51.4 L 37.397 -97.364 2.3 TES 12 1.0 1.8WTES 1
2017 821 2032 49.2 L 37.240 -97.572 3.2 TES 12 0.1 2.6WTES 1
2017 821 2032 49.0 L 37.250 -97.573 4.9 TES 11 0.3 3.0WTES 1
2017 821 2117 27.8 L 37.272 -97.506 5.9 TES 10 0.0 1.7WTES 1
2017 821 2117 28.3 L 37.282 -97.519 1.1 TES 10 0.3 1.7WTES 1
2017 821 2130 37.9 L 37.279 -97.515 5.3 TES 9 0.0 1.5WTES 1
2017 821 2130 38.0 L 37.286 -97.518 4.9 TES 8 0.0 1.7WTES 1
2017 821 2302 10.4 L 37.283 -97.511 3.7 TES 11 0.0 2.0WTES 1
2017 821 2302 10.3 L 37.285 -97.514 4.3 TES 9 0.0 1.9WTES 1
2017 822 0105 14.1 L 37.325 -97.512 7.2 TES 9 0.1 2.0WTES 1
2017 822 0105 14.5 L 37.307 -97.525 4.3 TES 10 0.4 1.9WTES 1
2017 822 0106 35.8 L 37.275 -97.506 5.5 TES 9 0.0 1.5WTES 1
2017 822 0106 36.3 L 37.270 -97.500 1.1 TES 8 0.3 1.5WTES 1
2017 822 0145 38.3 L 37.283 -97.514 3.8 TES 10 0.0 1.5WTES 1
2017 822 0145 38.0 L 37.281 -97.510 5.9 TES 10 0.1 1.6WTES 1

2017 822 0558 16.5 L 37.271 -97.501 5.8 TES 10 0.0 1.7WTES 1
2017 822 0558 16.8 L 37.282 -97.514 1.1 TES 9 0.1 1.4WTES 1
2017 822 0704 27.2 L 37.292 -97.533 9.7 TES 8 0.1 1.3WTES 1
2017 822 0704 28.3 L 37.281 -97.508 4.9 TES 7 0.1 1.2WTES 1
2017 822 0716 2.5 L 37.284 -97.515 4.1 TES 10 0.0 2.1WTES 1
2017 822 0716 2.6 L 37.284 -97.516 3.3 TES 11 0.1 2.2WTES 1
2017 822 0718 35.7 L 37.283 -97.518 4.6 TES 10 0.1 1.3WTES 1
2017 822 0718 36.9 L 37.290 -97.473 2.3 TES 7 0.1 1.2WTES 1
2017 822 0721 21.0 L 37.283 -97.514 1.0 TES 9 0.0 1.1WTES 1
2017 822 0721 20.9 L 37.284 -97.517 2.8 TES 8 0.2 1.1WTES 1
2017 822 0822 48.2 L 37.284 -97.521 3.9 TES 9 0.0 1.2WTES 1
2017 822 0822 48.3 L 37.287 -97.524 1.1 TES 7 0.1 1.3WTES 1
2017 822 0908 32.9 L 37.269 -97.507 6.4 TES 9 0.0 1.0WTES 1
2017 822 0908 32.6 L 37.224 -97.444 1.4 TES 6 0.3 1.4WTES 1
2017 822 0937 7.2 L 37.283 -97.515 4.2 TES 10 0.0 1.1WTES 1
2017 822 0937 6.7 L 37.277 -97.524 5.7 TES 9 0.4 1.6WTES 1
2017 822 1015 55.8 L 37.282 -97.517 4.2 TES 10 0.0 1.7WTES 1
2017 822 1015 56.2 L 37.283 -97.520 0.0 TES 10 0.3 1.6WTES 1
2017 822 1044 56.2 L 37.281 -97.518 2.6 TES 10 0.0 1.1WTES 1
2017 822 1044 55.9 L 37.279 -97.514 5.5 TES 8 0.1 1.5WTES 1
2017 822 1508 55.4 L 37.288 -97.524 5.4 TES 10 0.0 1.6WTES 1
2017 822 1508 55.7 L 37.286 -97.521 2.7 TES 9 0.2 1.6WTES 1
2017 822 1728 18.2 L 37.282 -97.514 1.6 TES 10 0.0 1.3WTES 1
2017 822 1728 18.1 L 37.280 -97.512 1.8 TES 10 0.1 1.7WTES 1
2017 822 1816 26.6 L 37.280 -97.510 4.3 TES 9 0.0 1.2WTES 1
2017 822 1816 26.6 L 37.258 -97.483 3.7 TES 8 0.2 1.3WTES 1
2017 822 2034 32.2 L 37.265 -97.500 1.3 TES 8 0.1 1.1WTES 1
2017 822 2034 31.1 L 37.293 -97.526 7.0 TES 9 0.2 1.5WTES 1
2017 822 2056 47.2 L 37.283 -97.516 5.2 TES 10 0.0 1.6WTES 1
2017 822 2056 46.7 L 37.300 -97.535 6.9 TES 10 0.3 1.8WTES 1
2017 822 2116 43.6 L 37.273 -97.509 5.7 TES 10 0.0 1.3WTES 1

2017 822 2116 42.7 L 37.300 -97.538 8.9 TES 9 0.4 1.7WTES 1
2017 822 2205 6.2 L 37.304 -97.502 4.4 TES 10 0.0 1.8WTES 1
2017 822 2205 6.0 L 37.325 -97.520 1.1 TES 9 0.1 1.9WTES 1
2017 822 2317 46.6 L 37.281 -97.516 1.0 TES 9 0.0 1.1WTES 1
2017 822 2317 44.3 L 37.281 -97.512 14.7 TES 7 0.5 1.4WTES 1
2017 823 0011 50.1 L 37.282 -97.515 3.7 TES 10 0.0 1.4WTES 1
2017 823 0011 50.0 L 37.285 -97.519 4.1 TES 10 0.1 1.7WTES 1
2017 823 0054 12.3 L 37.279 -97.512 4.4 TES 10 0.0 1.5WTES 1
2017 823 0054 12.4 L 37.287 -97.523 1.1 TES 8 0.1 1.4WTES 1
2017 823 0242 34.7 L 37.278 -97.515 4.6 TES 10 0.0 1.2WTES 1
2017 823 0242 34.6 L 37.279 -97.520 4.5 TES 8 0.2 1.5WTES 1
2017 823 0323 14.1 L 37.283 -97.515 3.8 TES 10 0.1 1.4WTES 1
2017 823 0323 14.0 L 37.289 -97.514 4.5 TES 10 0.2 1.7WTES 1
2017 823 0326 36.8 L 37.241 -97.572 4.2 TES 10 0.0 1.3WTES 1
2017 823 0326 37.2 L 37.252 -97.569 0.8 TES 7 0.3 1.6WTES 1
2017 823 0334 57.2 L 37.245 -97.571 3.2 TES 10 0.0 1.3WTES 1
2017 823 0334 57.4 L 37.254 -97.568 1.0 TES 9 0.4 1.7WTES 1
2017 823 0343 32.4 L 37.233 -97.577 4.6 TES 10 0.0 1.4WTES 1
2017 823 0343 32.8 L 37.254 -97.587 1.2 TES 9 0.4 1.4WTES 1
2017 823 0351 11.6 L 37.247 -97.571 2.6 TES 10 0.0 1.3WTES 1
2017 823 0351 11.6 L 37.256 -97.580 1.2 TES 9 0.3 1.3WTES 1
2017 823 0431 23.0 L 37.305 -97.500 4.6 TES 10 0.1 1.1WTES 1
2017 823 0431 22.1 L 37.324 -97.507 8.3 TES 9 0.3 1.5WTES 1
2017 823 0545 43.0 L 37.282 -97.519 2.9 TES 10 0.0 1.3WTES 1
2017 823 0545 43.2 L 37.281 -97.520 0.0 TES 10 0.2 1.4WTES 1
2017 823 0807 16.0 L 37.279 -97.500 7.4 TES 12 0.0 1.9WTES 1
2017 823 0807 16.1 L 37.286 -97.508 6.1 TES 10 0.2 1.8WTES 1
2017 823 0808 58.9 L 37.277 -97.509 5.3 TES 11 0.1 1.9WTES 1
2017 823 0808 58.9 L 37.278 -97.509 5.0 TES 9 0.1 1.8WTES 1
2017 823 0822 13.0 L 37.130 -97.610 5.6 TES 12 0.0 2.2WTES 1
2017 823 0822 13.8 L 37.192 -97.642 3.7 TES 9 0.3 2.0WTES 1

2017 823 0842 20.7 L 37.282 -97.514 1.8 TES 11 0.1 1.3WTES 1
2017 823 0842 20.6 L 37.289 -97.523 1.8 TES 8 0.1 1.3WTES 1
2017 823 0922 52.0 L 37.282 -97.515 1.7 TES 10 0.1 1.1WTES 1
2017 823 0922 52.0 L 37.278 -97.511 2.4 TES 8 0.1 1.5WTES 1
2017 823 1019 27.3 L 37.277 -97.513 4.0 TES 10 0.0 1.3WTES 1
2017 823 1019 27.0 L 37.280 -97.518 5.7 TES 8 0.2 1.4WTES 1
2017 823 1043 11.4 L 37.284 -97.515 3.4 TES 10 0.0 1.1WTES 1
2017 823 1043 11.4 L 37.291 -97.520 2.8 TES 9 0.2 1.3WTES 1
2017 823 1358 56.6 L 37.138 -97.517 1.7 TES 10 0.0 1.5WTES 1
2017 823 1358 57.2 L 37.172 -97.518 1.4 TES 6 0.4 1.8WTES 1
2017 823 1902 1.8 L 37.278 -97.515 5.1 TES 10 0.1 1.2WTES 1
2017 823 1902 1.5 L 37.312 -97.548 1.1 TES 8 0.2 1.6WTES 1
2017 823 2109 29.4 L 37.205 -97.506 2.3 TES 11 0.1 1.3WTES 1
2017 823 2109 29.6 L 37.212 -97.510 0.9 TES 9 0.3 1.8WTES 1
2017 823 2154 55.0 L 37.198 -97.510 3.2 TES 10 0.0 1.5WTES 1
2017 823 2154 54.9 L 37.184 -97.525 0.3 TES 7 0.3 2.0WTES 1
2017 823 2155 15.2 L 37.168 -97.511 1.0 TES 10 0.0 1.3WTES 1
2017 823 2155 16.1 L 37.210 -97.517 0.1 TES 7 0.3 1.8WTES 1
2017 823 2157 32.9 L 37.161 -97.518 0.6 TES 9 0.2 2.6WTES 1
2017 823 2157 55.4 L 37.285 -97.511 4.2 TES 10 0.0 2.0WTES 1
2017 823 2157 55.3 L 37.284 -97.510 4.3 TES 10 0.1 2.1WTES 1
2017 823 2207 30.6 L 37.187 -97.509 2.1 TES 12 0.0 1.7WTES 1
2017 823 2207 30.6 L 37.188 -97.510 2.7 TES 10 0.0 1.8WTES 1
2017 823 2331 47.6 L 37.228 -97.511 1.9 TES 10 0.1 1.6WTES 1
2017 823 2331 47.5 L 37.224 -97.511 2.1 TES 9 0.0 1.7WTES 1
2017 824 0006 11.2 L 37.221 -97.515 2.1 TES 11 0.0 1.2WTES 1
2017 824 0006 7.1 L 37.025 -97.636 1.4 TES 8 0.0 1.7WTES 1
2017 824 0056 32.5 L 37.279 -97.506 5.7 TES 11 0.0 1.6WTES 1
2017 824 0056 32.4 L 37.285 -97.514 5.6 TES 8 0.0 1.6WTES 1
2017 824 0058 19.7 L 37.176 -97.517 3.4 TES 11 0.0 1.7WTES 1
2017 824 0058 16.2 L 37.509 -97.433 34.3 TES 7 0.0 2.0WTES 1

2017 824 0107 29.5 L 37.214 -97.510 1.8 TES 11 0.0 1.5WTES 1
2017 824 0107 25.4 L 37.404 -97.738 27.4 TES 7 0.1 1.8WTES 1
2017 824 0150 15.5 L 37.173 -97.518 6.8 TES 11 0.0 1.5WTES 1
2017 824 0150 12.4 L 37.025 -97.629 1.9 TES 8 0.0 2.0WTES 1
2017 825 0150 21.1 L 37.115 -97.585 6.5 TES 10 0.0 2.0WTES 1
2017 825 0150 21.2 L 37.169 -97.600 16.5 TES 8 0.0 2.2WTES 1
2017 825 0608 23.6 L 37.129 -97.902 9.8 TES 10 0.0 1.7WTES 1
2017 825 0608 23.7 L 37.373 -97.951 10.3 TES 8 0.0 1.7WTES 1
2017 825 0940 2.2 L 37.286 -97.410 3.7 TES 7 0.0 0.9WTES 1
2017 825 0940 2.2 L 37.289 -97.428 3.8 TES 6 0.0 1.9WTES 1
2017 825 1449 14.1 L 37.273 -97.512 4.7 TES 10 0.0 1.6WTES 1
2017 825 1449 14.4 L 37.284 -97.513 0.4 TES 8 0.0 2.0WTES 1
2017 826 0319 41.7 L 37.850 -99.454 15.0 TES 8 0.0 2.6WTES 1
2017 826 0320 28.7 L 37.279 -97.666 5.0 TES 9 0.0 1.9WTES 1
2017 826 0426 55.1 L 37.279 -97.514 3.8 TES 10 0.0 1.3WTES 1
2017 826 0426 50.2 L 37.192 -97.660 8.0 TES 6 0.0 1.6WTES 1
2017 826 0545 43.4 L 37.191 -97.505 2.1 TES 11 0.0 2.1WTES 1
2017 826 0545 25.2 L 37.434 -97.433 93.2 TES 7 0.0 2.8WTES 1
2017 826 0802 11.2 L 37.282 -97.521 1.7 TES 10 0.0 1.1WTES 1
2017 826 0802 11.2 L 37.274 -97.508 0.8 TES 7 0.0 1.1WTES 1
2017 826 0811 34.0 L 37.283 -97.520 1.2 TES 9 0.0 1.1WTES 1
2017 826 0811 33.8 L 37.291 -97.530 3.1 TES 7 0.0 1.2WTES 1
2017 826 0828 58.8 L 37.281 -97.521 1.5 TES 11 0.0 1.3WTES 1
2017 826 0828 59.1 L 37.276 -97.511 0.1 TES 7 0.0 1.3WTES 1
2017 826 0831 56.6 L 37.283 -97.523 2.4 TES 9 0.1 1.2WTES 1
2017 826 0831 56.9 L 37.276 -97.513 0.0 TES 7 0.0 1.2WTES 1
2017 826 0856 57.9 L 37.166 -97.513 1.4 TES 10 0.0 1.4WTES 1
2017 826 0856 57.6 L 37.158 -97.512 0.8 TES 8 0.0 1.5WTES 1
2017 826 1024 14.0 L 37.268 -97.501 7.3 TES 10 0.1 1.3WTES 1
2017 826 1024 14.6 L 37.280 -97.513 0.2 TES 8 0.0 1.6WTES 1
2017 826 1026 44.7 L 37.283 -97.512 1.6 TES 10 0.0 1.2WTES 1

2017 826 1026 44.8 L 37.294 -97.524 0.1 TES 8 0.0 1.5WTES 1
2017 826 1058 12.6 L 37.286 -97.511 4.4 TES 10 0.1 1.2WTES 1
2017 826 1058 12.9 L 37.280 -97.506 0.8 TES 7 0.0 1.2WTES 1
2017 826 1103 3.5 L 37.280 -97.510 5.5 TES 10 0.1 1.4WTES 1
2017 826 1103 3.8 L 37.280 -97.511 0.3 TES 7 0.0 1.4WTES 1
2017 826 1126 55.6 L 37.277 -97.513 5.7 TES 11 0.0 1.9WTES 1
2017 826 1126 56.0 L 37.277 -97.513 1.0 TES 7 0.0 2.0WTES 1
2017 826 1222 16.7 L 37.284 -97.514 4.2 TES 10 0.0 1.3WTES 1
2017 826 1222 16.9 L 37.283 -97.511 1.0 TES 7 0.0 1.2WTES 1
2017 826 1224 45.1 L 37.279 -97.516 4.9 TES 10 0.0 1.5WTES 1
2017 826 1224 45.6 L 37.280 -97.516 0.1 TES 7 0.0 1.9WTES 1
2017 826 1241 58.7 L 37.278 -97.515 5.1 TES 10 0.0 1.2WTES 1
2017 826 1241 59.2 L 37.279 -97.516 0.0 TES 7 0.0 1.2WTES 1
2017 826 2307 34.4 L 36.318 -99.078 4.7 TES 6 0.0 2.1WTES 1
2017 826 2308 24.2 L 37.280 -97.520 3.7 TES 10 0.0 1.3WTES 1
2017 826 2314 28.5 L 36.638 -99.276 8.3 TES 6 0.0 2.0WTES 1
2017 826 2315 16.6 L 37.275 -97.510 6.9 TES 10 0.0 1.3WTES 1
2017 826 2337 50.3 L 37.283 -97.517 1.0 TES 8 0.0 1.4WTES 1
2017 826 2337 50.3 L 37.283 -97.517 0.9 TES 8 0.0 1.4WTES 1
2017 826 2339 24.6 L 37.276 -97.513 3.8 TES 9 0.1 1.3WTES 1
2017 826 2339 24.7 L 37.281 -97.519 0.5 TES 8 0.0 1.8WTES 1
2017 826 2342 0.0 L 37.279 -97.519 1.0 TES 10 0.0 1.2WTES 1
2017 826 2341 59.8 L 37.280 -97.519 0.1 TES 9 0.1 1.2WTES 1
2017 826 2345 40.5 L 37.392 -97.592 4.6 TES 10 0.0 1.2WTES 1
2017 826 2345 41.4 L 37.351 -97.576 3.5 TES 9 0.0 1.2WTES 1
2017 827 0117 23.9 L 37.353 -97.578 3.2 TES 10 0.0 1.3WTES 1
2017 827 0117 24.0 L 37.344 -97.576 3.5 TES 10 0.1 1.6WTES 1
2017 827 0117 49.9 L 37.346 -97.576 4.5 TES 12 0.1 1.8WTES 1
2017 827 0117 49.8 L 37.354 -97.577 5.3 TES 8 0.0 1.9WTES 1
2017 827 0338 6.7 L 37.266 -97.508 7.7 TES 11 0.0 1.6WTES 1
2017 827 0338 7.4 L 37.279 -97.517 0.6 TES 8 0.0 1.9WTES 1

2017 827 0352 16.7 L 37.273 -97.509 5.6 TES 9 0.0 1.2WTES 1
2017 827 0352 17.0 L 37.282 -97.517 0.7 TES 8 0.0 1.2WTES 1
2017 827 0354 55.1 L 37.277 -97.517 4.8 TES 10 0.1 1.4WTES 1
2017 827 0354 55.4 L 37.279 -97.517 0.7 TES 9 0.0 2.0WTES 1
2017 827 0551 58.0 L 37.275 -97.512 4.8 TES 8 0.0 1.4WTES 1
2017 827 0551 58.2 L 37.274 -97.516 4.3 TES 10 0.0 1.1WTES 1
2017 827 0926 1.5 L 37.279 -97.627 4.0 TES 10 0.0 1.5WTES 1
2017 827 0926 1.6 L 37.281 -97.624 3.7 TES 9 0.0 2.4WTES 1
2017 827 1338 17.5 L 37.198 -97.579 5.3 TES 10 0.0 1.5WTES 1
2017 827 1338 14.4 L 37.084 -97.589 1.1 TES 9 0.0 1.7WTES 1
2017 827 1435 7.3 L 37.286 -97.507 5.6 TES 10 0.0 1.4WTES 1
2017 827 1435 7.6 L 37.289 -97.511 0.5 TES 8 0.0 2.1WTES 1
2017 827 1436 4.9 L 37.286 -97.506 5.8 TES 10 0.1 1.4WTES 1
2017 827 1436 4.8 L 37.293 -97.516 6.0 TES 8 0.0 1.9WTES 1
2017 827 1501 16.0 L 37.244 -97.572 3.4 TES 11 0.0 2.7WTES 1
2017 827 1501 16.0 L 37.241 -97.572 3.8 TES 9 0.0 2.9WTES 1
2017 827 1626 5.7 L 37.281 -97.510 4.7 TES 10 0.0 1.5WTES 1
2017 827 1626 6.2 L 37.281 -97.508 8.1 TES 9 0.0 2.1WTES 1
2017 827 1656 13.3 L 37.241 -97.572 4.0 TES 11 0.0 1.6WTES 1
2017 827 1656 13.3 L 37.239 -97.571 4.3 TES 9 0.0 2.4WTES 1
2017 827 1928 39.5 L 37.294 -97.426 5.6 TES 8 0.0 1.4WTES 1
2017 827 1928 39.4 L 37.285 -97.435 5.2 TES 7 0.0 1.4WTES 1
2017 827 1929 4.3 L 37.288 -97.510 5.7 TES 9 0.0 1.1WTES 1
2017 827 1929 4.5 L 37.260 -97.476 4.3 TES 7 0.0 1.1WTES 1
2017 827 2049 55.9 L 37.445 -97.362 2.2 TES 9 0.1 1.4WTES 1
2017 827 2049 56.2 L 37.433 -97.377 0.1 TES 8 0.0 1.7WTES 1
2017 827 2232 21.1 L 37.166 -97.581 5.4 TES 9 0.0 1.5WTES 1
2017 827 2232 20.6 L 37.146 -97.583 5.3 TES 9 0.0 2.5WTES 1
2017 828 0234 41.5 L 37.250 -97.571 2.1 TES 10 0.0 1.3WTES 1
2017 828 0234 41.1 L 37.234 -97.572 4.7 TES 9 0.0 1.4WTES 1
2017 828 0436 4.0 L 37.283 -97.515 2.6 TES 10 0.0 1.2WTES 1

2017 828 0436 4.0 L 37.282 -97.511 0.2 TES 7 0.0 1.2WTES 1
2017 828 1829 15.3 L 37.281 -97.509 5.1 TES 10 0.0 1.7WTES 1
2017 828 1829 15.3 L 37.285 -97.514 5.1 TES 9 0.0 2.4WTES 1
2017 828 1907 23.3 L 37.283 -97.514 0.6 TES 10 0.0 1.5WTES 1
2017 828 1907 23.5 L 37.274 -97.501 1.0 TES 7 0.0 2.9WTES 1
2017 828 1927 50.4 L 37.285 -97.513 4.4 TES 10 0.0 1.6WTES 1
2017 828 1927 50.3 L 37.286 -97.515 4.6 TES 9 0.0 2.2WTES 1
2017 829 0224 14.8 L 36.988 -97.573 18.0 TES 11 0.0 2.1WTES 1
2017 829 0223 58.2 L 36.453 -97.617 0.3 TES 9 0.0 2.9WTES 1
2017 829 1531 35.8 L 37.138 -97.630 8.2 TES 12 0.0 2.0WTES 1
2017 829 1531 35.8 L 37.138 -97.630 8.2 TES 9 0.0 2.5WTES 1
2017 829 2358 52.2 L 37.285 -97.514 4.5 TES 9 0.0 1.4WTES 1
2017 829 2358 52.3 L 37.289 -97.519 3.5 TES 8 0.0 1.3WTES 1
2017 830 0325 56.6 L 37.287 -97.522 6.8 TES 9 0.0 1.2WTES 1
2017 830 0325 50.3 L 37.268 -97.530 31.9 TES 7 0.0 1.5WTES 1
2017 830 1046 22.6 L 37.328 -97.776 6.0 TES 10 0.0 1.7WTES 1
2017 830 1046 22.7 L 37.339 -97.772 4.2 TES 9 0.0 2.4WTES 1
2017 830 1201 16.4 L 37.285 -97.290 6.1 TES 10 0.0 1.6WTES 1
2017 830 1201 16.2 L 37.285 -97.279 5.5 TES 8 0.0 2.1WTES 1
2017 830 1214 10.9 L 37.285 -97.516 1.1 TES 9 0.1 1.1WTES 1
2017 830 1214 10.9 L 37.269 -97.495 0.4 TES 7 0.0 1.2WTES 1
2017 830 1607 56.5 L 37.283 -97.516 1.7 TES 10 0.0 1.3WTES 1
2017 830 1607 56.2 L 37.286 -97.519 4.6 TES 9 0.0 1.8WTES 1
2017 831 0239 18.9 L 37.601 -97.750 3.6 TES 10 0.0 1.7WTES 1
2017 831 0239 18.9 L 37.601 -97.743 7.1 TES 8 0.0 1.8WTES 1
2017 831 0707 35.5 L 37.686 -97.479 2.2 TES 11 0.0 1.9WTES 1
2017 831 0707 35.5 L 37.681 -97.459 9.7 TES 9 0.0 2.6WTES 1
2017 831 0721 15.3 L 37.614 -97.759 6.3 TES 11 0.0 3.2WTES 1
2017 831 0721 15.3 L 37.607 -97.767 10.9 TES 9 0.0 3.3WTES 1
2017 831 1022 33.7 L 37.350 -97.577 7.2 TES 10 0.0 1.2WTES 1
2017 831 1022 34.1 L 37.344 -97.574 4.6 TES 8 0.0 1.5WTES 1

```
2017  831 1914 30.0 L  37.294 -97.511  4.5  TES  9 0.0 1.2WTES          1
2017  831 1914 30.3 L  37.292 -97.509  1.0  TES  9 0.0 1.2WTES          1
2017  831 2243 51.8 L  37.290 -97.506  3.9  TES 11 0.0 1.6WTES          1
2017  831 2243 51.8 L  37.293 -97.507  4.4  TES  9 0.0 2.4WTES          1
```